UQAC
Université du Québec
à Chicoutimi

Prediction of retrogressive landslide in the sensitive clays with the material point method

By

Zinan Ara Urmi

Under the supervision of Dr. Ali Saeidi and the co-supervision of Dr. Alba Yerro

Thesis presented to the University of Quebec at Chicoutimi with a view to obtaining the degree of Doctor of Philosophy (PhD) in engineering (Civil)

BOARD OF EXAMINERS:

Dr. Mathieu Fiset, Department of Applied Sciences at UQAC, President of the Board

Dr. Mingliang Zhou, Associate Professor, College of Civil Engineering, Tongji University, External Member of the Board

Dr. Meghdad Payan, Associate Professor, University of Guilan, External Member of the Board

Dr. Ali Saeidi, Professor, Department of Applied Sciences at UQAC, Internal Member of the Board

Dr. Alba Yerro, Assistant Professor, Department of Civil & Environmental Engineering, Internal Member of the Board

Québec, Canada

RÉSUMÉ

Les glissements de terrain dans les argiles sensibles posent des défis significatifs dans des régions comme le Québec et l'Ontario au Canada, en raison de leurs styles de déformation uniques et de la diminution dramatique de la résistance au cisaillement. Cette thèse doctorale commence par une revue exhaustive de la littérature portant sur le comportement des argiles sensibles, les facteurs à l'origine des glissements de terrain dans ce type de sol, et les hypothèses concernant les mécanismes de glissement observés lors d'incidents passés. Cette thèse examine également les outils existants pour l'analyse des ruptures rétrogressives et évalue les avantages et les limites de chaque approche. La revue de la littérature scientifique indique que les méthodes traditionnelles ne parviennent pas à déterminer la courbe « contrainte-déformation » après le pic de rupture pour des niveaux élevés de déformation (>100%), en raison des complexités associées aux niveaux élevés de déformation. De plus, une évaluation critique des modèles constitutifs existants et des outils numériques révèle des lacunes significatives dans les approches conventionnelles, notamment leur incapacité à intégrer précisément la nature progressive et rétrogressive des glissements de terrain et les grandes déformations associées. Pour pallier ces limitations, cette thèse doctorale introduit une nouvelle méthode d'évaluation du comportement spécifique in situ après le pic de rupture des argiles sensibles, en examinant les caractéristiques de déformations élevées trouvées dans la littérature existante. De plus, une nouvelle équation exprimant la réduction de la résistance au cisaillement est proposée pour représenter précisément le comportement « contrainte-déformation » après le pic de rupture des argiles sensibles. Cette méthodologie est ensuite appliquée dans l'analyse du comportement après le pic de rupture de sept glissements de terrain historiques au Québec. Les résultats montrent que le comportement « contrainte-déformation » est bien reproduit, ce qui conduit à des glissements de terrain majeurs. Pour faciliter l'analyse des glissements de terrain, cette thèse doctorale s'appuie sur le logiciel Anura3D à cause de sa flexibilité pour produire des modèles de sol contrôlés par l'utilisateur, au sein d'un cadre robuste de la MPM (Material Point Method). La MPM simule les grandes déformations en utilisant une combinaison des approches eulérienne et lagrangienne. En utilisant la nouvelle équation produite dans le cadre de ce doctorat pour la réduction de la résistance au cisaillement dans un modèle constitutif basé sur Mohr-Coulomb, nos travaux de recherche permettent de valider à travers de multiples simulations de cisaillement simple direct (DSS). Suit ensuite la calibration du modèle constitutif avec des facteurs d'échelle, de manière à réaliser une implémentation dans une analyse réelle de glissement de terrain. Le modèle calibré est utilisé pour prédire l'initiation et la propagation de bandes de cisaillement conduisant à de grandes ruptures rétrogressives dans des pentes d'argile très sensibles. Trois études de cas notables démontrent que l'outil numérique prédit avec succès la rétrogression et la dispersion après les ruptures des glissements de terrain, en accord avec les observations de terrain et les mécanismes de glissement hypothétisés. Le projet doctoral explore également des techniques d'optimisation pour l'analyse numérique de rupture rétrogressive afin d'atteindre des résultats plus réalistes. Enfin, en prédisant avec succès le mouvement après rupture de l'un des glissements de terrain rétrogressifs les plus grands et les plus complexes du dernier siècle, la rupture rétrogressive de Lamieux en 1993, l'étude démontre l'efficacité de l'approche d'optimisation. La méthode de prédiction de rupture rétrogressive développée dans le cadre de cette thèse doctorale offre des indications fondamentales sur les mécanismes sous-jacents et les facteurs principaux entraînant des ruptures rétrogressives dans les argiles sensibles. Cette compréhension approfondie améliore la cartographie des risques géotechniques en permettant des prédictions plus précises des zones potentielles de glissement de terrain et de l'étendue potentielle des mouvements probables. De plus, cette connaissance améliore significativement l'analyse des risques, facilitant le développement de stratégies d'atténuation ciblées et de plans d'urgence.

Mots clés: Argile sensible, Glissement de terrain rétrogressif, adoucissement de la contrainte, Grande déformation, Méthode du point de matériau.

ABSTRACT

Landslides involving sensitive clays pose significant challenges in regions like Quebec and Ontario in Canada due to their unique deformation behaviors and dramatic reductions in shear strength. The study begins with an extensive literature review of the behavior of sensitive clays, the factors that trigger landslides in such soils, and the hypotheses regarding landslide mechanisms observed in past incidents. It also reviews existing tools for retrogressive failure analysis and evaluates the advantages and limitations of each approach. The review indicates that traditional methods often fail to accurately determine the post-peak stress-strain curve for large strains (>100%) due to the complexities at higher strain levels. Furthermore, a critical evaluation of existing constitutive models and numerical tools reveals significant gaps in conventional approaches, particularly their failure to accurately incorporate the progressive and retrogressive nature of landslides and the associated large deformations. To address these limitations, this study introduces a novel methodology for assessing the site-specific post-peak behavior of sensitive clays by examining their large deformation characteristics found in existing literature. This research develops a new strain-softening law to precisely represent the post-peak stress-strain behavior of sensitive clays. This methodology is then implemented to analyze the post-peak behavior of seven pre-historic landslide locations. The energy calculations from these curves demonstrate that the stress-strain behavior is well captured, leading to massive landslides. To facilitate landslide analysis, this study utilizes the Anura3D software for its flexibility in working with user-defined soil models within a robust Material Point Method (MPM) framework that handles large deformations using a combination of both Eulerian and Lagrangian approaches. Employing the strain-softening law in a Mohr-Coulomb-based strain-softening constitutive model, the research then validates the constitutive soil model through multiple Direct Simple Shear (DSS) simulations by effectively capturing the targeted post-peak stress-strain behavior. The research subsequently calibrates the constitutive model with scale factors for its implementation in real-scale landslide analysis. The calibrated model is then used to predict the initiation and propagation of shear bands leading to large retrogressive failures in highly sensitive clay slopes. Three prominent case studies demonstrate that the numerical tool successfully predicts the post-failure retrogression and runout of the landslides, closely aligning with field observations and hypothesized landslide mechanisms. The study also explores optimization techniques for the numerical analysis of retrogressive failure within this framework to increase accuracy and flexibility. Finally, by successfully predicting the post-failure movement of one of the largest and most complex retrogressive flowslides of the last century, the 1993 Lamieux landslide, the study demonstrates the effectiveness of the optimization approach. The retrogressive failure prediction method developed by this research offers invaluable insights into the underlying mechanisms and primary factors driving retrogressive failures in sensitive clays. This deeper understanding enhances hazard mapping by enabling more accurate predictions of potential landslide zones and the extent of likely movements. Furthermore, this knowledge significantly improves risk analysis, facilitating the development of targeted mitigation strategies and emergency response plans.

Keywords: Sensitive clay, Retrogressive landslide, strain softening, Large deformation, Material point method

TABLE OF CONTENTS

LIST OF TABLES

LIST OF FIGURES

LIST OF SYMBOLS

s_u: Undrained shear strength
s_{up}: Peak undrained shear strength
s_{ur}: Remolded undrained shear strength
s_{uR}: Residual undrained shear strength
S_t: Sensitivity

γ: Shear strain
γ_{95}: Shear strain corresponding to a 95% of the total strength decrease
γ_p: Peak shear strain
γ_R: Residual shear strain
γ_r: Shear strain on the onset of remolding
c': Effective cohesion
φ': Effective friction angle
c'_r: Residual cohesion
φ'_r: Residual friction angle
N_s: Stability number
I_r: Remolding index
w_L: Liquid limit

I_L: Liquidity index
I_P: Plasticity index
ν: Poisson's ratio
E_o: Lateral earth pressure co-efficient at rest
e_o: Initial void ratio
Δe: Change in void ratio
E: Young's Modulus
G: Shear Modulus

θ: Slope angle
H: Slope height
m: Unit weight of soil
$\bar{\varepsilon}_p$: Deviatoric plastic shear strain
$\bar{\varepsilon}_{pr}$: Deviatoric plastic shear strain on the onset of remolding
K: Linear softening co-efficient
P_w: Pore water pressure

δ: Shear deformation
$\dot{\gamma}$: Strain rate
τ_y: yield stress
η: plastic viscosity
σ: Total stress
w_N: Normalized strain energy
w_{LS}: Limit state strain energy
W_x: Strain energy per unit volume
σ_p': Pre-consolidation pressure
α, β: Site-specific strength reduction constants
E^P: Initial potential energy
E^R: Remolding energy
E^{KF}: Kinetic and frictional energy
I_D: Destruction index
R_D: Crest to crest retrogression distance
R_o: Runout distance from the slope's toe
ω: Proportional constant
I_B: Brittleness Index

LIST OF ABBREVIATIONS

NC:	Normally Consolidated	SLE:	Saint-Léon
OC:	Over Consolidated	LOU:	Louiseville
CU:	Consolidated Undrained	HIL:	Saint-Hilaire
TSP:	Total Stress Path	THU:	Saint-Thuribe
ESP:	Effective Stress Path	MAS:	Mascouche
DSS:	Direct Simple Shear	SAL:	Saint-Alban
FEM:	Finite Element Method	SJV:	Saint-Jean-Vianney
TL:	Total Lagrangian	SST:	Stress-Strain curves from Tavenas et al (1983) 's data
UL:	Updated Lagrangian	SSER:	Stress-Strain curves predicted by Einav and Randolph (2005)'s strain softening equation
ALE:	Arbitrary Lagrangian-Eulerian	MTMDET:	Quebec Ministry of Transport, Sustainable Mobility and Transport Electrification
RITSS:	Re-meshing and Interpolation Technique with Small Strain	NVE:	Norwegian Water Resources and Energy Directorate
CEL:	Coupled Eulerian-Lagrangian	MP:	Material Points
PFEM:	Particle Finite Element Method	CN:	Computational Nodes
SPFEM:	Smoothed Particle Finite Element Method	PIC:	Particle in Cell
MPM:	Material Point Method	GIMPM:	Generalized Interpolation Material Point Method
LEA:	Limit Equillibrium Analysis		

DEDICATION

To my mother,

I owe my entire being to you.

ACKNOWLEDGMENTS

I would like to express my sincere gratitude to the individuals whose guidance, support, and encouragement have been instrumental in the completion of my PhD thesis.

First and foremost, my eternal gratitude goes to Dr. Ali Saeidi, my supervisor, for his unwavering trust and belief in my abilities. His support and encouragement enabled me to pursue my PhD studies abroad. I have never met a more flexible and easy-to-work-with person like him. Dr. Saeidi's prudent guidance and generous understanding of my limitations have been invaluable.

Likewise, I sincerely appreciate Dr. Alba Yerro, my co-supervisor, for her timely and insightful guidance. Her expertise and steadfast support were indispensable in overcoming my research challenges. Her critical thinking and judicious responses to my inquiries have taught me to tackle critical questions adeptly. Her unwavering work ethic and brilliance have inspired me endlessly as a scholar and woman.

I am profoundly grateful to Dr. Rama Vara Prasad Chavali, my mentor, for imparting essential knowledge and teaching me the basics of writing research papers. His guidance and expertise have been instrumental throughout this journey. His readiness to clarify my doubts whenever they arose has been a testament to his dedication. Having a mentor like him has been a true blessing.

My thanks also extend to Sarah, with whom I have shared this entire journey. Starting together, facing challenges, and growing together as academics have been a significant part of my PhD experience. I will always cherish our discussions about our research. Additionally, I want to acknowledge the valuable feedback and comments from our research group, R2eau, during our monthly meetings.

I owe a debt of gratitude to my undergraduate and MSc supervisor, Dr. Mehedi Ahmed Ansary, who instilled in me the first seed of confidence that I could achieve something meaningful in academia. His belief in me has been foundational. Likewise, I am thankful to my former organization, Environment and Infrastructure Management Solutions (EIMS) Ltd, Bangladesh, for granting me a 3-year study leave, no questions asked.

My deepest gratitude extends to my family for their unconditional love, understanding, and support throughout this journey. Their encouragement and sacrifices have been the bedrock of my success. I am indebted to my husband for being my best friend, a constant from childhood. I am grateful to my child, Uzair, for being a constant source of encouragement and love. Your presence has inspired me to overcome challenges and reach this significant milestone in my academic career. Lastly, my heartfelt thanks go to my best friend, Eva, who has been my pillar of support and kept me grounded during moments of emotional turmoil throughout my PhD.

I am genuinely grateful to each of you for contributing to my academic and personal growth. Thank you for believing in me and being an integral part of this remarkable journey.

CHAPTER 1

INTRODUCTION

1.1 GENERAL

Landslides in sensitive clays are recurrent events in the northern countries of the world, especially in Canada and Norway. The impact of landslides is catastrophic to both the population and the economy. Natural resources Canada [1] has reported that the annual damages by landslides are worth $200 to $400 million in Canada. Around a thousand people have died in landslide events all over the country from 1771 to 2018, among which 134 fatalities were recorded solely in the Québec region due to the glaciomarine-sensitive clay failures in the St. Lawrence Lowlands [2]. Because of the nature of sensitive clay, runouts, and affected areas are generally very large. In the sensitive clays of Norway, the Gjerdrum landslide (2020) spanned a flow-off area of 210 000 m^2 and additionally affected 90 000 m^2 by debris flow. A total of 1,000 people were evacuated, 10 people died, 31 houses were destroyed, and the mitigation works were worth $20 million without the rebuilding cost of infrastructure or environmental damages [3]. Therefore, understanding the triggering factors, failure mechanisms, and post-failure consequences of these landslides is vital for risk assessment and improving the resiliency of the affected communities.

Understanding how material sensitivity controls soil behavior is paramount in analyzing landslides in sensitive clays. The unique nature of sensitive clays is that under shear loading, after reaching the peak shear strength, there is a dramatic reduction in shear strength with increasing strain [4]; this phenomenon is generally called "strain-softening." In this context, "sensitivity" is the ratio of the peak shear strength to the reduced shear strength that expresses the loss of strength when the soil experiences large deformation. The development of sensitivity of the clays is attributed to the depositional features of sensitive clays and the ongoing weathering effect on embankment soils. Sensitive clays are believed to have been deposited in marine environment depressions left by the Laurentian ice sheet around 14000 to 6000 years ago from the present time [5]. Due to the exposure to seawater with high salt concentration, the clays formed a flocculated structure with high undisturbed shear strength. With the deglaciation of the ice sheets over time, the lands that were once depressed by the massive weight of the ice sheets rose above the sea level (iso-static rebound). Due to this uplift of the

clay deposition above the seawater, the clays were exposed to fresh water. When the freshwater flows through the soil, the salt concentration within the soil mass reduces due to the leaching out of salt into the fresh water. As a result, even though the clays retain their flocculated structure, they do not have the salt ions that keep the structure stable. This structure is meta-stable and highly susceptible to disturbance, leading to very low remolded strength. This metastable structure is destroyed upon remolding, and the liberated interparticle surface water transforms the clay into a liquid-like fluid, commonly referred to as remolded clays [6]. During this process, the shear strength reduces from peak (s_{up}) to remolded (s_{ur}) strength and the sensitivity (S_t) of the soil is quantified as the ratio of the peak and remolded shear strength (s_{up}/s_{ur}). When subjected to loading, the potential to liquefy or get remolded is one of the leading agents governing the post-failure behavior of sensitive clays. When excessive stress surpasses their peak shear strength, narrow shear bands with localized strain form, triggering the structural transformation that remolds the soil mass. The remolded clays within the shear bands can either spread laterally or drift away from their original position, resulting in a series of failures that progress in either a progressive or retrogressive manner [7]. These landslides can extend over kilometers, resulting in widespread destruction and devastating aftermath in the affected areas. The catastrophic consequences of landslides occurring in sensitive clays have sparked significant interest among researchers, who have extensively investigated the behavior of these materials under different loading conditions. The accurate prediction of the post-failure mechanism and the potentially affected area can significantly facilitate the evaluation of disaster risk and the development of effective mitigation measures.

The mechanism behind retrogressive failure in sensitive soil involves various complex features, including the landslide trigger, the formation of shear bands or multiple failure surfaces, the movement of remolded soil, and the progression of the landslide. These complexities pose significant challenges when conducting numerical analyses of sensitive clay landslides. Traditional methods, such as limit equilibrium or finite element strength reduction techniques, face two major issues that render them unsuitable for application in sensitive clay slopes. Firstly, these conventional approaches have limited capability in predicting landslide initiation and cannot at all predict subsequent failures or runouts in retrogressive landslides. Secondly, the large deformations associated with these landslides can cause mesh tangling in conventional finite element methods. The strain-softening behavior exhibited by sensitive clays, responsible for the intricate failure mechanism, necessitates using sophisticated constitutive soil models and advanced numerical tools capable of handling large

deformation problems. The capability to reproduce realistic strain-softening characteristics in the material model is necessary for more accurate numerical analyses of large deformation problems in such materials [8].

Over the past two decades, considerable progress has been made in addressing large deformation problems in geotechnical engineering. Various mesh-based and meshless numerical frameworks, such as the arbitrary Lagrangian finite element method, the particle finite element method, and the material point method, have been successfully implemented to capture some key characteristics of large retrogressive failures [9–11]. Additionally, the development of strain-softening constitutive soil models has further enhanced the ability to model these phenomena effectively. Numerical modeling of sensitive clay slopes offers valuable insights into failure mechanisms and post-failure runout, which are crucial for landslide hazard mapping in such areas.

1.2 PROBLEM STATEMENT

Ideally, the strain value required to reach the remolded shear stress is extremely large. Stark and Contreras [12] suggested that a completely remolded state may occur when the specimen is sheared to several hundred millimeters, corresponding to several hundred percent of the shear strain in soil specimens subjected to conventional laboratory tests [12]. Stress-strain curves obtained from triaxial compression tests are limited to only 10–20% strain [13]. Generally, ring shear tests, reversal shear box tests, or direct simple shear tests are used to study the large deformation behavior, but these laboratory-scale shear tests could only achieve strains up to 30%–45% [14–18]. Thakur et al. [19] examined the stress-strain behavior of sensitive clays using field vane shear testing [19]. However, the residual torque at 90◦ rotation could not reach the remolded level even after multiple manual turns due to factors associated with the drainage in the failure zone around the vane [20]. Thus, predicting post-peak stress-strain behavior is one of the major challenges in analyzing sensitive clay landslides where large deformation is involved. Some researchers used the linear strength degradation equation for simplicity [16, 21, 22], but strain softening in sensitive clays can be highly nonlinear [14–18]. As per the author's knowledge, the very first equation to represent the strain-softening behavior of sensitive clay for measuring the resistance of soil around a cone penetrometer was proposed by Einav and Randolph [23] as follows,

$$s_u = s_{ur} + (s_{up} - s_{ur})e^{-\frac{3\gamma}{\gamma_{95}}} \quad 1\text{-}1$$

where s_{up} is the peak shear strength, s_u is the degraded shear strength after the peak, s_{ur} is the remolded shear strength, γ is the strain corresponding to s_u, and γ_{95} is the strain when the strength is reduced by 95% of the supposed total reduction ($s_{up} - s_{ur}$). Given the absence of a suitable method to assess the large deformation characteristics of sensitive clays, recent studies predominantly revolve around retroactively analyzing past landslides. This involves iteratively adjusting large deformation parameters until they align more closely with observed field behavior. Consequently, as of now, no analytical tool is capable of predicting the potential extent of retreat or advancement in a sensitive clay landslide.

Several research questions arise based on the complexities and challenges identified in analyzing the post-peak stress-strain behavior of sensitive clays, particularly in the context of large deformations involved in landslide events. These questions aim to deepen the understanding and improve predictive models:

1. How can the complete strain-softening behavior of sensitive clays up to the remolded state be determined to reflect the nonlinear degradation of shear strength observed in field and laboratory tests?

2. What modifications are necessary to the existing strain-softening equation to adequately capture the large deformation characteristics of sensitive clays in a way that aligns with observed field behavior during landslides?

3. Can a new or improved method be developed to assess and predict the potential extent of retreat or advancement in sensitive clay landslides based on more accurate large deformation parameters?

4. To what extent can the iterative adjustment of large deformation parameters in numerical simulations be optimized to enhance the accuracy and reliability of landslide prediction models?

Addressing these questions could significantly advance the study of sensitive clay landslides, enhancing theoretical understanding and practical applications in geotechnical engineering.

1.3 RESEARCH OBJECTIVES

The primary purpose of this study is to develop a numerical tool for the successful prediction of sensitive clay landslides. The study aims to bridge the gap arising from the limitations of conventional laboratory shear tests for evaluating the large-deformation parameters of sensitive clay. The objective is to develop a strain-softening constitutive soil model that can accurately predict the post-failure behavior of sensitive clays. Subsequently, this model will be incorporated into a numerical framework capable of effectively handling extensive deformations, thereby facilitating the accurate prediction of retrogressive landslides in sensitive clay areas. Consequently, the specific research objectives are outlined as follows:

- Develop the complete post-peak curve up to remolding, proficiently replicating post-peak stress-strain curves to address the limitation of evaluating the large deformation parameters through laboratory testing.
- Integrate the post-peak behavior to a constitutive soil model into the Material Point Method framework.
- Calibrate the softening behavior from laboratory to field scale modeling.
- Validate the proposed numerical tool by predicting retrogressive failure in previously documented landslides.
- Optimize the numerical simulations using the proposed predictive tool to enhance reliability.

1.4 METHODOLOGY

The research methodology is divided into four main parts: Development of a complete post-peak curve up to remolding, integration of the constitutive model in a numerical framework, calibration and validation of the model, and optimization of the simulation process. Each step of the methodology is presented in the following chart.

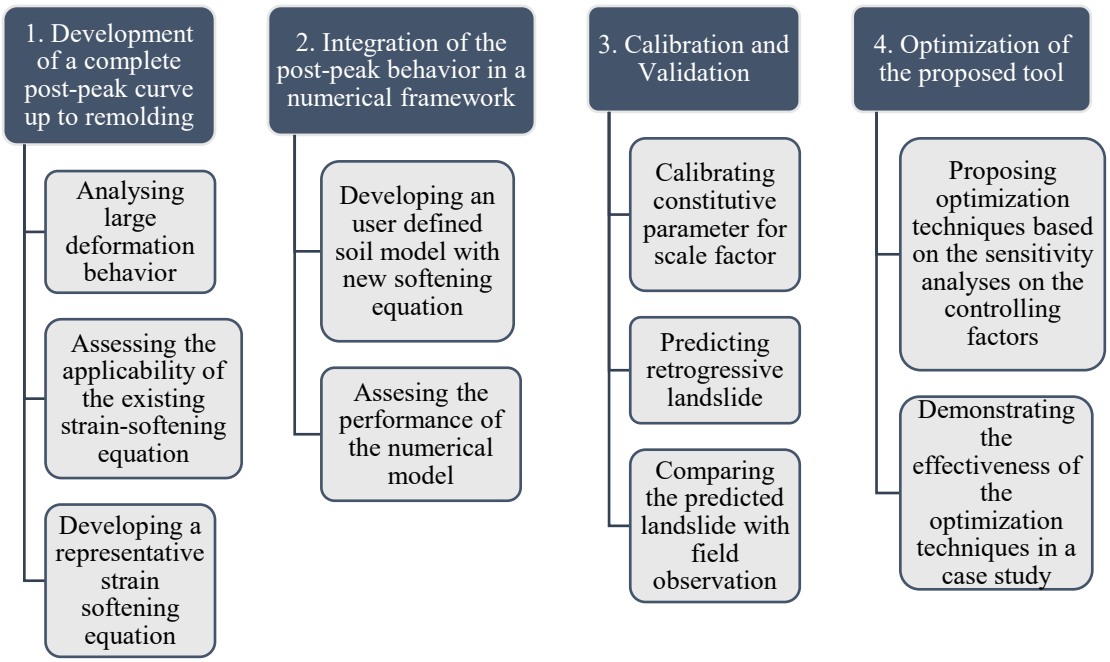

Figure 1-1. Flow chart of the methodology adopted for the study

1.4.1 Development of a complete post-peak curve up to remolding

Extensive investigations are conducted into the large deformation behavior, laying the foundation for developing the constitutive equation. An analytical approach is employed to construct a stress-strain curve capable of encompassing significant strains, drawing upon experimental data from 9 distinct locations featuring eastern Canadian Sensitive clay. Building on the insights gained from the limitations of existing strain-softening equations in accurately representing stress-strain curves derived from experimental data, a novel site-specific strain-softening criterion is formulated. This criterion serves as a means to effectively anticipate the post-failure behavior of sensitive clays.

1.4.2 Integration of the post-peak behavior in a numerical framework

The study adopts the open-source material point method (MPM) framework, Anura3D, to integrate the post-peak behavior of sensitive clays for numerical modeling. Within the MPM framework of Anura3D, a user-defined soil model incorporating the newly developed strain-softening equation is integrated. The efficiency of

the numerical model in replicating the strain-softening behavior of the newly developed equation is validated by simulating a direct shear test.

1.4.3 Calibration and Validation

As the softening equation is obtained from direct simple shear test data, the element size of the numerical model is kept the same as the direct shear test sample while simulating the test. While simulating direct shear tests with extremely small element sizes (0.014 m) provides accurate results, employing the same element size for real-scale landslide simulations becomes computationally very expensive. On the other hand, using a larger mesh size can lead to erroneous outcomes because employing strain softening in conventional continuum numerical methods often results in mesh-dependent strain localization problems. The smeared crack approach is commonly employed as a regularization technique to address the issue [24]. This approach assumes that the total work dissipated by a shear band is equivalent to the fracture energy dissipated in a discrete crack, and consistency in the dissipated work across shear bands of different element sizes ensures consistent results, irrespective of the mesh size employed. This can be achieved by conducting numerical shear tests using various mesh element sizes. By calibrating constitutive moduli, it is possible to ensure that the area under the stress-strain curve (dissipated work) is equal for each element size used for discretizing the shear band. If the dissipated energy is equal in the shearing process, the post-failure movements should be more or less similar per the smeared crack approach. Applying this methodology, the constitutive parameters are calibrated for the scale factor. After obtaining the calibrated parameters, the numerical tool was employed at three landslide locations to predict the post-failure runout and retrogression. Finally, the predicted results have been compared to the field observation to determine the model's validity.

1.4.4 Optimization of the model

Following the validation of the model against three landslide events, we conducted a sensitivity analysis to assess how model parameters influence the simulated outcomes. Subsequently, we proposed optimization techniques to increase the model's reliability and reduce costs. The effectiveness of these techniques was demonstrated through a real-world scenario. This step focused on optimizing the model parameters to accurately simulate large-scale, complex, retrogressive failures in sensitive clays.

1.5 ORIGINALITY

The research aims to make groundbreaking contributions to deepen the understanding and improve predictions of retrogressive landslides in sensitive clays. The study proposes the development of a novel strain-softening equation informed by experimental data, recognizing the intricacies prevalent in the post-peak stress-strain curves of sensitive clays. This forthcoming equation is envisioned to capture the extensive stress-strain behavior of sensitive clays during large deformations, potentially overcoming the constraints associated with traditional laboratory shear tests. By anchoring the model to the authentic behavior of sensitive clays under pronounced deformations, accurate projections of post-peak stress-strain curves up to remolded shear stress levels are anticipated. Furthermore, this innovation aims to precisely compute the remolding energy within sensitive clay slopes, potentially introducing a new means to assess landslide susceptibility to retrogressive failure through the remolding energy criterion.

The intended model, once validated with field observations, is expected to be a valuable tool for landslide prediction. It is hypothesized that aligning predictions of retrogressive failures, derived from the proposed strain-softening equation and prospective calibrated constitutive parameters, with real-world observations will not only validate the model's relevance but also highlight the potential efficiency of the smeared crack approach in mitigating mesh dependency in continuum frameworks. Moreover, it is anticipated that the numerical model will visually represent the evolution of shear band formation during retrogressive landslide movements, offering deeper insights into this vital process. By aligning the model's hypothesized failure mechanisms with theoretical constructs from existing literature, its credibility and expanded applicability aim to be ensured.

This research aspires to pioneer a transformative strain-softening equation, provide pivotal insights into retrogressive landslide prediction in sensitive clays, and expand knowledge on shear band formation. By drawing a congruence between anticipated outcomes and observations, the aim is to validate the model's utility and pave the way for further inquiries and tangible implementations in slope stability analysis.

1.6 THESIS OUTLINE

Four journal papers are the outcome of this thesis and are presented separately in Chapters 2 to 5. The general structure of the articles comprises the Abstract, Introduction, Numerical framework and Constitutive soil model, Analysis, Discussion, and Conclusion.

CHAPTER 1 begins by providing a detailed discussion of the research topic, aiming to portray the key research questions. Expanding on this foundation, the chapter articulates the research objectives. Subsequently, it delves into a comprehensive description of the methodology employed to achieve these objectives. Finally, the chapter concludes with an overview of the overall structure of the thesis, providing readers with a clear roadmap of what to expect.

CHAPTER 2 commences with an in-depth review of pertinent literature concerning the distinctive stress-strain behavior of sensitive clays, particularly focusing on their susceptibility to retrogressive failure. Next comes a thorough discussion of the failure mechanisms observed in retrogressive landslides based on previous studies. Subsequently, an evaluation of existing constitutive soil models is conducted, aimed at replicating the strain-softening behavior inherent in sensitive clays, emphasizing their applicability to specific cases. This is followed by a detailed review of advanced numerical frameworks to address the challenge of large deformations associated with landslides in sensitive clays. Finally, the chapter highlights the contributions of previous studies in elucidating the intricate post-failure behavior of sensitive clays and outlines avenues for future research based on their limitations.

CHAPTER 3 presents an analytical methodology to develop a strain-softening equation tailored to capture the large deformation behavior of sensitive clays. This approach integrates experimental data from nine pre-historic Eastern Canadian sensitive clay landslide locations. A new, site-specific strain-softening criterion is formulated by addressing the shortcomings observed in existing strain-softening equations regarding their accuracy in representing stress-strain curves derived from experimental data. This criterion serves as a valuable tool for predicting the post-failure behavior of sensitive clays.

CHAPTER 4 calibrates and validates a constitutive soil model using the developed strain-softening equation from Chapter 3. It integrates this model into the Anura3D software and validates its efficiency through direct shear test simulations. Additionally, constitutive parameters are calibrated for the scale factor using a smeared crack approach to mitigate mesh-dependent strain localization. The calibrated parameters are applied to predict post-failure runout and retrogression at three landslide locations, with results compared to field observations to validate the model.

CHAPTER 5 examines the impact of certain model parameters, such as element size, number of material points, geometrical representation, and methods for triggering failure in the numerical model on simulation outcomes, building on the methodology proposed in Chapter 4. The primary objective is to refine these parameters to develop a more accurate and cost-effective approach, emphasizing the critical nature of these adjustments when using the proposed numerical tool for simulating sensitive clay landslides. Moreover, this chapter demonstrates the effectiveness of these optimizations for accurately predicting one of the most complex and large retrogressive failures of eastern Canada.

CHAPTER 6 presents the most important outcomes of the present work and the directions for future research.

CHAPTER 2

Article 1: Failure Mechanism, Existing Constitutive Models and Numerical Modeling of Landslides in Sensitive Clay: A Review

Zinan Ara Urmi [a] *, Ali Saeidi [a], Rama Vara Prasad Chavali [a] and, Alba Yerro[b]

[a] Department of Applied Sciences, University of Quebec at Chicoutimi, Saguenay, G7H 2B1, QC, Canada

[b] Department of Civil and Environmental Engineering, Virginia Tech, Blacksburg, Blacksburg, VA 24061, United States

Published, Geoenvironmental Disasters, Volume 10 (14), 26 May 2023, 111866
https://doi.org/10.1186/s40677-023-00242-9

Competing interests

The author(s) declare(s) that they have no competing interests.

Funding

This research was partially funded by the Natural Sciences and Engineering Research Council of Canada (NSERC) and Hydro-Quebec under projects funding no. RDCPJ 521771–17 and NSERC- 950-232724.

Authors' contributions

Idea conceptualization: Ali Saeidi

Literature review and preparation of the complete initial draft: Zinan Ara Urmi

Repeated review, restructuring, re-writing, and proof-reading: All Authors

2.1 ABSTRACT

Landslides involving sensitive clays are recurrent events in the world's northern regions and are especially notorious in eastern Canada. The two critical factors that separate sensitive clay landslides from traditional slope stability analysis are the highly brittle behavior in undrained conditions (strain-softening) characteristic of progressive or retrogressive failures and the large deformations associated with them. Conventional limit equilibrium analysis has numerous shortcomings in incorporating these characteristics when assessing landslides in sensitive clays. This paper presents an extensive literature review of the failure mechanics characteristics of landslides in sensitive clays and the existing constitutive models and numerical tools to analyze such slopes' stability and post-failure behavior. The advantages and shortcomings of the different techniques to incorporate strain-softening and large deformation in the numerical modeling of sensitive clay landslides are assessed. The literature review depicts that elastoviscoplastic soil models with non-linear strain-softening laws and rate effects represent the material behavior of sensitive clays. Though several numerical models have been proposed to analyze post-failure runouts, the amount of work performed in line with sensitive clay landslides is very scarce. That creates an urgent need to apply and further develop advanced numerical tools for better understanding and predicting these catastrophic events.

Keywords: Progressive landslide, Sensitive clay, Numerical modeling, Strain-softening, Constitutive soil model, and Large deformation.

2.2 INTRODUCTION

Landslides in sensitive clays are recurrent events in the northern countries of the world, especially in Canada and Norway. The impact of landslides is catastrophic to both the population and the economy. Natural resources Canada (NRCan) has reported that in Canada, the annual damages by landslides are worth $200 to $400 million [1]. A total of 778 people have died in landslide events all over the country from 1771 to 2018, among which 134 fatalities are recorded solely in the Québec region due to the glaciomarine-sensitive clay failures in the St. Lawrence Lowlands [2]. Because of the nature of sensitive clay, the runout and affected area of these landslides are generally very large. In the sensitive clays of Norway, the Gjerdrum landslide (2020) spanned a flow-off area of 210 000 m^2 and additionally affected 90 000 m^2 by debris flow. A total of 1 000

people were evacuated, ten people died, 31 houses were destroyed, and the mitigation works were worth $20 million without the rebuilding cost of infrastructure or environmental damages [3]. Therefore, understanding the triggering factors, failure mechanisms, and post-failure consequences of these landslides is vital for risk assessment and improving the resiliency of the affected communities.

Understanding how material sensitivity controls soil behavior is of utmost importance in analyzing landslides in sensitive clays. The unique nature of sensitive clays is that under shear loading, after reaching the peak shear strength, there is a dramatic reduction in shear strength with increasing strain [4]; this phenomenon is generally referred to as "strain-softening." In this context, "sensitivity" is defined as the ratio of the peak shear strength to the reduced shear strength that expresses the loss of strength when the soil experiences large deformation [25, 26]. The development of sensitivity of the clays is attributed to the depositional features of sensitive clays as well as the ongoing weathering effect on embankment soils. Sensitive clays are believed to be deposited in marine environment depressions left by the Laurentian ice sheet around 14000 to 6000 years ago from the present time [5, 27]. Due to the exposure to seawater with high salt concentration, the clays formed a flocculated structure with high undisturbed shear strength. With the deglaciation of the ice sheets over time, the lands which were once depressed by the huge weight of the ice sheets rose above the sea level (iso-static rebound). Due to this uplift of the clay deposition above the seawater, the clays got exposed to fresh water. When the freshwater flows through the soil, the salt concentration within the soil mass reduces due to the leaching out of salt into the fresh water. As a result, even though the clays retain their flocculated structure, they do not have the salt ions that were keeping the structure stable. This structure is called meta-stable, which is highly susceptible to disturbance and leads to very low remolded strength. Some marine clay deposits exhibit exceptionally high sensitivity after the significant reduction in shear strength with increasing strain; the soil completely loses its structural stability and transforms from a solid to a liquid-like substance [6, 28]. This process is termed "remolding of sensitive clays," and the shear strength at which the process of remolding begins is termed the "remolded shear strength." These soil deposits are also referred to as "quick clays." Sensitivity values for quick clays are generally greater than 30 with remolded shear strength less than 0.5 kPa [29]. Crawford [26] reported that eastern Canadian quick clays have a sensitivity value ranging from 20 to several hundred. In a sensitive clay landslide, the initially deformed soil deposits get remolded and flow away from the source area, leaving the newly formed slope unsupported, which may initiate another instability. This

process can lead to a series of failures extending far beyond the crest of the initial slope [30]. Hence, for highly sensitive clays, the slope failure initiation is not the only concern, but the post-failure analysis is also critical. The subsequent sliding is referred to as "progressive" if the failure progresses forward and "retrogressive" if the failure propagates rearward [31].

The current state of knowledge related to the detailed analysis of landslides in sensitive clays depicts that computational modeling is more adaptable than other approaches, such as theoretical analysis, empirical analysis, and experimental investigations. Conventional limit equilibrium analysis has numerous shortcomings in incorporating complex geometry, non-linear soil behavior, and real-life field condition. Moreover, it cannot predict post-failure runout. Alternatively, numerical modeling is a handy tool for slope stability analysis because it requires fewer assumptions, especially regarding the failure mechanism, and can account for complex constitutive behaviors. Even though numerical modeling for landslides has come a long way in the last three decades, a few works have focused on the challenging features of sensitive clays (e.g., strain-softening, the transition from solid to liquid form, and post-failure large deformation) [9, 32, 33]. The reasons for this lack of information are, for example, that the simulation of strain-softening materials is challenging in continuum numerical frameworks, strains tend to develop and localize along narrow shear bands, and several mesh-regularization techniques need to be adapted to obtain mesh-independent results [8, 22, 34]. In addition, a well-established constitutive framework is required to capture the transition from solid to liquid behavior. Finally, the modeling of post-failure behavior in history-dependent materials is complex, and current state-of-practice numerical techniques (i.e., finite elements and finite differences) suffer from mesh tangling when dealing with large deformations [35].

The objective of this paper is to provide an extensive review of (a) the behavior of sensitive clays under shear loading, (b) the landslide mechanisms in sensitive clays, and (c) the available numerical models (i.e., constitutive laws and numerical frameworks) used for the assessment of such landslides by examining the concerns and advancements of each technique. The paper is organized as follows. First, the post-peak stress-strain behavior of sensitive clays is presented. Then, typical sensitive clay landslides' triggering and failure mechanisms (i.e., flows and spreads) are outlined. After that, the existing numerical tools used for the evaluation of sensitive clay landslides are revised. In particular, the specific utility of constitutive models that address

strain-softening and numerical frameworks that cover large deformation problems in the assessment of landslides are discussed. Finally, the literature review is compiled in a summary table, and the conclusions and future research lines are highlighted.

2.3 BEHAVIOR OF SENSITIVE CLAYS

When subjected to monotonic shear loading in drained conditions, sensitive clays have a robust collapsible nature for both normally consolidated (NC) or over consolidated (OC) state. Due to the depositional history of sensitive clays, during drained shear failure, they experience a dispersion in their meta-stable structure and a simultaneous decrease in porosity [36]. In contrast, the non-sensitive clays show dilative or contractive nature in drained shearing based on being OC and NC state, respectively. This difference in volumetric behavior in drained conditions directly impacts the undrained behavior of clays. Although no volumetric deformation is expected in undrained conditions, the material's tendency to contract or dilate governs the sign of the excess pore pressure (positive or negative, respectively) generated during the loading process, impacting the undrained shear strength and the soil behavior. While non-sensitive OC clays generate negative pore pressure (suction) and experience enhanced undrained shear strength (with respect to the drained condition), non-sensitive NC clays generate (positive) excess pore water pressures leading to reduced undrained shear strength. Mild strain-softening behavior might be observed in either case, but it does not greatly impact shearing resistance. On the contrary, in sensitive clays (NC or OC), the strong tendency to collapse leads to a massive generation of excess pore pressure, the shearing resistance is reduced to a negligible value, and the strain-softening behavior is exacerbated in comparison with the one experienced by non-sensitive clays [37]. Both non-sensitive and sensitive OC clays exhibit similar strain-softening behavior in drained conditions.

Early studies on the stress-strain behavior of sensitive clays explicated strain-softening phenomenon based on experimental results [25, 38]. Skempton [38] illustrated that if overconsolidated clays are strained, the shear strength would initially increase up to a certain point (peak shear strength). Then, the strength would start to decrease gradually with increasing strain to a residual value at a large displacement. He stipulated that post-peak strain-softening occurs due to the reduction of the effective cohesion (c') and friction angle (φ') of such clays to a residual value (c'_r and φ'_r) (Figure 2-1). Bjerrum [39] suggested that in undrained shearing,

increasing pore pressure with increasing strain might cause a decrease in shearing resistance due to the diminished effective stress. Consistent with this idea, several researchers in the last two decades stipulated that the post-peak shear strength reduction in soft sensitive clays is governed by shear-induced pore pressure rather than by a reduction of the values of the strength parameters (φ′ and c′) [22, 40, 41]. Figure 2-2 represents the stress-strain relationship and stress paths of CU triaxial testing, where the undrained effective stress path (ESP) follows a unique failure line when subjected to undrained shearing [13]. The resulting undrained strain-softening behavior is related to the increasing shear-induced pore pressure (P_w), thereby reducing the effective stress. Thakur et al. [13] supported that reductions in φ′ and c′ are possible when sensitive clays are subjected to very large strains, which was demonstrated in constant volume ring shear test results on low-sensitive Drammen plastic clay [42].

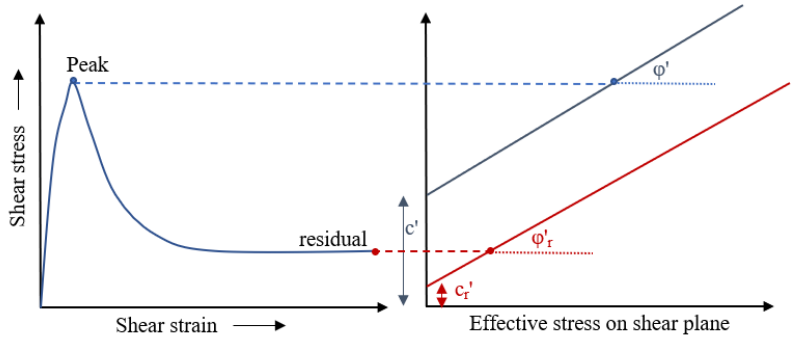

Figure 2-1. Drained behavior of an overconsolidated clay under shear loading (after [38]).

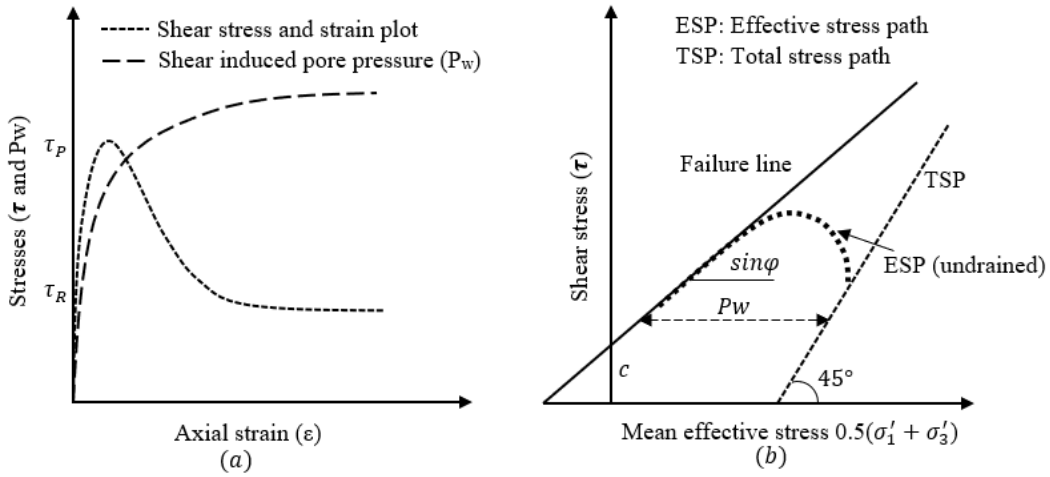

Figure 2-2. Illustration of the strain-softening mechanism (a) Development of excess pore water pressure resulting in reduced shear strength; and (b) Effective stress path and total stress path following a unique failure line indicating no reduction in effective cohesion and friction angle (after [13]).

Canadian sensitive clays can have a remolded undrained shear strength s_{ur} less than 1.5 kPa measured by Swedish fall cone tests [17, 18, 43]. Tavenas et al. [44] determined the strain energy required to remold sensitive clays up to a certain percentage (75%-90%) for different locations in eastern Canada and plotted the remolding index (I_R) vs. strain energy curves. Later on, Quinn et al. [45] converted those curves to stress-strain curves and pointed out that the shear strain required for 75%-90% of remolding is far beyond 100% (Figure 2-3a). Stark and Contreras [12] also suggested that a wholly remolded state may occur when the specimen is sheared to several hundred millimeters, equivalent to several hundred percent shear strain in soil specimens subjected to conventional laboratory tests. But such large strains cannot be attained by standard laboratory shear testing. Stress-strain curves obtained from triaxial compression tests are limited to only 10-20% strain [13]. Generally, ring shear tests, reversal shear box tests, or direct simple shear tests are used to study the large deformation behavior, but these laboratory-scale shear tests could only achieve strains up to 30%-45% [14, 15, 17, 18, 46]. This limitation warrants the need for strain-softening equations to predict the complete post-peak softening behavior up to the remolded stress [47]. Figure 2-3b illustrates DSS results in undrained conditions for sensitive clays from five different locations in Canada; it can be observed that strain-softening in sensitive clays is highly non-linear.

a)

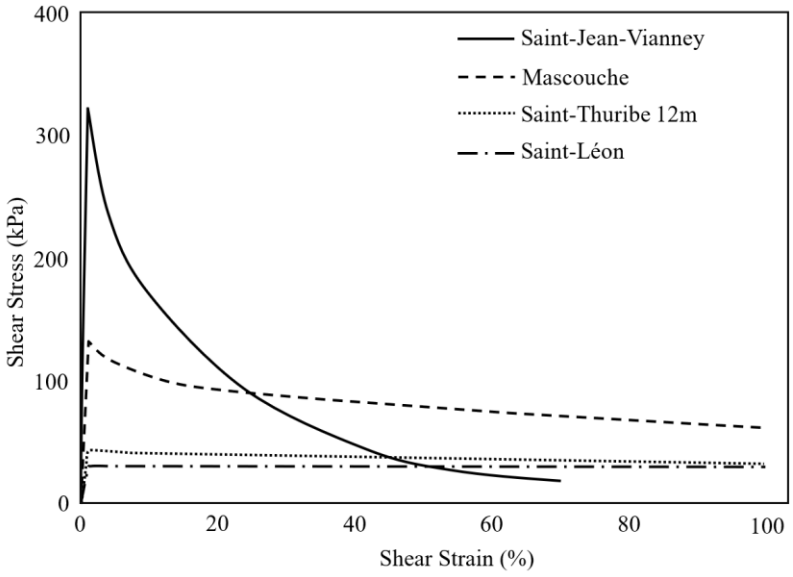

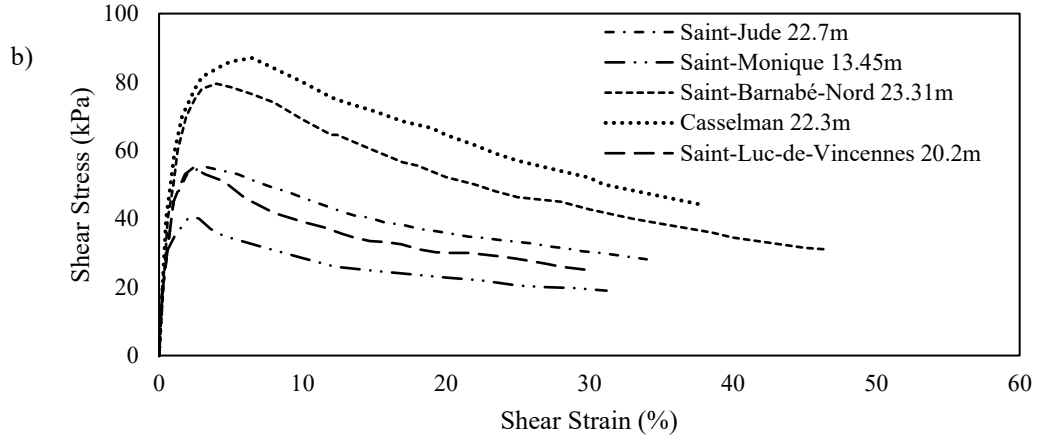

Figure 2-3. (a) Analytically interpreted stress-strain curves based on the data of the remolding index vs. normalized strain energy curves by Tavenas et al. [44] (after [45]) (b) Experimental DSS test results showing strain-softening behavior of sensitive clays for different locations in Canada; the legends show the depth of the sample along with the location name (after [14, 15, 17, 18, 46])

The behavior of sensitive clays is significantly affected by the deformation rate. Vaid et al. [48] performed one-dimensional and isotropic consolidation triaxial tests on heavily consolidated sensitive clay. They observed that the compressibility and the undrained shear strength considerably depend on the development of time-dependent strain, generally known as creep. Creep is a phenomenon in which a soil mass undergoes a slow and gradual deformation over time while subjected to constant effective stress [49]. It was noted that low strain rates caused increased compressibility and reduced shear strength. Other studies on sensitive Leda clay also support the fact that the undrained shear strength of the soil increased by about 6–12 % for a ten-times increase in strain rate [50, 51]. Lefebvre and Leboeuf [52] found a linear variation of shear strength with the logarithm of strain rate by performing several monotonic and cyclic triaxial tests on three undisturbed sensitive clay samples from eastern Canada (Figure 2-4). Field observations of sensitive clay landslides have indicated that the creep behavior significantly influences the field conditions for landslide initiation in glacimarine-sensitive clays [53]. Creep development leading to failure has three stages, a primary stage when the strain rate decreases over time, a secondary stage where the strain rate is constant, and a tertiary phase when the change in strain rate accelerates until global failure occurs [49, 53]. Neglecting the impact of strain rate during the primary stage can promote the initiation of failure. However, during the tertiary phase, not considering strain rate can lead to overestimating the velocity of flowing debris, resulting in more significant retrogression and runout.

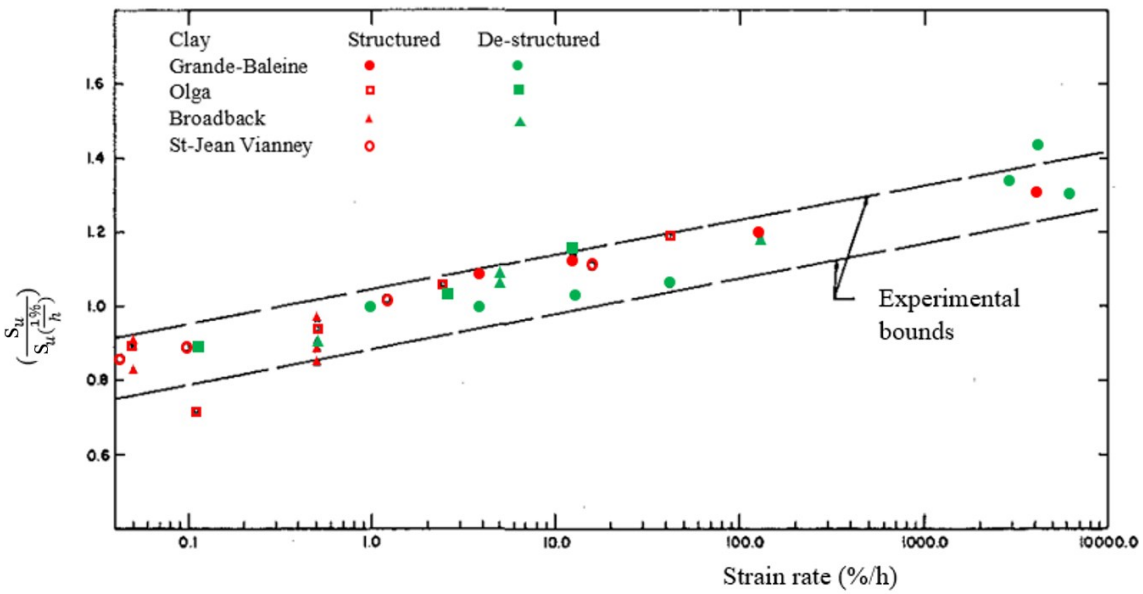

Figure 2-4. Change in undrained shear strength ratio with strain rate (after [52])

In sensitive clays, the sliding surface may develop in a narrow shear band due to the strain-softening response before any significant movement occurs. The strength degradation process is initiated when the gravitational shear stress surpasses the peak strength. As a result, unbalanced stresses are transferred to the surrounding areas, potentially overstressing the neighboring points. This process eventually leads to the development of a continuous weak zone where all the subsequent plastic deformation occurs, generally known as a shear band [54]. The energy released during strain softening acts as the driving force for the propagation of the shear band. The shear band propagates steadily as long as the mobilized strength within the shear band is lower than the peak strength but greater than the remolded strength. When plastic deformations further reduce the shear strength in the weak zone to the remolded strength, the shear band can progressively propagate without additional external load [45]. The required length for the catastrophic propagation of the shear band is known as the characteristic length or the critical length of the shear band. Several analytical and numerical methods exist to evaluate this critical length [55–57]. Propagation of shear bands beyond their critical length leads to large retrogressive failures in sensitive clays. Detailed descriptions of the formation of the sliding surface in sensitive clay landslides can be found in Locat et al.'s [58] work.

2.4 LANDSLIDE TYPES AND FAILURE MECHANISMS

Sensitive clays (quick clays) are postglacial marine deposits found primarily in North America (Eastern Canada and Alaska) and Scandinavia [59]. The largest deposits of postglacial marine clays were formed in the Champlain Sea in the Saint-Lawrence lowland, approximately 12,500 to 10,000 years BP [60]. Lefebvre [61] identified landslides as an important feature of valley formation caused by erosion of rivers and streams. He emphasized that the erodibility of the clay layers and change in groundwater regime in these deposits are major causes of instability. Demers et al. [43] illustrated that the majority of the landslides in Canadian sensitive clays have occurred along the watercourses where erosion acted as the main triggering factor. Quinn et al. [45, 56] stated that the development of a failure surface in a sensitive clay landslide might be very slow (years of small erosions) or rapid (earthquake, pile driving, blasting, or other sudden shocks) depending on the triggering factor. However, if a slope has marginal stability, a small increase in stress in the slope (e.g., due to seasonal variation of pore water pressure) can cause a catastrophic failure [27, 45, 62]. Various hydrological factors, including precipitation, piezometric pressure, groundwater flow, and other processes, are recognized as contributors to triggering retrogressive failures in sensitive clays [61, 63, 64]. Case studies and discussions of large landslide events in glaciomarine clay often identify hydrogeological factors, such as rainfall, snowmelt or anomalous weather leading up to the event, as a possible trigger [65, 66].

Different authors tried to classify landslides in the presence of sensitive clays. Varnes [31] identified two kinds of landslide, "spreading by lateral failure" and "earth flow" if the mass slides or flows, respectively. Carson and Lajoie [67] classified the landslides in the sensitive marine sediments into five categories: two-dimensional spreading failures, aborted retrogression, excess retrogression, multidirectional retrogression, and flakeslides. The last four are comparable to the earth flows defined by Varnes [31]. Tavenas [68] and Karlsrud et al. classified the landslides observed in the sensitive clays of Canada and Scandinavia based on the type of movement involved in the slides as single rotational slides, multiple retrogressive slides (earth flows/flow slides), translational progressive flake slides, and spreads. [58] identified the last three types to occur suddenly and affect large areas. Hungr et al. [69] updated Varnes's [31] classification into 21 separate categories, among which landslides observed in sensitive clays are divided into sensitive clay flow-slides (multiple retrogressive slides (earth flows/flow slides) and translational progressive (flake slides) and sensitive clay spreads. The

following two subsections present a literature review on the two most important mechanisms: flow slides and spreads in sensitive clay.

Although spreads and flow slides are well distinguished in the literature, there is no clear agreement on how to differentiate their occurrence based on the material properties and characteristics of the slope. Demers et al. [43] analyzed the characteristics of historically recorded flow slides (over 60) and spreads (about 40) and showed similar material properties for both mechanisms. Some researchers pointed out that spreads can occur in soils with low sensitivity where a flow slide will not occur [70–72]. Quinn et al. [73] suggested that spread occurs where the thickness of the crust is larger compared to the sensitive clay layer; thus, the remolded clay flows underneath and squeezes up through the cracks. In the event of flow slides, the upper crust is relatively thin compared to the sensitive clay layer; hence the crust is carried away with the remolded clay. Demers et al. [43] found that spreads occur when the sensitive clay layers exist below the watercourse level, contrary to flow slides.

2.4.1 Flow slides

Flow slides initiate with a single rotational failure that is usually a result of a slow decrease of the shear strength in the sensitive clays due to leaching out of salt through pore water in the process of erosion over decades (i.e., drained conditions) [74]. Consistently, the initial failure should be analyzed in drained conditions except for the cases when it is initiated by sudden loading (e.g earthquake or intense rainfall). In soils that are not sensitive, the initially mobilized mass rapidly becomes stable (Figure 2-5 a,b). However, in sensitive clays, the shear strength within the failure surface and the deformed mass reduces dramatically down to the remolded shear strength (Figure 2-5c). When the soil mass becomes remolded, it behaves like a viscous liquid (debris) and flows out of the newly formed crater with a considerable velocity. This movement and stress redistribution trigger a series of retrogressive rotational failures (Figure 2-5d). The rapid removal of lateral support combined with the low permeability of the sensitive clay generates negative excess pore water pressures in the back scarp (i.e., undrained conditions) increasing the effective stress [7]. Therefore, each successive retrogression must overcome a greater average shearing resistance due to the changing initial stress conditions as the back scarp

becomes further removed from the initial slope. Eventually, the back scarp remains stable, no more debris can flow out, and the sliding mass stabilizes (Figure 2-5e).

Mitchell and Markell [75] estimated that the transition between drained and undrained conditions happens at a horizontal distance from the toe of the slope between $3H\sec\theta$ and $4H\sec\theta$ (H being the slope height and θ the slope angle) because the stresses within the slope drastically changes from K_0 condition at the mentioned horizontal distance. Therefore, the author suggested that, for a failure starting in drained condition, retrogression beyond a horizontal distance of $3H\sec\theta$ to $4H\sec\theta$ from the toe of the slope should be considered as an undrained or short-term failure. For the undrained analysis, a flow slide occurs if the stability number, $N_s = mH/s_{up}$ is larger than 6 (m being the soil's natural unit weight and s_{up} the undrained shear strength), and it terminates due to topographic/stratigraphic restrictions or when the energy dissipated in the flowing debris becomes equal to the energy released at the back scarp.

Other studies on flow slides in sensitive clays focus on the criteria for the occurrence of large retrogressive landslides. Lebuis and Rissman [76] stated that large retrogressive landslides occur if the liquidity index (I_L) is greater than 1.2 or the remolded shear strength (s_{ur}) is less than 1 kPa. Tavenas et al. [44] argued that the condition based on mechanical soil parameters is necessary for assessing retrogression potential but is inadequate. One must account for whether the energy dissipated by the initial slide is large enough to remold the clay so that it can flow out of the crater. They summarized all the conditions to assess retrogression potential in four points. Firstly, an initial slope failure must occur against long-term stability. Secondly, the back-scarp failure in undrained conditions will occur only if $N_s>4$. Thirdly, the deformed soil mass from the first slide will get remolded if the remolding index (I_R) >70% or liquid limit (w_L) <40%. Finally, the remolded debris will flow if $I_L>2$ or s_{ur} <1kPa. Lebuis et al. also stressed that the energy required for the clay to be wholly remolded should be dissipated from the first slide. They added another observation from case studies that earth flows with retrogression of 100m occurs when the sensitivity (S_t) is greater than 25 and remolded shear strength (s_{ur}) is less than 1 kPa. Later studies somewhat agree with the previous criteria for large retrogressive failure.

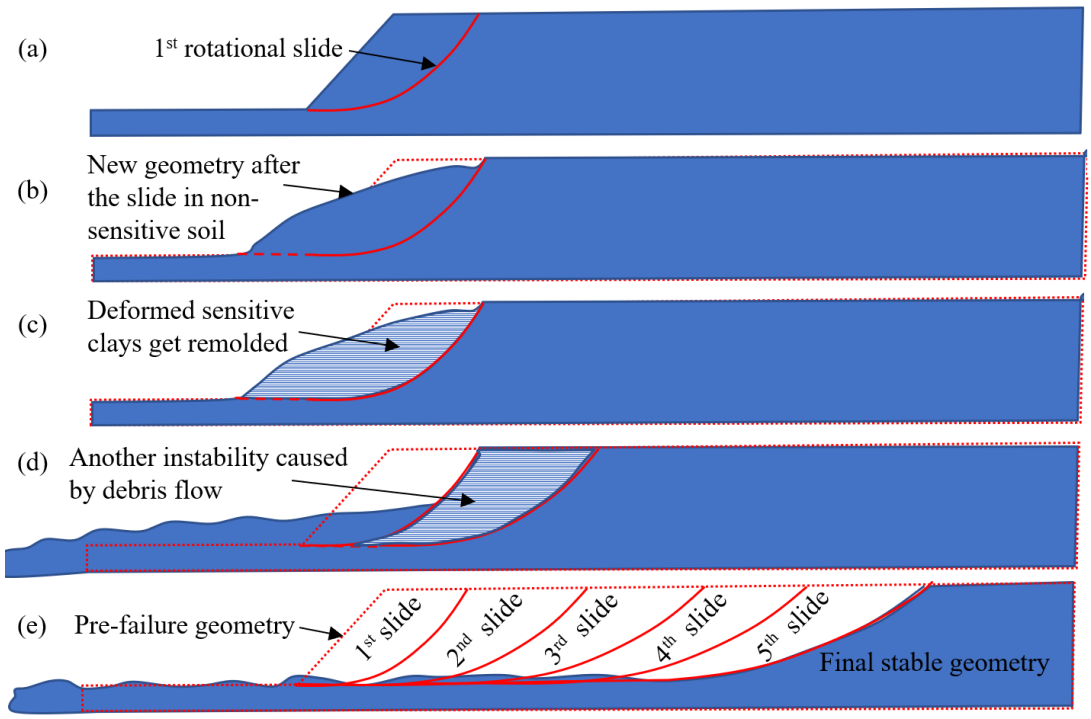

Figure 2-5 (a-e). Flow slide mechanism (after the description of [74])

For example, Lefebvre [27] stated that slopes with N_s>6 and s_{ur}<1.5 kPa have the risk of retrogressive failure after an initial slide; Thakur and Degago [77] stated that soils having s_{ur}>1 kPa are less likely to initiate large retrogressive failure. Demers et al. [43] showed by analyzing the previously occurred flow slides that most sites have very low remolded shear strength (<0.8kPa) and a very high liquidity index (1.5-16). To summarize, the aforementioned researchers acknowledged that large flow slides are most likely to occur when the following conditions are met: S_t>25, N_s>4, w_L <40%, I_L >1.2, and s_{ur} <1kPa.

2.4.2 Spread

Spreads are identified by their unique structure of alternative crests and level surfaces after failure, generally known as horst and grabens (Figure 2-6). The mechanism of spread was first described as a retrogressive failure by Odenstad [78] for the Skottorp landslide in the Lidan river. Odenstad [78] stated that the slide started with a part of the riverbank slipping into the river. The driving factor for the failure initiation was not distinctly identified, but erosion, leaching of salt, or blasting activity near the river could be responsible for the slow reduction of the stability of the slope over time. The formation process of horst and grabens is depicted in Figure 2-6. When a slope experiences instability, the strength of the weak soil layer drops due to

stress concentration within this layer and failure propagates horizontally through the layer opposite to the river producing a slide bottom "ba", simultaneously, a slip surface "bc" is formed at an angle of 45° parallel to the riverbank (Figure 2-6a). When stresses along "bc" reach near to zero it starts to slip forming a wedge "bb'c'c" (Figure 2-6b). When "bb'c'c" slips from position 1 to 2, it stops at a depth where it reaches the slide bottom forming a graben (Figure 2-6c). The drag of this slip causes a rupture "de" parallel to "bc". By this time, the slide bottom has already reached point "d" (Figure 2-6c). The horizontal drag and vertical slip cause a secondary failure surface along "cd" creating a wedge "cde" (Figure 2-6d). The wedge "cde" sinks from position 3 to 4, creating a graben which leaves a horst at "bcd" (Figure 2-6e). This is how the whole strip "SS'" forms in a retrogressive and discontinuous manner (Figure 2-6f) and finally slips into the river with an almost horizontal (slightly inclined towards the bottom) translatory movement.

Mollard and Hughes [79] argued that the landslides in the Grondines and Trois Rivieres Areas, Quebec, explained by Karrow [65] as multiple rotational retrogressive slides are instead a spreading failure. They reasoned that earthflow cannot explain the formation of parallel ridges. Their description agrees with Odenstad's [78] that the trigger for the initial instability could be any of the natural or anthropogenic reasons and that there exists a weak sensitive clay layer below the ground surface.

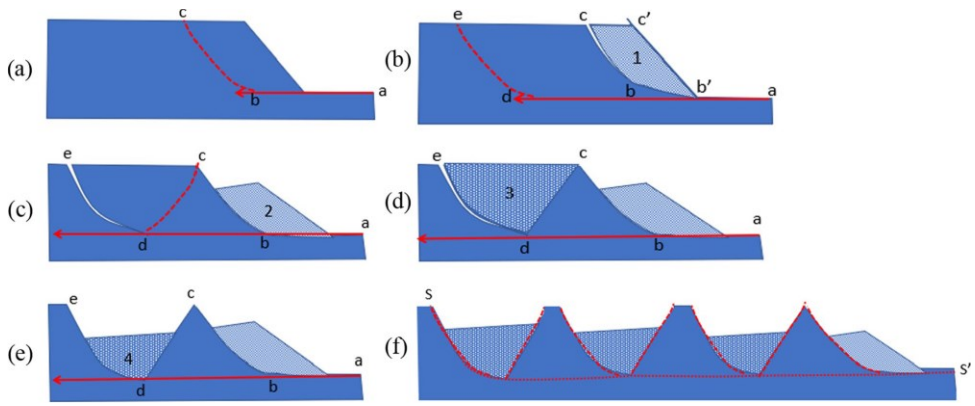

Figure 2-6. (a-f) Spread mechanism (after [78])

Unlike Odenstad's [78] horizontal propagation of the slide bottom, they stated that with appreciable stress concentration, the sensitive clay layer gets remolded and spreads laterally like a liquid (Figure 2-7a-f). The

remolded clay is squeezed up through the cracks towards the top layer, and the top layer is stretched and separated into segmented blocks (Figure 2-7b), which might have some rotational movements due to frictional drag. This produces ridge or rib-like patterns (Figure 2-7c). The failure stops with the increased frictional resistance of the squeezed-up liquid and increasing strength due to pore pressure dissipation in the soil (Figure 2-7d). Mollard and Hugh's [79] explanation lacks the detailing of the influence of the tension cracks to create the prism-like structures in a spread.

Carson [70] modified Odenstad's [78] spread mechanism and described the development of tension cracks in addition to horizontal subsidence (Figure 2-8). He analytically explained the mechanism of the squeezed-up remolded clay in tension cracks aiding the formation of horst and grabens, combining both descriptions above. He postulated that the width of the cracks filled up with remolded clay at the end of the landslide equals the total volume of remolded clay in the weak layer. He emphasized that spread could occur regardless of the sensitivity being high or low; the important factor is how rapidly the soil gets disturbed to generate a rapid flow.

Grondin and Demers [80] suggested that the formation of horst and grabens may not be discontinuous as the description by Odenstad [78] and Carson [70] because, in the landslide of St-Ligouri, the top surface of the grabens was connected by grass (Figure 2-10). They suggested the landslide occurred due to horizontal subsidence that caused the dislocation of the upper soil mass.

A well-described discussion on the mechanism of spread can also be found in Locat et al. [58]. They described this mechanism as progressive (upward progressive failure) rather than retrogressive [15, 73]. As per their hypothesis, a failure surface in the sensitive clay layer, almost horizontal to the ground, moving upward starting near the toe of the slope, is formed before any noticeable movement occurs. The failure initiates with a slow translational movement of the soil mass above the failure surface. Then, the sensitive clay along the failure surface becomes remolded and liquefies due to the accumulated deformation. The movement accelerates the translational slide. Finally, the rapid progression of the soil mass above the liquified clay results in horst and grabens (Figure 2-9).

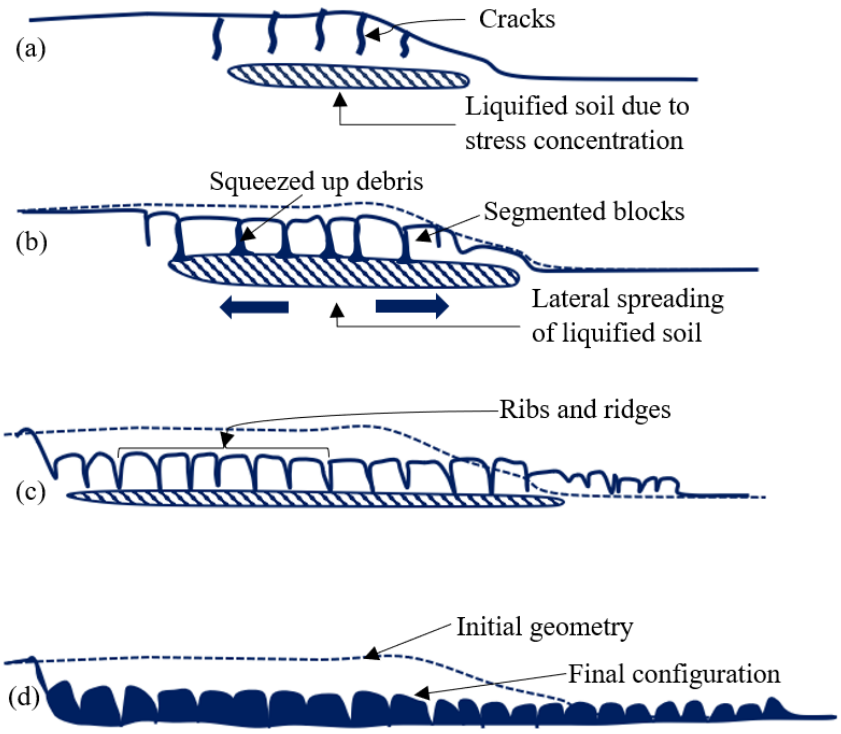

Figure 2-7 (a-d). Mechanism of spread (after [79])

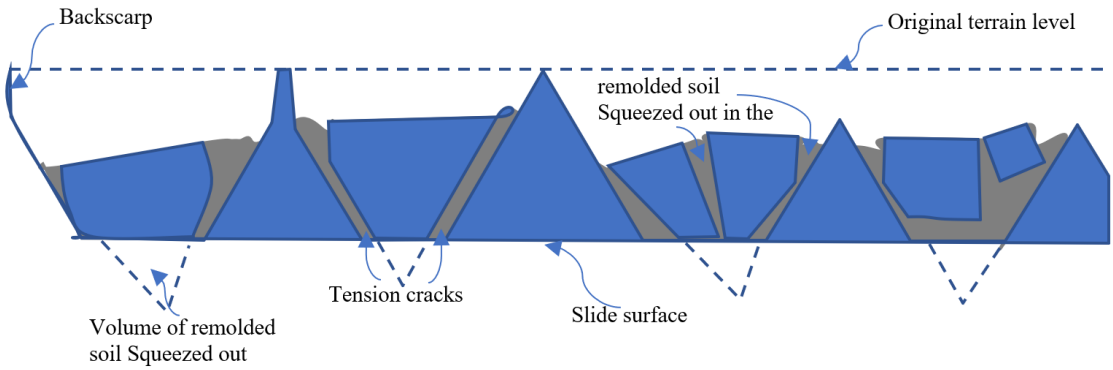

Figure 2-8. Spread mechanism (after [70])

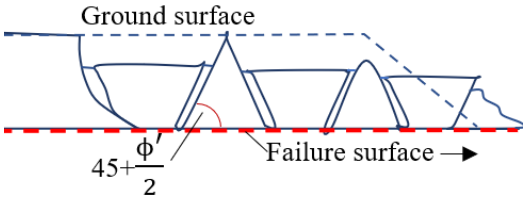

Figure 2-9. Spread mechanism (after [58])

Figure 2-10. Saint-Ligouri landslide (after [58])

2.5 NUMERICAL ANALYSIS OF SENSITIVE CLAY LANDSLIDES

Numerical modeling of sensitive clay landslides should address three particular challenges: strain-softening, remolding (solid-to-liquid transition), and large deformations. The following subsections present and discuss the prospect of the constitutive soil models and numerical frameworks considered in the literature to model sensitive clay landslides.

2.5.1 Constitutive soil models for the study of sensitive clays

The constitutive soil model, which represents the stress-strain behavior of the soil, is the most critical component for modeling sensitive clay slopes. The capability to reproduce realistic strain-softening characteristics in the material model is necessary for more accurate numerical analyses of large deformation problems in such materials. The constitutive models used in previous works for modeling sensitive clay landslides are summarized below. Their ability to deal with (a) strain-softening behavior, (b) strain-rate effects, and (c) rheological behavior of remolded soil is discussed. For completion, stress-strain curves numerically predicted by some of the models are compared with DSS data from sensitive clays. In particular, those

constitutive models that have been used in the literature to reproduce real case scenarios with available stress-strain DSS curves such data are considered for comparison [9, 17, 81]. Otherwise, the stress-strain curve of Saint-Barnabé-Nord [15] is considered for reference.

2.5.1.1 Von-Mises based models

The Von-Mises model is one of the simplest elastoplastic models to simulate the undrained behavior of clay. The model generally considers associated plastic flow and, at failure, it does not allow for volumetric strain. It requires only two parameters: the undrained elastic modulus (E) and the undrained shear strength (s_u). The Poisson's ratio is assumed constant (ν=0.5). Wang et al. (2016a, 2016b) used this model to simulate retrogressive failure features in sensitive clays together with a strain-softening law (Equation 2-1), where the undrained shear strength linearly reduces with deviatoric plastic shear strain ($\bar{\varepsilon}_p$) from the peak (s_{up}) to a residual value (s_{ur}) (

Figure 2-11a).

$$s_u(\bar{\varepsilon}_p) = \begin{cases} s_{up} + K\bar{\varepsilon}_p & ; \bar{\varepsilon}_p < \bar{\varepsilon}_{pr} \\ s_{ur} & ; \bar{\varepsilon}_p > \bar{\varepsilon}_{pr} \end{cases} \qquad 2\text{-}1$$

where $\bar{\varepsilon}_{pr}$ is the plastic deviatoric strain at the onset of the remolded strength, and K is the linear softening coefficient.

The capacity of this model to reproduce the stress-strain curve of Saint-Barnabé-Nord [15] is presented in Figure 12b. For the determination of the softening modulus, the value of the strain at remolded shear strength is required. Based on Thakur et al. [71], the strain at remolded shear strength is estimated to be 300% for Norwegian sensitive clays. Assuming the strain at remolded shear strength as 60-150% and considering $s_{up} = 79.5$ kPa and $s_{ur} = 1.6$kPa based on the experimental results from Locat et al. [71], the value K varies between -135 to -52 kPa. It is observed from

Figure 2-11(b) that the linear approximation either overpredicts or underpredicts the actual curve obtained from laboratory testing. Even though a linear approximation cannot capture the non-linearities of the softening behavior of sensitive clays, a reasonable approximation can be achieved when the areas between the

stress-strain curves produced by the constitutive model and the actual stress-strain curve compensate (e.g., the case with remolded strain taken as 100%).

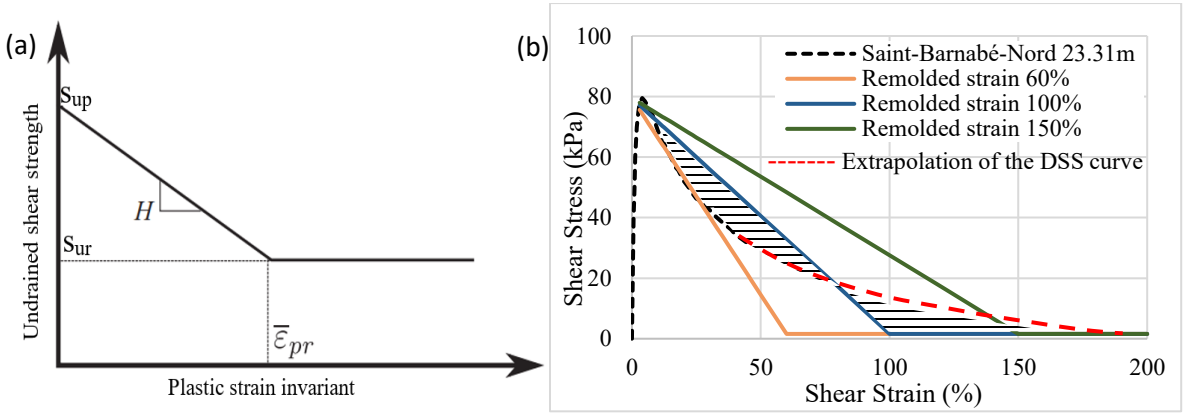

Figure 2-11. (a) Stress-strain behavior in a cohesion softening model [82, 83] (b) comparison between model [84, 85] and Saint-Barnabé-Nord clay.

A group of researchers [32, 86–88] used the same yield criterion with a non-linear strength degradation as a function of plastic shear displacement (Figure 2-12) as follows,

$$\frac{s_u}{s_{up}} = \begin{cases} \frac{s_{uR}}{s_{up}} + \left(1 - \frac{s_{uR}}{s_{up}}\right) e^{-\frac{3\delta'}{\delta_{95}}} & \text{if } 0 \le \delta' < 2\delta_{95} \\ \frac{s_{uR}}{s_{up}} - \frac{s_{uR} - s_{ur}}{s_{up}} \frac{\delta' - 2\delta_{95}}{\delta_r - 2\delta_{95}} & \text{if } 2\delta_{95} \le \delta' < \delta_r \\ \frac{s_{ur}}{s_{up}} & \text{if } \delta' \ge \delta_r \end{cases} \qquad 2\text{-}2$$

where s_u is the mobilized undrained shear strength; $\delta' = \delta_t - (\delta_e + \delta_{pc})$ with δ_e and δ_t being the elastic and total shear displacements, respectively; δ_{95} is the value of δ' at which the undrained shear strength is reduced by 95% of $(s_{up} - s_{uR})$. s_{uR} is the degraded strength at a displacement of $2\delta_{95}$ after the peak. δ_r is the value of δ' remolded shear strength (s_{ur}).

The non-linear part of Equation 2-2 (curve "bcd" in Figure 2-12) is a modified form of the strength degradation equation proposed by Einav and Randolph [23] as follows,

$$\frac{s_u}{s_{up}} = \frac{s_{ur}}{s_{up}} + \left(1 - \frac{s_{ur}}{s_{up}}\right) \times e^{-\frac{3\gamma}{\gamma_{95}}} \qquad 2\text{-}3$$

where displacements relate to the strain as $\delta = \gamma t$ (t =shear band thickness).

The linear-elastic pre-peak segment (line "oa" in Figure 2-12) is defined using undrained stiffness parameters. The peak undrained shear strength (s_{up}) is mobilized at point "a" and remains constant up to point "b" for a displacement of δ_{pc} from point "a". The rest of the curve corresponds to Equation 2-2.

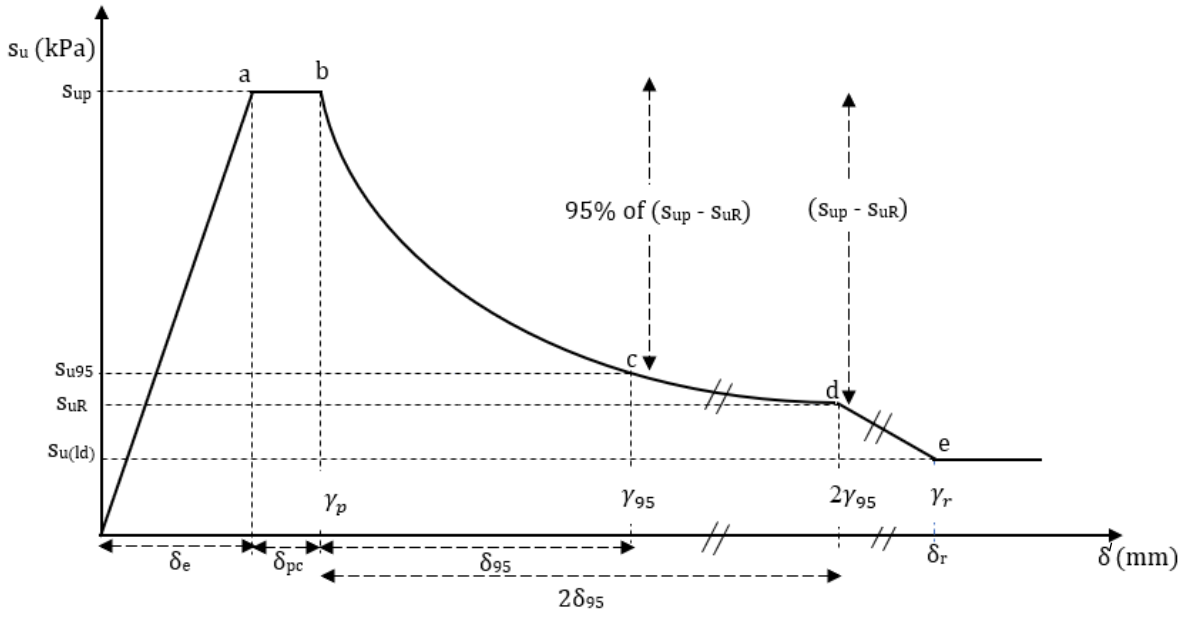

Figure 2-12. Stress-strain behavior of sensitive clay [32]

The comparison between the post-peak stress-strain relationship predicted by Equation 2-3 and the DSS stress-strain curve of Saint-Barnabé-Nord [15] is presented in Figure 2-13. The comparison has been made in terms of shear strain instead of displacement. After a calibration process, the most fitting curve is obtained with γ_{95}=130%. The predicted curve shows some discrepancies with the DSS data up to 20% strain, but it exactly matches from 20-46% strain.

It can be concluded that exponential strain softening is better suited than linear strain-softening laws to capture the strain-softening from sensitive clays, but much uncertainty prevails in the accurate estimation of the parameters like γ_r and γ_{95}. The wrong approximation of these parameters can significantly reduce the accuracy of the strain-softening equation for field conditions.

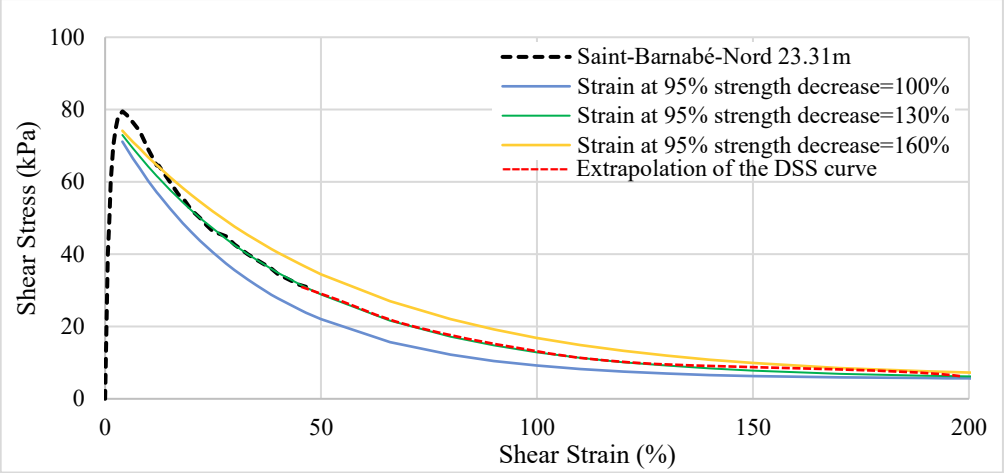

Figure 2-13. Comparison between the exponential strain-softening law with different γ_{95} to the stress-strain behavior from DSS test from Saint-Barnabé-Nord clay.

Wang et al. [33, 89] added strain-rate effects on the shear strength using Equation 2-4. They considered the undrained shear strength (s_u) as a function of a shear strain-softening factor (f_1) and a strain rate factor (f_2) as,

$$s_u = s_{uy}\,(f_1 f_2) \qquad 2\text{-}4$$

where s_{uy} is the undrained shear strength at a very low strain rate (i.e., quasi-static).

Generally, the dependency of undrained shear strength of clays on applied strain rate has customarily been characterized in terms of a semi-logarithmic relation [51, 90] (Equation 2-5) and a power law (Equation 2-6) [23] expressed as,

$$s_u = \left[1 + \mu \log\left(\frac{\dot{\gamma}}{\dot{\gamma}_{ref}}\right)\right] s_{u,ref} \qquad 2\text{-}5$$

$$s_u = \left(\frac{\dot{\gamma}}{\dot{\gamma}_{ref}}\right)^{b} s_{u,ref} \qquad 2\text{-}6$$

where $\dot{\gamma}$ is the shear strain rate, $\dot{\gamma}_{ref}$ is the strain rate at a reference shear strength $s_{u,ref}$, the coefficient μ and b give the proportional change in shear strength for each order of magnitude change in strain rate, which lies in the range of 0.05–0.2 and 0.05-0.1, respectively.

Again, the behavior of liquified remolded sensitive clays in debris flow can be described with a strain rate dependent fluid mechanics framework (Herschel–Bulkley model) relating the yield stress (τ) with strain rate ($\dot{\gamma}$) based on fluid viscosity (η) and a shear thinning index (n) as [91],

$$\begin{cases} \dot{\gamma} = 0 & \text{for } |\tau| \leq \tau_0 \\ \tau = \tau_0 + \eta|\dot{\gamma}|^n & \text{for } |\tau| > \tau_0 \end{cases} \quad 2\text{-}7$$

For the sensitive clays, the effect of strain rate on the undrained shear strength would be present in the solid phase as well as in the liquid phase when it flows like debris. To capture the strain rate effect on strength in both the phases Zhu and Randolph [92] proposed a unified equation that originates from the power-law (Equation 2-6) but also incorporates the viscosity and shear thinning index like Herschel–Bulkley model. This unified equation is termed an "additive power law" model and expressed as,

$$s_u = \left[1 + \eta\left(\frac{\dot{\gamma}}{\dot{\gamma}_{ref}}\right)^n\right] s_{u,ref} \quad 2\text{-}8$$

Wang et al. [33, 89] used equation 2-8 in his constitutive model to incorporate strain rate, and the second function in equation 2-4 is defined as,

$$f_2 = \left[1 + \eta\left(\frac{\dot{\gamma}}{\dot{\gamma}_{ref}}\right)^n\right] \quad 2\text{-}9$$

By incorporating strain rates, constitutive models can effectively evaluate the impact of a time-dependent strain or creep behavior on both the onset and advancement of failure.

2.5.1.2 Tresca-based models

Tresca is also an elastoplastic model, very similar to the Von Mises model. Its simplicity inspired some researchers to model sensitive clays by adding strain-softening laws [9, 57, 93, 94]. Locat et al. [16] modeled the spread mechanism in sensitive clays, assuming a hyperbolic elasticity model up to the peak stress and linear plasticity in post-peak strain softening (Figure 2-14a). The strain-softening is linear and defined with a softening modulus K as follows,

$$K = \frac{s_{up} - s_{ur}}{\delta_r - \delta_p} \qquad 2\text{-}10$$

where δ_p and δ_r are the shear displacement at peak and remolded strength, respectively.

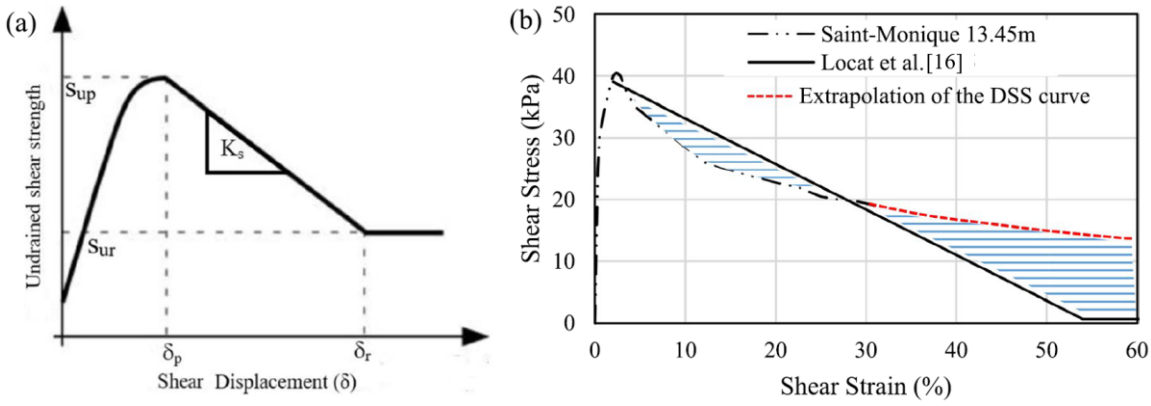

Figure 2-14. (a) Shear stress-displacement relationship [16], (b) Comparison of assumed strain-softening with the laboratory test result.

This model has also been applied to study the post-peak behavior of the Sainte-Monique landslide in Quebec [17], assuming $\gamma_p = 2\%$ and $\gamma_r = 55\%$. The comparison between the linear approximation and the measured stress-strain curve is presented in Figure 2-14b. It is evident that linear approximations significantly deviate from the actual stress-strain curves.

Zhang et al. [57] investigated the initiation and propagation of a fully softened shear zone in submarine sensitive clay landslides with both linear (Equation 2-11) and non-linear (Equation 2-12) strain-softening laws. The latest (Equation 2-12) is based on Einav and Randolph [23] (Figure 2-15).

They compared the critical length of the softened zone predicted by the numerical model with the analytical evaluation and concluded that linear degradation overestimates the length of the shear band by 10-15% more than non-linear degradation. The softening equations are as follows,

$$s_u = s_{up} - (s_{up} - s_{ur})\frac{\gamma}{\gamma_r} \qquad 2\text{-}11$$

$$s_u = s_{ur} + (s_{up} - s_{ur})e^{-\frac{\gamma}{\gamma_{95}}} \qquad 2\text{-}12$$

where s_u is the degraded undrained shear strength at displacement increment γ after reaching the peak, and γ_{95} is the plastic strain increment required to reduce the strength by 95% of $(s_{up} - s_{ur})$ from the peak strength (s_{up}),

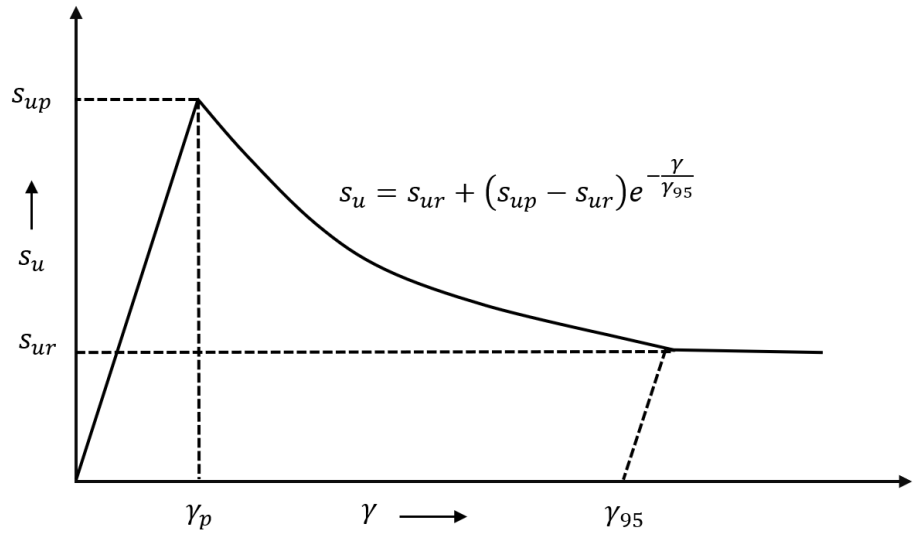

Figure 2-15. Stress-strain behavior with exponential strain-softening [57]

Shan et al. [95] added strain-rate effects and depth-wise variation on shear strength to Equation 2-11 as

$$s_u = \max\left(s_{up} - (s_{up} - s_{ur})\frac{\gamma}{\gamma_r}, s_{ur}\right)\left(1 + \overline{K}\left|\frac{\dot{\gamma}}{\dot{\gamma}_{ref}}\right|^n\right) \qquad 2\text{-}13$$

where n is the power index (usually varies from 0.4 to 0.6 for Canadian sensitive clay), and $\overline{K}$ is the viscosity coefficient ($\overline{K} \approx 0.028 s_{up}^{0.28}$). The depth-wise variation of peak strength was defined as follows:

$$s_{up} = \begin{cases} s_{up1} & 2m \le h < 5m \\ s_{up1} + a(h-5) & h \ge 5m \end{cases} \qquad 2\text{-}14$$

where h is the soil depth, s_{up1} is the undrained shear strength in the first clay layer (h =2m-5m), and "a" is the strength gradient along the depth h in the second clay layer (h >5m).

Tran and Sołowski [96] proposed a modified version of the elastoplastic Tresca model with a non-associated flow rule for modeling the progressive failure behavior of sensitive clays and used it to simulate the Sainte-Monique landslide. They added features to the model for replicating the field soil behavior, including strain-rate effects, the effect of water content, and soil depth on the shear strength. The non-linear strain-softening law describes the strength degradation as follows,

$$s_u = s_{u,ref}\left(\frac{\dot{\gamma}}{\dot{\gamma}_{ref}}\right)^{\beta}\left[\frac{1}{S_t} + (1-\frac{1}{S_t})e^{-3\gamma/\gamma_{95}}\right] \text{ when } \gamma > \gamma_e \qquad 2\text{-}15$$

where γ_e is the accumulated elastic strain. The reference undrained shear strength depends on the water content (w) and depth (h) as:

$$s_{u,ref}(w,h) = \left(a_1 w^{-b_1}\right)\left[s_{uh,ref} + \Delta s_u(h - h_{ref})\right] \qquad 2\text{-}16$$

where, a_1 is the undrained shear strength at w = 100% at a reference strain rate (γ_{ref}), w (%) is the water content and b_1 is the model parameter, $s_{uh,ref}$ is the reference undrained shear strength at the reference depth h_{ref}, and Δs_u is the increase of strength per unit depth after the reference depth. The stress-strain prediction of this model is compared with laboratory DSS test result (Sainte-Monique landslide), which shows that this model is better suited compared to previous linear models discussed above in terms of capturing the non-linear stress-strain behavior of sensitive clays (Figure 2-16).

Jin et al. [97] simulated retrogressive failure in sensitive clays with a cohesion softening model which is comparable to the Tresca softening model where the peak and residual cohesion (c_p and c_r) are equivalent to the peak and remolded undrained shear strengths (s_{up} and s_{ur}) of sensitive clays. The softening is defined as,

$$s_u = s_{ur} + (s_{up} - s_{ur})e^{-\eta\bar{\varepsilon}_p} \qquad 2\text{-}17$$

where η is the shape factor that controls the rate of strength decrease. They evaluated mesh dependency and the effect of the shape factor η on post-failure behavior of the landslides. It can be seen in Figure 2-17 that,

the softening curve is significantly dependent on the value of the shape factor (η). For the case of Sainte-Monique landslide, $\eta = 2$ is more representative of the field behavior.

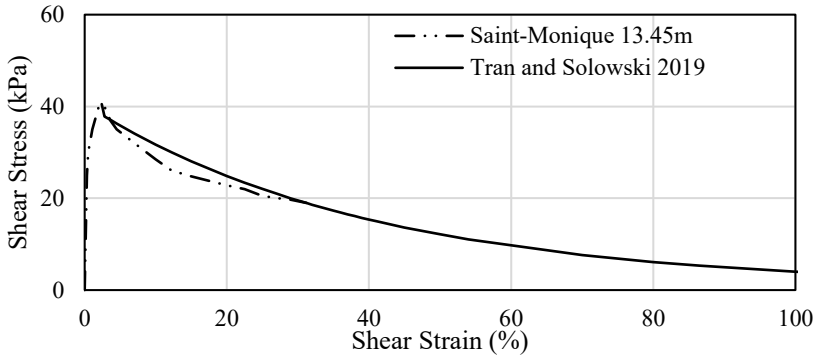

Figure 2-16. Comparison of stress-strain behavior of DSS test result with the numerical model of Tran and Solwoski [96].

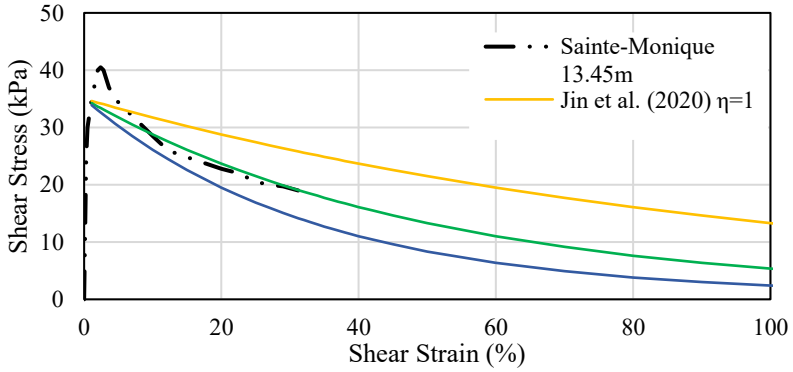

Figure 2-17. Comparison between DSS test results vs. stress-strain behavior of Jin et al. [97] with different η values

2.5.1.3 Bingham-Tresca based models

The constitutive models described above are common in the study of soil mechanics, and most of them do not directly consider the rheological properties of the clay, which may affect the prediction of runout distances in retrogressive flow slides. In the field of fluid mechanics, the Bingham plastic model is a common constitutive law that considers non-Newtonian rheology to predict the flow behavior using its yield stress (τ_y) and plastic viscosity (η). As shown in Figure 2-18, the fluid starts to flow after reaching its yield stress, and the yield stress increases linearly with the shear rate. Several rheological models have been used for simulating the

debris flow of sensitive clays, including the Herschel–Bulkley model [98–100]. The Bingham model is a limiting case of Herchel-Bulkley rheology. It should be noted that these models only consider the liquid flow of the sensitive clays and do not capture the transition from solid to a liquid phase.

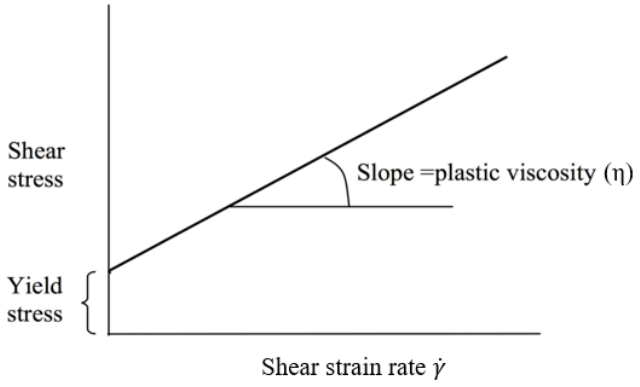

Figure 2-18. Bingham plastic model

With the idea of capturing the transition from solid to liquid behavior of sensitive clay, Zhang et al.[101] came up with an elastoviscoplastic model that combines an elastoplastic model with a viscous model using the concept of strain-based transition initially proposed by Prime et al. [102]. In particular, they combined the Bingham model and the Tresca model with linear strain softening [11, 81, 101]. Total strain rate ($\dot{\gamma}$) for the elastoviscoplastic material is defined as the summation of an elastic strain rate ($\dot{\gamma}^{e}$) and a visco-plastic strain rate ($\dot{\gamma}^{vp}$).

$$\dot{\gamma} = \dot{\gamma}^{e} + \dot{\gamma}^{vp} \qquad 2\text{-}18$$

The strain is purely elastic when the stress state is below the Tresca yield surface, whereas viscoplastic strain starts to develop when the stress state crosses the yield surface. Strain softening is incorporated by reducing the undrained shear strength s_u using a bilinear function (similar to

Figure 2-11a) of the equivalent deviatoric plastic strain. In this case, the softening modulus K is a function of the viscoplastic strain (γ^{vp}).

The classical Bingham model is utilized to describe the rheological behavior of sensitive clays, and the total stress is defined as,

$$\sigma = \tau + \eta\dot{\gamma}^{vp} \qquad 2\text{-}19$$

where τ is the stress lying on the boundary of the Tresca yield surface, η is the viscosity coefficient and $\dot{\varepsilon}^{vp}$ is the viscoplastic strain. When the viscosity is zero, the model reduces to the classic Tresca model. This model is comparable to the strain-rate-based models, where the strain-rate dependency of liquified debris is derived from the Herschel–Bulkley model (Equation 7-9). Zhang et al. [81] used this constitutive soil model to simulate the Saint-Jude landslide (2010) and showed that ignoring rheological properties overestimates the runout distance. However, the linear strain-softening is not representative of the actual stress-strain behavior (Figure 2-19).

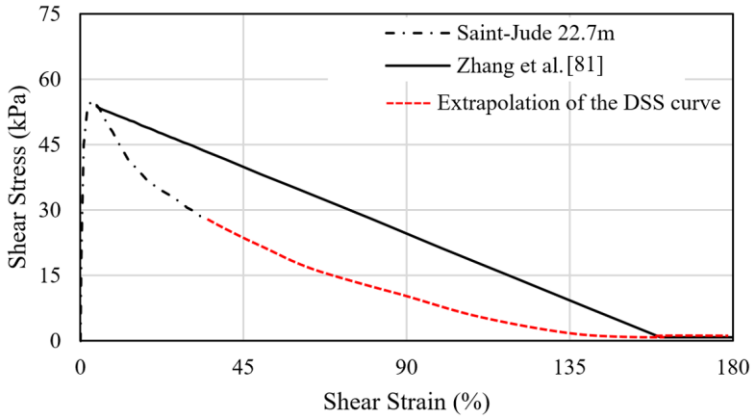

Figure 2-19. Comparison between DSS test results vs. stress-strain behavior of Zhang et al. [81].

2.5.2 Numerical frameworks for modeling landslides in sensitive clays

Numerical analysis has two prominent approaches, i.e. continuum mechanics and discrete mechanics. In continuum analysis, each particle within a material is not treated explicitly, and the material is modeled as a continuous entity; the change in the properties of the geomaterial under loading conditions is represented by a constitutive model. On the other hand, discontinuum methods model the geomaterial as a collection of distinct particles which may or may not represent a real particle arrangement, and the particles interact through their contacts with other particles and boundaries. Numerical analysis for large deformation problems in geomechanics has been a prominent issue in recent times. Both continuum and discontinuum numerical

frameworks for modeling geomaterials, particularly for large deformation problems, have been summarized by Augarde et al. [103]. Before that, Soga et al. [104] and Wang et al. [105] compared the advantages and disadvantages of existing numerical frameworks used in slope stability analysis and other geotechnical problems, respectively. In the following section, large deformation numerical frameworks that have particularly been used in the analysis of landslides with strain-softening materials or sensitive clays will be discussed, which are mainly different formulations in continuum approaches.

2.5.2.1 Updated Lagrangian Finite Element Method

The most popular approach used in geotechnics is the standard finite element method (FEM) with classic Lagrangian formulation (known as the total Lagrangian, TL). The TL is a continuum method that uses the undeformed initial geometry as its frame of reference for computing the static and kinematic variables as well as formulating the discrete equations. In the cases where deformations are substantial with respect to the initial geometry, this formulation suffers from mesh distortion and produces inaccurate results. The updated Lagrangian (UL) formulation is an upgraded version of the classic lagrangian formulation to solve the mesh distortion problem for its implementation in large deformation problems [106]. In UL formulation, the variables are computed, and equations are formulated for the deformed state in the previous calculation step. Therefore, the positions of the nodes are updated based on the displacement calculated in the last increment. The UL framework is available in some commercial FEM software, making it flexible to work with. The limitation of this method is that when very large deformation is encountered, elements become too distorted. This distortion reduces the accuracy of the results and creates computational instabilities that make the calculation impossible [103]. Mohammadi and Taiebat [21] have used the UL FEM formulation to simulate progressive failure in strain-softening soil slopes. In their model, mesh distortion was encountered for higher sensitivity ($RF=1/S_t$), as shown in Figure 2-20.

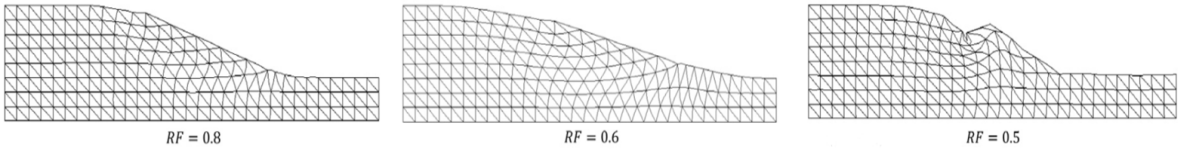

Figure 2-20. The deformed FEM mesh for different RF values with UL (after [21])

2.5.2.2 Arbitrary Lagrangian-Eulerian (ALE) Methods

ALE is the upgraded version of UL, which offers a solution to the mesh distortion by substituting the distorted mesh with a new mesh (re-meshing). This requires the transfer of state variables (re-mapping), which might reduce the accuracy of the solution when these are history-dependent. This method is referred to as arbitrary Lagrangian-Eulerian because the process of material state transformation from the old mesh to the new one is similar to that of the Eulerian description. Several re-meshing and re-mapping methods have produced several branches of the ALE formulation. The Re-meshing and Interpolation Technique combined with Small Strain (RITSS) approach is a widely popular re-meshing technique. The RITSS approach addresses large strain problems by dividing them into smaller Lagrangian strain increments [107]. At the end of each increment, the deformed body is re-meshed with new undistorted elements. To ensure an accurate transfer of information, solution variables such as stresses, deformations, velocities, nodal pore pressures, etc., are then interpolated from the old mesh to the new mesh [108]. The RITSS process can be broken down into four main steps, which include the generation of an initial mesh, conducting an incremental step of the Lagrangian analysis, updating boundaries and re-meshing, and mapping stresses and material properties from the old to the new mesh. These steps are repeated until the entire large deformation analysis is completed using a standard Lagrangian finite element package [109]. This process, thus, overcomes mesh distortion and allows for the modeling of various geotechnical problems, including those with fully drained, undrained, or intermediate drainage conditions. It's important to note that the accuracy and success of this process depend on the choice of interpolation scheme and mesh density. The RITSS approach can be flexibly used in any FEM code but is computationally very expensive. Zhang et al. [57] used the RITSS approach to simulate the initiation and propagation of a shear band in a fully softened weak zone. Zhang et al. [110] simulated a landslide in submarine sensitive clays with the same framework. Shan et al. [95] simulated the Sainte-Monique landslide in Quebec in 1994 with RITSS and successfully simulated the features of the retrogressive failure. The final runout and the post-failure profile were found to be close to the field conditions.

One of the most popular versions of ALE is the Coupled Eulerian-Lagrangian (CEL) method, also known as multi-material ALE. This method utilizes the advantages of both the Lagrangian and Eulerian approaches [111]. This method has two different domains for material description. One is the classic Eulerian, and the other

is the updated Lagrangian. Stiffer materials are described with the Lagrangian domain. When stresses are applied on these stiffer materials, it causes the softer materials in the vicinity to experience large deformation. The Eulerian description allows these softer materials to deform freely. The two domains interact with each other through some contact algorithms. The CEL approach is also available in commercial software like ABACUS. Dey et al. [32, 86, 87, 112] used this framework to model progressive failures leading to spreads in submarine sensitive clay slopes. Islam et al. (2019) used this framework to model retrogressive failure initiated by earthquake loads. Wang et al. [33, 89] modeled retrogressive failures resulting from erosion with some practical applications using this method. The authors adapted the techniques to reduce the mesh dependency of the models.

2.5.2.3 Particle Finite Element Method (PFEM) and Smoothed Particle Finite Element Method (SPFEM)

The Particle Finite Element Method (PFEM) is also an approach mainly developed to overcome the mesh distortion suffered by FEM. In this method, the mesh nodes are regarded as particles that can freely move even beyond the initial computational domain. The particles carry all information. The boundary of the domain is marked by connecting the outermost particles, and each internal particle is connected through the Delaunay triangulation technique. After the mesh is established, the governing equations are solved as it is in a conventional FEM simulation. The updated positions of the mesh nodes are used to form a new cloud of particles, and the process repeats (Figure 2-21).

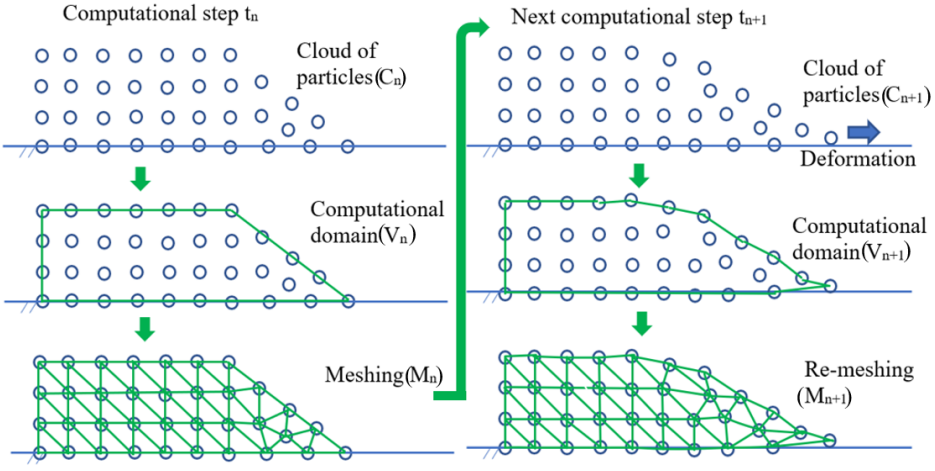

Figure 2-21. Steps for the PFEM modeling of a landslide.

The main advantage of this method is that it shows convergence behavior regardless of a large change in the state variables from the previous calculation step to the current step, which is very useful for modeling history-dependent materials like sensitive clay landslides Zhang et al. [101, 113]. Zhang et al. [81] utilized this framework to simulate the Saint-Jude landslide in Quebec, Canada. It has been able to reproduce the failure mode and the progressive failure process of the Saint-Jude landslide and correctly estimated its final runout distance, retrogression distance, and failure surface. The infinitesimal strain assumption in this method is likely to result in several errors, including excess strain for rigid body motion. Zhang et al. [101] reported that the error is limited to 1% for a converged solution. Contact between solid-solid and solid-liquid is complex in this method. Frequent re-meshing in large deformation problems requires extreme precision in transferring history-dependent information from the old mesh to the new one to maintain the accuracy of the calculation [103].

The Smoothed Particle Finite Element Method (SPFEM) is an improved form of PFEM where the equilibrium of the governing equations is established at the nodes instead of the Gaussian points with the help of strain-smoothing cells covering each node. This reduces the error in re-mapping the history-dependent variables. This method is more accurate and computationally flexible than PFEM [114]. With this framework, Yuan et al. [93] simulated retrogressive failure in sensitive clays. This simulation used the simplest form of the strain-softening Tresca model. Therefore, the applicability of this framework with a more sophisticated constitutive model with rate effects and non-linear softening is yet to be studied.

2.5.2.4 Material point method (MPM)

MPM is a combination of particle-based and mesh-based methods. The computational domain is discretized with a number of particles (i.e. material points) and a fixed background mesh. The material points are described in the Lagrangian formulation. Each material point represents a part of the computational domain and moves through the fixed background mesh. All the physical properties of the continuum are carried by the material points. The background mesh is described in Eulerian formulation. The state variables are transferred from the material points to the mesh nodes in each computational step (Figure 2-22), and the balance equations are solved at the nodes of the Eulerian mesh. Updated properties are mapped back to the material points, and the calculation proceeds to the next step. The background mesh must contain the problem domain geometry, and the material deformation is carried by the material points. Thus, the mesh remains undistorted throughout

the calculation, and mesh distortion is completely avoided. Some numerical difficulties of MPM are cell crossing instability, generation of nonphysical stiffness, and the mapping from material points to nodes and back.

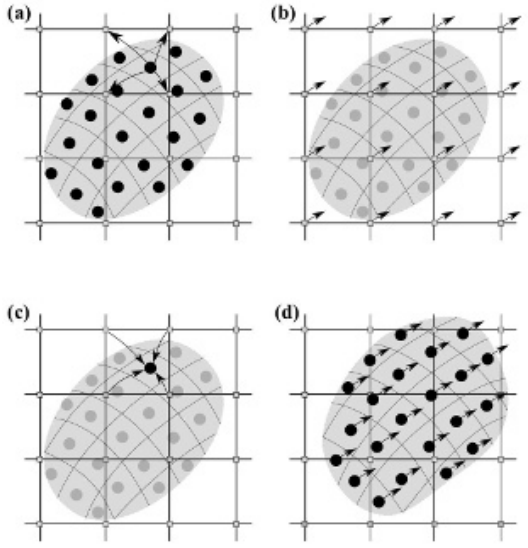

Figure 2-22(a-d). MPM Computational cycle [115]

The full process of retrogressive failure of sensitive clay triggered by erosion has been simulated using MPM framework by Wang et al. [84] and Tran and Solwoski [96]. The simulations well captured the features of a retrogressive landslide.

2.6 CONTRIBUTION OF NUMERICAL ANALYSIS TO UNDERSTAND THE CONTROL PARAMETERS OF SENSITIVE CLAY LANDSLIDES

Various combinations of the constitutive models and numerical frameworks described in the previous section have been implemented to model different landslides in sensitive clays. Some of these works explore the failure mechanisms in detail and provide new insights. Numerical simulations also help understand which geometrical and material parameters control the occurrence and post-failure behavior of sensitive clay landslides. The following section focuses on how the numerical results aided in understanding the critical factors for sensitive clay landslides.

2.6.1 Effect of the geometry of the slope on the occurrence and post-failure behavior

Several numerical studies have evaluated how the geometrical variations of the soil layer or the slope change the failure pattern, retrogression, and runout distances. In particular, the effect of the thickness of the sensitive clay layer, height and width of the slope, slope angle, and inclination of the soil layer are some aspects that have been assessed.

Dey et al. [116] showed that a minimum thickness of the sensitive clay layer is required to initiate retrogressive/progressive failure, while Zhang et al. [81] concluded that an increase in the thickness of the sensitive clay layer (H_{St}), keeping the crust thickness constant, increases retrogression distance. Additionally, an increase in H_{St} changes the failure pattern from spread to flow slide [32, 88]. Studies show that for a fixed slope height, an increase in slope width increases the retrogression and runout up to an optimum value. After this point, further width increase results in no significant change in post-failure behavior; that is, slope width has an optimum value for the occurrence of large retrogressive failure [93]. The frictional coefficient of the base layer also controls the retrogression. It is observed that the larger the basal friction, the less susceptible to retrogressive failure [84, 93]. The slope angle controls the failure mechanism and post-failure behavior to a great extent. For a varying slope angle (θ) of a horizontal soil layer (Figure 2-23a), steeper slopes are more susceptible to larger retrogressive failure [16, 86–88]. Jin et al. [97] showed that a higher θ value reduces the time to reach failure for sensitive clay slopes. For a varying inclination of the clay layer θ' with the horizontal (Figure 2-23b), a higher θ' changes the slide movement from rotational to translational and produces a higher number of secondary slip planes with smaller failure blocks [83]. Islam et al. [88] further demonstrated with a varying upslope inclination (θ") (Figure 2-23c) that flow slide occurs for low and high values of θ". In contrast, the failure pattern for intermediate θ" is spread. Overall, these numerical results align with the literature that the susceptibility and extent of progressive failure are high on steep slopes [117].

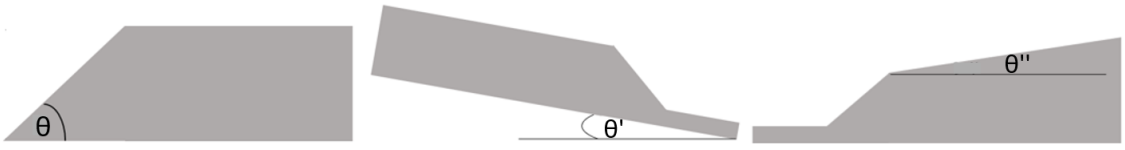

Figure 2-23. Different types of slope inclination

2.6.2 Effect of material properties on the occurrence and post-failure behavior

The effect of different material parameters on the initiation and the extent (retrogression and runout distance) of the sensitive clay landslides has been assessed in light of different numerical simulations. Dey et al. [32] showed that progressive failure would not occur for very low sensitivity (S_t< 3), spread occurs with medium sensitivity (S_t~5-7), and the failure pattern changes to a flow slide with higher sensitivity (S_t≥10). Moreover, they found that decrease in the shear strength of the crust changes the failure pattern from spread to flow slides. In contrast, Islam et al. [88] illustrated that the failure pattern changes from a flow slide to a combined spread and flow slide type with increased sensitivity. Even though both Dey et al. [32] and Islam et al. [88] used the same softening constitutive model and numerical framework, the differences in their conclusions might be due to the different triggering factors considered in their analysis, i.e., toe erosion [32] and earthquake Islam et al. [88]. In any case, both works coincide in that higher sensitivity caused higher retrogression and runout distances. Zhang et al. [11] illustrated that in addition to the increased retrogression and runout, it takes a longer time for the sliding front to stop entirely with increased sensitivity.Yuan et al. [93] added that the failed soil mass would reach a longer runout distance with higher sensitivity, owing to a smaller dissipation of potential energy for remolding, leading to higher kinetic energy.

Tran and Solwoski [9] showed that large retrogressive landslides are also dependent on low remolded strength (s_{ur}< 2kPa) with high sensitivity (S_t>25). Several researchers demonstrated that the retrogression distance is significantly controlled by the remolded shear strength. Increased remolded strength s_{ur} (keeping all other material and geometrical parameters fixed) reduces the retrogression distance, and a further increase in s_{ur} completely stops the retrogression [9, 16, 83, 88]. Likewise, when the remolded strength approaches zero, there is a sharp increase in retrogression and runout [11]. It can also be said that highly brittle soils are more susceptible to progressive failure. Brittleness of soil is generally quantified by the brittleness index (I_B) defined as Bishop [118]

$$I_B = \frac{s_{up} - s_{ur}}{s_{up}} \qquad 2\text{-}20$$

If retrogressive failure initiates, increased brittleness of the soil changes the failure type from spread to flow slide [33]. Displacement at remolded shear strength (δ_r) also controls the post-failure behavior [32, 88]. Dey et al. [119] reported that an increase of δ_r changes the failure pattern from spread to flow slide. Increased δ_r results in an increase in remolding energy (area under the stress-strain curve up to remolded shear strength and strain) as well as a decrease in softening modulus. Simulation results show that increased remolding energy decreases the retrogression [88] and increased softening modulus increases the retrogression [16, 83]; that is, a higher δ_r will result in lower retrogression [86].

Wang et al. [33] assessed the effect of stability number (N_s) on the occurrence of retrogressive failure and suggested that retrogressive failure doesn't occur for N_s =3.8 but occurs for N_s =4.9 and 6.8. They concluded that sites characterized by a low stability number are less prone to large retrogression than sites with a high stability number. Earth pressure at rest (K_{oi}) also affects the extent of retrogression. Slopes with higher K_{oi} are susceptible to large progressive spreads rather than flow slides [16, 33].

The viscosity of remolded clay also affects the post-failure behavior. An increase in viscosity leads to a decrease in both the runout distance and the retrogression distance of a retrogressive failure because highly viscous fluid would consume more energy to flow [93, 101, 113]. Zhang et al. [113] reported that the effect of viscosity is more significant for the soils with higher sensitivity and low remolded strength. Their simulation demonstrated that the unaccounted viscosity overestimates the runout distance by 35% and the retrogression distance by 20%. Mobility of the liquified debris also affects the failure mechanism. If the liquified debris moves out of the crater easily once the retrogression has started, a flow slide is more likely to occur; on the contrary, if the liquified debris has slower movement, the failure may result in spread [33].

Tran and Solwaski [96] demonstrated that overlooking the impact of strain rate on shear strength may overestimate the retrogression distance. Wang et al. [10] provided further clarity on this topic, explaining the effect of strain rate during failure with respect to the reference strain rate in the constitutive model. They concluded if the strain rate at the time of failure exceeds the reference strain rate, it may overestimate the post-failure movement. Conversely, if the strain rate is lower than the reference strain rate, it may underestimate of the final retrogression and runout distance.

Wang et al. [82] illustrated the effect of spatial variability of undrained peak and remolded shear strength on the retrogression distance and showed that spatial variability alters the distance of retrogression. He concluded that heterogeneity significantly affects the initiation and failure mechanism, and a deterministic analysis may result in erroneous outcomes.

2.6.3 Effect of field conditions on the occurrence and post-failure behavior

The impact of field conditions on landslides is not straightforward and is often very complex. Landslides will respond to the combined effect of several hydrological and hydrogeological parameters [120]. Therefore, establishing a direct correlation between specific parameters and landslide occurrence is challenging and difficult to incorporate into the numerical analysis. Hence, studies on this issue are scarce and highlight the need for more research. Wang et al. [121] simulated the steady-state seepage condition with his strain rate-dependent strain softening constitutive soil model (Equation 2-4). Pore water pressure and seepage forces are calculated using a thermal-hydraulic analogy to model the in-situ stress condition for retrogressive failure in sensitive clay slopes. They concluded that seepage significantly influences landslide triggers. An elevated artesian pore pressure close to the slope's toe may initiate substantial failure. A rise in the earth pressure coefficient, coupled with an increase in shear strength, can alter the failure pattern from flow slide to spread and thus affect the retrogression distance.

2.7 FINAL DISCUSSION

In this study, the distinct characteristics of sensitive clay landslides and the advancement for modeling those landslides have been discussed in detail, focusing on the landslide types, constitutive models, numerical frameworks, and critical factors controlling landslides mechanism. It is observed that, the unique mechanism of sensitive clay landslides, i.e, its progressive or retrogressive nature is completely attributed to the strain softening nature of the soil. Whether the failure advances as successive rotational flowslide or a translational movement resulting in spread or a combination of both, it is always a result of the movement of the liquified clay. Therefore, the most essential component for the modeling of sensitive clay slopes is the constitutive soil model, which reproduces realistic strain-softening characteristics for accurately capturing the complex landslide mechanism in sensitive clays. Though several numerical frameworks are well-suited to capture the large

deformation associated with retrogressive failure, the constitutive models need much improvement to represent the accurate post-failure behavior of sensitive clays. The different numerical models concerning sensitive clay landslides have been compiled in Table 2-1. The table presents a list of literatures on the numerical modeling of sensitive clay landslides with the constitutive model and numerical framework used, the type of landslide that has been modeled, and the outcomes of each study to give a general idea about the recent advancement and challenges in simulating landslides in sensitive clays.

Based on the review of the existing works on the numerical modeling of sensitive clay landslides, some areas that require further study are noted below.

- The most advanced constitutive model discussed in section 2.5.1 is by Wang et al. [33] which considered the strain rate effects, including the rheological property of soil, non-linear strength degradation, and variation of effective stress with depth. The accuracy of this model vastly depends on the large-deformation parameter, displacement at 95% strength degradation δ_{95}. A physical method to determine this parameter on the field or laboratory scale is required.
- Constitutive models used in the literature to account for sensitive clay behavior are formulated in a total stress framework which is more relevant to accounting for undrained shear strength behavior. The development of advanced effective-stress-based constitutive models is essential to evaluate in a unified coupled hydro-mechanical numerical framework long-term triggering factors with short-term rapid post-failure runouts without the need to predefine the change in calculation mode from drained to undrained analysis.
- Most of the research has been focused on landslides initiated by toe erosion, whereas research simulation related to seismic loading and other triggering factors is scanty. The influence of different field and weather conditions on failure initiation and post-failure behavior is still largely unknown and warrants further studies.
- All the numerical studies of sensitive clay landslides have been done in plane-strain conditions. Still, in reality, spatial variability in soil parameters could affect the failure mechanism to a great extent. Further investigation of 3D effects is required.

- There is scope for implementing advanced constitutive models and geometries in large deformation numerical frameworks. These tools need to be further exploited in sensitive clay landslides. For instance, constitutive models with thermo-hydro-mechanical formulations can assess the thermal effects on the creep behavior of sensitive clays [122] and the mobility of retrogressive rock failures [123]. It is essential to evaluate whether these models also apply to sensitive clay landslides.
- A limited amount of work has been performed to evaluate the effect of geometrical and material parameters for the prediction of different types of retrogressive/progressive failures in sensitive clays. Further understanding of the critical parameters is essential for landslide prediction and risk assessment of such events.

2.8 CONCLUSION

This study presents an elaborate review of failure mechanisms, constitutive soil models, and numerical frameworks for the simulation of sensitive clay landslides. Additionally, the results from numerical studies have been compiled in a summary table. It has been found that modeling landslides with sensitive clays is extremely challenging, mainly due to the distinctive soil behavior. Therefore, the constitutive model is one of the most important issues when simulating these landslides. Strain localization, formation of the shear band, failure initiation, and landslide mechanism vastly depend on the stress-strain relationship of the soil. The inclusion of a well-fit complete stress-strain curve up to the point of remolding is essential for modeling sensitive clay landslides. Furthermore, precise estimation of runout distance is not possible without considering the rheological behavior of sensitive clays after remolding. Another challenging factor is its progressive nature which requires stability analysis in both drained (failure initiation) and undrained conditions (during progressive failure) in a single simulation. Moreover, the large deformation associated with the progressive failure requires a numerical framework that captures large deformation without numerical instability and computational inaccuracy.

Table 2-1: Summary of recent studies for numerical modeling of sensitive clay landslides

Name of the researcher	Constitutive model with strain softening	Numerical framework for Large deformation	Type of sensitive clay landslide	Triggering factor	Contribution on prediction of landslides	Limitations
1. Locat et al. [16]	NGI-ANISOFT constitutive soil model with linear strain-softening	BIFURC	Spread	Erosion	• Steeper slopes with high K_{oi}, slope with low stiffness, low remolded shear strength, high rate of strain-softening are more susceptible to large progressive failure • Spread occurs in highly over-consolidated clays	• Linear strain-softening • Strain rate effect and depth-wise variation of shear strength not considered • Rheological property of remolded clay not considered • Homogeneous slope • No demonstration for dislocation of soil mass or formation of horst and grabens
2. Dey et al. [119]	Von-mises with exponential strain-softening	Coupled Eulerian-Lagrangian	Spread	Erosion	• Illustration for the formation of horst and grabens • Steeper slope, higher sensitivity, lower δ_{ld} are more likely to cause large progressive failure • Increase in δ_{ld} , S_t, H_{St}, and decrease in s_u of the crust changes the failure pattern from spread to flow slide	• Strain rate effect and depth-wise variation of shear strength not considered • Rheological property of remolded clay not considered
3. Dey et al. [116, 124]			Combined	Erosion + surcharge load	• Instantaneous velocity and surcharge load accelerate the propagation of the shear band, causing progressive failure	
4. Wang et al. [84, 85]	Von-mises with linear strain-softening	Implicit & Random material point method	Retrogressive	Gravity load	• Failure surface forms in the weakest soil layer • Shear band propagation is governed by residual strength • For S_t=5 the failure is translational forming horst and grabens • Spatial variability alters landslide initiation and propagation	• Linear strain-softening • Strain rate effect and depth-wise variation of shear strength not considered • Rheological property of remolded clay not considered • Homogenous slope • No clarification on the failure mechanism concerning failure type
5. Zhang et al.[11], Zhang et al. [81, 101]	Bingham-Tresca with linear strain-softening	Particle finite element method	Flow slide	Erosion	• Illustration for the multiple rotational slides • Ignoring the viscosity of the remolded clay over-estimates the retrogression and runout. • Minimum sensitivity is required to initiate flow slide	• Linear strain-softening • Depth-wise variation of shear strength not considered • Homogeneous slope

Name of the researcher	Constitutive model with strain softening	Numerical framework for Large deformation	Type of sensitive clay landslide	Triggering factor	Contribution on prediction of landslides	Limitations
					• Higher sensitivity increases the retrogression and runout • Effect of viscosity is higher for highly sensitive clays • Flow slides can result in horst and grabens	
6. Tran and Solowski [96]	Tresca with exponential strain-softening with strain rate effect	Material point method	Spread	Erosion	• Sensitive clay slope with S_t>25 and τ_{ld}<2kPa are susceptible to large progressive failure • Strain rate has a significant impact on the propagation of progressive failure	• Rheological property of remolded clay not considered
7. Islam et al. [88]	Tresca with exponential strain-softening	Coupled Eulerian-Lagrangian	Flow slide	Seismic loading	• Steeper and inclined slopes have increased retrogression and runout • Upslope surcharge load increases retrogression and runout • Increased thickness of highly sensitive clay changes the failure pattern from spread to flow slide • Increased remolding energy decreases retrogression • A combination of rotational flow slide and translational spread can be possible in a large retrogressive failure	• Strain rate effect and depth-wise variation of shear strength not considered • Rheological property of remolded clay not considered • Assumption of static stress-strain behavior of soil under dynamic loading
8. Wang et al. [10, 89]	Tresca with exponential strain-softening and rate effect	Coupled Eulerian-Lagrangian	Flow slide and Spread	Erosion	• The occurrence of flow slide or spread depends on the movement of liquified debris, brittleness of soil, lateral earth pressure • Lower strain rate increases the mobility of the debris leading to a large flow slide	• No conclusive relationship between remolding energy and retrogression • Increasing stability number did not result in increasing retrogression • Some estimated input parameters (δ_{95}, β, η) for the constitutive model had high uncertainty
9. Zhang et al. [114], Yuan [93]	Strain-softening Tresca Model	Smoothed particle finite element method (SPFEM)	Retrogressive failure	Erosion	• Suitability of SPFM for retrogressive failure • Increased softening modulus increases retrogression and runout	• Linear strain-softening • Strain rate effect on shear strength not considered • Rheological property of remolded clay not considered • Homogenous slope

Name of the researcher	Constitutive model with strain softening	Numerical framework for Large deformation	Type of sensitive clay landslide	Triggering factor	Contribution on prediction of landslides	Limitations
10. Shan et al. [95]	Elastoviscoplastic model	Re-meshing and interpolation technique with small strain (RITSS)	Retrogressive failure leading to spread	Decreasing shear strength of soil	• Increased S_t, decreased τ_{ld}, decreased viscosity of the remolded clay and increased riverbed width increases the retrogression	• Linear strain-softening • Homogenous slope

CHAPTER 3

Article 2: Prediction of post-peak stress-strain behavior for sensitive clays

Zinan Ara Urmi [a] *, Ali Saeidi [a], Alba Yerro [b,] Rama Vara Prasad Chavali [a]

[a] Department of Applied Sciences, Université du Québec à Chicoutimi, Saguenay, G7H 2B1, Saguenay, QC, Canada

[b] Department of Civil and Environmental Engineering, Virginia Tech, Blacksburg, Blacksburg, VA 24061, United States

Published, Engineering Geology, Volume 323, 20 September 2023, 107221

https://doi.org/10.1016/j.enggeo.2023.107221

Credit authorship contribution statement

Zinan Ara Urmi: Conceptualization, Data curation, Formal analysis, Resources, Writing – original draft, Writing – review & editing. **Ali Saeidi:** Supervision, Methodology, Resources, Writing – review & editing. **Alba Yerro:** Supervision, Writing – review & editing. **Rama Vara Prasad Chavali:** Writing – review & editing.

Declaration of competing interest

The authors declare the following financial interests/personal relationships which may be considered as potential competing interests: Ali Saeidi reports financial support was provided by Natural Sciences and Engineering Research Council of Canada (Grant ID: NSERC- 950- 232724). Ali Saeidi reports financial support was provided by HydroQu´ebec (Grant ID: RDCPJ 521771–17). If there are other authors, they declare that they have no known competing financial interests or personal relationships that could have appeared to influence the work reported in this paper.

3.1 ABSTRACT

Unlike typical soils, sensitive clays undergo extensive post-peak strength degradation with increasing strain and finally disintegrate into a remolded liquid state. Realization of post-peak stress-strain behavior of sensitive clay up to large strains is vital in assessing large deformation problems such as landslides and mud flows. The conventional experimental approaches are uncertain about accurately determining the post-peak stress curve up to large strains (>100%) owing to rapidly increasing testing problems at increasing strains. This necessitates the exploration of an alternative scientific approach to predict the complete stress-strain curve for sensitive clays, which is addressed in this paper. Post-peak stress-strain curves of sensitive clays for different sites are obtained by converting remolding index vs. strain energy curves. Using site-specific data from eastern Canada sites, a mathematical expression is proposed to predict the complete stress-strain curve. Subsequently, an equation is developed for predicting remolding energy based on the stress-strain curve. Finally, it is observed that the post-peak stress-strain behavior is highly site-specific and can be mathematically expressed with a combination of exponential and linear strain-softening curves. Overall, the knowledge of the complete stress-strain behavior contributes greatly to the prediction of post-failure movements closer to reality.

Key Words: Strain-softening, Stress-strain behavior, Sensitive clays, Large deformation, Remoulding energy, Retrogression distance

3.2 INTRODUCTION

3.2.1 General background

The post-failure behavior of sensitive clays is attributed to the reduction in strength after reaching peak strength under shear loading, which is also known as strain softening [4]. Sensitive clays generally have high intact shear strength, but the shear strength reduces to a significantly low value (remolded shear strength) when subjected to disturbance in undrained condition [26, 38]. The strength reduction reaches a point where the clay completely loses its intact structure and disintegrates to a liquid-like mass (remolded clay) that can flow [6, 28]. Thus, the soil is referred to as "sensitive" because its post-peak strength is sensitive to disturbance. The sensitivity (S_t) of soil is quantified by the ratio between the peak (s_{up}) and remolded (s_{ur}) shear strength [25].

In analyzing landslides in sensitive clays, understanding how material sensitivity controls soil behavior is of utmost importance. Once the failure starts in sensitive clay slopes, the clay layer gets remolded and keeps moving away from its original position. The drag of this liquified soil results in subsequent failures (progressive or retrogressive) until the flow of this liquified clay stops or is unable to initiate another failure. Thus, the extent of the failure of sensitive clay slopes is enormous compared to slope failure in non-sensitive soil. For example, the recently occurred Gjerdrum landslide (2020) in the highly sensitive clays of Norway spanned a flow-off area of 210,000 m^2 and additionally affected 90,000 m^2 by debris flow [3].

The devastating aftermath of landslides in sensitive clays intrigued researchers to extensively investigate the behavior of these materials that leads to the initiation and progress of extremely large landslides under different loading conditions. Due to strain-softening behavior, the mobilized strength along a potential failure surface varies from the peak to the remolded shear strength, unlike a constant value used in limit equilibrium (LE) methods [16, 38, 58, 118, 125]. Therefore, analysis of sensitive clay slopes requires peak shear strength and detailed information about the strain-softening behavior, which fundamentally cannot be incorporated into conventional LE analysis [126]. Recent studies suggest that the stability analysis of sensitive clay slopes requires advanced numerical modeling tools to capture the retrogressive nature of these landslides [11, 32, 88, 96, 127]. Numerical modeling of sensitive clay slopes offers valuable insights into failure mechanisms and post-failure runout, which are crucial for landslide hazard mapping in such areas. The constitutive soil model, which represents the stress-strain behavior of the soil, is the most critical component for modeling sensitive clay slopes. The capability to reproduce realistic strain-softening characteristics in the material model is necessary for more accurate numerical analyses of large deformation problems in such materials [8]. Additionally, for retrogressive failure to occur, the soil must be capable of being wholly remolded and flowing out of the crater [44, 70, 74, 79]. The energy required for the remolding process is termed “remolding energy” and can be quantified from the area under the post-peak stress-strain curve with the principle of fracture mechanics [45, 128]. If the available potential energy of the slope is greater than the remolding energy of the clays, the slope is then considered susceptible to retrogressive failure [44, 129]. Hence , it is possible to evaluate the likelihood of a location being prone to retrogressive landslides by using post-peak stress-strain behavior up to the point of remolding.

3.2.2 Relevant works on large deformation behavior of sensitive clays

Ideally, the strain value required to reach the remolded shear stress is extremely large. Stark and Contreras [12] suggested that a completely remolded state may occur when the specimen is sheared to several hundred millimeters, corresponding to several hundred percent of the shear strain in soil specimens subjected to conventional laboratory tests. Stress-strain curves obtained from triaxial compression tests are limited to only 10-20% strain [13]. Generally, ring shear tests, reversal shear box tests, or direct simple shear tests are used to study the large deformation behavior, but these laboratory-scale shear tests could only achieve strains up to 30%-45% [14–18]. Thakur et al. [19] examined the stress-strain behavior of sensitive clays using field vane shear testing. However, the residual torque at 90˚ rotation could not reach the remolded level even after multiple manual turns due to factors associated with the drainage in the failure zone around the vane [20]. Thus, predicting post-peak stress-strain behavior is one of the major challenges in analyzing sensitive clay landslides where large deformation is involved.

Stress-strain data close to the remolded state of sensitive clays can only be found in Tavenas et al.'s [44] work. They determined the strain energy required to remold the clay with four innovative test methods, including impact on a rigid surface, impact from falling objects, extrusion through a narrowing tube, and shearing through oscillating simple shear in a large shear box. They considered the reduction of shear strength from its peak strength to the remolded strength as 100% remolding. They defined a parameter called the remolding index, which represents the amount of strength reduction as a percentage of the total strength reduction from the peak to the remolded state as follows,

$$I_r = \frac{s_{up} - s_u}{s_{up} - s_{ur}} \times 100\% \qquad 3\text{-}1$$

where s_{up}, s_u, and s_{ur} are the undrained shear strength at the peak, at any point after the peak, and at the remolded state. Additionally, the normalized strain energy (w_N) corresponding to a particular I_r is defined as

$$w_N = \frac{W_x}{w_{Ls}} \times 100\% \qquad 3\text{-}2$$

where W_x is the energy per unit volume (kN-m/m^3) to reduce the strength from s_{up} to s_u and w_{Ls} is the energy per unit volume (kN-m/m^3) required to reach the peak strength, i.e. the limit state energy. As per Tavenas et al. [130], the energy needed to reach the peak stress (limit state energy) for Champlain Sea clay can be expressed as,

$$w_{LS} = 0.013\sigma_p' \qquad 3\text{-}3$$

where σ_p' is the pre-consolidation pressure.

Finally, they generated the remolding index (I_r) vs. normalized strain energy (w_N) curves for different locations of eastern Canadian sensitive clays. The soil properties and the I_r vs. w_N curves of Tavenas et al.'s [44] work are presented in Table 3-1 and Figure 3-1, respectively. Quinn et al. [45] converted those remolding-index vs. strain-energy curves to stress-displacement curves (Figure 3-2).

As per the author's knowledge, the very first equation to represent the strain-softening behavior of sensitive clay for measuring the resistance of soil around a cone penetrometer was proposed by Einav and Randolph [23] as follows,

$$s_u = s_{ur} + (s_{up} - s_{ur})e^{-\frac{3\gamma}{\gamma_{95}}} \qquad 3\text{-}4$$

where s_{up} is the peak shear strength, s_u is the degraded shear strength after the peak, s_{ur} is the remolded shear strength, γ is the strain corresponding to s_u, and γ_{95} is the strain when the strength is reduced by 95% of the supposed total reduction ($s_{up} - s_{ur}$). Dey et al. [124] calibrated Equation 3-4 using Quinn et al.'s [45] interpreted curves (Figure 3-2) for its application in the landslide analysis of sensitive marine clay. However, the authors acknowledged the uncertainty in evaluating the large deformation parameter (γ_{95}) used in the softening equation.

Table 3-1. Soil properties of each location of Tavenas et al.'s [44] work

Name of the site	Sample depth (m)	Peak shear strength s_{up} (kPa)	Remolded shear strength s_{ur} (kPa)	Pre-consolidation pressure, σ_p' (kPa)
Saint-Léon (SLE)	4.8	30	1.10	100
Saint-Léon (SLE)	9.3	49.5	2.10	180
Louiseville (LOU)	6	39	1.30	125
Saint-Hilaire (HIL)	5.6	35	0.80	115
Saint-Thuribe (THU)	6	55	0.40	175
Saint-Thuribe (THU)	12	42	0.07	195
Mascouche (MAS)	9	135	1.30	400
Saint-Alban (SAL)	6.6	21	0.20	85
Saint-Jean-Vianney (SJV)	30	320	1.20	1000

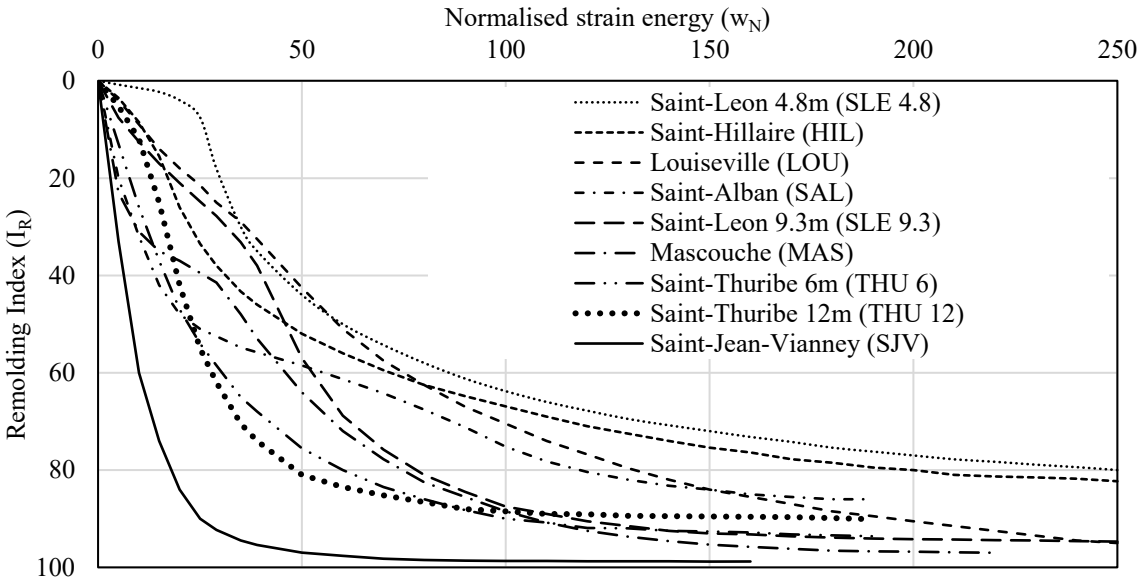

Figure 3-1. Relationship between normalized energy and remolding index for Champlain clay samples (replotted from Tavenas et al. [44]).

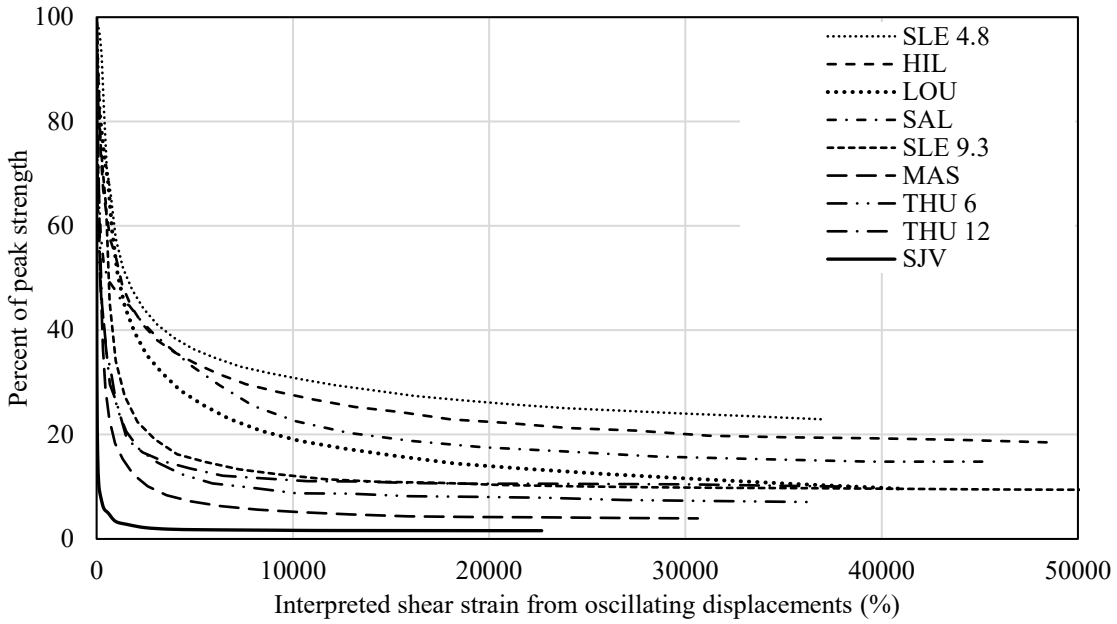

Figure 3-2. Stress-strain curves interpreted by Quinn et al. [45] from the remolding index vs. normalized strain energy curves of Tavenas et al. [44].

Some researchers used the linear strength degradation equation for simplicity [16–18, 131, 132] but strain softening in sensitive clays can be highly non-linear [14–18]. Most of the recent studies on the simulation of sensitive clay landslides [9, 11, 89, 93, 127] used Einav and Randolph's strain-softening equation (Equation 3-4). Generalized application of this equation without site-specific verification and without an accurate estimation of the large-deformation parameter, γ_{95}, might result in erroneous outcomes. Site-specific applicability of this equation has been discussed in detail in section 3.4.1.

3.2.3 Study outline

In a nutshell, even though post-peak stress-strain behavior is crucial in the analysis of post-failure behavior of sensitive clay landslides, existing work related to the prediction of the stress-strain curve of sensitive clays is limited. This study aims to provide a methodology to obtain a complete post-peak stress-strain curve up to the point of remolding based on site-specific geotechnical investigation results and a suitable strain-softening equation. To achieve this objective, firstly, the remolding index-strain energy curves [44] are converted to stress-strain curves. Then, focusing on the shortcomings of the existing strain-softening equation,

a new site-specific strain-softening criterion is established to predict the post-failure behavior and determine the remolding energy of sensitive clays. Next, the criterion is applied to predict the complete stress-strain curves of five different locations. Finally, an equation is proposed to determine the distance of retrogression of spreading kind of failure based on the calculated remolding energies from the predicted curves of those five locations.

3.3 DEVELOPMENT OF SHEAR STRESS-STRAIN CURVE FROM REMOLDING INDEX-STRAIN ENERGY CURVE

Quinn et al. [45] first interpreted the energy curves from Tavenas et al.'s [44] data as stress-strain and stress-displacement curves considering basic assumptions. In particular, they assumed that the strain was linear-elastic up to the peak strength; therefore, the energy required to reach the peak strength (w_{LS}) was defined as,

$$w_{LS} = \frac{1}{2} \times \gamma_p \times s_{up} \qquad 3\text{-}5$$

Additionally, they assumed that, $\gamma_p = 1\%$ and $w_N = W_x$, that is, $w_{LS} = 1$ as per Equation 3-2. However, the assumption that both γ_p and w_{LS} equal to 1 is unrealistic because it results in a constant peak strength value for all sites as per Equation 3-5. The authors of this present paper re-interpreted those curves, and the reasons will be clarified further in this section.

In this work, a stress-strain curve has been considered for sensitive clays, as shown in Figure 3-3. The soil is assumed to be perfectly elastic up to the peak (i.e., no energy dissipation during this part of the curve). Consider two points in the curve after the peak at a stress s_{ux-1} and s_{ux} having strains γ_{x-1} and γ_x, respectively. Therefore, the strain energy required for the reduction of the stress from s_{ux-1} to s_{ux} is the shaded area under the stress-strain curve in Figure 3-3. This energy is the difference between the energies at these two points (i.e., W_{x-1} and W_x), and it can be approximated as such,

$$\frac{1}{2}(s_{ux-1} + s_{ux})(\gamma_x - \gamma_{x-1}) = W_x - W_{x-1} \;\rightarrow\; \gamma_x = \frac{2(W_x - W_{x-1})}{(s_{ux-1} + s_{ux})} + \gamma_{x-1} \qquad 3\text{-}6$$

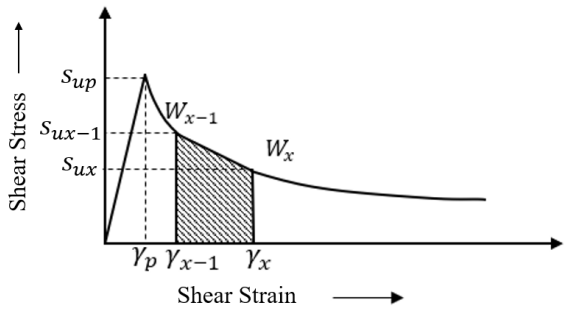

Figure 3-3. Stress-strain curve of a sensitive clay

To evaluate the γ_x for the first point of the post-peak stress-strain curve, the value of s_{ux-1}, γ_{x-1}, and w_{x-1} would be the peak shear stress (s_{up}), peak strain (γ_p), and the energy required to reach the peak stress (w_{LS}). That is, for the current step, the value of s_{ux-1}, γ_{x-1}, and w_{x-1} would be the stress, strain, and energy value of the previous incremental step. While s_{ux} can be determined by rearranging Equation 3-1.

$$s_{ux} = s_{up} - I_{rx}(s_{up} - s_{ur}) \qquad 3\text{-}7$$

where, I_{rx} is the remolding index corresponding to stress s_{ux}.

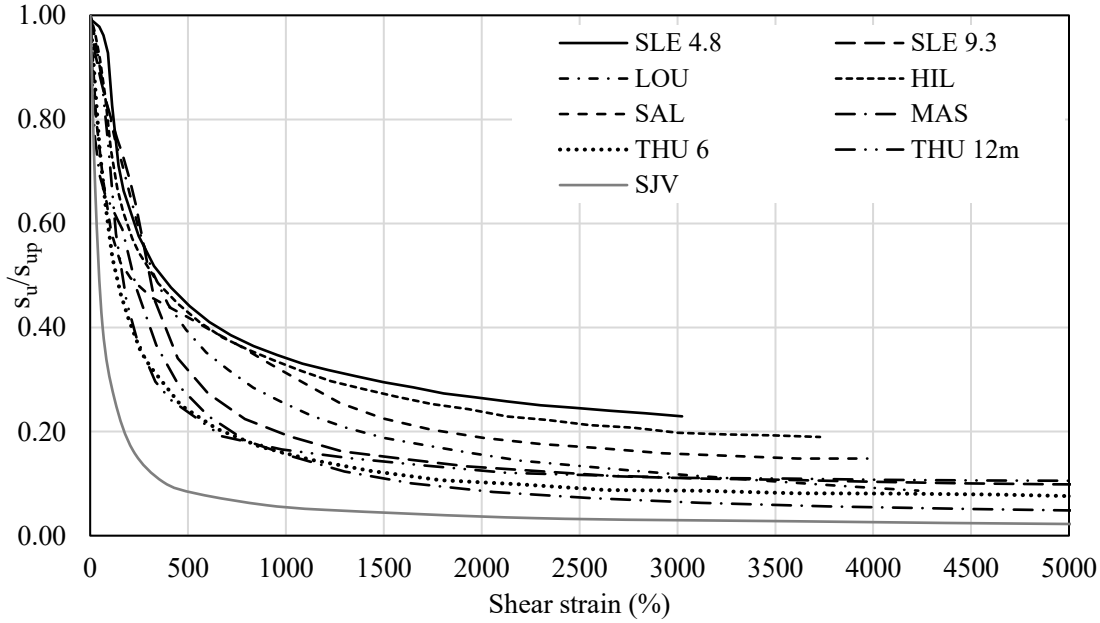

Figure 3-4. Stress-strain curves produced from Tavenas et al.'s [44] data.

Using the data from Table 3-1 and Equations 3-2, 3-3, 3-5, 3-6, and 3-7, I_r vs. w_N curves can be converted to stress-strain curves for each site. Figure 3-4 shows the stress-strain curves produced from the data of Tavenas et al.'s [44] I_r vs. w_N curves (Figure 3-1).

For the evaluation of strains (γ_x) from Tavenas et al.'s [44] data, Quinn et al. [45] proposed the following equation,

$$\gamma_x = \frac{2w_N}{(s_{ux-1} + s_{ux})} + \gamma_{x-1} \qquad 3\text{-}8$$

It can be noted that instead of using the difference of energies between two incremental stresses, $W_x - W_{x-1}$, Equation 3-8 considers the normalized strain energy of the current step (w_N), that is, the energy required for the strain accumulation from γ_{x-1} to γ_x has been taken as $\frac{W_x}{w_{Ls}}$ which represents what fraction of the limit state energy is required to reach γ_x from $\gamma = 0$. Therefore, the inconsistency in Equation 3-8 is that even though the strains are incremental, the energy is not. By comparing the stress-strain curve produced by Quinn et al. [45] (Figure 3-2) and the curves produced by this study (Figure 3-4), we can see that the strain values in Quinn et al.'s [45] interpretation are considerably higher, for example, in Saint-Alban, the strain value corresponding to a normalized strain energy value =190 corresponds to a strain value of 45485% by Quinn et al., [45]. In contrast, the same strain energy corresponds to a strain value of 3970% as per this study. The difference between the interpreted strain values of Figure 3-2 [45] and Figure 3-4 (this study) is evident in Figure 3-5, where stress-strain curves produced by both studies are plotted together (dashed lines represent this study, solid lines represent Quinn et al. [45], and the locations are color-coded). To determine which interpretation is more consistent with Tavenas et al.'s [44] data, the experimental setup for evaluating the strain energy values in Tavenas et al.'s [44] work has been analyzed. The description of these experiments can be found in Flon et al. Tavenas et al. [44] determined the strain energy from four methods, one of which was simple shearing. For the determination of strain energy by simple shearing, the sample size was 12x12x10cm, and each half cycle of simple shearing was equivalent to a displacement of 8cm. The highest number of cycles for each sample varied between 60 to 90. Therefore, the highest strain for each sample could be in the range of 8000-12000%. From this study, the highest values of interpreted strains for the maximum values of strain energies are in the range of 3200-12000%, which is comparable with Tavenas et al.'s [45] test methods. In comparison, the maximum

strain values for different locations by Quinn et al. [45] are in the range of 14000-55000%, which is inconsistent with Tavenas et al.'s [45] experimental setup. That is why the re-interpretation of the strains was considered important in this study.

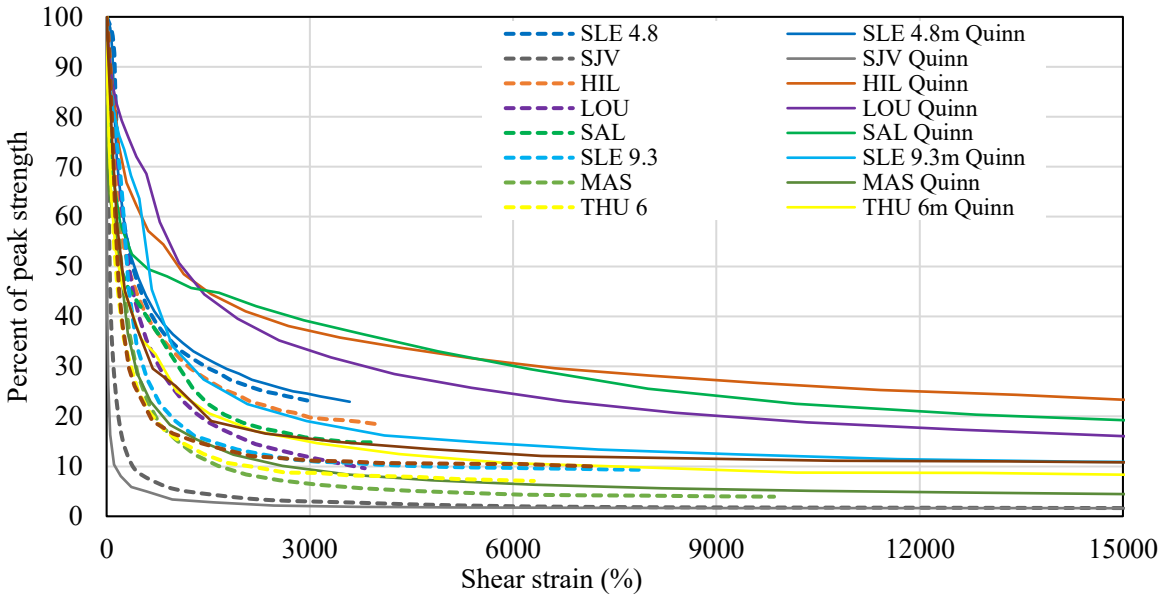

Figure 3-5. Comparison of the stress-strain curves interpreted by this study with Quinn et al. [45].

3.4 DEVELOPMENT OF STRAIN-SOFTENING EQUATION FOR SENSITIVE CLAY

3.4.1 Applicability of existing equation

It is evident from the stress-strain curves (Figure 3-4) that the post-peak strength decreases with increasing strain is non-linear. Einav and Randolph's [23] strength degradation equation (Equation 3-4) was the very first equation describing the non-linear strain softening behavior of sensitive clays in large deformation problems and had become increasingly popular for its application in the numerical simulations of sensitive clay landslides . To assess the applicability of Equation 3-4 for predicting the post-peak behavior of the sensitive clays of Tavenas et al.'s [44] studied locations, stress-strain curves produced from Tavenas et al.'s [44] data (these curves would be referred to as "SST curves" from here on) and stress-strain curves predicted by Einav and Randolph's [23] strain-softening equation (these curves would be referred as "SSER" curves from here on) have been plotted for comparison in Figure 3-6.

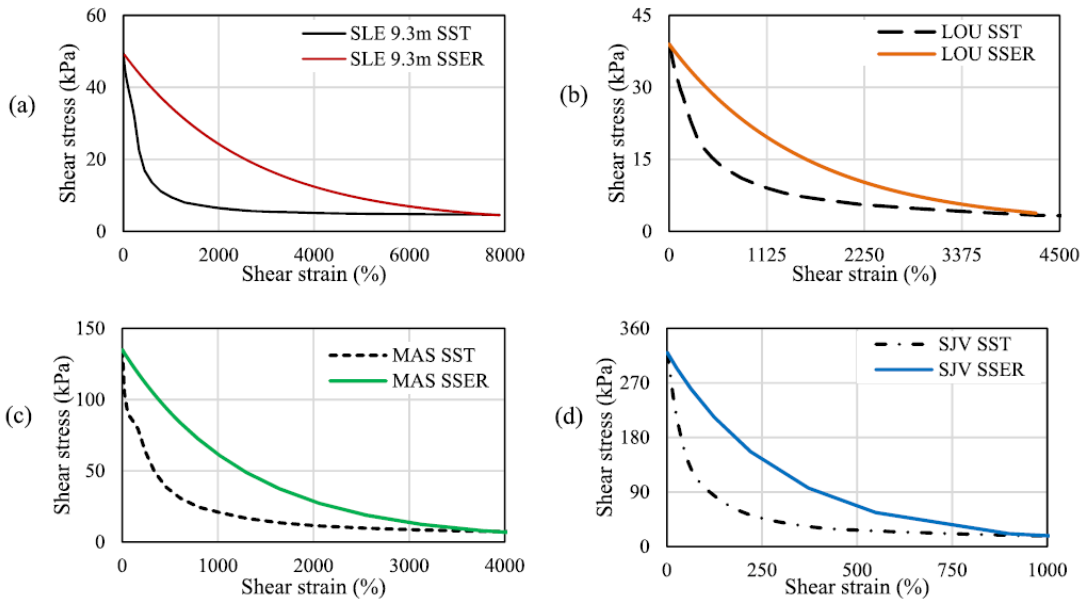

Figure 3-6. Comparison of the stress-strain curves produced from Tavenas et al.'s [44] experimental data with Einav and Randolph's [23] strain softening equation for four sensitive clays from different sites.

As per the definition of γ_{95}, it is the value of strain corresponding to an $I_R = 95\%$. From Tavenas et al. 's [44] experimental results, samples from only four sites could reach up to 95% of remolding, that is, γ_{95} was obtainable only for four sites. Despite the reduced amount of data, these four locations have a wide range of peak shear stress (40-320kPa), plasticity index (13-46%), sensitivity (24-260), and pre-consolidation pressure (25-1000kPa); therefore, it is reasonable to assume that the soils from these sites are a good representation of sensitive clays with varying soil properties. It is observed from Figure 3-6 that in all cases, Equation 3-4 overpredicts the stress-strain curves produced from the experimental data to a significant extent. The rate of strength decrease is slower in SSER curves compared to SST curves. Additionally, the SSER curves have a uniform exponential decrease, whereas the rate of strength decrease in the SST curves is higher in the initial parts at smaller strains compared to the final parts at larger strains. For example, in the Saint-Jean-Vianney (SJV) SST curve, 80% of the strength decrease happens within 125% strain value, but it takes another 800% of strain to reach 95% of strength reduction. It can be concluded that for a more accurate prediction of the stress-strain curves, modification is required in the exponent part of the strain-softening equation ($e^{-\frac{3\gamma}{\gamma_{95}}}$) which controls the rate of strength decrease. For a more precise understanding, developing a strain softening equation compatible with laboratory-obtained shear test results from a specific site requires two essential parameters.

First, a parameter is needed to initiate the curve at the correct peak stress, and second, a parameter is necessary to regulate the curve's exponent, preventing over- or underestimation. For example, in Figure 3-7, the stress-strain curves from two sites, a and b, can be re-presented with a strain-softening equation if the starting point and exponent of the softening equation can be calibrated based on the site-specific results. The development process is further clarified in the next section.

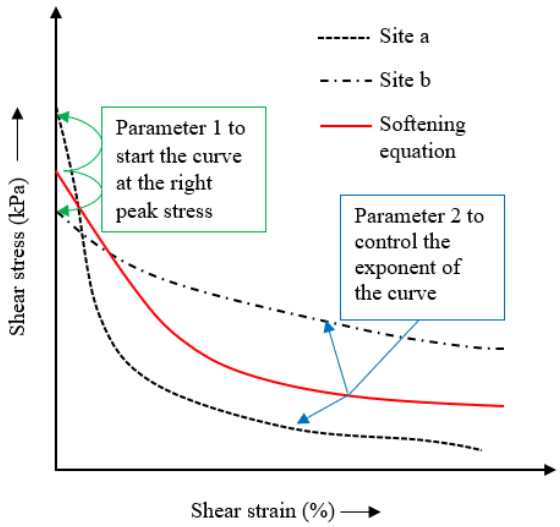

Figure 3-7. Development of a site-specific strain softening equation

3.4.2 Development of a new strain-softening equation

The exponential term in Equation 3-4 represents the fraction of the total shear strength reduction required to reach the remolded strength. To understand this term more clearly, at the peak strength, the fraction of total reduction required to reach the remolded strength is 1 (100%), so the equation gives $s_u = s_{up}$. Again, at remolded shear strength, the fraction of total reduction required to reach the remolded shear strength is 0; thus the equation gives $s_u = s_{ur}$. By rearranging Equation 3-4 we get,

$$e^{-\frac{3\gamma}{\gamma_{95}}} = \frac{s_u - s_{ur}}{s_{up} - s_{ur}} \qquad 3\text{-}9$$

As per Equation 3-9, plotting the $\frac{s_u - s_{ur}}{s_{up} - s_{ur}}$ against strain (γ), the exponential nature of the curves can be analysed better. After examining the trend of the curve, it is observed that even though the change in the fraction of total reduction required to reach the remolded strength is exponential up to a certain strength (s_{uR}) but does not exactly follow the equation $e^{-\frac{3\gamma}{\gamma_{95}}}$, rather it follows $\alpha e^{-\beta\gamma}$, where α and β are site-specific strength reduction constants (Figure 3-8). It is essential to understand how these site-specific constants play an important role in capturing the particular stress-strain behavior of the site. In a physical sense, α controls the starting point of the curve, and β controls the rate of exponential strength reduction. For example, let us consider a particular site, Louiseville (LOU), for different α values keeping the β value fixed. It can be observed from Figure 3-9(a) that a precise α value helps in initiating the curve at the correct peak strength. To understand how β controls the stress-strain curve, we have performed a sensitivity analysis considering different values of β while keeping α constant for the Louiseville site (LOU). Figure 3-9(b) shows that β represents the rate of strength reduction to its final remolded shear strength.

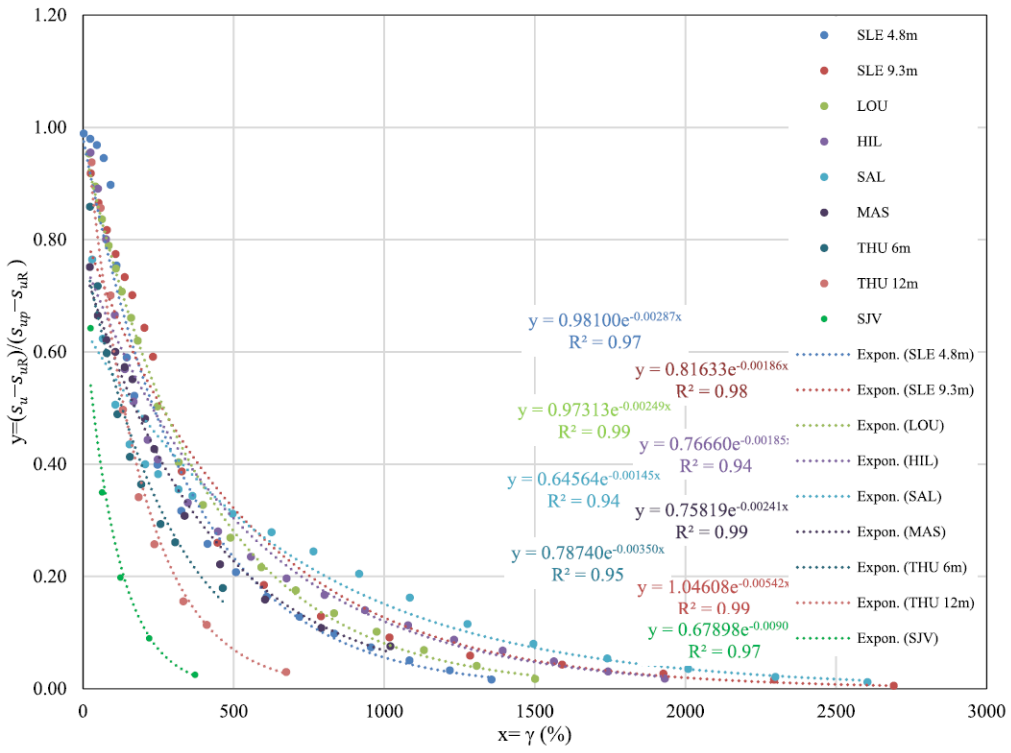

Figure 3-8. $\frac{s_u - s_{uR}}{s_{up} - s_{uR}}$ vs. γ curves, along with their exponential trend color-coded by location.

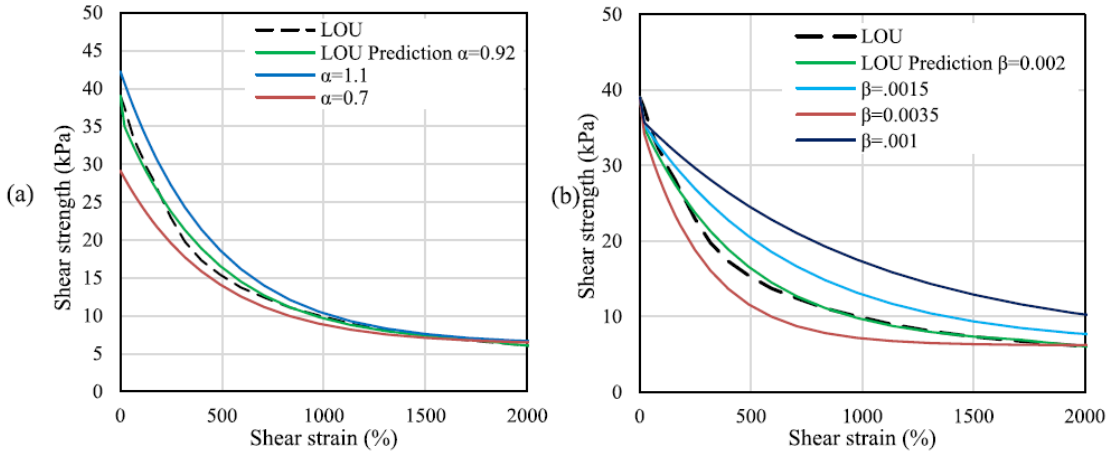

Figure 3-9. (a) Effect of α on the stress-strain curve; (b) effect of β on the stress-strain curve

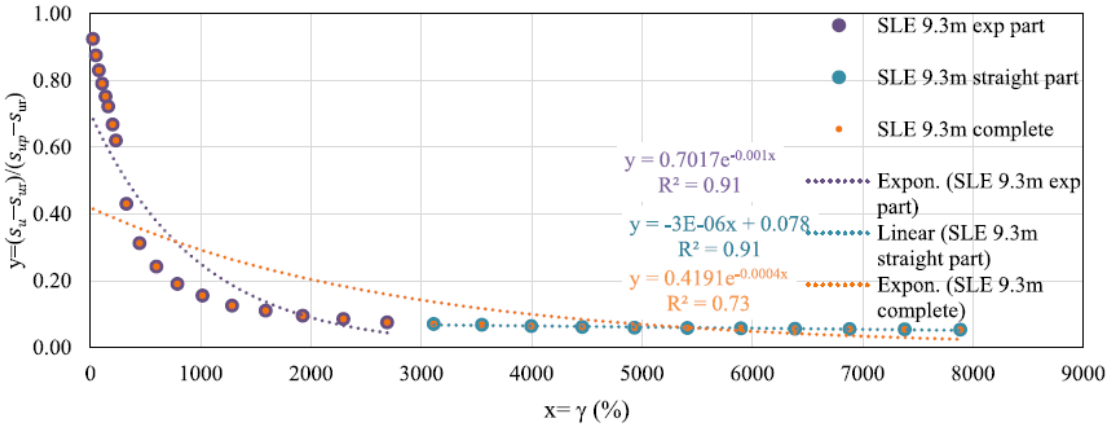

Figure 3-10. $\frac{s_u - s_{uR}}{s_{up} - s_{uR}}$ vs γ curve for Saint-Leon 9.3m

From the $\frac{s_u - s_{ur}}{s_{up} - s_{ur}}$ vs. γ curves, it is also evident that the shear strength reduces exponentially up to a certain percentage of the total reduction, and the remaining can be considered a linear decrease. For example, for Saint-Leon (SLE) 9.3m sample, a combination of an initial exponential reduction (up to 93% of the total reduction) and final linear reduction gives an R^2=0.9. In contrast, it reduces to R^2=0.7 if the whole softening is considered exponential (Figure 3-10). Therefore, the strain-softening equation can be divided into two parts, an exponential initial part, and a final linear part, as

$$s_u = \begin{cases} s_{uR} + (s_{up} - s_{uR})\alpha e^{-\beta\gamma}, & s_u \geq s_{uR} \\ s_{uR} - (s_{uR} - s_{ur})\dfrac{\gamma - \gamma_R}{\gamma_r - \gamma_R}, & s_{uR} > s_u \geq s_{ur} \end{cases} \qquad 3\text{-}10$$

Where, s_{uR} is the degraded strength up to which the strength reduction is exponential and γ_R is the corresponding strain. It is found that the value s_{uR} is dependent on the peak shear strength (s_{up}) by the following correlation (Figure 3-11),

$$s_{uR} = 0.095 s_{up} \quad 3\text{-}11$$

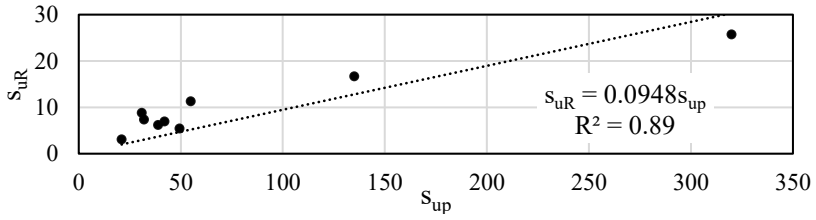

Figure 3-11. Correlation between s_{up} and s_{uR}

All the parameters required in Equation 3-10 for the prediction of stress-strain curves in all the considered sites are presented in Table 3-2. It can be seen that the value of α varies from 0.64 to 1.04, whereas Einav and Randolph [23] (Equation 3-4) considered a constant value of 1. Additionally, the strain softening is not exponential up to 95% of strength decrease for every site as assumed in Equation 3-4. The value of $\gamma_R\beta$ varies from 3.84 to 5.79, unlike a constant value of $\gamma_{95}\beta = 3$ as taken in Einav and Randolph's [23] equation. An extremely small change in the exponent (i. e. $\gamma_R\beta$) of the strain softening equation significantly changes the post-failure retrogression and runout in sensitive clay landslides [133]. Another concern in applying Equation 3-4 in real-case scenarios is the uncertainty in the prediction of γ_{95} when the complete stress-strain curve is unknown. On the other hand, in the solution presented here, γ_R can be determined by calibrating the values of α, β, and s_{uR}. In particular, the site-specific constants α and β can be determined from the $\frac{s_u - s_{ur}}{s_{up} - s_{ur}}$ vs. γ plot of a partial stress-strain curve (up to 30-40% of strain) obtained from conventional laboratory test results.

To complete the stress-strain curve up to the point of remolding, the strain at remolded shear stress γ_r is required. As mentioned earlier, the I_R vs. w_N curves could not attain 100% of remolding. The last point of those curves represents a point in between s_{uR} and s_{ur}; therefore, the strain value (γ_r) corresponding to the remolded strength (s_{ur}) cannot directly be determined from those curves. Considering the assumption of this study that

the strain softening is linear after s_{uR}, it is possible to determine γ_r by rearranging the linear part of Equation 3-10 as follows

$$\gamma_r = \frac{(\gamma - \gamma_R)(s_{uR} - s_{ur})}{s_{uR} - s_u} + \gamma_R \qquad 3\text{-}12$$

Where, s_u and γ are the stress and strain values of any points in between s_{uR} and s_{ur}.

With conventional laboratory testing, however, a point in between s_{uR} and s_{ur} might not be available. Therefore, it was thoroughly assessed whether γ_r can be determined from a reliable empirical equation. From the peak strength vs. $\frac{\gamma_r}{\gamma_R}$ relationship, a linear correlation (Figure 3-12) between these two parameters can be determined as per the following equation,

$$\frac{\gamma_r}{\gamma_R} = 0.13 s_{up} \qquad 3\text{-}13$$

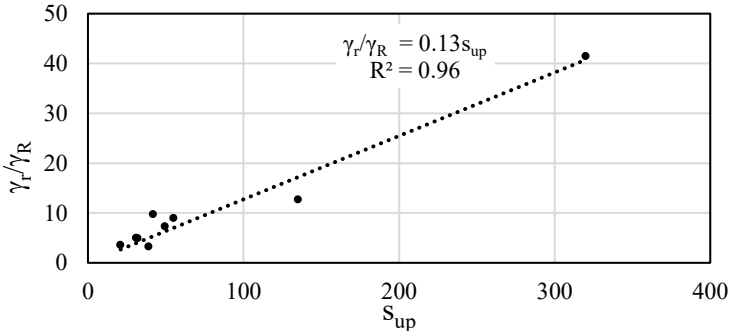

Figure 3-12. Correlation between s_{up} and $\frac{\gamma_r}{\gamma_R}$

Using all the parameters determined in Table 3-2, stress-strain curves are predicted with the new strain softening equation (Equation 3-10). It is observed that the proposed new softening equation immensely improves the accuracy of the prediction (Figure 3-13). For the evaluation of the site-specific strain softening parameters, α and β mentioned in 3-10, $\frac{s_u - s_{uR}}{s_{up} - s_{uR}}$ vs. γ curves had all the strain values up to γ_R (Figure 3-8), but with conventional laboratory testing, the maximum available strain (γ) is very low (at most up to 50% of the total strength reduction, γ_{50}). Therefore, it was important to assess the reliability of α and β values determined from partial stress-strain curves where strain value is available up to γ_{50}.

Table 3-2. Parameters for prediction of stress-strain behavior of sensitive clays.

Sites / Parameters	SLE 4.8m	SLE 9.3m	LOU	HIL	SAL	MAS	THU 6m	THU 12m	SJV
s_{up} (kPa)	31	49.5	39	32	21	135	55	42	320
s_{uR} (kPa)	8.85	5.42	6.20	7.34	3.11	16.68	11.32	6.97	25.75
γ_R (%)	1501	3114	1944	2129	3614	1298	646	978	549
α	0.98	0.816	0.917	0.766	0.638	0.813	0.875	1.04	0.679
β	0.0029	0.0019	0.0022	0.0019	0.0013	0.0031	0.006	0.0054	0.0090
%Reduction up to s_{uR}	74	93	87	79	86	89	80	84	92
$\gamma_R\beta$	4.31	5.79	4.22	3.94	4.84	4.06	3.84	5.30	4.97
s_{ur} (kPa)	1.1	2.1	1.3	0.8	0.2	1.3	0.4	0.07	1.2
γ_r (%)	7503	22767	6399	10600	13071	16485	5793	9542	22781

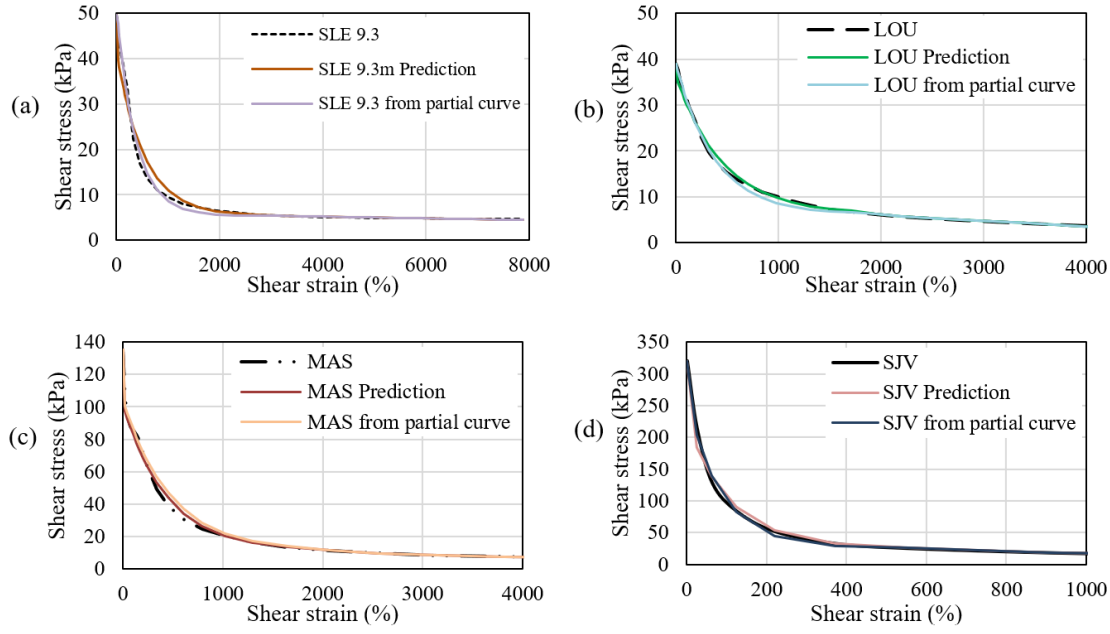

Figure 3-14 illustrates the change of the predicted curves if α and β are obtained from a partial stress-strain curve. It can be observed that the prediction from the new strain-softening equation suits well with the SST curves even if α and β are determined from partial stress-strain curves.

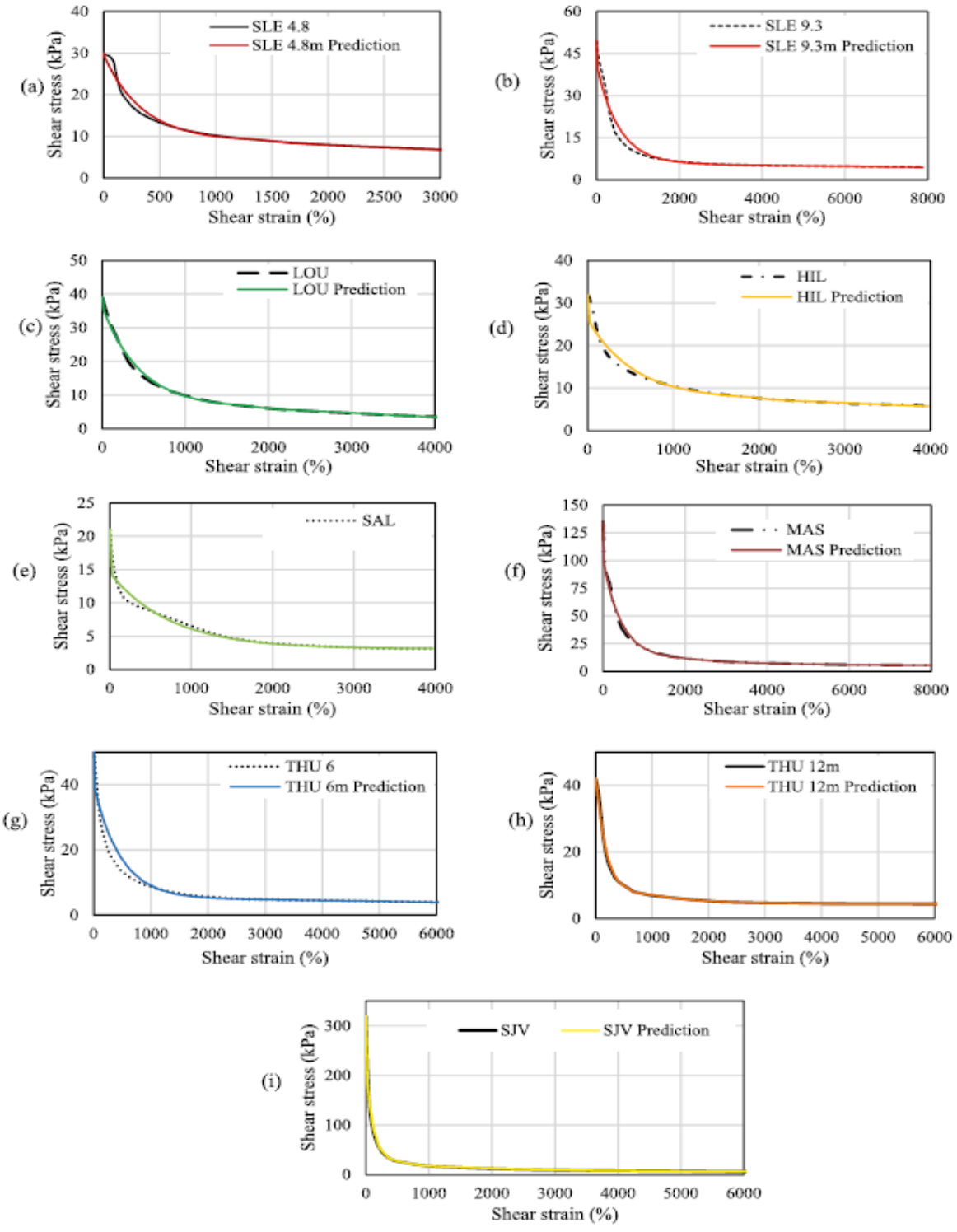

Figure 3-13. Comparison of the SST curves with the stress-strain curves predicted with the new strain softening equation (Equation 3-10) for different sites

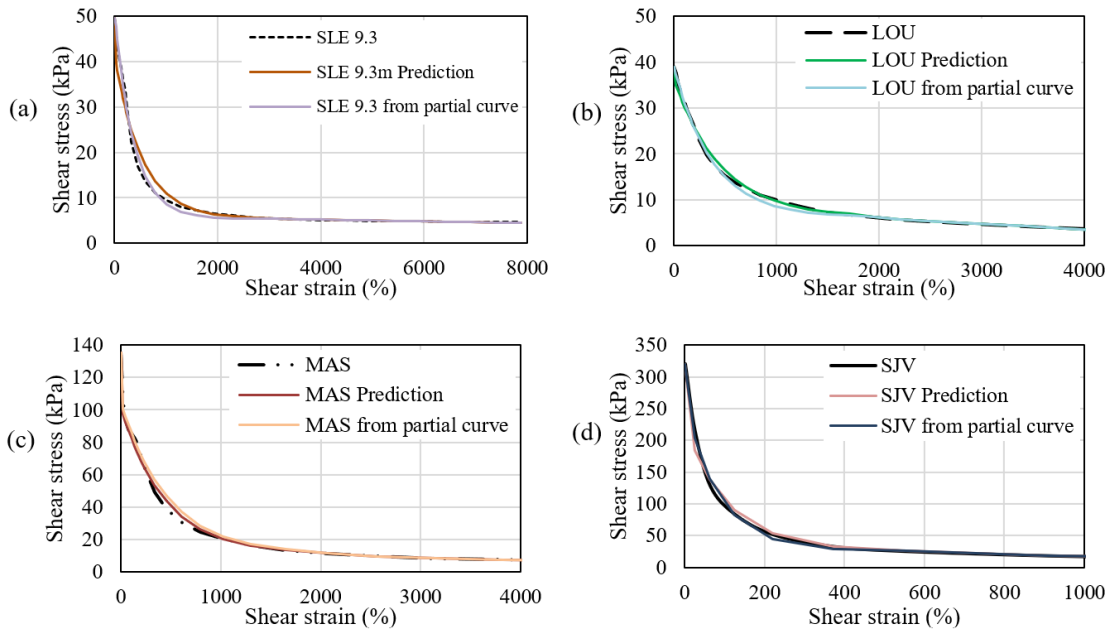

Figure 3-14 (a-d). Comparison of the SST curves, prediction by new equation, and updated prediction when the site-specific parameters are obtained from a partial stress-strain curve.

3.4.3 Methodology for the prediction of post-peak stress-strain behavior of sensitive clays using the established strain-softening criterion

The site-specific data required for the prediction of the post-peak stress-strain behavior of a particular site using Equation 3-10 are the peak shear strength, the remolded shear strength, and a partial post-peak stress-strain curve. The following steps need to be followed:

1. From the partial stress-strain curve, plot $\frac{s_u - s_{uR}}{s_{up} - s_{uR}}$ vs. γ to evaluate the value of α and β from the exponential trend of the plot, as shown in Figure 3-15. Here, s_{uR} is obtained from Equation 3-11. With the values of s_{up}, s_{uR} , α and β plot the exponential part of Equation 3-10 as shown in the first blue rectangle of Figure 3-16.
2. Estimate the strain value (γ_R) corresponding to the stress s_{uR} from the plotted curve and estimate γ_r from Equation 3-12.
3. With the values of s_{uR}, s_{ur}, γ_R and γ_r complete the linear part of the curve as shown in the second blue rectangle of Figure 3-16.

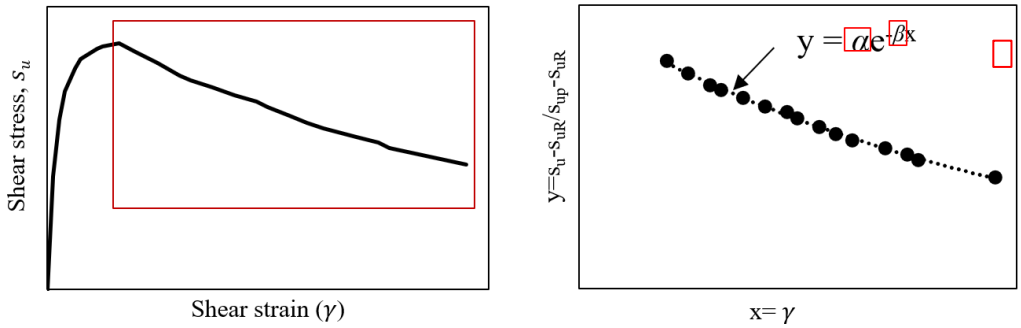

Figure 3-15. Estimation of α and β from the partial stress-strain curve

Figure 3-16 shows the complete stress-strain curve for a particular site where the curve up to the peak comes from laboratory experiment and the post-peak curve comes from the methodology described above.

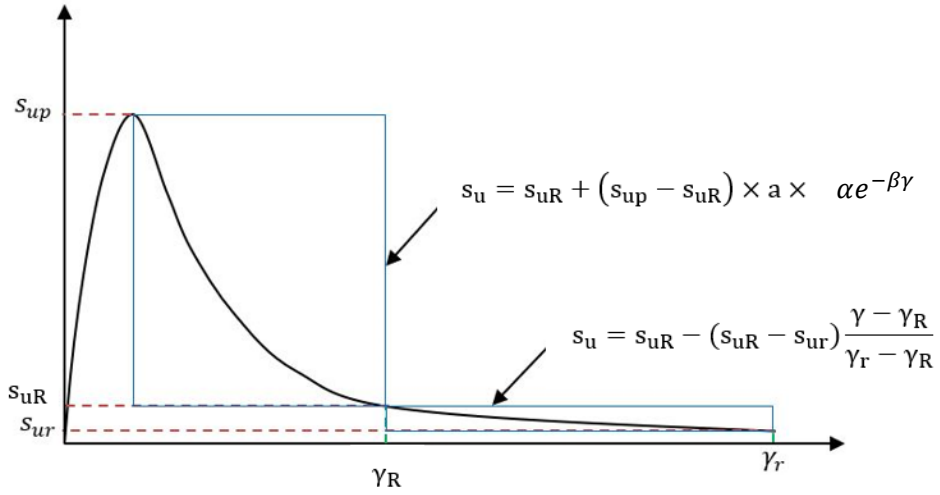

Figure 3-16. Prediction of post-failure stress-strain behavior of sensitive clays

3.4.4 Analytical framework for the estimation of remolding energy based on the post-peak stress-strain curves

During a sensitive clay slide, the initial potential energy (E^P) is divided into the energy required to remold the clay (remolding energy E^R) and the movement of the slide (kinetic and frictional energy, E^{KF}).

$$E^P = E^R + E^{KF} \quad 3\text{-}14$$

The movement of the slide, thus, entirely depends on how much energy is required to remold the soil and whether there is enough energy left for the remolded debris to flow [44, 129, 134]. Remolding energy is generally defined as the strain energy dissipated in the process of remolding. Tavenas et al. [44] illustrated the effect of the remolding energy on initiating retrogressive failure. They measured the total strain energy required to remold the clay and normalized it with respect to the limit state energy (w_{LS}) as the remolding process started after the peak. They showed that retrogression happens only when enough energy is available to remold the clay to a certain percentage. The concept of remolding energy to evaluate the susceptibility of landslides to retrogressive failure surfaced as a result of the observation that several landslide locations did not adhere to the evaluation criteria based on sensitivity, liquidity index, and remolded shear strength for predicting the occurrence of retrogressive failure [44, 129]. Building upon the data presented by Tavenas et al. [44], Leroueil et al. [135] identified a correlation between remolding energy and the multiple of plasticity index (I_p) and peak shear strength (s_{up}) as follows,

$$E^R = 16\, s_{up} I_p \quad 3\text{-}15$$

Using this formula, Locat et al. [136] estimated the remolding energies of 22 Canadian sensitive clay landslide locations and defined a parameter destruction index ($I_D = \frac{E^P}{E^R}$) to evaluate the effect of remolding energy on the landslide runout (D) (Figure 3-17). In their observations, a notable finding was the existence of a linear relationship between debris run-out and the destruction index when $I_D < 1$. When the destruction index is below one, it indicates that the remolding energy surpasses the available potential energy, leading to insufficient potential energy for effectively remolding the soil. This inadequate energy availability ultimately results in minimal run-out, as depicted in the figure. This observation aligns with the argument put forth by Tavenas et al. [44]. However, for thirteen out of the twenty-two sites examined, no such relationship between the destruction index and run-out was discovered. Locat et al.'s Locat et al., 2008) reasoning behind this discrepancy suggests that the significant depthwise variation in the plasticity index of a specific site poses a challenge in determining the appropriate index to utilize for accurately estimating remolding energy from Equation 3-15. Additionally, the discrepancy may stem from the fact that the concept of the destruction index

does not consider the frictional resistance exhibited by the moving debris, which plays a substantial role in influencing the magnitude of run-out.

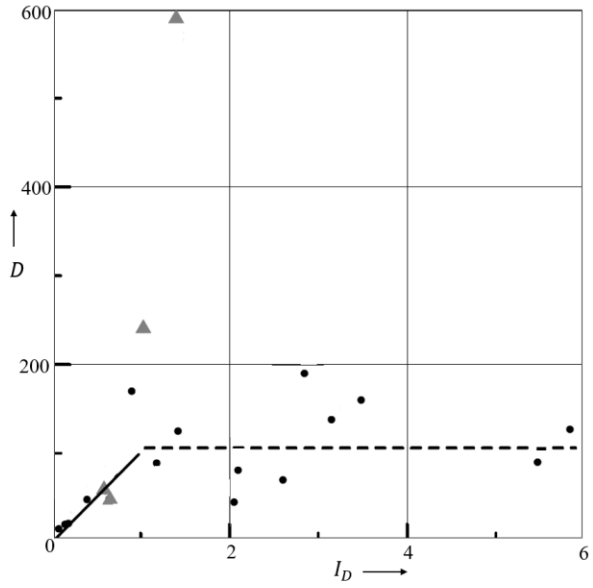

Figure 3-17. Relationship between run out of debris (D) and destruction index (I_D) (after [136])

Later on, Thakur et al. [128] employed an analytical approach to determine energy dissipated in the process of remolding by calculating the area under the post-peak stress-strain curve up to remolded shear strength. They assumed an idealized stress-strain behavior, considering that strain softening is linear from the peak to the remolded shear strength (Figure 3-18). However, strain softening is highly non-linear. Determination of the area under the stress-strain curve with a linear assumption may only work if the underpredicted area and the over-predicted area are almost equal, as in the case marked by a red dashed line in Figure 3-18. However, without the knowledge of the actual stress-strain curve, a linear assumption may result in a highly overpredicted or underpredicted area under the stress-strain curve, as illustrated in Figure 3-18 with green and blue dashed lines, respectively. The limitations of this approach become more evident when examining the determination of remolding energy for Klett clay, which was one of the cases studied by Thakur et al. [128]. This site had a peak shear strength (s_{up}) of 17 kPa, and remolded shear strength (s_{ur}) of 0.1 kPa. The vane shear test results indicated that strength reduction was only achieved up to 7 kPa at the maximum vane rotation. In their analysis, Thakur et al. [128] extended the initial linear portion of the stress-strain curve

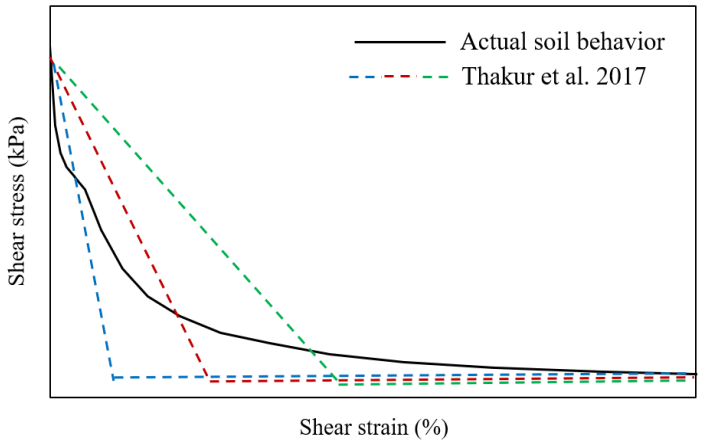

Figure 3-18. Stress-strain behavior of sensitive clays compared with the assumption of Thakur et al. [128].

up to the remolded strength and determined the area under the stress-strain curve as an estimate for the remolding energy (Figure 3-19a). However, based on the findings of this study regarding the post-peak stress-strain behavior of sensitive clays, it was established that the strength reduction follows an exponential decay pattern up to s_{uR}, followed by a linear decrease up to s_{ur}. Consequently, the partial stress-strain curve is extended exponentially up to 1.6 kPa (as per Equation 3-10) and then linearly up to 0.1 kPa (Figure 3-19b). It is observed that the linear approximation based on the partial stress-strain curve used by Thakur et al. [128] for Klett clay substantially underestimates the actual remolding energy.

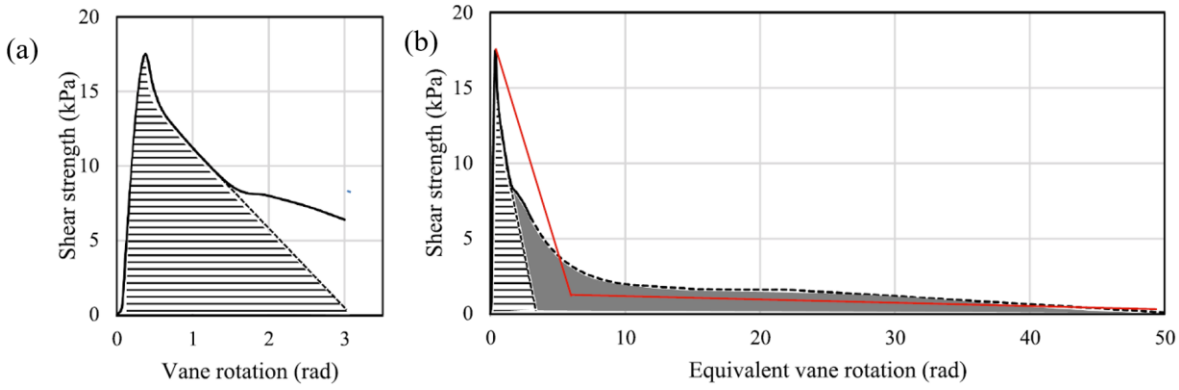

Figure 3-19. (a) Determination of remolding energy with linear approximation from a partial softening curve (after [128]) (b) Comparison between the remolding energy estimation by linear approximation vs. actual non-linear stress-strain behavior.

The viability of linear estimation relies on a balanced offset between over-prediction and under-prediction, as exemplified by the red line in Figure 3-19b. However, it is essential to note that such assumptions

cannot be made without access to the complete stress-strain curve. Furthermore, if the complete curve is already obtainable, the necessity for a linear approximation becomes redundant.

This study proposes a methodology for obtaining the complete post-peak stress-strain curve, which enables the straightforward estimation of remolding energy by calculating the area beneath the stress-strain curve. The area under the non-linear stress-strain curve i.e. the remolding energy (Figure 3-20a), can be mathematically represented as,

$$E^R = \int_{\gamma=\gamma_p}^{\gamma=\gamma_r} s_u \, d\gamma \qquad 3\text{-}16$$

Where s_u is the shear strength that varies from the peak to the remolded state.

It is possible to estimate the remolding energy by integrating the degrading shear strength (s_u) in Equation 3-10 with respect to strain (γ) from $\gamma = \gamma_p$ to $\gamma = \gamma_r$ as illustrated in Figure 3-20b. Therefore, the analytical expression for the remolding energy would be,

$$E^R = \int_{\gamma_p}^{\gamma_R} \left[s_{uR} + (s_{up} - s_{uR})\alpha e^{-\beta\gamma}\right] d\gamma + \left[\frac{1}{2}(s_{uR} + s_{ur})(\gamma_r - \gamma_R)\right] \qquad 3\text{-}17$$

(a)

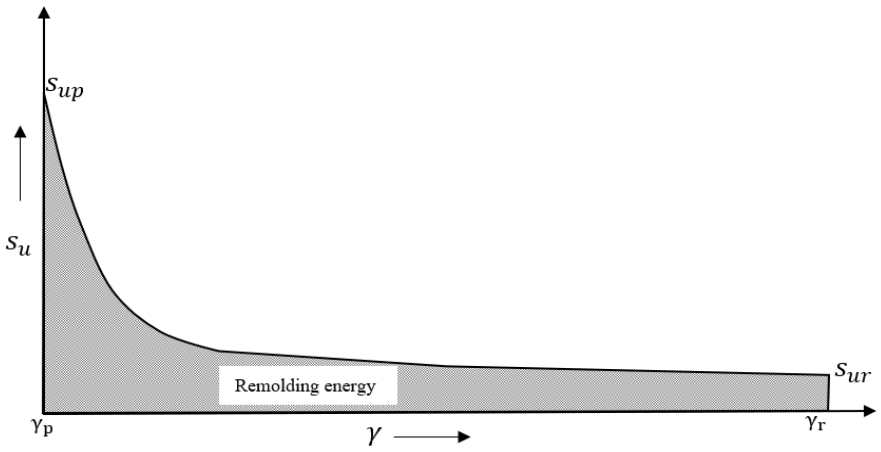

(b)

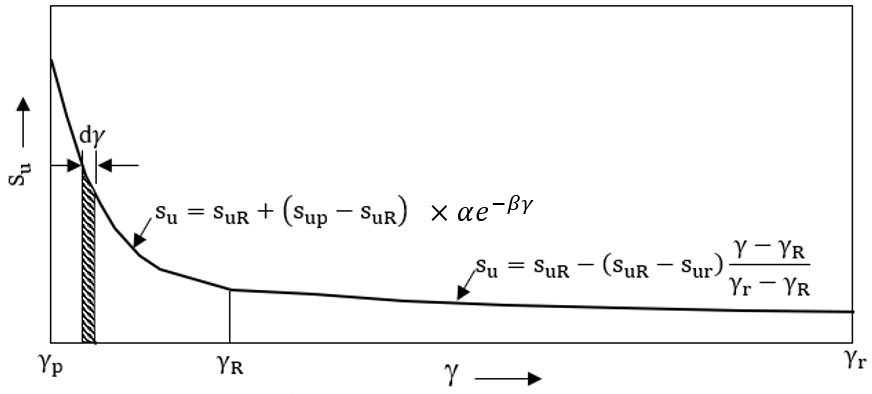

Figure 3-20 (a-b). Determination of area under the post-peak curve by integration

3.5 APPLICATION TO REAL CASES

3.5.1 Prediction of the stress-strain curve

The methodology described in section 3.4.3 has been applied to seven different landslide locations (6 eastern Canadian and 1 Norwegian) to predict the post-peak stress-strain behavior of sensitive clays. The landslides presented here are all identified as a spread retrogressive/progressive failure. The geotechnical properties of these sites are well described in the literature [14–18, 39, 137–139]. One of the major challenges in working with laboratory test data of sensitive clays involves the effect of sample disturbances. The quality of soil samples is a critical consideration in laboratory-based soil testing methods, particularly in the case of sensitive clays where sampling disturbance can significantly impact the mechanical properties of the clay [140–142]. If soil properties are taken from bad quality samples, the finite element numerical analysis of a sensitive clay slope may have a 25% lower safety factor compared to a high-quality sample [143]. Lunne et al. [144] have proposed criteria for assessing sample disturbance in marine clays with OCR between 1 and 2. These criteria involve categorizing sample quality based on the normalized change in the void ratio (Δe/e0) resulting from sample consolidation to assumed in situ effective stresses. These guidelines can be employed to ensure the quality of anisotropically consolidated samples compressed under undrained conditions (CAU) using the triaxial apparatus. The laboratory test data used in this study for most of the sites had geotechnical investigation reports verifying sample quality [14–18, 145]. It is crucial to obtain laboratory test results from high-quality samples to estimate post-peak stress-strain behavior accurately.

Table 3-3. Geotechnical properties for the sensitive clays of different landslide locations

Sites / Parameters	Cassel-man	Saint-Barnabé-Nord	Saint-Jude	Saint-Luc-de-Vincennes	Saint-Monique	Rockcliffe	Bekkelaget
Unit weight (m) kN/m^3	17	16	16.5	16	16	17	18.9
Plasticity Index (P_I) %	15	15	24	15	28	36	10
Liquidity Index (I_L) %	2	1.1	1.2	1.5	1	2	2.4
Slope Height (H) m	44	70	30	35	45	12.2	16
Sensitivity (S_t)	58	50	60	40	55	55	80
Peak strength (s_{up}) kPa	87.0	79.5	55.2	55.0	40.5	54.9	16.2
Remolded strength (s_{ur}) kPa	1.50	1.59	0.92	1.38	0.74	1.0	0.2
Peak strain γ_p %	6.5	4.0	3.2	2.4	2.4	3.0	6.6
s_{uR} (from eq 11) kPa	8.27	7.55	5.24	5.22	3.85	5.22	1.54

The geotechnical properties of each site are described in Table 3-3, the partial stress-strain curves from direct shear test results are illustrated in Figure 3-21, evaluation of α and β for each site from $\frac{s_u - s_{uR}}{s_{up} - s_{uR}}$ vs. γ curves are illustrated in Figure 3-22 (a-g), with estimated values of α, β, γ_R and γ_r for all locations are presented in Table 3-4. Finally, the complete stress-strain curves are constructed in Figure 3-23 (a-b).

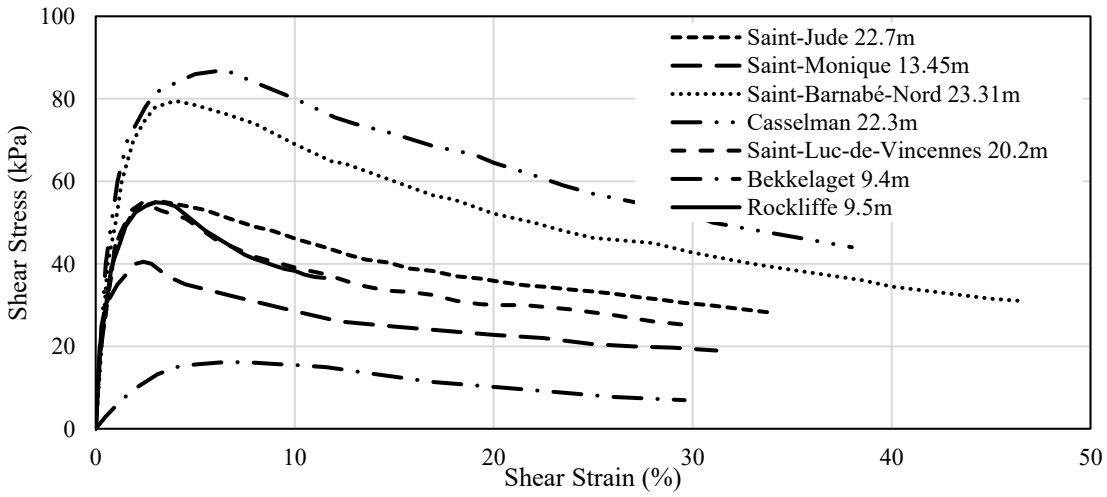

Figure 3-21. Partial stress-strain curve from DSS test results for different sensitive clay landslide locations.

Table 3-4. Additional parameters required for the prediction of the complete stress-strain curves

Sites / Parameters	Casselman	Saint-Barnabé-Nord	Saint-Jude	Saint-Luc-de-Vincennes	Saint-Monique	Rockcliffe	Bekkelaget
α	1.157	1.091	1.049	0.945	0.952	1.208	1.526
β	-0.024	-0.026	-0.025	-0.029	-0.028	-0.060	-0.048
γ_R (%)	250	230	240	195	180	95	120
γ_r(%)	2828	2377	1722	1394	948	678	253

From the final prediction of the stress-strain curves (Figure 3-23), it can be observed that the rate of strain softening is extremely low for larger strain values (>100%). Beyond the exponential softening, the rate of strength reduction is so low that the linear parts of the softening curves seem almost horizontal, indicating that the strain value at the remolded strength is extremely high. To assess whether the post-peak stress-strain behavior is consistent with the observed landslide movement, remolding energies using these stress-strain curves were determined as per Equation 3-17 (Table 3-5). In all the cases, the available potential energy of the slope was greater than the estimated remolding energies required for the remolding of the clay, which suggests that the slopes were susceptible to retrogressive failure.

Interestingly, for three sites, the estimated remolding energy from the empirical equation proposed by Leroueil et al. [135] closely matched the calculated remolding energies of this study. However, for other sites, overestimation or underestimation of remolding energy was observed, as depicted in Figure 3-24. In particular, at the Rockliffe site, Leroueil et al.'s [135] equation yielded higher remolding energy than the available potential energy, suggesting that the occurrence of large retrogressive failure may not align precisely with Tavenas et al.'s [44] remolding energy criterion. It is worth noting that the plasticity index for this site was significantly higher than the other sites.

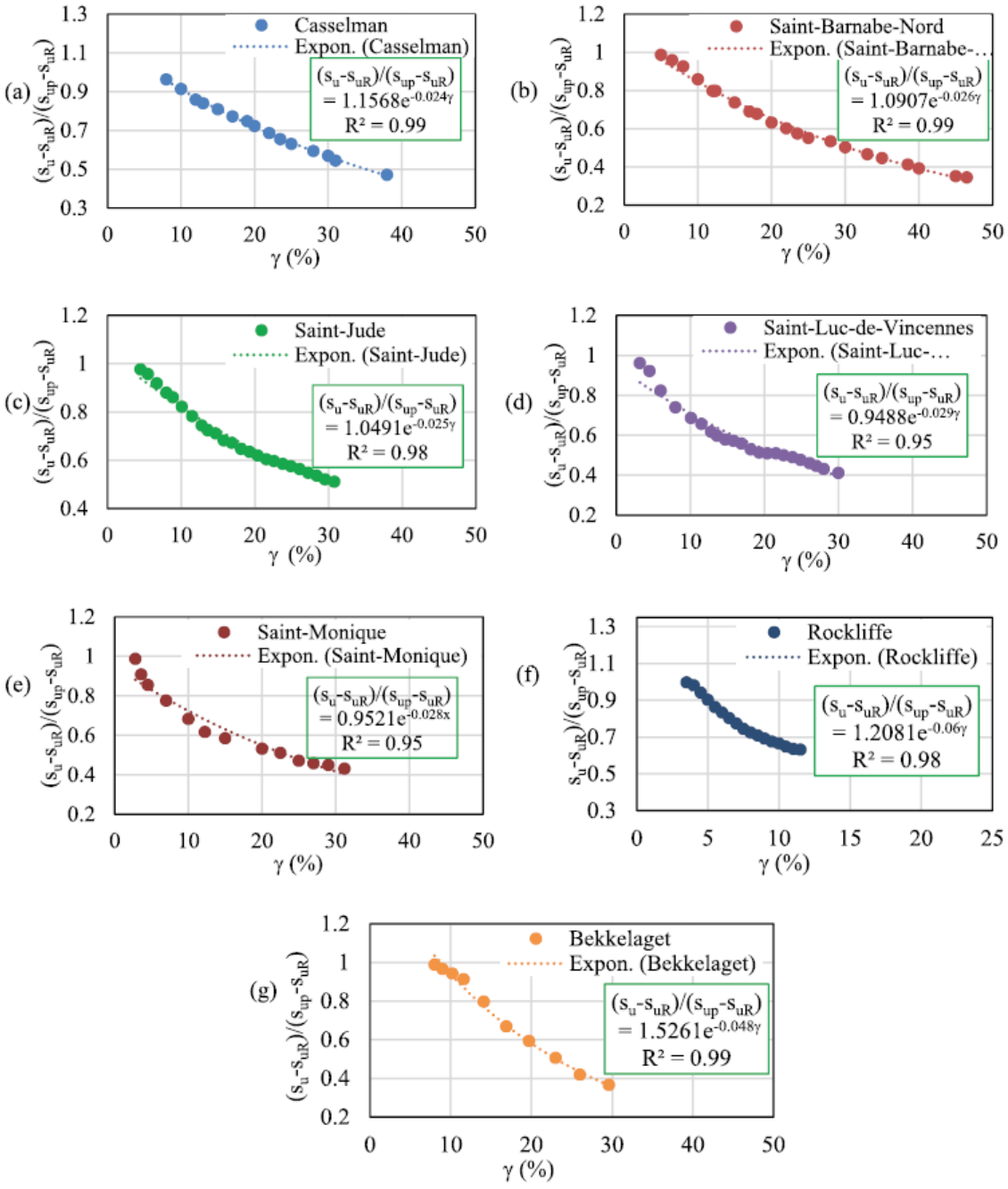

Figure 3-22 (a-g). Estimation of α and β for different sensitive clay landslide locations.

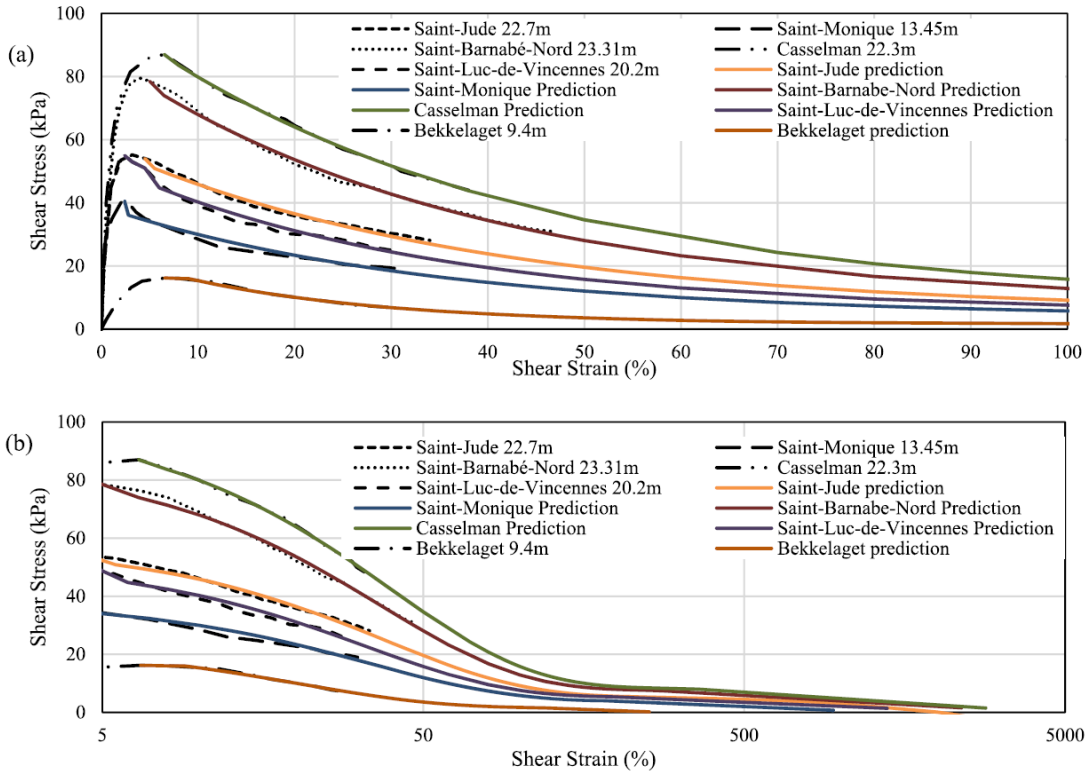

Figure 3-23. (a) Comparison between the predicted stress-strain curves and curves from DSS results. (b) Stress-strain curves plotted on a semi-logarithmic scale to illustrate the entire post-peak behavior

Table 3-5. Determination of remolding energies for the prediction of retrogressive failure occurrence

Locations	Cassleman	Saint-Barnabé-Nord	Saint-Jude	Saint-Luc-de-Vincennes	Saint-Monique	Rockcliffe	Bekkelaget
Potential energy E^P (2mH/3) kN-m/m^3	498.7	746.7	330.0	373.3	480.0	138.3	201.6
Remolding energy E^R (kN-m/m^3)	374.8	298.1	186.0	142.9	88.0	79.8	29.05
Occurrence of large retrogressive failure $E^P > E^R$	Yes	Yes	Yes	Yes	Yes	Yes	Yes

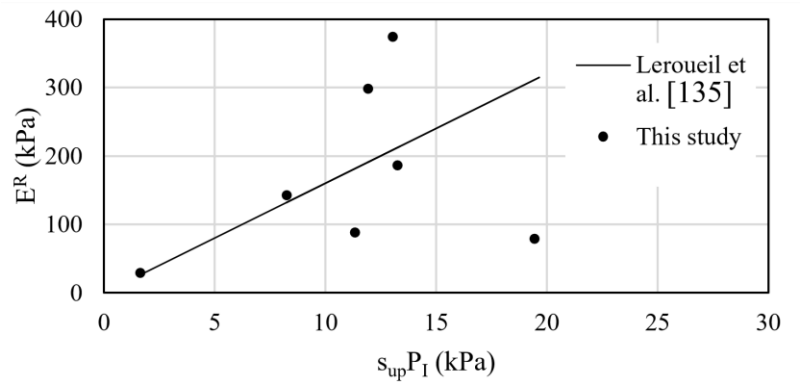

Figure 3-24. Comparison between the remolding energy estimation by Leroueil et al. [135] with this study

3.5.2 Prediction of the movement of remolded clay from the estimated remolding energies using the stress-strain curves

There are several empirical methods available for the estimation of retrogression distances. Mitchell and Markle [75] correlated the stability number ($N_s = mH/s_{up}$) with retrogression distance assuming that retrogression will not occur for $N_s < 6$. Later, other researchers linked retrogression distance with geometrical constraints like slope height and angle [45, 146]. However, Demers et al. [43] concluded that these correlations do not work well for Eastern Canadian landslides, especially for the Quebec region. The Norwegian Water Resources and Energy Directorate uses a simple method for mapping hazard zones that involves drawing a $1V:15H$ line from the toe of the slope to represent the maximum retrogression distance of potential flow slides in sensitive clay. But recent data shows that some landslides in Norway have exceeded this distance [147]. Turmel et al. [148] showed that in the Quebec region, observed retrogression distances for historical cases may vary between 2 to 50 times the height of the slope (H). Quebec Ministry of Transport, Sustainable Mobility and Transport Electrification (MTMDET) uses a statistical approach based on retrogression distances of historical landslides and ancient scars. Suppose a potential site satisfies the geotechnical and geomorphological requirements. In that case, the retrogression distance is assessed by applying a third-order moving average to the retrogression distance of previous scars in the vicinity. This method provides better results for regions where previously recorded landslide data is available [148]. Recently, numerical analysis of sensitive clay landslides has been used to predict post-failure retrogression [9, 11, 16, 127]. For an accurate estimation of retrogression

distance through numerical simulation, a site-specific strain-softening constitutive model for sensitive clays is required. The main aim of this paper was to produce an accurate strain-softening behavior model for sensitive clays designed explicitly for site-specific application, which can then be used to simulate sensitive clay landslides. It is worth noting that the post-peak stress-strain behavior model proposed in this study has a broader range of applications. Specifically, using the remolding energies estimated from these curves, an equation for calculating the retrogression distance may be developed using only laboratory test data of these locations.

As discussed in section 3.4.4, when remolded clay moves down a slope, the distance it travels (in retrogression and run out) depends on the available potential energy (E^P), the remolding energy (E^R), and the kinetic energy (E^{KF}) that develops during the movement of the slide. In spread failures, retrogression (the backward movement of the landslide toe) contributes to the lateral spreading of the slide mass. As the remolded clay spreads laterally within the slope, rather than flowing out of the crater as a cohesive mass, run-out distance (i.e., the distance the material travels downslope) is typically relatively low in spreads compared to earth flows. It can be assumed that most of the kinetic and frictional energy (E^{KF}) contributes to the retrogression distance.

By rearranging Equation 3-14, we get,

$$E^{KF} = E^P - E^R \qquad 3\text{-}18$$

By expanding the potential and remolding energies, we get,

$$E^{KF} = \frac{2}{3}mH - \int_{\gamma_p}^{\gamma_R}\left[s_{uR} + (s_{up} - s_{uR})\alpha e^{-\beta\gamma}\right]d\gamma + \left[\frac{1}{2}(s_{uR} + s_{ur})(\gamma_r - \gamma_R)\right] \qquad 3\text{-}19$$

where m is the unit weight of the soil, and H is the average height of the slope.

The amount of energy left for the movement of the remolded clay vastly depends on the frictional resistance i.e. the viscosity and unit weight of the liquified clay. If the retrogression distance of the landslide is represented with "RD", Equation 3-19 can be rewritten as follows,

$$\omega \times RD = \frac{2}{3}mH - \int_{\gamma_p}^{\gamma_R}\left[s_{uR} + \left(s_{up} - s_{uR}\right) \times a \times e^{-b\gamma}\right] d\gamma - \left[\frac{1}{2}\left(s_{uR} + s_{ur}\right) \times \left(\gamma_r - \gamma_R\right)\right] \quad 3\text{-}20$$

where ω is a proportional constant for the movement of the remolded clay, which is dependent on the viscosity and unit weight of the liquified clay. ω can be determined using the potential and remolding energy of previously occurred landslide locations with known retrogression distances (Table 3-6).

Table 3-6. Determination of ω for previously occurred landslide locations.

Locations	Cassleman	Saint-Barnabé-Nord	Saint-Jude	Saint-Luc-de-Vincennes	Saint-Monique	Rockcliffe	Bekkelaget
E^{KF} (kN-m/m^3)	182.53	448.57	144.00	230.43	391.97	58.5	172.55
RD (m)	450	180	80	110	142	76	145
$\omega=\frac{E^{KF}}{RD}$	0.41	2.49	1.80	2.09	2.76	0.77	1.19

Again, the viscosity of the remolded clay depends on the liquidity index of the clay [149]. Therefore, ω was calibrated against the unit weight and liquidity index of the clay using five out of the seven available landslide locations, while the remaining two sites will be reserved for validation purposes. It should be noted that the range for liquidity index (I_L) for the calibration of the proportional constant ω was extremely narrow. A linear correlation (Figure 3-25) between the product of I_L and m, and ω was obtained as follows,

$$\omega = 4.2 - 0.1 I_L m \quad 3\text{-}21$$

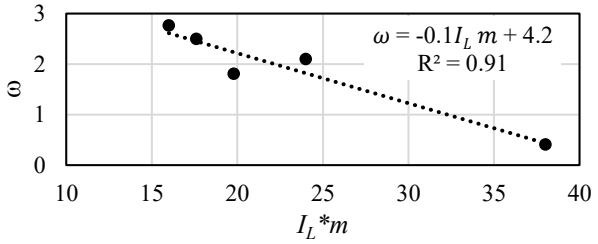

Figure 3-25. Determination of the dependency of ω on the clay unit weight (m) and the liquidity index (I_L)

Replacing ω in Equation 3-20, the equation to determine retrogression distance is,

$$RD = \frac{\frac{2}{3}mH - \int_{\gamma_p}^{\gamma_R}\left[s_{uR} + \left(s_{up} - s_{uR}\right) \times \alpha \times e^{-\beta\gamma}\right]d\gamma - \left[\frac{1}{2}\left(s_{uR} + s_{ur}\right) \times \left(\gamma_r - \gamma_R\right)\right]}{4.2 - 0.1 \times I_L \times m} \qquad 3\text{-}22$$

This equation is now applied to the two remaining locations for validation. For the eastern Canadian site, Rockcliffe equation 3-22 gives a retrogression distance very close to what was observed in the field. But for Bekkelaget, equation 3-21 provides a negative value of ω because the unit weight and liquidity index value for this Norweigian site are higher than the Canadian sites with which the ω value has been calibrated. Due to the difference in overall soil properties in Norweigian quick clays to Eastern Canadian sensitive clays, it is suggested that ω should be separately calibrated for Norweigian and Canadian sites. Other empirical methods for estimating the retrogression distance have been compared with the results of Equation 3-22 (Table 3-7). Unlike the previous empirical equations, the proposed equation considers geotechnical and geometrical parameters for the prediction. This equation has the potential for a closer approximation of the observed field data if calibrated against a large data set.

Table 3-7. Comparison of retrogression distances measured from Equation 3-22 with other empirical methods.

Locations	Observed retrogression distance on the field	RD (m) from Equation 22	Average Slope Angle	RD (m) from Quinn et al. (2011) RD = H/6sinA (A = slope angle)	RD (m) from Carson and Lajoie (1981) RD = 4H ~ 27H	RD (m) from Mitchell and Markell (1974) RD = 100 (Ns − 4)	RD (m) from NVE RD = 15H
Cassleman	450	456	20º	21	176~ 1188	560	660
Saint-Barnabé	180	184	37º	19	140 ~1890	1009	1050
Saint-Jude	80	65	16º	18	60 ~ 810	497	450
Saint-Luc-de-Vincennes	110	128	4.5º	74	70 ~ 945	618	525
Sainte-Monique	142	150	24º	18	90 ~ 1215	1377	675
Rockcliffe	76	73	16º	7.37	48.8 ~ 329	N/A	183
Bekkelaget	145	N/A	3º	49	64 ~ 432	1566	240

3.6 CONCLUSIONS

- A new strain-softening equation for sensitive clays was proposed, which effectively reproduces the non-linear behavior observed in post-peak stress-strain curves (Equation 3-10). The equation comprises two distinct segments: an initial exponential strength reduction characterized by a higher rate of strain softening, followed by a final linear strength reduction where the rate of softening is minimal.
- The newly proposed strain-softening equation effectively addresses the challenge of accommodating the large deformation stress-strain behavior of sensitive clays, surpassing the limitations associated with conventional laboratory shear tests. Formulating the equation based on the actual behavior of sensitive clays under large deformations enables accurate prediction of post-peak stress-strain curves for up to the remolded shear stress. This constitutive equation thus may serve as a valuable tool in simulating large deformation problems specific to sensitive clays, enhancing its practicality and utility in such scenarios.
- The comprehensive stress-strain curves generated by the new equation facilitate accurate calculation of the remolding energy in sensitive clay slopes, thereby enabling the prediction of landslide susceptibility to retrogressive failure based on the remolding energy criterion.
- The estimated remolding energies hold the potential for predicting post-failure landslide movements, as exemplified by the formulation of Equation 22, which enables the estimation of post-failure retrogression in six eastern Canadian sites. To further advance the understanding and applicability of the proposed approach, additional studies should be conducted to encompass multiple landslides and explore their suitability in broader contexts. Moreover, undertaking calibration against a larger dataset could significantly improve the equation's capability to closely approximate observed field data.

CHAPTER 4

Article 3: Prediction of retrogressive landslide in the sensitive clays: Incorporating a novel Strain Softening Constitutive Model into the Material Point Method

Zinan Ara Urmi[a], Alba Yerro[b], Ali Saeidi[a] , and Rama Vara Prasad Chavali[a]

[a] Department of Applied Sciences, University of Quebec at Chicoutimi, Saguenay, G7H 2B1, QC, Canada

[b] Department of Civil and Environmental Engineering, Virginia Tech, Blacksburg, Blacksburg, VA 24061, United States

Published, Engineering Geology, Volume 340, 31 July 2024, 107669
https://doi.org/10.1016/j.enggeo.2023.107221

Credit authorship contribution statement

Zinan Ara Urmi: Writing – original draft, Visualization, Validation, Software, Methodology, Formal analysis, Data curation, Conceptualization. **Alba Yerro:** Writing – review & editing, Supervision, Software, Methodology. **Ali Saeidi:** Writing – review & editing, Supervision, Methodology, Funding acquisition. **Rama Vara Prasad Chavali:** Writing – review & editing.

Declaration of competing interest

The authors declare the following financial interests/personal relationships which may be considered as potential competing interests: Ali Saeidi reports financial support was provided by Natural Sciences and Engineering Research Council of Canada (Grant ID: NSERC- 950- 232724). Ali Saeidi reports financial support was provided by HydroQu´ebec (Grant ID: RDCPJ 521771–17). If there are other authors, they declare that they have no known competing financial interests or personal relationships that could have appeared to influence the work reported in this paper.

4.1 ABSTRACT

Sensitive clays, when subjected to large strains, exhibit a unique strain-softening behavior, transforming into a remolded liquid with remarkably low shear strength. When a slope fails, this behavior leads to the remolded clay moving away from its original position, triggering subsequent failures and catastrophic outcomes. To accurately predict such scenarios, it is crucial to incorporate realistic strain-softening characteristics into the constitutive soil model. This paper presents a novel yet practical strain-softening law developed by the authors that effectively captures the post-peak behavior of sensitive clays down to their remolded strength. The softening law is implemented in an elastoplastic Mohr-Coulomb model and incorporated into Anura3D, an open-source software that uses the Material Point Method to simulate large deformations. The constitutive model is calibrated by simulating the stress-strain behavior through direct shear tests conducted at three sensitive clay landslide locations. The accuracy of the overall numerical framework is assessed by predicting the post-failure movements of these landslides. Notably, two of the landslides, Sainte-Monique (1994) and Saint-Jude (2010), have previously been analyzed using other numerical tools, allowing for a comparative analysis with the method presented here. The third landslide, the Saint-Luc-de-Vincennes landslide, representing a composite flow slide and spread, has been numerically simulated for the first time. The post-failure behavior observed in the landslide events is compared with field observations and other numerical analyses. The results show that the MPM models with the proposed strain-softening law can reasonably predict post-failure retrogression and runout distance, which are crucial parameters for determining the risk of landslides in sensitive clays.

Key words: Retrogressive landslide, sensitive clay, numerical modelling, material point method.

4.2 INTRODUCTION

The mechanism behind retrogressive failure in sensitive soil involves various complex features, including the landslide trigger, the formation of shear bands or multiple failure surfaces, the movement of remolded soil, and the progression of the landslide [150]. These complexities pose significant challenges when conducting numerical analyses of sensitive clay landslides. Traditional methods, such as limit equilibrium or finite element strength reduction techniques, face two major issues that render them unsuitable for application

in sensitive clay slopes. Firstly, these conventional approaches have limited capability in predicting landslide initiation and cannot anticipate subsequent failures or runouts in retrogressive landslides. Secondly, the large deformations associated with these landslides can cause mesh tangling in conventional finite element methods. The strain-softening behavior exhibited by sensitive clays, responsible for the intricate failure mechanism, necessitates using sophisticated constitutive soil models and advanced numerical tools capable of handling large deformation problems.

Over the past two decades, considerable progress has been made in addressing large deformation problems in geotechnical engineering. Various mesh-based and meshless numerical frameworks, such as the arbitrary Lagrangian finite element method, the particle finite element method, and the material point method, have been successfully implemented to capture key characteristics of large retrogressive failures [9–11, 94]. Additionally, the development of strain-softening constitutive soil models has further enhanced the ability to model these phenomena effectively. In recent studies, highly non-linear post-peak strain-softening of sensitive clays has inspired the implementation of an exponential strength degradation equation (Equation 4-1) to capture the post-peak soil behavior [9, 10, 93].

$$s_u = s_{ur} + (s_{up} - s_{ur})e^{-3\gamma/\gamma_{95}} \qquad 4\text{-}1$$

where s_u is the degraded shear strength after the peak, γ is the strain corresponding to s_u, and γ_{95} is the strain when the strength is reduced by 95% of the supposed total reduction ($s_{up} - s_{ur}$). Even though 95% strength reduction does not correspond to a wholly remolded state, the strain value at 95% strength reduction is so large that it cannot be attained with conventional laboratory shear tests [44]. To effectively model sensitive clay landslides using the strain-softening equation, one requires the value of the large deformation parameter γ^{95}, which represents the strain value at 95% strength reduction. However, on a laboratory scale, shear tests can reach the strain value, corresponding to at most 40-50% strength reduction with DSS tests and 25-30% with Triaxial tests. This limitation makes it difficult to obtain γ^{95} directly from laboratory tests. Due to the unavailability of γ^{95}, researchers resort to the back analysis method to model sensitive clay landslides. They start with an assumed value of γ^{95}, later, this parameter is adjusted to match the simulation outcome with field observations.

To eliminate the need for back analysis and improve the numerical modeling of sensitive clay landslides, Urmi et al. [151] developed an empirical/ indirect method to determine the large deformation parameter with available laboratory and field investigation results. In the development process, it was found that the strain-softening equation requires modification based on site-specific data. The strain-softening patterns of the nine prehistoric sensitive clay landslide sites revealed that the exponent of the strain-softening curve ($-3/\gamma_{95}$ in equation 1) varies from site to site and isn't constant regarding its relation to the large deformation parameter, γ^{95}. Moreover, the strength reduction is not entirely exponential; at greater strain values, the exponent of the exponential curve reduces to zero; thus, the strength reduction becomes linear. These observations inspired Urmi et al. [151] to propose a new site-specific strain-softening equation (Equation 4-2) based on the strain-softening pattern observed in the sensitive clays of prehistoric landslide locations. Based on the unique non-linear strain-softening behavior each site, it was observed that the exponential strength decrease required two site-specific parameters (α, β) for a better representation. These parameters are derivable from shear stress-strain curves from laboratory shear test results specific to the site in question. Direct Simple Shear (DSS) tests are preferred because they better represent the large deformation strain-softening behavior for progressive failure than triaxial tests [17]. Urmi et al. [151] demonstrated that the exponential behavior characterized by site-specific parameters (α, β), derived from a laboratory-scale partial stress-strain curve, closely approximates the actual behavior of sensitive clays at high strain levels. The crucial aspect is identifying the pattern of exponential decay; even when derived from a limited number of data points on a partial curve, the results remain comparable because the strength decrease adheres to a unique law for a particular site.

The proposed softening equation is a combination of an exponential and linear strength reduction as represented by (Equation 4-2) (Figure 4-1).

$$s_u = \begin{cases} s_{uR} + (s_{up} - s_{uR})\alpha e^{-\beta\gamma}, & s_u \geq s_{uR} \\ s_{uR} - (s_{uR} - s_{ur})\,(\gamma - \gamma_R)/(\gamma_r - \gamma_R), & s_{uR} > s_u \geq s_{ur} \end{cases} \qquad 4\text{-}2$$

Where, s_{uR} is the residual strength defined as the degraded strength up to which the strength reduction is exponential and can be determined by

$$s_{uR} = 0.095 s_{up} \quad 4\text{-}3$$

γ_R is the corresponding residual strain at s_{uR}. γ_r is the strain at the remolded shear strength s_{ur} that can be estimated as,

$$\gamma_r = 0.13 s_{up} \gamma_R \quad 4\text{-}4$$

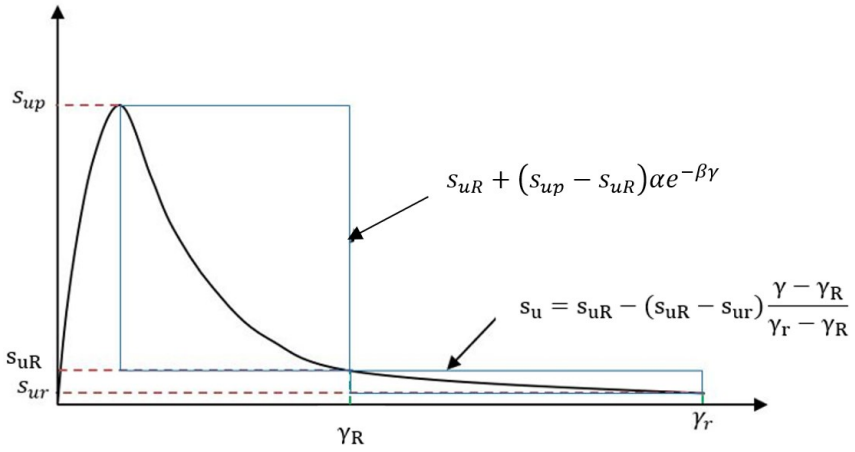

Figure 4-1. Strain-softening behavior of sensitive clays (after [151])

Using equation 4-2 facilitates the determination of the strain value at remolded shear stress (γ_r). The strain value at the remolded shear stress is particularly important because it completes the strength reduction curve and thus facilitates the evaluation of dissipated energy during the remolding, which is the area under the stress-strain curve. For more detailed information on the development process of equation 4-2 and its application to landslide risk analysis, readers are encouraged to read Urmi et al. [151].

In this study, the strength of the sensitive clay was modeled using a non-associated Mohr-Coulomb constitutive model with an additional strain-softening law described by equation 4-2, where the reduction in cohesion is equivalent to the degradation of undrained shear strength. For retrogressive failure analysis under undrained conditions, the friction angle in the Mohr-Coulomb model is set to zero, making it comparable to the Tresca softening model. For this study, equation 4-2 has been employed on an elastoplastic constitutive model obeying the Tresca failure criterion, which considers the undrained shear strength (s_u) of the material as an

input parameter. Although this is a basic constitutive model, the incorporation of strain softening law on the Tresca or Von Mises criteria has been frequently used in simulating sensitive clay landslides under undrained conditions [9, 10, 93, 94, 152].

The primary objective of this paper is to validate the effectiveness of the new strain-softening equation to simulate sensitive clay landslides by implementing it in the Anura3D software, which utilizes a Material Point Method (MPM) framework [153]. The choice of MPM is motivated by its previous successful use in demonstrating its capabilities to capture large deformations and shear band formation in retrogressive sensitive clay spread failures [9, 83].

The objective of the study is to implement and test a novel strain-softening law in Anura3D for predicting retrogressive landslides in sensitive clay. This objective was achieved through the following steps. Firstly, direct shear tests were simulated to validate the implementation of the strain-softening equation in a user-defined constitutive soil model in Anura 3D. This step evaluates the numerical model's reliability in predicting site-specific post-peak stress-strain behavior of sensitive clays. Next, the constitutive parameters of the softening equation were calibrated using the smeared crack approach through direct shear tests with different mesh sizes to mitigate the effect of mesh dependency when implementing strain-softening in a continuum numerical framework. The model was then validated by predicting the post-failure movement of three previously occurred sensitive clay landslides. A comparison was then conducted between the predicted post-failure behavior and the observed behavior in the field for all three case studies, allowing for insights into the use of numerical analysis in understanding the underlying mechanism of such failures.

This study focuses on three distinct landslide events in Quebec, Canada: Sainte-Monique (1994), Saint-Jude (2010), and Saint-Luc-de-Vincennes (2016). It leverages the available numerical simulations of the Sainte-Monique and Saint-Jude landslides for comparative analysis and testing the effectiveness of the employed numerical framework. The Saint-Luc-de-Vincennes landslide, a composite flow slide and spread, presents a unique challenge and opportunity: it has not been previously modeled. Therefore, this study is the first one to apply the proposed constitutive model to this complex event, assessing its suitability in capturing the dual nature

of the landslide; it highlights the need for innovative approaches in the analysis of retrogressive failure in sensitive clays.

4.3 BASIS OF MPM FRAMEWORK

The Material Point Method (MPM) represents a computational methodology initially formed by Harlow as the Particle-In-Cell method (PIC) at Los Alamos National Laboratory [154]. Primarily designed for fluid dynamics, the methodology was later expanded by Sulsky and Schreyer [35] at New Mexico University to accommodate solid mechanics challenges, specifically discretizing the dynamic momentum balance equation [155]. Positioned between particle-based techniques and the Finite Element Method (FEM), MPM employs a dual discretization approach. In the first frame, the continuum undergoes discretization into material points (MPs), each signifying a sub-domain with an invariant mass to ensure conservation (Figure 4-2). The classical MPM assumes mass concentration at the respective MP, encapsulating velocities, strains, and stresses. These MPs exhibit Lagrangian characteristics as they move with the deformations of the body. The second frame involves a computational mesh like the conventional FEM, encompassing the complete problem domain. Discrete governing equations are solved at mesh nodes, and variables are mapped from MPs to mesh nodes using mapping functions, typically linear shape functions. Boundary conditions may be imposed at mesh nodes or MPs, and the governing equations are incrementally solved. Finally, Material Point (MP) quantities are updated by interpolating mesh results without storing mesh information permanently. Not storing this information allows the mesh to be redefined at the end of each time step, although conventionally, the mesh stays the same.

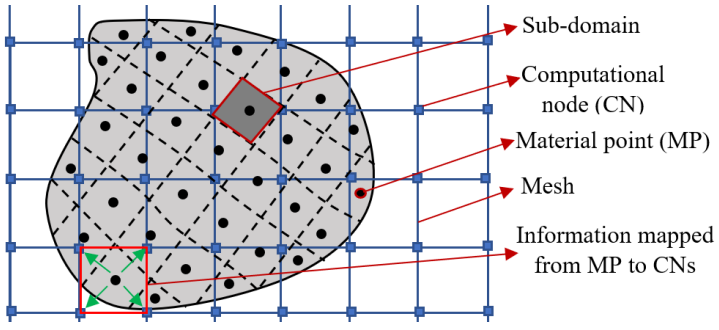

Figure 4-2. Spatial formulation of MPM framework (after [133])

The MPM approach provides a robust framework for analyzing complex geotechnical problems. Through its unique formulation and data transfer mechanism between MPs and computational nodes, the MPM technique can accurately simulate the behavior of slopes and other geotechnical systems, capturing their dynamic responses and interactions [156–159].

4.4 STRAIN-SOFTENING MODEL CALIBRATION: SIMULATION OF DIRECT SHEAR TESTS

Locat et al. [17, 18, 46] and Durand [14] conducted multiple direct simple shear (DSS) tests using soil samples taken from the sensitive clay layers at three sites affected by previous landslides, i.e., Sainte-Monique, Saint-Jude, and Saint-Luc-de-Vinecenne. They aimed to study the shear behavior of the clay involved in such landslides. Soil samples, with dimensions of 14mm in height and 67.8mm in diameter, were subjected to consolidation under a vertical stress level that closely matched the in-situ conditions corresponding to the depths from which the samples were obtained. The samples were placed inside plastic rings to prevent lateral deformation during consolidation. Shearing was conducted laterally by a motor, applying a horizontal strain rate of 0.7 mm/min at the top of the sample while the base remained fixed.

These tests were replicated in Anura3D, considering loading and boundary conditions consistent with the laboratory tests, as shown in Figure 4-3. In particular, plain strain conditions were considered, and an initial rectangular domain (with a height equal to the sample's height as measured in laboratory testing) was divided into triangular elements (base length = height = 0.014m) discretized with 46 MPs each. A total stress analysis is performed in undrained conditions. A prescribed velocity of 0.01mm/sec, consistent with the horizontal strain rate used in the laboratory shear test, was applied at the top of the row of nodes to generate the DSS total stress path. A damping factor is assumed to be 2% to reduce numerical instabilities, consistent with similar studies [160] . Input material parameters for the simulations are listed in Table 4-1. Soil properties are obtained from the respective sites' detailed field investigation reports by Locat et al. (2017, 2015, 2013) and Tremblay-Auger et al. (2021). Specific parameters ($s_{uR}, \alpha, \beta, \gamma_R, \gamma_r$) for the softening equation (Equation 4-2) are based on laboratory test results obtained with a detailed methodology described in [151]. The earth-pressure coefficient and Poisson's ratio are adopted from previous studies that have conducted numerical analyses specifically on the sites under consideration [9, 18, 93, 160]. The shear modulus of Eastern Canadian sensitive clays is typically

lower than that of other clay soils, with values ranging from approximately $G \cong 30s_{up}$ to $100s_{up}$ [45]. For this study, the shear modulus is directly interpreted from the shear stress-strain curve obtained from the laboratory DSS test for each site, assuming that the behavior is elastic up to peak shear strength (Shear modulus, $G=s_{up}/\gamma_p$).

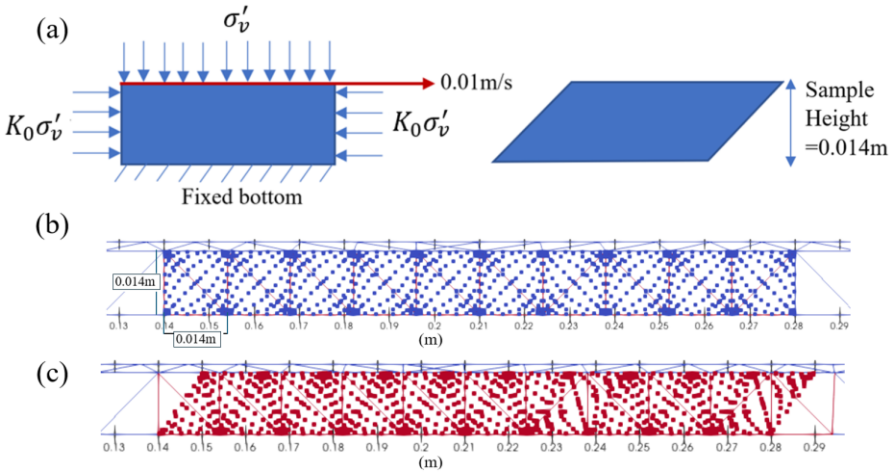

Figure 4-3. (a) Loading conditions; configuration of material points (b) initial and (c) final.

Table 4-1. Input parameters for the numerical simulation of DSS tests

Parameter	Sainte-Monique	Saint-Jude	Saint-Luc-de-Vincennes
Natural weight of soil, m	16 kN/m^3	16.5kN/m^3	16 kN/m^3
Effective vertical stress, σ_v'	93kPa	170kPa	168kPa
The coefficient of lateral earth pressure at rest, K_0	0.5	0.5	0.5
Shear Modulus, $G=\frac{s_{up}}{\gamma_p}$	4050kPa	4580kPa	4583kPa
Undrained Poisson's ratio, μ	0.45	0.45	0.45
Peak shear strength, s_{up}	40.5 kPa	55 kPa	55 kPa
Peak shear strain, γ_p	0.01	0.014	0.012
Remolded shear strength, s_{ur}	0.736 kPa	0.92 kPa	1.375 kPa
Residual strain, γ_R	1.8	2.4	1.95
Site-specific constant, α	0.95	1.049	0.945
Site-specific constant, β	2.8	2.5	2.9

Figure 4-4 (a-c) shows the stress-strain behavior predicted by the model and the softening equation and how well it complies with the laboratory direct shear test results. It can be observed that the constitutive equation has been well implemented in the numerical model to accurately depict the stress-strain behavior of sensitive clays up to the remolded strength. Additionally, the simulated direct shear test results closely resemble those

obtained from laboratory tests, particularly within the laboratory's maximum strain range. These observations suggest that this constitutive model is a reliable tool for predicting the material behavior of sensitive clays under undrained shear loading.

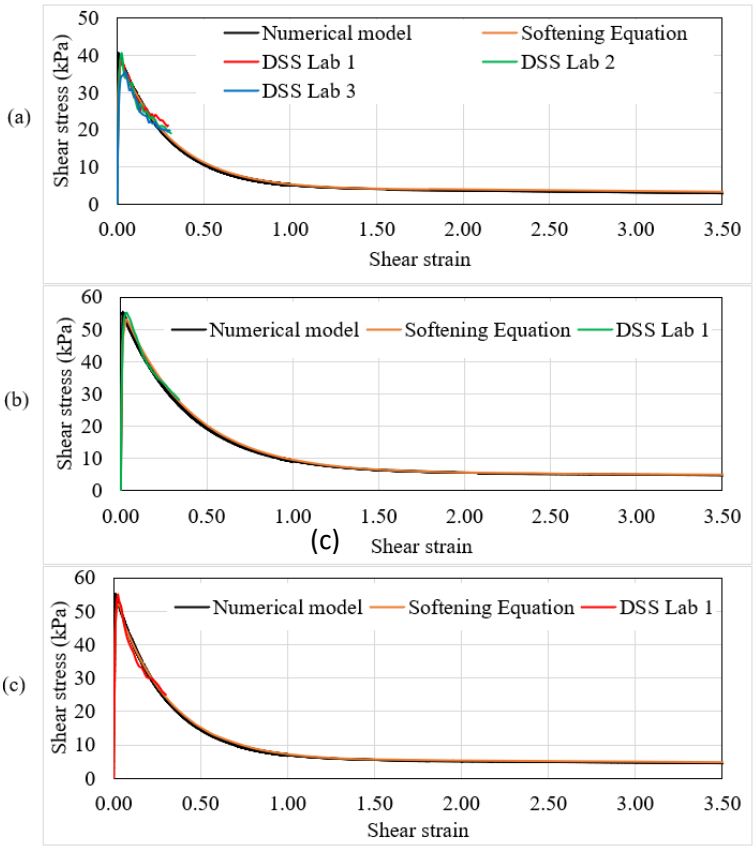

Figure 4-4 (a-c). Stress-strain behavior is depicted in the numerical model, softening equation, and DSS laboratory tests for Sainte-Monique, Saint-Jude, and Saint-Luc sites, respectively.

4.5 DESCRIPTION OF THE NUMERICAL MODELS

Figure 4-5 illustrates two-dimensional plane strain models for the numerical simulation of the Sainte-Monique (1994), Saint-Jude (2010), and Saint-Luc-de-vincennes (2016) landslide. The models' dimensions are determined based on the in-situ topography, as detailed in a study by Locat et al. [17, 18, 46] and Trembley-Auger et al. [161].

For the Sainte-Monique site (Figure 4-5a), the dimensions of the left-hand riverbank in the studied area are 21.7 meters in height and 183 meters in length. The right-hand embankment, which prevents further sliding, is 11 meters high and 57 meters long. The length of the slope at the left side of the brook is 37 m with a slope angle of 24°, while the right-hand slope is 25 m in length with a slope angle of 26°. The soil slope comprised a very thin 2m sandy crust (C1), with a thick sensitive clay layer up to 40m depth. According to the soil investigation results (Figure 4-6a), the undrained shear strength remains relatively constant from a depth of 2 to 10m, measuring at 25kPa. Progressing to a depth of 10 to 20m, an increase from 30 to 50kPa is observed, resulting in an average overall shear strength of 40kPa. Notably, a direct shear test at 13.5m depth revealed a shear strength of 40.5kPa. The shear strength rises from 50 to 70kPa between 20 to 25m depth. A layer of sensitive clay (S1) has been incorporated up to the slope's toe, showcasing a peak shear strength matching that of the Direct Shear Test (DSS) at 40.5kPa. A 5-m layer of sensitive clay (B1) below the slope's toe is taken to account for the higher shear strength observed in deeper layers. This lower layer has a shear strength of 55kPa, contributing to a more comprehensive representation of the subsurface conditions. The material properties for the numerical model of the Sainte-Monique site are listed in Table 4-2. The crust layer is defined with an elastic, perfectly plastic constitutive soil model.

Table 4-2. Input parameters for the numerical simulation of the Sainte-Monique landslide.

Parameter	Crust (C1)	Sensitive clay layer1 (S1)	Sensitive clay layer2 (B1)
Natural weight of soil, m	18 kN/m^3	17 kN/m^3	17 kN/m^3
The coefficient of lateral earth pressure at rest, K_0	0.5	0.5	0.5
Shear Modulus, $G=\frac{s_{up}}{\gamma_p}$	-	4050kPa	4050kPa
Elastic modulus, E	10000kPa	-	-
Undrained Poisson's ratio, μ	0.45	0.45	0.45
Peak shear strength, s_{up}	90 kPa	40.5 kPa	55 kPa
Peak shear strain, γ_p	-	0.01	0.01
Remolded shear strength, s_{ur}	-	1 kPa	1 kPa
Residual strain, γ_R	-	1.8	1.8
Site-specific constant, α	-	.95	.95
Site-specific constant, β	-	2.8	2.8

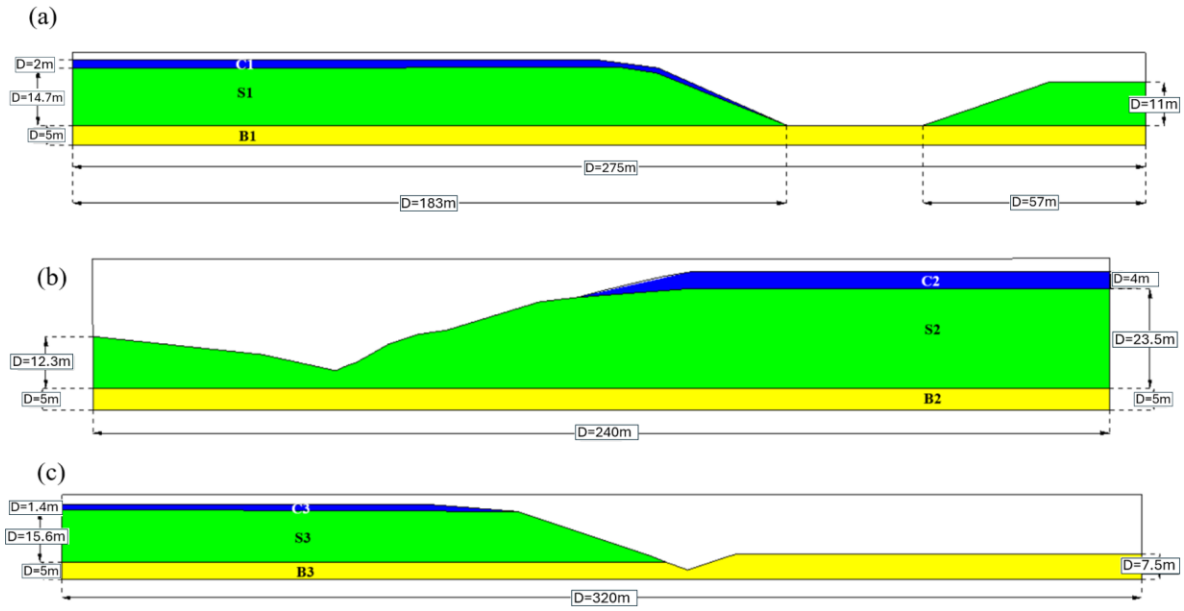

Figure 4-5. The geometry of the slope used in the numerical model (a) Sainte-Monique, (b) Saint-Jude, (c) Saint-Luc-de-Vincennes.

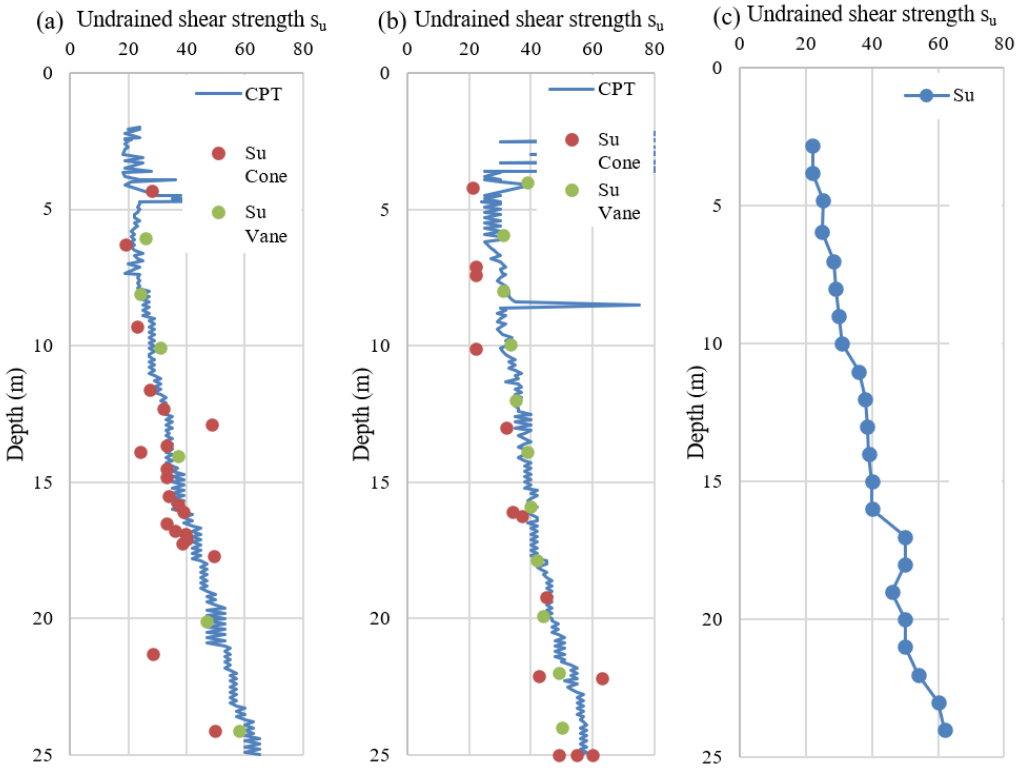

Figure 4-6. Depth-wise variation of undrained shear strength ; (a) Sainte-Monique, (b) Saint-Jude, (c) Saint-Luc-de-Vincennes.

For the Saint-Jude site (Figure 4-5b), the slope profile is based on stereophotogrammetry and field investigation data from the report by Locat et al. [18]. The bottom of the river channel is 4.5 m above the lower boundary of the sensitive clay layer. The total height of the slope on the right side of the river is 32.5m, with a slope angle near the toe of 40˚, transitioning to a milder angle ranging between 12 and 20˚ in the upper part. The ground surface on the right side of the slope crest is almost horizontal. The profile consists of a 4-m thick crust below the ground surface (Material C2), followed by a 23.5m thick sensitive clay layer (Material S2). In the field investigation report, there were three soil layers with relatively high shear strength are found below the sensitive clay layer and above the bedrock. These layers had a combined thickness of approximately 17m. For the numerical modeling, these three layers have been simplified as a single soil layer (Material B2) with a depth of 5m, as varying the layers' thickness or number of layers did not significantly affect the slope failure behavior [62]. The material properties for the numerical simulation of the Saint-Jude site are presented in Table 4-3. An elastic, perfectly plastic model defines the crust and the stiffer layer. The shear strength parameters of the crust and the till layer are obtained by averaging the shear strength data obtained through field investigation (Figure 4-6b), corresponding to specific depths of the layers.

Table 4-3. Input parameters for the numerical simulation of the Saint-Jude landslide.

Parameter	Crust (C2)	Sensitive clay layer (S2)	Stiffer soil layer (B2)
Natural weight of soil, m	18 kN/m^3	16.5 kN/m^3	17 kN/m^3
The coefficient of lateral earth pressure at rest, K_0	0.5	0.5	0.5
Shear Modulus, $G=\frac{s_{up}}{\gamma_p}$	-	4580kPa	-
Elastic modulus, E	10000 kPa	-	10000 kPa
Undrained Poisson's ratio, μ	0.45	0.45	0.45
Peak shear strength, s_{up}	30 kPa	55 kPa	80 kPa
Peak shear strain, γ_p	-	0.014	-
Remolded shear strength, s_{ur}	-	0.92 kPa	-
Residual strain, γ_R	-	2.4	-
Site-specific constant, α	-	1.04	-
Site-specific constant, β	-	2.5	-

For the Saint-Luc-de-Vincennes site, the analyzed slope extends over 320m, with the left and right embankments measuring 25m and 10m in height, respectively [161]. The geological composition exhibits

distinct layers. Starting from the uppermost stratum, a silty-sandy crust layer (Material C3) persists down to a depth of 1.4m, succeeded by a sensitive clay unit spanning from 1.4 to 15.5m (Material S3), followed by a stiffer sensitive clay layer (Material B3). In the analysis, two distinct layers of sensitive clay are considered to account for the variation in undrained shear strength with depth (Figure 4-6c). For the first layer (S3), a constant peak shear strength of sensitive clay is considered in the model, which is consistent with the DSS test. To represent the sharp increase in shear strength after 15.5m, a sensitive clay layer (B3) with a higher peak strength has been considered beyond this point. All material parameters of the simulation are summarized in Table 4-4. The crust layer is defined with an elastic, perfectly plastic constitutive soil model.

Table 4-4. Input parameters for the numerical simulation of the Saint-Luc-de-Vincennes landslide.

Parameter	Crust (C3)	Sensitive clay layer 1(S3)	Sensitive clay layer 2 (B3)
Natural weight of soil, m	18 kN/m^3	17 kN/m^3	17 kN/m^3
The coefficient of lateral earth pressure at rest, K_0	0.5	0.5	0.5
Shear Modulus, $G=\frac{s_{up}}{\gamma_p}$	-	4583kPa	4583kPa
Elastic Modulus, E	10000kPa	-	-
Undrained Poisson's ratio, μ	0.45	0.45	0.45
Peak shear strength, s_{up}	25 kPa	55 kPa	70 kPa
Peak shear strain, γ_p	-	0.012	0.012
Remolded shear strength, s_{ur}	-	1.375 kPa	1.375 kPa
Residual strain, γ_R	-	1.95	1.95
Site-specific constant, α	-	0.945	0.945
Site-specific constant, β	-	2.9	2.9

When simulating real-scale landslides, selecting an appropriate mesh size is crucial when dealing with mesh-based continuum numerical methods that incorporate strain-softening features because they result in mesh-dependent strain localization problems and can result in different failure and post-failure predictions [162]. While simulating direct shear tests with a mesh size consistent with the soil specimen tested in the lab (laboratory scale) provides accurate stress-strain results, employing the same element size for real-scale landslide simulations becomes computationally very expensive. On the other hand, while coarser meshes are computationally more efficient, they can lead to erroneous outcomes if localization problems are not addressed.

The smeared crack approach [24] is a simple regularization technique that has been previously used in MPM to address the issue [159, 163, 164]. This approach assumes that the total work dissipated by a shear band is equivalent to the fracture energy dissipated in a discrete crack, and consistency in the dissipated work across shear bands of different element sizes ensures consistent results, irrespective of the mesh size employed. This can be achieved by conducting a series of numerical shear tests using various element sizes suitable for field scale modeling. By calibrating large deformation parameters of the softening equation, it is possible to ensure that the area under the stress-displacement curve (dissipated work) is equal for field scale and laboratory scale element sizes. If the dissipated energy is equal in the shearing process, the post-failure movements should be similar per the smeared crack approach.

To achieve this, direct shear tests are simulated for all three sites using a mesh size of 0.5m, which is the mesh size adopted in the landslide models at the field scale. Both laboratory and field scale direct shear tests provide individual stress-strain curves. The stress-displacement curves for each case are obtained by multiplying the strain values by the element size. The dissipated energy in the shearing process is calculated by integrating the areas under the stress-displacement curves for each element size. To reduce mesh dependency, it is essential to ensure these areas are equal. Since the major part of the stress-displacement curves is exponential, the most straightforward method to adjust the area under the curve is by modifying the exponent of the curve, referred to as the β value. Calibrating the β value, a unique value of β was obtained for each field scale DSS simulation that produces an equal area under the stress-displacement curve obtained from the laboratory scale DSS simulation.

The stress-displacement curves employed for the β calibration are depicted in Figure 4-7, and the calibrated β values are presented in Table 4-5.

Table 4-5 . Calibration of β for 0.5m Element Size (ES).

Parameter	Sainte-Monique	Saint-Jude	Saint-Luc-de-Vincennes
For Element Size 0.014m Site-specific constant, β	2.9	2.5	2.9
For Element Size 0.5m Site-specific constant, β	105	80	90

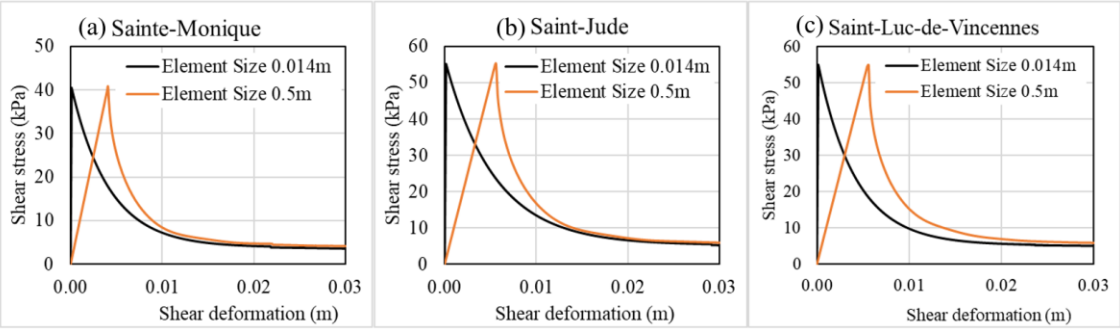

Figure 4-7 (a-c). Calibration of β for 0.5m Element Size (ES).

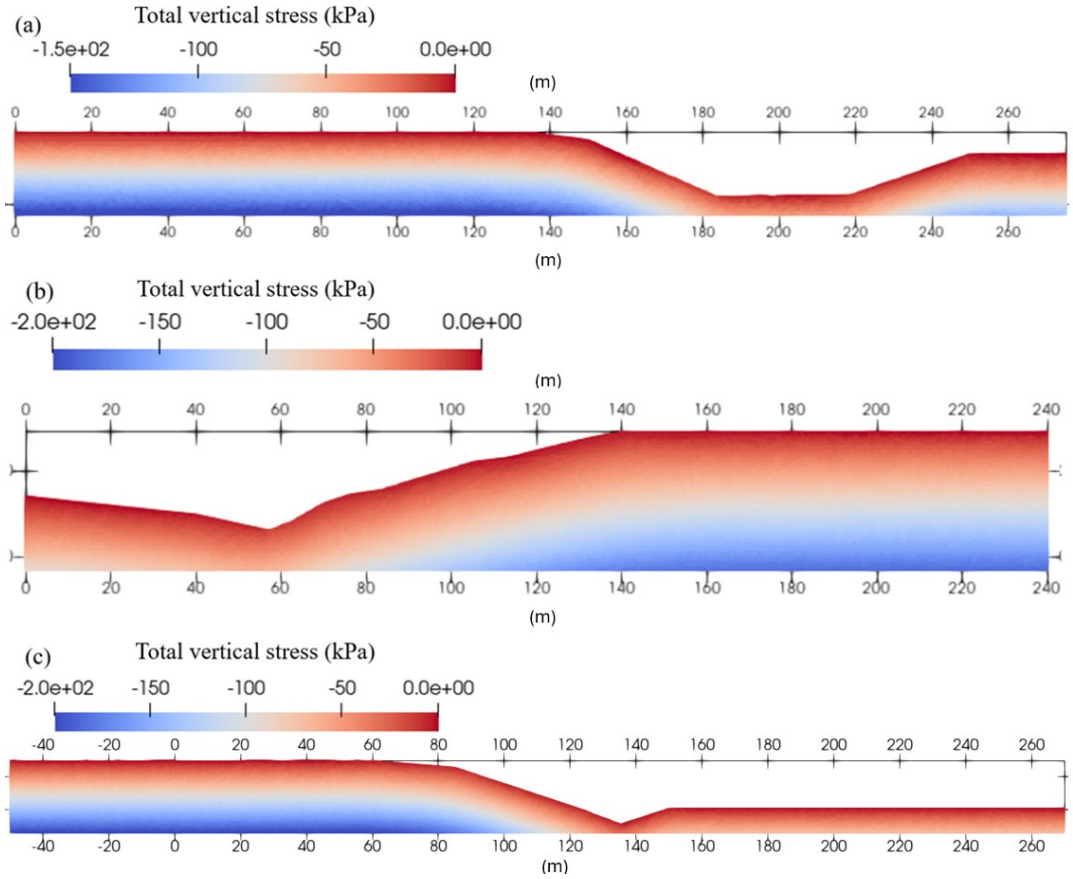

Figure 4-8. Total vertical stress of the slope; (a) Sainte-Monique, (b) Saint-Jude, (c) Saint-Luc-de-Vincennes

For all three cases, a single-phase total stress MPM formulation is considered; hence, excess pore pressure is not calculated. It is generally believed that the undrained strain softening is the result of increased

pore water pressure in undrained shearing. By implementing the strain-softening behavior, the numerical model captures the response of increased pore water pressure in undrained shearing, simulating the reduction in effective stress and its impact on shearing resistance. The left and right boundaries were fixed horizontally, and the bottom boundary was fixed vertically. The initial stress conditions (Figure 4-8) were generated by gravity loading in drained condition using drained shear strength obtained from site investigation as presented in

Table 4-6 [17, 18, 161]. As the clay is normally to slightly overconsolidated, the earth pressure coefficient Ko was selected to be 0.5. The effective poisson's ratio was 0.33, derived from Ko.

Table 4-6. Material parameters for the initial stress condition by gravity loading

Parameter	C1	S1	B1	C2	S2	B2	C3	S3	B3
Effective cohesion, c′ (kPa)	0	3.7	3.7	0	7.7	7.7	2	7.6	7.6
Friction angle, φ′ (Degrees)	35	30.6	30.6	35	35	45	30	32	32

The calculation process can be summarized in two main steps follows.

- First, the stresses were initialized by applying gravity loading using drained soil strength parameters Table 4-6 using an elastoplastic Mohr-Coulomb constitutive soil model was used without strain softening, and slope stability was attained. In this stage, the material behaves mainly elastically, and failure was consistently not reached. The homogeneous local damping in this stage was set to 0.75, given that stress initialization should be a quasi-static problem, and the approach of applying artificial local damping is utilized to enhance numerical convergence speed, as recommended by Ceccato and Simonini [165].
- In the second calculation step, the failure is triggered by switching the material parameters to be consistent with undrained conditions, as summarized in Table 4-2, Table 4-3, Table 4-4 and with the calibrated β value for 0.5m element size from Table 4-5. A local damping of 0.02 is employed in this stage to facilitate dynamic analysis.

4.6 RESULT AND DISCUSSION

4.6.1 Failure mechanism observed in the simulation compared to the literature and field observation

4.6.1.1 Sainte-Monique Landslide

After the gravity loading (Figure 4-9a), the soil is stable with an undrained shear strength of 40kPa, and the strain starts to localize in a thin shear band as soon as strain softening is activated from step 3 (Figure 4-9b). Failure propagates horizontally through the layer opposite to the river producing a slide bottom "ba"; simultaneously, a slip surface "bc" is formed at an angle of 55^{o} parallel to the slide bottom (Figure 4-9c). When stresses along "bc" reach near zero, the soil mass starts to slip, forming a wedge "abc" (Figure 4-9c). When "abc" moves forward, the drag of this slip causes a rupture "de" almost parallel to "bc." By this time, the slide bottom has already reached point "d" (Figure 4-9d), and a secondary failure surface along "cd" creates a wedge "cde". The wedge "cde" sinks from its original position, creating a graben which leaves a horst at "bcd" (Figure 4-9e). Thus, the whole strip "AA'" forms in a retrogressive and discontinuous manner (Figure 4-9f) and slips into the river with an almost horizontal (slightly inclined towards the bottom) translatory movement. During the movement, tension cracks are formed within the wedges, contributing to the formation of horst and graben-like structures. Similarly, strips BB' (Figure 4-9j) form. During the formation of strip CC' (Figure 4-9k), the front portion of the moving debris is arrested on the other side of the river, and the landslide movement starts to cease. Then, strips CC' (Figure 4-9n) and DD' (Figure 4-9p) are formed. After this point, no more tension cracks are formed, and the formation of horst and grabens is straightforward, with the formation of primary and secondary alternate failure surfaces, as presented in Figure 4-9c-d. Similarly, strips DD', EE', and FF' forms, each having one horst and one graben (Figure 4-9l-n). The landslide completely stops when strip FF' propagates about 4m from its original position (Figure 4-9n). The final retrogression distance is about 103m from the original position of the crest. The tip angles of the horsts are 70 degrees on average. The failure observed mechanism perfectly complies with the description of the spread mechanism of Odenstad [78] and Carson [70] as summarized in Urmi et al. [150].

The numerical simulation accurately captured the retrogression observed in the field, resulting in a similar retrogression distance and post-failure geometry (Figure 4-10). The crest-to-crest retrogression was

100m observed in the field and 103m as per the numerical model. A comparison of the simulation's post-failure features with the field observation by Locat et al. [17] reveals several similarities.

- The landslide debris remained inside the crater, with the opposite side of the brook obstructing the flow and resulting in minimal lateral movement, as observed in the field.
- Several ridges were visible with intact material, and some had sharp tips pointing upwards, referred to as horsts, with tip angles mostly varying between 70 degrees. The field observations noted that the tip angle of the horst closely resembled the active failure angle observed in eastern Canadian clays, approximately 60 degrees. Other blocks within the debris had flat, horizontal tops called grabens, which were not entirely separated and could be connected by vegetation, as observed in the field.
- The soil mass moved horizontally in an active failure mode, similar to the field.

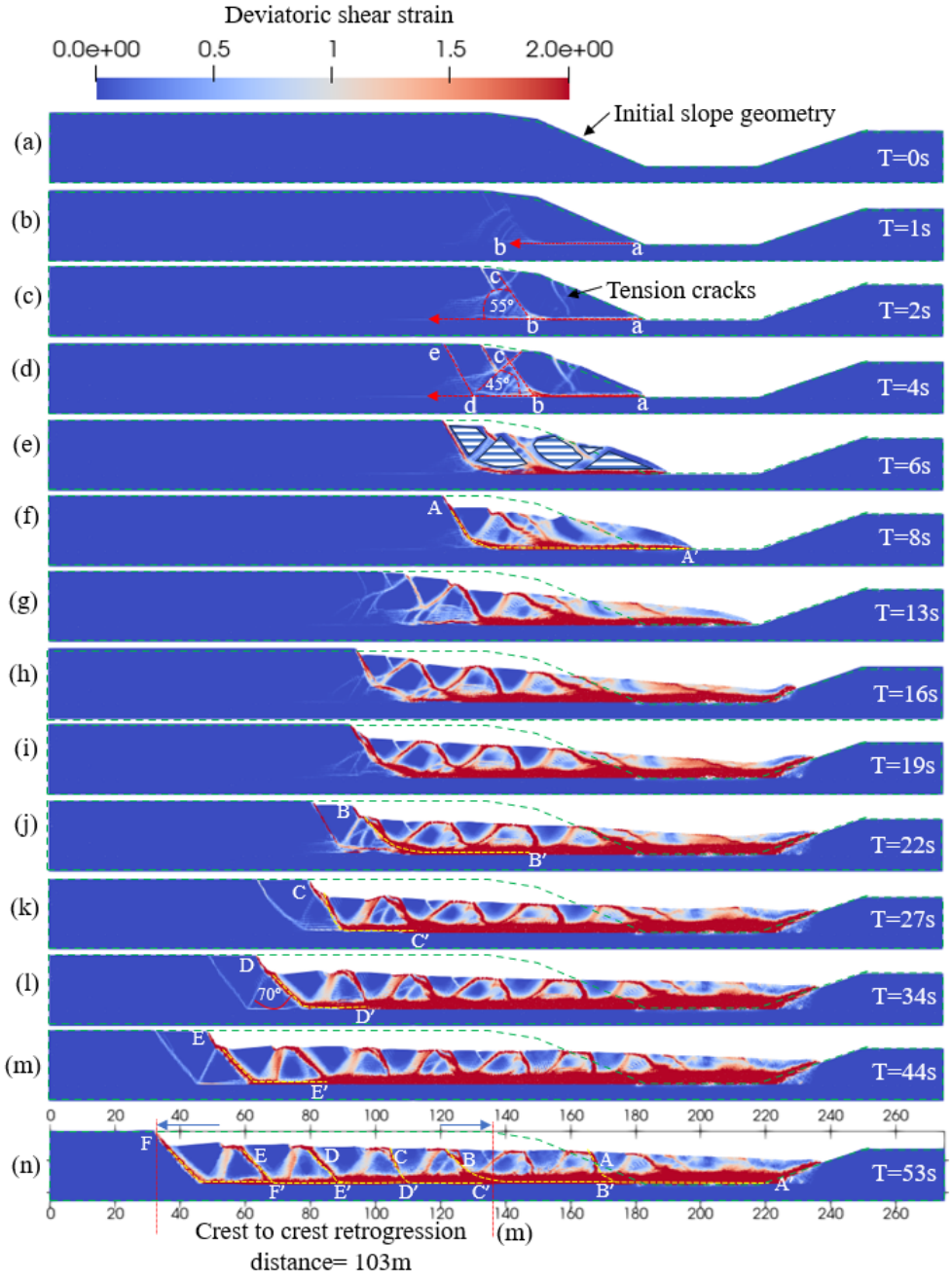

Figure 4-9. The failure mechanism of simulated retrogressive Sainte-Monique landslide

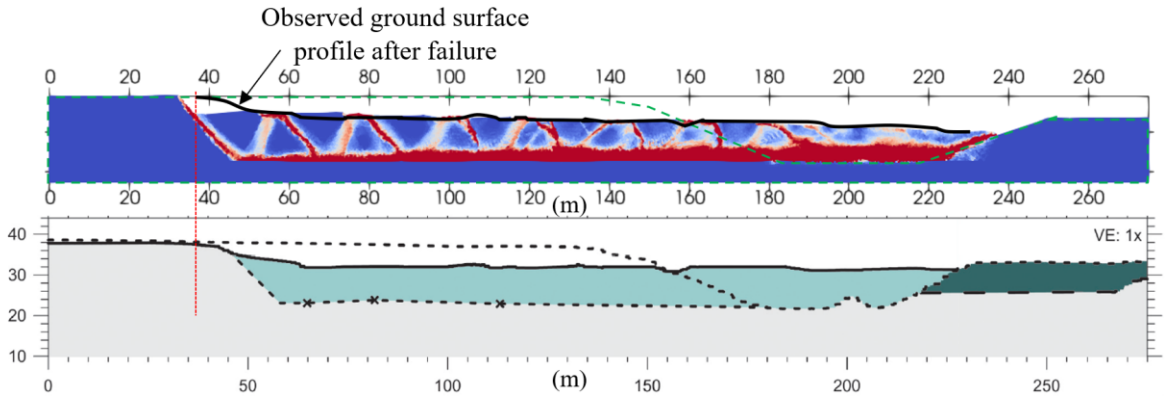

Figure 4-10. Comparison of the post-failure geometry of the simulated model and field observation by Locat et al. [17] of Sainte-Monique landslide

.

4.6.1.2 Saint-Jude landslide

After the gravity loading (a), the slope is stable with an undrained shear strength of 55kPa, and the strain starts to localize in a thin shear band as soon as strain softening is activated from step 3 (Figure 4-11b). A circular failure surface, “abc” forms from the toe of the slope. When stresses along the shear band reduce, resulting from the large straining and the strain-softening behavior, the clay within becomes fully remolded, and the slope mass starts displacing towards the river in a translatory movement (Figure 4-11c). As strain concentration intensifies within the shear band, the enclosed soil mass experiences lateral spreading. This lateral expansion leads to strain localization within the central portion of the moving soil, dividing the soil mass into two distinct segmented blocks (Figure 4-11d-e). The movement of the liquified debris generates another failure surface, labeled “def,” characterized by numerous secondary shear bands. These shear bands fracture the soil mass into segmented blocks. These segmented blocks appear as horst and grabens, generally observed in spread failures. This mechanism of spread failure is similar to Mollard and Hughes's [79] description of spread failure. The third and final rupture occurs as a wedge “ghi,” and the movement of the debris ceases at 32s after the failure is triggered, with a final crest-to-crest retrogression distance of 70m, which is 10m less than that of the field observation. The prediction of the model was 87.5% accurate. Despite this difference, the post-failure geometry of the simulated slope is very similar to the field observation (Figure 4-12). A comparison of the simulation's post-failure features with the field observation by Locat et al. [18] reveals the following similarities and deviations.

- The failure surface was identified as 2.5m below the river's level by CPTu and progressed nearly horizontally for 100 m within the undisturbed deposit. In the numerical analysis, the failure surface formed around 3m beneath the river elevation and propagated roughly 65m horizontally within the intact deposit.
- In line with the field data, the modeled slope moved to the opposite side of the river, causing minimal disturbance in the debris. Behind it, the soil mass split into multiple segments, adopting horst and graben formations.
- A secondary failure surface, approximately 10m higher than the primary one, was also identified using CPTUs. In contrast, the failure surfaces in the model were at the same elevation.
- The simulated debris movement was mainly translational with minimal or no rotation with a continuous failure surface, as observed in the field.
- The location of the crust layer after failure observed in both the field and the numerical analysis closely align with each other, as illustrated in Figure 4-13.

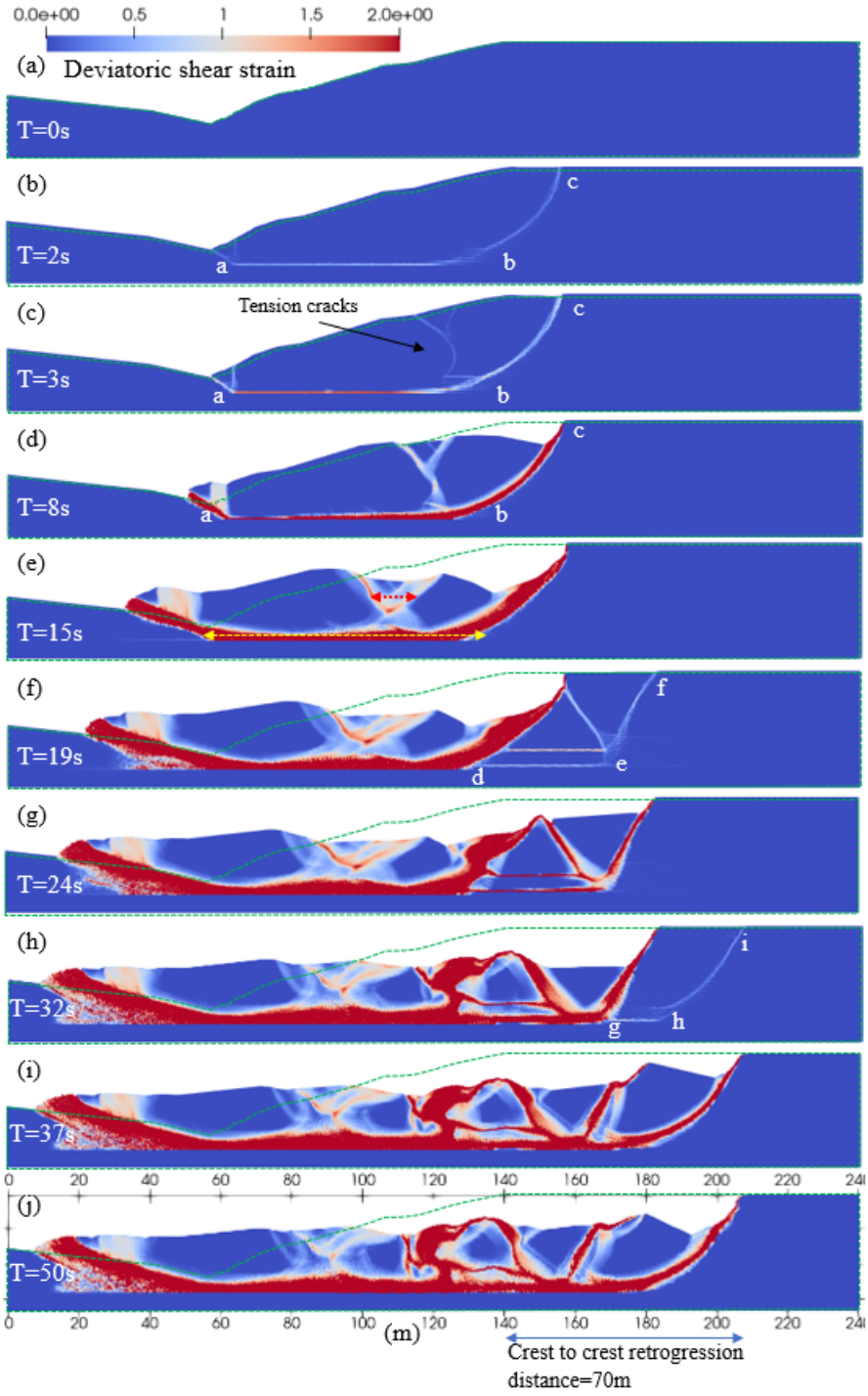

Figure 4-11. The failure mechanism of simulated retrogressive Saint-Jude landslide.

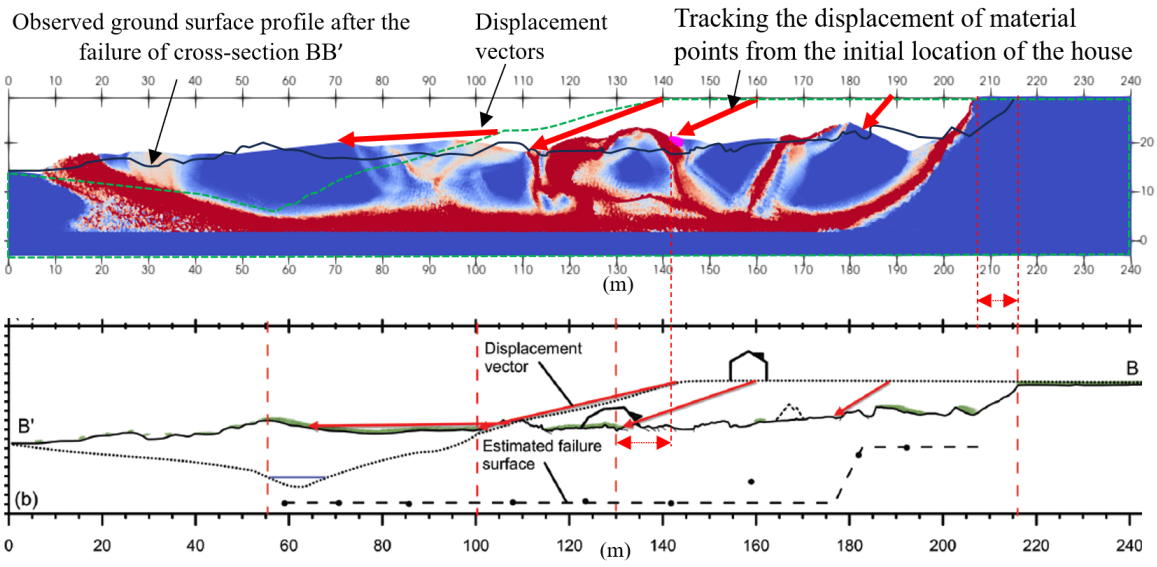

Figure 4-12. Comparison of the post-failure geometry of the simulated model and field observation of Saint-Jude landslide of Locat et al. [18].

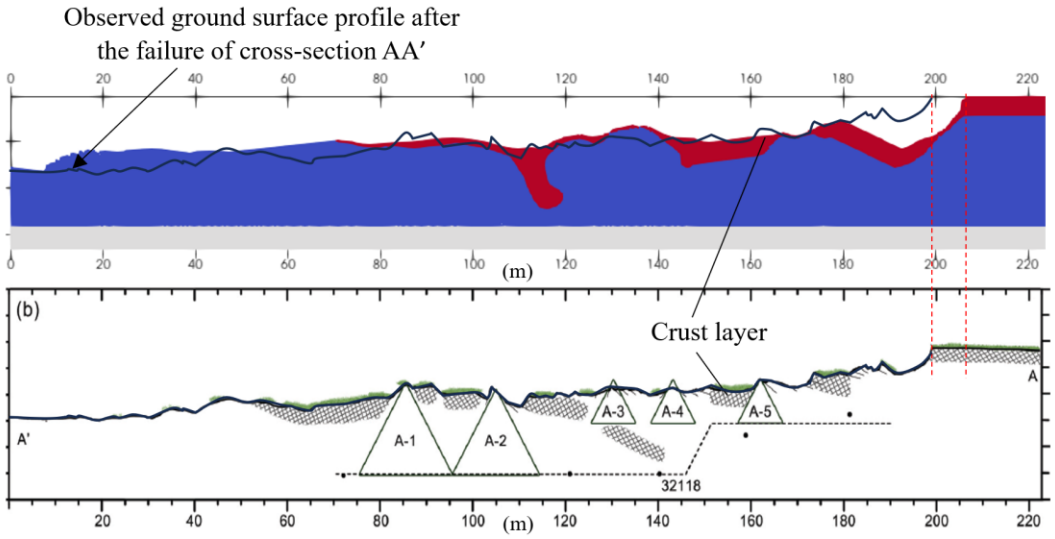

Figure 4-13. Comparison of the position of the crust layer the numerical simulation of this study with Locat et al.'s [18] post-failure field observations of Saint-Jude landslide.

4.6.1.3 Saint-Luc-de-Vincennes

After the initial gravity loading as depicted in Figure 4-14a, the soil remains stable, exhibiting an undrained shear strength of 55kPa. However, upon activating strain softening from step 3, as illustrated in Figure 4-14b, strain begins to localize within a narrow shear band. This shear band formation is analogous to

that observed in the Saint-Monique landslide, where tension cracks and alternating shear bands lead to the formation of strip AA' (Figure 4-14e). This strip then experiences rapid flow (Figure 4-14e-l) over the riverbed, resulting in the disappearance of the initially formed horst and graben structures due to this movement (Figure 4-14n). The rest of the horst and graben structures are formed in successive strips and remain in the crater because their movement is restricted by the debris left from the flow of the initial strip. Finally, when the slope finally stabilitzes, the landslide displays evident horst and grabens from the final backscarp to a distance of 62m, designating this region as a spread failure. The remaining portion of the landslide is classified as a flow slide, as depicted in Figure 4-14o. Overall, the simulated landslide led to a retrogression of approximately 94m and had a runout of about 135m from the initial crater. Typically, in spread failures, the runout is substantially shorter than the retrogression distance. However, this particular failure presented both horst and graben structures, as well as a significant zone of remolded debris, constituting what can be described as a combined failure mode.

As per the numerical simulation, the reason behind the soil blocks within the first strip transforming completely into liquid debris is the lack of geometrical restrictions to block their rapid movement. Notably, the mechanism of shear band formation and its propagation remains consistent between the Saint-Monique landslide and the present case, apart from the fact that the sliding front ceases to move due to the restriction of the opposite riverbank.

In comparison with field observations (Figure 4-17), the simulation results present both remarkable similarities and notable differences:

- The simulated landslide initiated with two rotational failure surfaces, as shown in Figure 13c, which flowed rapidly out of the crater. Following these initial slides, alternate shear bands gave rise to horst and graben configurations, resulting in a composite spread and flow slide failure, mirroring the field observations.
- In the field, the observed failure surface inclined progressively upwards with each retrogression. However, the simulation revealed a consistently horizontal failure surface, positioned approximately 4m below the rupture plane observed in the field.

- Although the simulation identified the zone of spread failure nearly at the same distance from the final crater as observed in the field (62m in the model, 66m in the field), the model underestimated the final retrogression distance by 18m. The model's prediction was 84% accurate for the retrogression distance and 90% accurate for the spread limit.

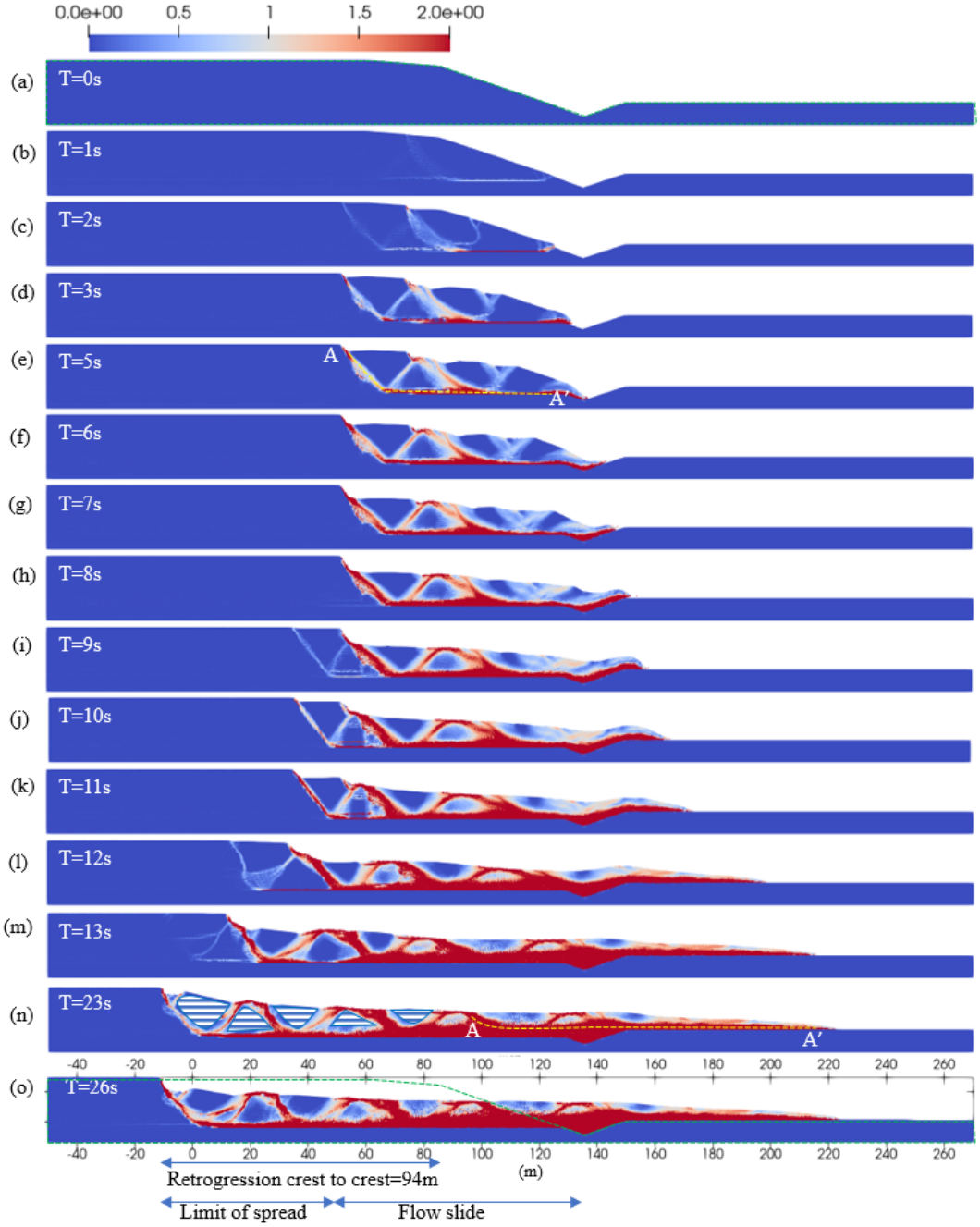

Figure 4-14. The failure mechanism of simulated retrogressive Saint-Luc-de-Vincennes landslide.

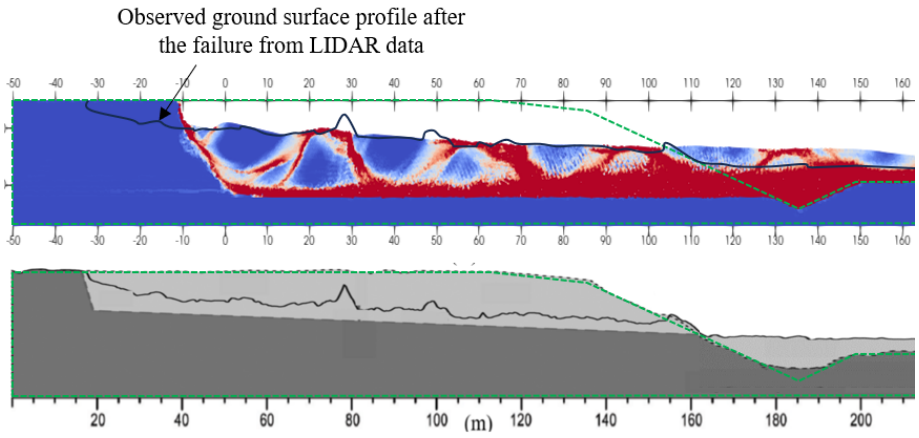

Figure 4-15. Comparison of the post-failure geometry of the simulated model and field observation of Saint-Luc-de-Vincennes landslide of Tremblay-Auger et al. [161].

4.6.2 Comparison of the simulation results with other numerical simulations of the same landslide

Tran and Solwoski [9] and Shan et al. [94] undertook modeling of the Sainte-Monique landslide. They adopted different strain-softening equations, integrating them into the Generalized Interpolation MPM framework (GIMPM) and the Particle Finite Element Method (PFEM) with the RITSS technique, respectively. A significant similarity in their approaches was the consideration of the strain rate's effect on shear strength and the depthwise fluctuation in peak shear strength.

Tran and Solwoski [9] developed a numerical model that predicted retrogression distances equal to the field using remolded undrained shear strengths of 1.6 kPa, 2.5 kPa, and 3 kPa at the failure surface, coupled with strain rate parameters (β) of 0, 0.06, and 0.17, respectively. These cases correspond to sensitivities of 25, 16, and 13.3. Their sensitivity analysis revealed that increasing β necessitates a higher remolded strength and a lower sensitivity to align more closely with field observations. For the base case (Figure 4-16b), they selected a remolded shear strength (s_{ur}) of 1.6 kPa and a sensitivity (S_t) of 25, as this combination most closely matched the real field parameters of Sur=0.7 kPa and S_t=55. Intriguingly, they also found that choosing β=0.17, while keeping s_{ur} at 1.6 kPa and S_t at 25, yielded a retrogression distance similar to field observations. This similarity in outcomes across different β values, specifically between β=0 and β=0.17, with the same s_{ur} and S_t, was not explicitly explained in their findings, raising questions about the influence of β on model predictions under these conditions. The failure mechanism and post-failure dynamics of their study were similar to this study.

Shan et al.'s [94] results (Figure 4-16c) diverged from several field observations, notably the missing ridges and the complete fragmentation of the soil mass into separate blocks. This study utilized a more straightforward constitutive model compared to the previous studies. Despite the simplicity, the constitutive model has more effectively captured the post-failure behavior, as demonstrated in Figure 4-16. This enhanced behavior might be traced back to the strain-softening equation, derived after scrutinizing the large-deformation stress-strain behavior of multiple sensitive clay sites in eastern Canada [151]. Furthermore, this study's parameters for large deformation were directly rooted in laboratory direct shear test data, while Shan et al. [94] calibrated the model by doing sensitivity analysis on the large deformation parameter, displacement at remolded shear strength with δ=0.05, 0.1, 0.2 and 0.4m and selected δ= 0.1 because it yielded to the observed retrogression distance of the field.

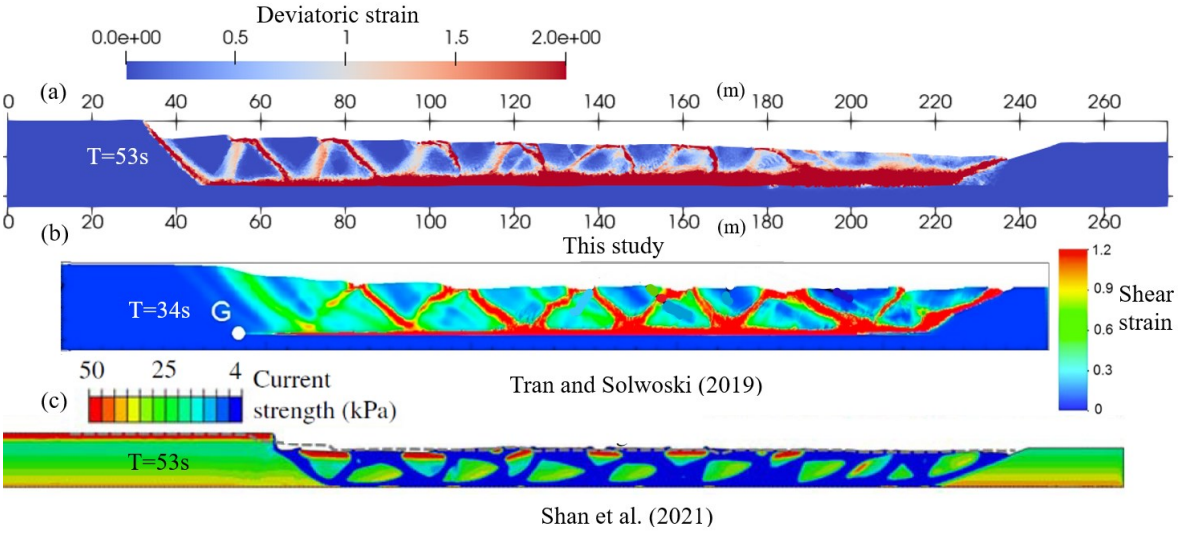

Figure 4-16. Comparison of the post-failure geometry of the simulated model of this study and other numerical simulations of the Sainte-Monique landslide; (a) This study; (b) Tran and Solwoski [9]; (c) Shan et al. [94]

On the other hand, Wang et al. [121], Zhang et al. [81] and Shen et al. [166] analyzed the Saint-Jude landslide; Zhang et al. [81] and Shen et al. [166] employed linear strain softening within a viscoplastic soil constitutive model, integrating the soil model in the particle finite element and arbitrary Lagrangian finite element frameworks, respectively. Both studies depicted the Saint-Jude landslide as a multiple rotational retrogressive failure, a portrayal that contrasted with actual field observations (Figure 4-17b,c). Even so, the post-failure dynamics regarding runout and retrogression from these studies aligned well with this research.

Wang et al. [89] used the same numerical framework as Shen et al. [166], but the constitutive soil model is more advanced, with an exponential strain softening that accounted for strain rate and variations in the peak shear strength based on depth. While Wang et al. [89] depicted segmented blocks that formed horst and grabens differently from our study, the similarities are striking (Figure 4-17a,c). Additionally, Wang et al. [89] replicated the post-failure retrogression witnessed in field observations, whereas our model predicted a retrogression shorter by 20 meters.

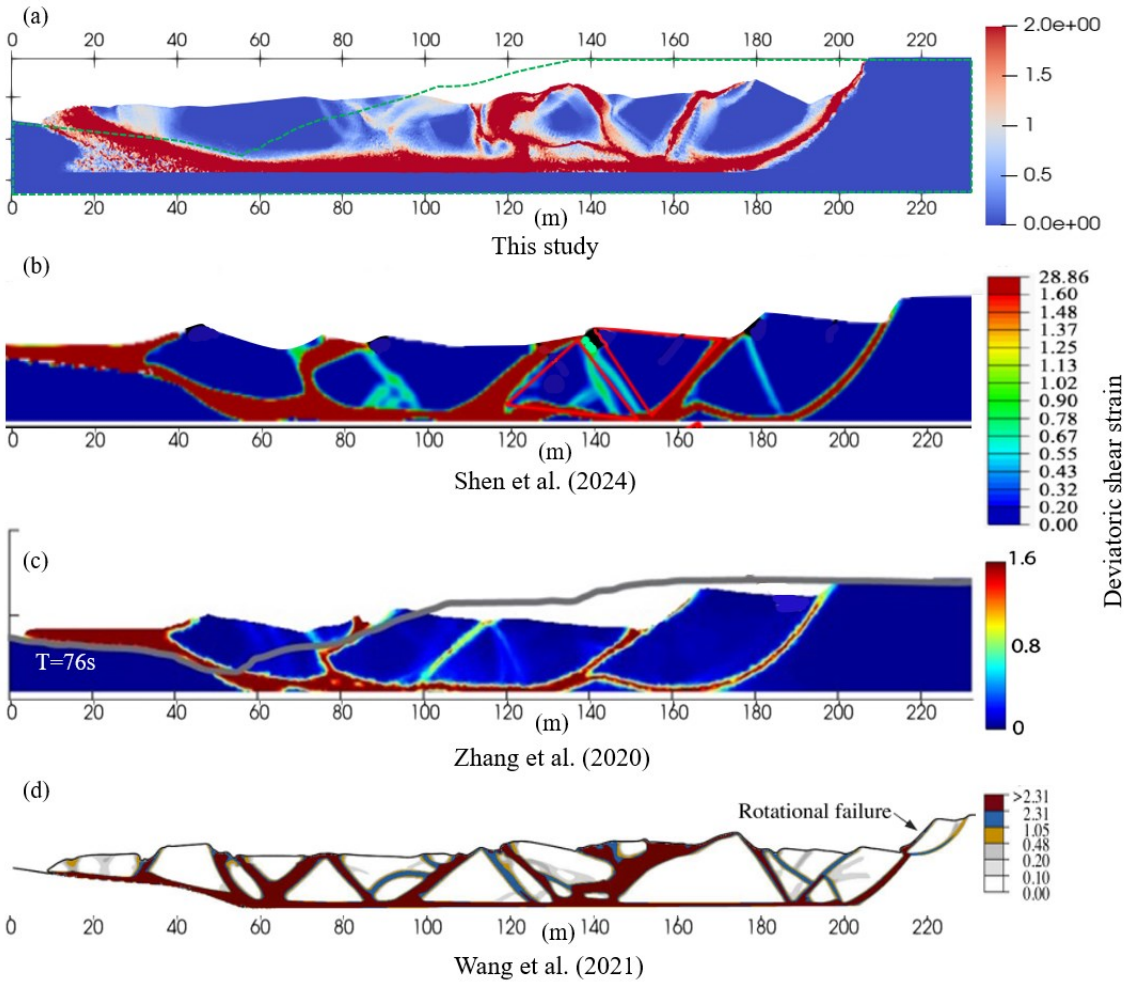

Figure 4-17. Comparison of the post-failure geometry of the simulated model of this study and other numerical simulations of the Saint-Jude landslide (a) This study; (b) Shen et al. [166]; (c) Zhang et al. [81]; (d) Wang et al. [89].

The numerical framework and the constitutive soil model are different in these studies and our study. Still, the key difference in the modeling methodology lies in the evaluation and incorporation of the large deformation parameters (γ_R, γ_r) in the numerical model. Shen et al. [166] and Zhang et al. [81] used a visco-

elastic Tresca model that considers linear strain softening. The difficulty with considering a linear softening behavior has been discussed in Urmi et al. [151, 167]. It demonstrates that a realistic outcome considering linear behavior is only possible when the energy dissipated by the remolding process in both the actual non-linear behavior and assumed linear behavior is equal. As per fracture mechanics, if the area under the stress-strain curve in both cases is equal, that represents similar strain-softening behavior. It is only possible when, in linear strength decrease, the over-estimated area under the strain softening curve is compensated by the underestimated area. Without the complete curve up to the point of remolding, uncertainty remains with the selection of the large deformation parameter (residual shear strain) from laboratory shear test data. Both Shen et al. [166] and Zhang et al. [81] stated that the value of residual shear strain is determined from the strain-softening pattern of Canadian sensitive clays as per Quinn et al.'s [45] study. Both studies considered the value of residual shear strain as 1.6 (160%) without specifying the detailed methodology for obtaining it Quinn et al.'s [45] data or whether any sensitivity analysis has been done to obtain the large deformation parameter that produces simulation result close to the field observation. The focus of this study is to reduce the uncertainty in determining the residual shear strain by providing a clear methodology for obtaining the residual and remolded strain (γ_R, γ_r) in equation 2 so that the complete strain-softening curve is readily available to provide the input parameters for effective prediction of the post-failure behavior.

A pervasive gap in previous research efforts was the inability to foresee post-failure outcomes. This was primarily due to the lack of an appropriate methodology for gauging the large deformation characteristics inherent to sensitive clays. Hence, most prior studies focused on retrospective examinations of past landslides. This generally involved iterative tweaks to large deformation parameters to better fit observed field behavior. Therefore, in contrast to our research, earlier studies did not forecast the potential extent of either retreat or advancement in sensitive clay landslides. However, it is important to emphasize that since the depthwise variation of peak shear strength was not considered, the failure surface emerged directly above the point where the deeper layer was characterized by greater strength in the numerical model. Although the soil layer selection was based on field investigation reports and engineering judgment, studies that specifically addressed variations in peak shear strength depicted a continuous sensitive clay layer where the failure surface naturally formed at its weakest point, providing a more realistic representation.

This work introduces a novel constitutive model specifically designed to capture the large strain behavior of sensitive clays. This model allows for effective prediction of clay behavior under stress, eliminating the need for rigorous and often time-consuming back analysis typically required in such studies. The primary advantage of the proposed constitutive soil model lies in its simplicity, as it only requires input parameters that can be easily obtained from basic soil tests, making it both practical and accessible for widespread use. The methodology detailed in this paper is particularly useful for predicting the post-failure runout and retrogression of future landslides in sensitive clays, which are common in the landslide-prone areas of eastern Canada. By accurately simulating these post-failure behaviors, the model helps in understanding and anticipating the movement of remolded clay after a landslide event. This ability to predict such movements is crucial for the development of effective hazard maps and risk assessments. By providing reliable data and predictions, the model helps prepare for potential landslides, enhances community safety and resilience, and offers a valuable tool for mitigating impacts and improving structural stability on sensitive clay deposits.

4.7 CONCLUSION

- This research introduced a novel strain-softening constitutive soil model for sensitive clays within the framework of the material point method. One can derive the large deformation parameters of sensitive clay for specific sites from geotechnical investigation reports. Furthermore, laboratory test outcomes adequately supply the model's necessary input parameters. This is the uniqueness of the constitutive model. The softening equation utilizes site-specific parameters α, β, residual stress s_{uR}, residual strain γ_R and , remolded shear strain γ_r which are obtainable from laboratory and field investigation data. Therefore, this model doesn't require sensitivity analysis on the large deformation parameters and allows for actual prediction. A parameter in the model can be calibrated to reduce mesh dependency on the results, bridging the gap between laboratory tests and larger mesh element sizes employed in real-world scenarios through the smeared crack approach.
- Three different Canadian landslides in sensitive clay have been numerically modeled, i.e., Sainte-Monique, Saint-Jude, and Saint-Luc-de-Vincennes landslides. The numerical findings underscore the feasibility of predicting most features in retrogressive failures. The landslides

modeled in this research demonstrate the formation and advancement of shear bands consistent with field observations. Moreover, the numerical simulations validate prior characterizations of spread failure mechanisms in the existing literature.

- The Saint-Luc-de-Vincennes landslide is a composite spread and flow type that was not attempted to model numerically before this study. This numerical tool has been able to predict the post-failure movement of a composite landslide with around 90% accuracy.
- While the current constitutive model prizes simplicity, there is potential for further refinement. This enhancement could consider pivotal elements currently overlooked, including depth-dependent variations in peak shear strength, strain rate effects, and soil's long-term creep behavior. Incorporating these aspects would elevate the model's precision and range of application.

CHAPTER 5

Article 4: Balancing Advanced Numerical Techniques and Engineering Judgment in Predicting Retrogressive Landslides in Sensitive Clays for Increased Reliability

Zinan Ara Urmi[a], Ali Saeidi[a], Alba Yerro[b], Rama Vara Prasad Chavali[a]

[a] Department of Applied Sciences, University of Quebec at Chicoutimi, Saguenay, G7H 2B1, QC, Canada

[b] Department of Civil and Environmental Engineering, Virginia Tech, Blacksburg, Blacksburg, VA 24061, United States

Submitted to a journal

Credit authorship contribution statement

Zinan Ara Urmi: Writing – original draft, Visualization, Validation, Software, Methodology, Formal analysis, Data curation, Conceptualization. **Alba Yerro:** Writing – review & editing, Supervision, Software. **Ali Saeidi:** Writing – review & editing, Supervision, Methodology, Funding acquisition. **Rama Vara Prasad Chavali:** Writing – review & editing.

Declaration of competing interest

The authors declare the following financial interests/personal relationships which may be considered as potential competing interests: Ali Saeidi reports financial support was provided by Natural Sciences and Engineering Research Council of Canada (Grant ID: NSERC- 950- 232724). Ali Saeidi reports financial support was provided by Hydro Quebec (Grant ID: RDCPJ 521771–17). If there are other authors, they declare that they have no known competing financial interests or personal relationships that could have appeared to influence the work reported in this paper.

5.1 ABSTRACT

Retrogressive landslides in sensitive clays pose significant challenges due to their complex failure mechanisms. This paper investigates the reliability of the numerical model for predicting these failures using the material point method combined with user-defined strain-softening constitutive soil. It begins by evaluating the effectiveness of a regularization technique to reduce element size dependency in simulations using the case study of the Sainte-Monique landslide. The study then examines the impact of varying the number of material points per element on simulation outcomes. Additionally, the study assesses the consistency of numerical results with field observations across different cross-sections and discusses effective methods for triggering failure in the numerical model. Optimization strategies based on engineering judgment are discussed for each factor. These strategies are applied to a detailed analysis of the Lemieux Landslide, which occurred on June 20, 1993, in the South Nation Valley, one of the largest retrogressive failures in eastern Canadian sensitive clays. The numerical model achieved a 90% accuracy rate in predicting post-failure retrogression distances, highlighting that while advanced numerical techniques are invaluable, engineering judgment is essential for instilling confidence in their application for anticipating future landslide occurrences in susceptible areas.

Keywords: Sensitive clay landslides; large deformation numerical modeling; Material point method, Mesh regularization; Retrogressive flowslide.

5.2 INTRODUCTION

Landslides occurring in regions with sensitive clays are recurring phenomena, notably prevalent in northern countries such as Canada and Norway. The ramifications of these landslides extend beyond mere geological events, as they inflict catastrophic consequences on both the population and the economy [2]. Sensitive clays experience a significant reduction in post-peak shear strength with increasing strain and transform into a liquid-like substance; this phenomenon is known as the remolding of sensitive clays. Under loading conditions, the susceptibility to remolding becomes a key determinant governing the post-failure behavior of sensitive clays [44]. Excessive stress exceeding their peak shear strength leads to the formation of

narrow shear bands with localized strain, initiating the structural transformation that remolds the soil mass [132]. The remolded clays within these shear bands may either spread laterally or drift away from their original position, resulting in a series of failures that progress progressively or retrogressively [75].

These complex features of retrogressive failures make it challenging to model using conventional numerical methods. The strain-softening behavior of sensitive clays requires a suitable constitutive soil model and an advanced numerical tool capable of handling large deformation [62]. The capability to reproduce realistic strain-softening characteristics in the material model is necessary for more accurate numerical analyses of large deformation problems in such materials. In the last two decades, significant development has been made to accommodate large deformation problems in geotechnical engineering. Several mesh-based and meshless numerical frameworks like arbitrary Lagrangian finite element method, particle finite element method, material point method, etc., have successfully been implemented to model some key characteristics of large retrogressive failures [10, 81, 93, 95, 96]. However, each of those numerical methods has its inherent limitations and advantages. It's extremely important to carefully select all the model parameters that influence the simulation outcome.

All mesh-based continuum numerical methods that incorporate strain-softening features suffer from mesh-dependent strain localization problems. Zhang et al. [11] addressed this issue in the numerical modeling of sensitive clays using the Particle Finite Element Method, particularly for strain-softening behavior in a rate-independent elastoviscoplastic constitutive model with linear strain softening. They noted that mesh size affects the width of a shear band, impacting its formation and progression and, thus, the overall failure pattern. To counter this problem, they introduced a length scale tied to the boundary-value problem, focusing on achieving converged solutions for failure patterns and kinematics in progressively retrogressive failures, rather than pinpointing the exact shear bandwidth. Their findings showed that converged solutions were not obtained for element sizes larger than 0.6m. Tran and Solwoski [96] studied the influence of grid density on numerical solutions for simulating retrogressive failure using the Generalized Interpolation Material Point Method (GIMP). Unlike Zhang et al. [11], they found that grid density significantly affects run-out distance prediction if the shear band's exact thickness is not considered in the simulation. They proposed a regularization technique where incremental shear strain is calculated based on the generated shear strain of the model, multiplied by the

ratio of the assumed shear bandwidth to the actual shear bandwidth. Simulations incorporating shear band thickness showed reduced grid dependence and improved results. Different cell sizes (0.4m, 0.3m, 0.2m) with varying numbers of material points were tested, revealing that higher grid densities led to smaller errors because the assumed shear bandwidth approached the actual shear bandwidth. However, the uncertainty in this regularization technique includes the selection of the actual shear band thickness, which varies from 2-3mm [168] in scale to a few decimeters in situ. Wang et al. [84] pointed out that mesh dependency in Material Point Method simulations is related to both mesh size and the number of material points per mesh. However, Tran and Solowski [96] did not address the impact of changing the number of material points per element, consistently using four material points per element. Jin et al. [97] evaluated the impact of mesh density on retrogressive failure development using node-based and edge-based algorithms of Smoothed Particle Finite Element Methods (SPFEM). They analyzed three mesh sizes (0.2m, 0.15m, and 0.12m) and found that both SPFEMs could effectively model spread retrogressive landslides with horsts and grabens using the adopted soil model but exhibited considerable mesh dependency. However, the node-based algorithm had a smaller computational time for finer mesh sizes, which is advantageous when dealing with mesh dependency. Urmi et al. [169] utilized a smeared crack approach to mitigate mesh dependency in the simulation of three pre-historic sensitive clay landslides using a user-defined constitutive soil model in the MPM framework using the Anura3D software. This method suggests that the total work dissipated by a shear band is equivalent to the fracture energy dissipated in a discrete crack. Ensuring consistency in the dissipated work across shear bands of varying element sizes yields reliable results, regardless of the mesh size used [104]. Urmi et al. [169] showed that matching the energy dissipated during the strain softening process in a laboratory direct shear test with the energy dissipated in field-scale numerical modeling resulted in predicted retrogression and runout distances that closely aligned with actual field observations. This energy-based regularisation technique addresses the uncertainty associated with determining the actual thickness of the shear band during failure. However, the author didn't compare whether there is an effect on the formation and progression of the shear band and overall post-failure behavior using different element sizes for the field scale. Based on the existing literature, mesh dependency is a significant concern when modeling large deformation characteristics of strain-softening materials. Proper regularization is crucial to obtaining results that are least affected by mesh dependency to optimize the outcome.

Another important aspect of modeling in 2D plane strain frameworks is the geometrical representation. Several numerical studies have explored the impact of geometrical variations on failure patterns, retrogression, and runout distances in sensitive clay slopes. Urmi et al. [167] highlighted key findings: a minimum thickness of the sensitive clay layer is required for failure initiation, and increased thickness leads to greater retrogression and changes in failure patterns [81, 88]. Steeper slope angles increase the likelihood and speed of failure [97], and increased riverbed width between opposite banks increases retrogression distance [95]. When working with a 2D cross-section, it is crucial that any minor changes in geometry, such as slight alterations in slope angle or riverbed width, are accurately reflected in the retrogression and runout distances. This ensures that the model responds sensitively to these variations when compared to field observations.

Additionally, it is crucial to carefully consider the triggering mechanism when numerically simulating sensitive clay landslides. Landslides triggered by erosion are often modeled numerically as excavation, which is the most common method for initiating retrogressive failure in sensitive clays [10, 96]. While 90% of retrogressive landslides in eastern Canada are directly or indirectly triggered by long-term erosion [43], Urmi et al. [62] examined the triggering factors of 15 prehistoric landslides and observed that, in most cases, erosion reduces the factor of safety to a borderline condition in a drained state. Retrogressive failure is typically initiated by a final trigger of increased pore water pressure, activating undrained strain softening in the sensitive clay layer. There have been no studies comparing different approaches to landslide triggers and their effects on the landslide mechanism, nor any studies comparing the final retrogression and runout distances.

An optimized numerical simulation means assessing the impact of each of these factors to ensure the highest reliability. The paper begins with a detailed examination of the influence of element size on strain softening within a continuum framework, introducing a mesh regulation scheme designed to enhance reliability. It then delves into the effect of the integration scheme on the accuracy of simulation results by varying the number of material points per element (material point density). The study then explores the role of geometrical representations in 2D plane strain simulations, specifically if the numerical model can capture the onset and development of retrogressive failures while dealing with variations in site geometry and irregularities across different cross-sections. Furthermore, the study assesses the influence of two different approaches for landslide triggers on the simulation results. To further validate the effectiveness of these optimization strategies, the

Lemieux Landslide is simulated using the same approach. This landslide was chosen because it is one of the largest retrogressive failures, which will demonstrate whether the optimization techniques work when the numerical model is very long, and the mesh size is on the coarser domain. The straightforward geometry and known erosion trigger of this landslide make it an ideal case to demonstrate the effectiveness of the optimization techniques. The post-failure movement observed in the field is closely aligned with the simulated outcome. This comprehensive approach addresses technical aspects and emphasizes the importance of engineering judgment in predicting and understanding sensitive clay landslides through numerical modeling.

5.3 NUMERICAL FRAMEWORK AND CONSTITUTIVE SOIL MODEL

5.3.1 Basics of MPM

The Material Point Method (MPM) originated as the Particle-In-Cell method (PIC) at Los Alamos National Laboratory, later expanded by Sulsky and Schreyer in 1994 at New Mexico University for solid mechanics challenges [155]. MPM employs a dual discretization approach, where the continuum is discretized into material points (MPs) representing sub-domains with invariant mass (Figure 5-1). MPs encapsulate velocities, strains, and stresses, exhibiting Lagrangian characteristics. A computational mesh, similar to Finite Element Method (FEM), covers the problem domain. Governing equations are solved at mesh nodes, and variables are transposed from MPs to mesh nodes using linear shape functions. Boundary conditions can be imposed at either nodes or MPs. During each time increment, equations of motion are established by mapping information from MPs to computational nodes. Nodal accelerations are solved to update MP attributes. The absence of permanent mesh information storage allows for flexible mesh redefinition, although the mesh typically remains fixed. Post-mesh adjustments involve updating the assignment of MPs to finite elements.

Anura3D, a notable MPM code used in this study, provides a robust framework for analyzing complex geotechnical problems by effectively incorporating the behavior of multiphase materials. Through its unique formulation and data transfer mechanism between material points and computational nodes, the MPM technique can accurately simulate the behavior of slopes and other geotechnical systems, capturing their dynamic responses and interactions [159, 170–172].

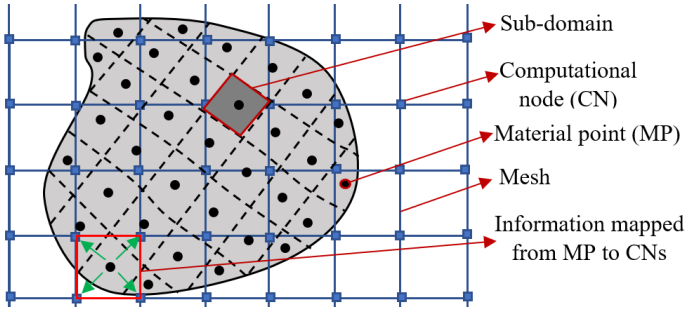

Figure 5-1. Spatial formulation of MPM framework (after [133]).

5.3.2 Constitutive soil model

Recent studies have focused on modeling the highly non-linear post-peak strain-softening behavior of sensitive clays. The development of strain-softening constitutive soil models has further enhanced the ability to simulate these phenomena effectively. An exponential strength degradation equation has been widely used in recent years to capture post-peak soil behavior,

$$s_u = s_{ur} + (s_{up} - s_{ur})e^{-3\gamma/\gamma_{95}} \qquad 5\text{-}1$$

where s_u is the degraded shear strength after the peak, γ is the strain corresponding to s_u, and γ_{95} is the strain when the strength is reduced by 95% of the supposed total reduction ($s_{up} - s_{ur}$). However, obtaining the large deformation parameter γ_{95}, is not possible using conventional laboratory tests because laboratory shear tests typically reach only 40-50% strength reduction with DSS tests and 25-30% with triaxial tests. Therefore, researchers often resort to back analysis, starting with an assumed γ_{95} and adjusting it to match field observations. To eliminate the need for back analysis, Urmi et al. [151] developed an empirical method to determine γ_{95} using available laboratory and field data. They found that the exponent of the strain-softening curve varies by site and is not constant. Furthermore, the strength reduction becomes linear at greater strain values. This led to the proposal of a new site-specific strain-softening equation that uses two parameters (α, β) derived from shear stress-strain curves from laboratory shear tests. Direct Simple Shear (DSS) tests are preferred for their better representation of large deformation strain-softening behavior in progressive failure. Urmi et al. [151] demonstrated that the exponential behavior characterized by site-specific parameters closely approximates the actual behavior of sensitive clays at high strain levels. Identifying the pattern of exponential

decay, even from a limited number of data points, ensures the results remain comparable, as the strength decrease follows a unique law for each site. The study employed the same strain-softening equation proposed by Urmi et al. [151]. The following equation was developed based on the site-specific strain-softening pattern observed in the sensitive clays of several Canadian sites.

$$s_u = \begin{cases} s_{uR} + (s_{up} - s_{uR})\alpha e^{-\beta\gamma}, & s_u \geq s_{uR} \\ s_{uR} - (s_{uR} - s_{ur})\,(\gamma - \gamma_R)/(\gamma_r - \gamma_R), & s_{uR} > s_u \geq s_{ur} \end{cases} \quad 5\text{-}2$$

Where, s_{uR} is the residual strength defined as the degraded strength up to which the strength reduction is exponential and can be determined by

$$s_{uR} = 0.095 s_{up} \quad 5\text{-}3$$

γ_R is the corresponding residual strain at s_{uR}, α and β are site-specific parameters/constitutive modulas that can be determined from a direct shear test result of a specific site. γ_r is the strain at the remolded shear strength s_{ur} that can be estimated as,

$$\gamma_r = 0.13 s_{up}\gamma_R \quad 5\text{-}4$$

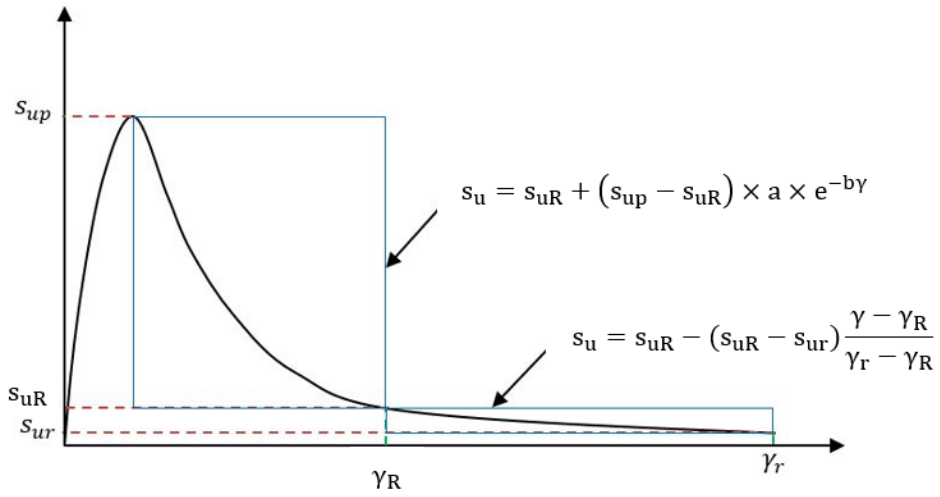

Figure 5-2. Strain-softening behavior of the model (after [151])

Using equation 5-2 facilitates the determination of the strain value at remolded shear stress (γ_r). The strain value at the remolded shear stress is particularly important because it completes the strength reduction curve and thus facilitates the evaluation of dissipated energy during the remolding, which is the area under the stress-strain curve. For more detailed information on the development process of equation 5-2 and its application to landslide risk analysis, readers are encouraged to read Urmi et al. [151].

In this study, the strength of the sensitive clay was modeled using a non-associated Mohr-Coulomb constitutive model in Anura3D software with an additional strain-softening law described by equation 5-2, where the reduction in cohesion is equivalent to the degradation of undrained shear strength. For retrogressive failure analysis under undrained conditions, the friction angle in the Mohr-Coulomb model is set to zero, making it comparable to the Tresca softening model. Although this is a basic constitutive model, the incorporation of strain softening law on the Tresca or Von Mises criteria has been frequently used in simulating sensitive clay landslides under undrained conditions [10, 93, 95, 96, 169].

5.4 OPTIMIZATION OF THE CONTROLLING FACTORS

5.4.1 Regularization of the Effect of Element Size

This section of the study examines the effectiveness of the smeared crack approach in regularizing mesh dependency. It does so by comparing the formation and progression of shear bands, as well as the overall retrogression and runout distances, using different mesh sizes. The smeared crack approach [24] is a simple regularization technique previously used in MPM to address mesh dependency issues [104, 163, 164, 173]. This approach assumes that the total work dissipated by a shear band equals the fracture energy of a discrete crack, ensuring consistent results regardless of the mesh size. This can be achieved by conducting numerical shear tests with various element sizes suitable for field-scale modeling. By calibrating the parameters of the softening equation, it is possible to ensure that the area under the stress-displacement curve (dissipated work) is equal for both field-scale and laboratory-scale element sizes. If the dissipated energy is equal in the shearing process, the post-failure movements should be similar per the smeared crack approach.

This section uses the Sainte-Monique landslide as a case study to simulate the post-failure behavior using three mesh sizes: 0.5m, 1m, and 1.5m. First, a laboratory-scale simulation of the direct shear test (element size=0.014m) is conducted, replicating laboratory conditions (Figure 5-3), as detailed by Urmi et al. [169]. The stress-strain curve obtained from this simulation, which represents equation 5-2, is comparable with the actual stress-strain curve from the laboratory [169]. The stress-displacement curve is then derived by multiplying the strain values by the element size. The dissipated energy in the shearing process is calculated by integrating the area under the stress-displacement curve, which serves as the reference dissipated energy.

Next, direct shear tests are simulated using mesh sizes of 0.5m, 1m, and 1.5m, corresponding to the mesh sizes adopted in the landslide models at the field scale. Each field-scale direct shear test provides an individual stress-strain curve. The dissipated energy in the shearing process is calculated similarly by integrating the areas under the stress-deformation curve. To reduce mesh dependency, it is essential to ensure that the dissipated energy in field-scale shear tests (ES=0.5m, 1.0m, and 1.5m) matches the dissipated energy in the lab-scale shear test (ES=0.014m). Since the stress-displacement curves are primarily exponential, the simplest method to adjust the area under the curve is by modifying the exponent, referred to as the β value. Through calibration, a unique β value was obtained for each field-scale DSS simulation, ensuring an equal area under the stress-displacement curve as obtained from the laboratory-scale DSS simulation. This calibration process adjusts the calibration factor to ensure consistency in the dissipated energy during failure across different mesh sizes (Figure 5-4). Model parameters are presented in Table 5-1.

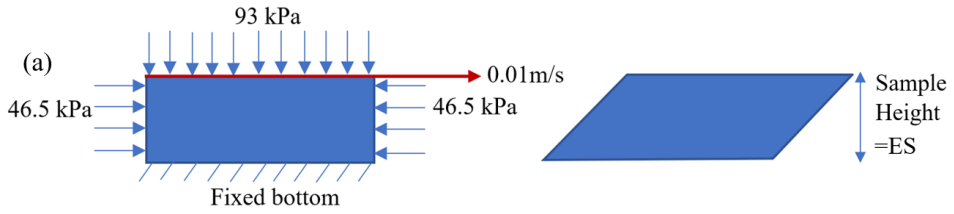

Figure 5-3. Numerical simulation of DSS tests (a) Loading conditions; initial and final configuration of material points for (b) 0.5m and (c) 1m mesh.

Table 5-1: Input parameters for the simulations

Parameter	ES=0.014m	ES=0.5m	ES=1m	ES=1.5m
Natural weight of soil, m	16 kN/m^3	16 kN/m^3	16 kN/m^3	16 kN/m^3
Effective vertical stress, σ_v'	93kPa	93kPa	93kPa	93kPa
The coefficient of lateral earth pressure at rest, K_0	0.5	0.5	0.5	0.5
Shear Modulus, G	5000kPa	5000kPa	5000kPa	5000kPa
Poisson's ratio, μ	0.45	0.45	0.45	0.45
Peak shear strength, s_{up}	40.5 kPa	40.5 kPa	40.5 kPa	40.5 kPa
Remolded shear strength, s_{ur}	0.736 kPa	0.736 kPa	0.736 kPa	0.736 kPa
Residual strain, γ_R	1.8	1.8	1.8	1.8
Site-specific constant, α	0.95	0.95	0.95	0.95
Site-specific constant, β	2.9	105	140	160

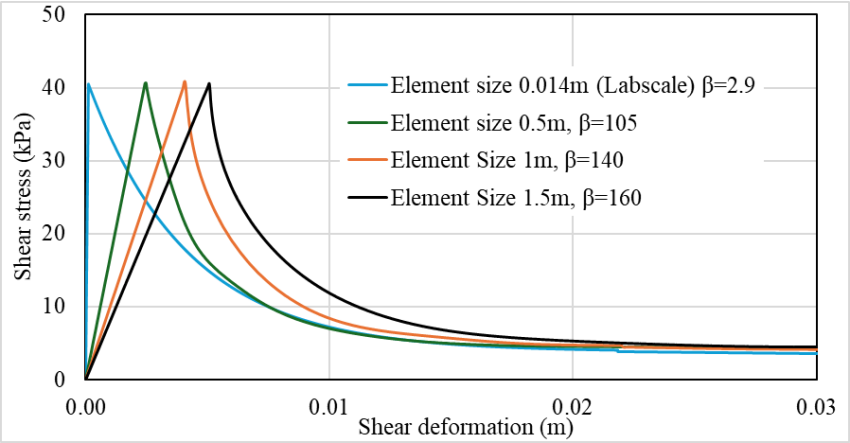

Figure 5-4. Calibration of the constitutive moduli for different element sizes with the smeared crack approach

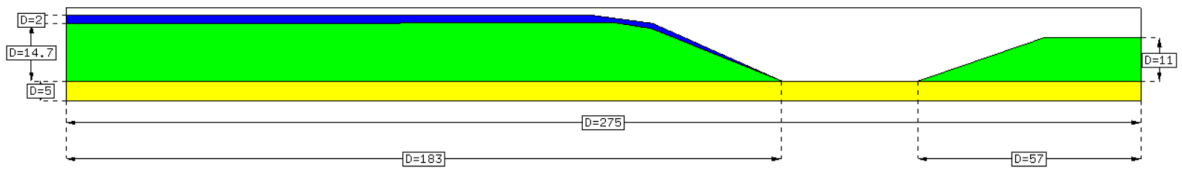

Figure 5-5: The geometry of the slope used in the numerical model of the Sainte-Monique Slope (after [17])

The landslide simulation is performed after achieving the calibrated parameters for each mesh size. Figure 5-5 illustrates a two-dimensional plane strain model for the numerical simulation of the Sainte-Monique landslide. The models' dimensions are determined based on the in-situ topography, as detailed in Locat et al. [17]. The dimensions of the left-hand riverbank in the studied area are 21.7m in height and 183m in length. The right-hand embankment, which prevents further sliding, is 11m high and 57m long. The length of the slope at the left side of the brook is 37m with a slope angle of 24°, while the right-hand slope is 25 m in length with a slope angle of 26°. The soil slope in the field comprised a thin 2m sandy crust, with a thick sensitive clay layer up to 40m depth. In the numerical model, a layer of sensitive clay has been incorporated up to the slope's toe after the 2m crust layer, showcasing a peak shear strength of 40.5 kPa. A 5-meter layer of sensitive clay below the slope's toe is considered for the higher shear strength observed in deeper layers. This lower layer has a shear strength of 55 kPa, which is the average shear strength of this depth as per the field investigation report. The crust layer is defined with an elastic, perfectly plastic material model. For this layer, the elastic modulus was taken as E=10000kPa, the lateral earth pressure coefficient was taken as K0=0.5, and the undrained Poisson's ratio is 0.45, consistent with similar studies on this site [94, 160]. Gravity loading generated the initial stress conditions. Failure was initiated by activating undrained strain softening; the calculation process is detailed in Urmi et al. [169].

When comparing the final retrogression and runout distances (Figure 5-6f) for different element sizes, the crest-to-crest retrogression distances for the 0.5m, 1m, and 1.5m meshes are 106m, 102m, and 108m, respectively, while the runout distances from the toe of the slope are 53m, 52m, and 49m, respectively. The horst and graben structure for final deposition is similar. Compared to the actual retrogression and runout distances observed in the field, which were 100m and 52m, respectively, all simulations produced close

approximations with over 92% accuracy. This indicates that the mesh regularization technique worked well in producing similar outcomes across different mesh sizes.

However, differences in landslide progression can be observed when comparing the movement and development at each time step for different mesh sizes [Figure 5-7(a-b)]. Coarser meshes achieve the retrogression distance rapidly but reach the runout distance more slowly compared to finer meshes. The 0.5m mesh size produces seven subsequent retrogressive slides, whereas the 1.0m and 1.5m meshes produce six and five slides, respectively. Each subsequent retrogressive slide is more pronounced and stable with the finer mesh. From a computational accuracy perspective, finer meshes ensure numerical accuracy as they can capture stress gradients across the elements more accurately.

When conducting numerical simulations to predict disaster risks by estimating probable retrogression and runout distances, using any of these mesh sizes can yield a close-to-realistic preliminary estimation with this regularization technique. However, as mesh size increases, computational time decreases almost exponentially (Figure 5-8), making it significantly more economical. Therefore, landslide analysts must balance computational time and accuracy to best serve the analysis's purpose.

It should be noted that actual computational time depends on the device's capacity for numerical modeling. However, since all modeling was performed on the same device, Figure 8 provides a reliable basis for comparative analysis. Additionally, this regularization technique offers a broader range of element size variations (0.5-1.5m) compared to other studies addressing mesh dependency in modeling sensitive clay landslides.

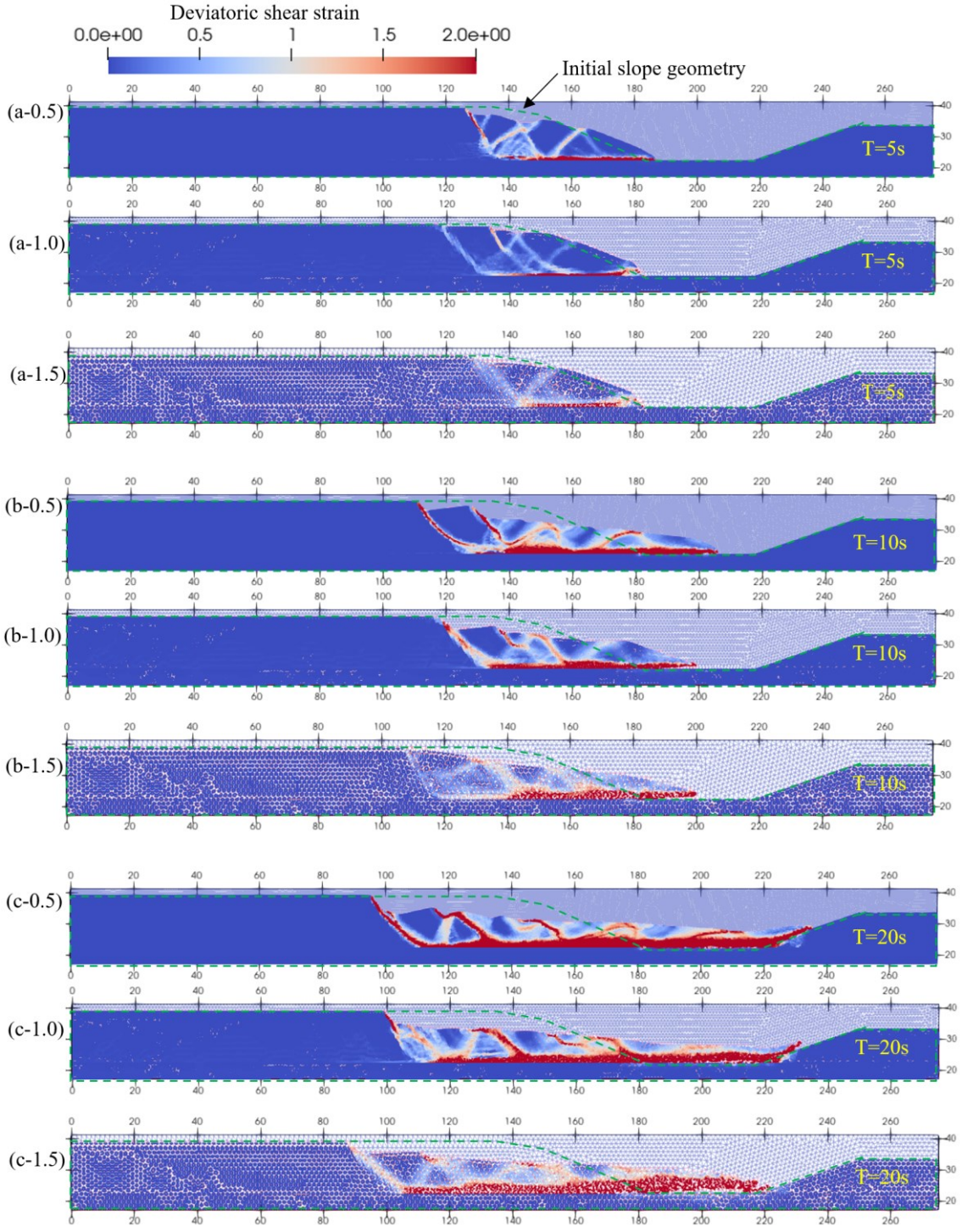
Deviatoric shear strain
0.0e+00
0.5
1
1.5
2.0e+00
Initial slope geometry
(a-0.5)
T=5s
(a-1.0)
T=5s
(a-1.5)
T=5s
(b-0.5)
T=10s
(b-1.0)
T=10s
(b-1.5)
T=10s
(c-0.5)
T=20s
(c-1.0)
T=20s
(c-1.5)
T=20s

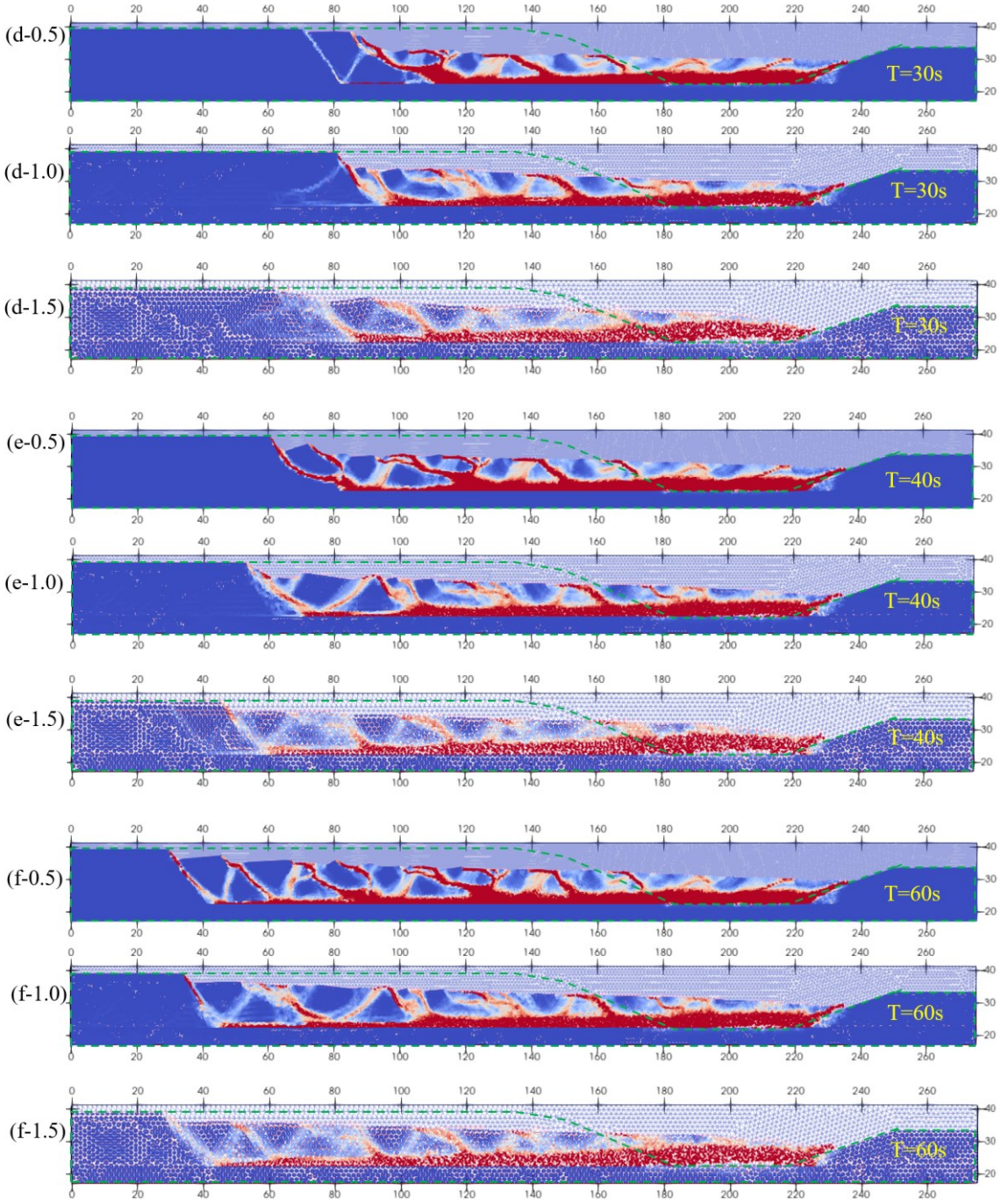

Figure 5-6 (a-f): Simulation of the Sainte-Monique landslide with different element sizes

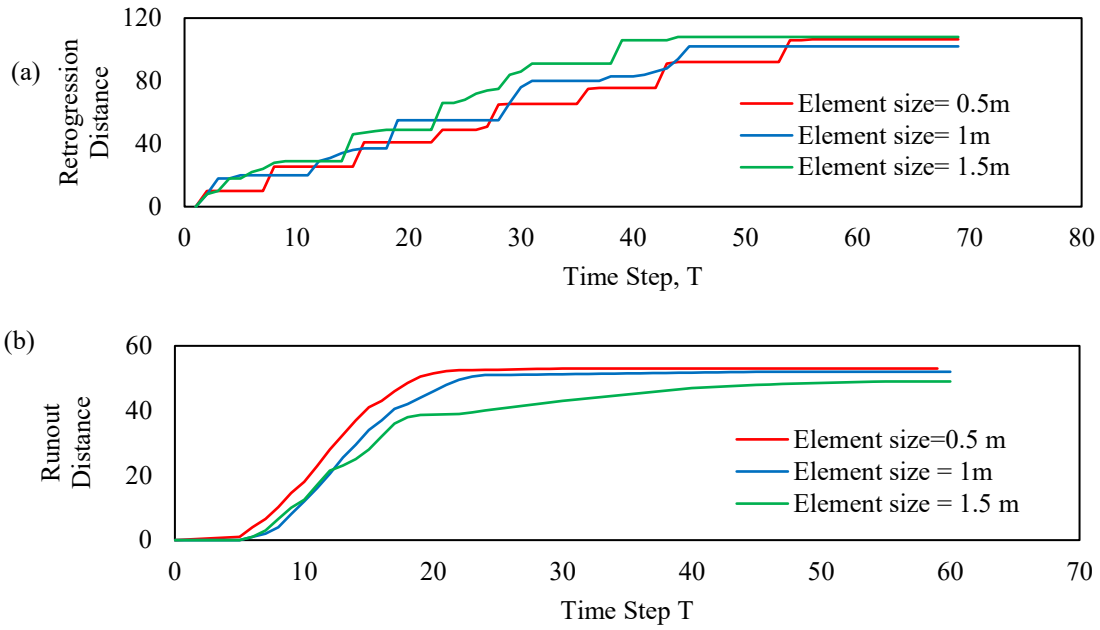

Figure 5-7: Progression of the landslide with time for different mesh sizes, a) Retrogression, b) Runout

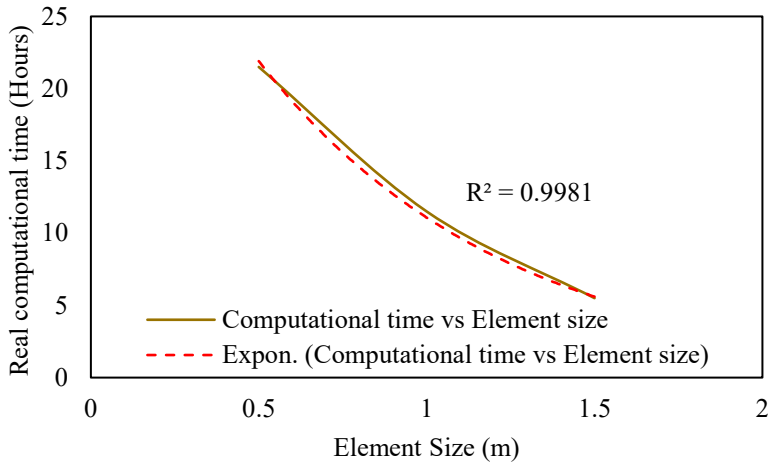

Figure 5-8: Real computational time vs. element size

5.4.2 Number of material points per element

This paper segment evaluates how the number of MPs per element influences simulation outcomes and identifies ways to optimize these results. To illustrate, the Saint-Monique landslide is simulated using different densities of MPs per element (1, 3, 6, and 12) while maintaining a uniform element size of 1m and adhering to the material properties specified in Table 5-1. The simulations indicate that employing a single MP per element

fails to capture the formation of shear bands, leading to an inaccurate portrayal of the failure mechanism (Figure 5-9). Conversely, in simulations with 3, 6, and 12 MPs per element, the final retrogression distances are 102m, 111m, and 112m, and runout distances are 52m, 53m, and 54m (Figure 5-10f). Compared to the final retrogression distance observed in the field, 3MPs, 6MPs, and 12MPs are respectively 97, 93, and 92 % close to the observed result; for runout distances, they provide over 99% accuracy in all cases. This study demonstrates that 3MPs per element for a 300m long model provides the most accurate results beyond or below, which reduces the accuracy of the prediction. With an increasing number of MPs per element, the progression of retrogression is more rapid (Figure 5-11a); however, there is no significant difference in the progression of the remolded debris, which is the run-out distance. An increased number of MPs per element for a particular mesh size increases computational time (Figure 5-12). The authors suggest that using this framework, an initial approach for field-scale modeling could involve using 3 MPs per element. If the model results in instability, the number of MPs per element should be increased. According to this analysis, the minimum count of MPs per element that accurately replicates the actual landslide mechanism may yield the most optimal solution.

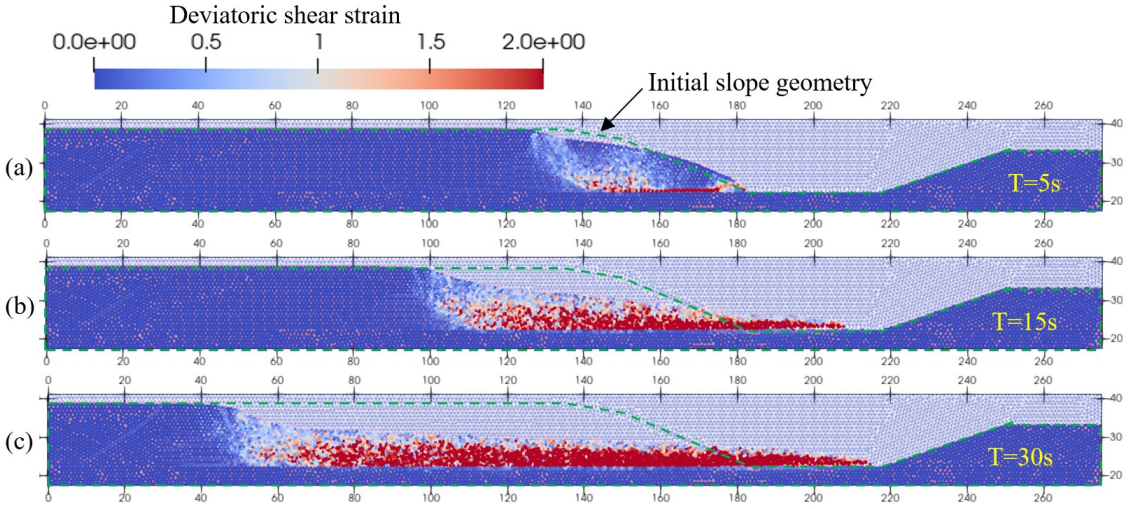

Figure 5-9 : Post-failure behavior with 1MP per element

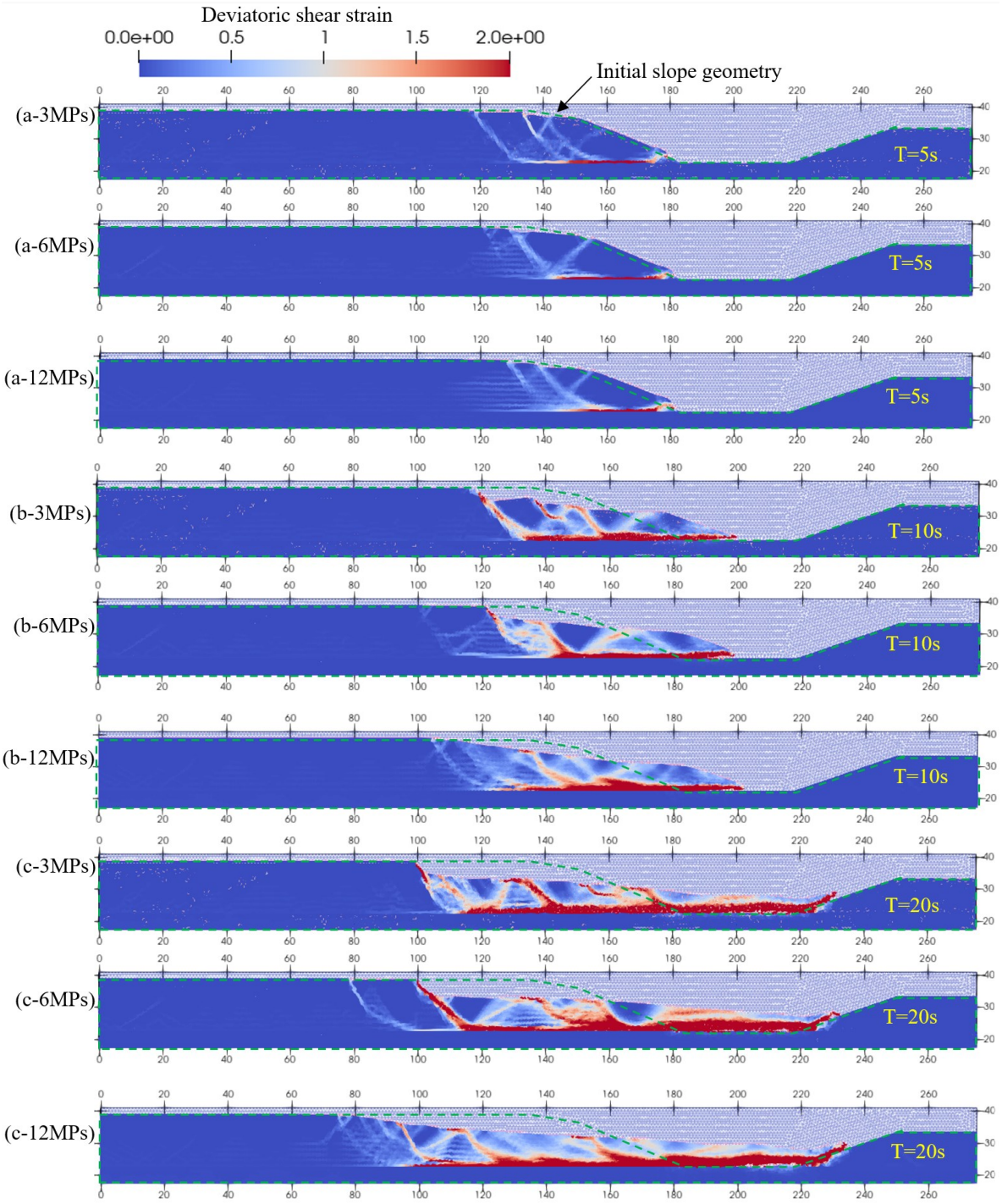
Deviatoric shear strain
0.0e+00
0.5
1
1.5
2.0e+00
Initial slope geometry
(a-3MPs)
T=5s
(a-6MPs)
T=5s
(a-12MPs)
T=5s
(b-3MPs)
T=10s
(b-6MPs)
T=10s
(b-12MPs)
T=10s
(c-3MPs)
T=20s
(c-6MPs)
T=20s
(c-12MPs)
T=20s

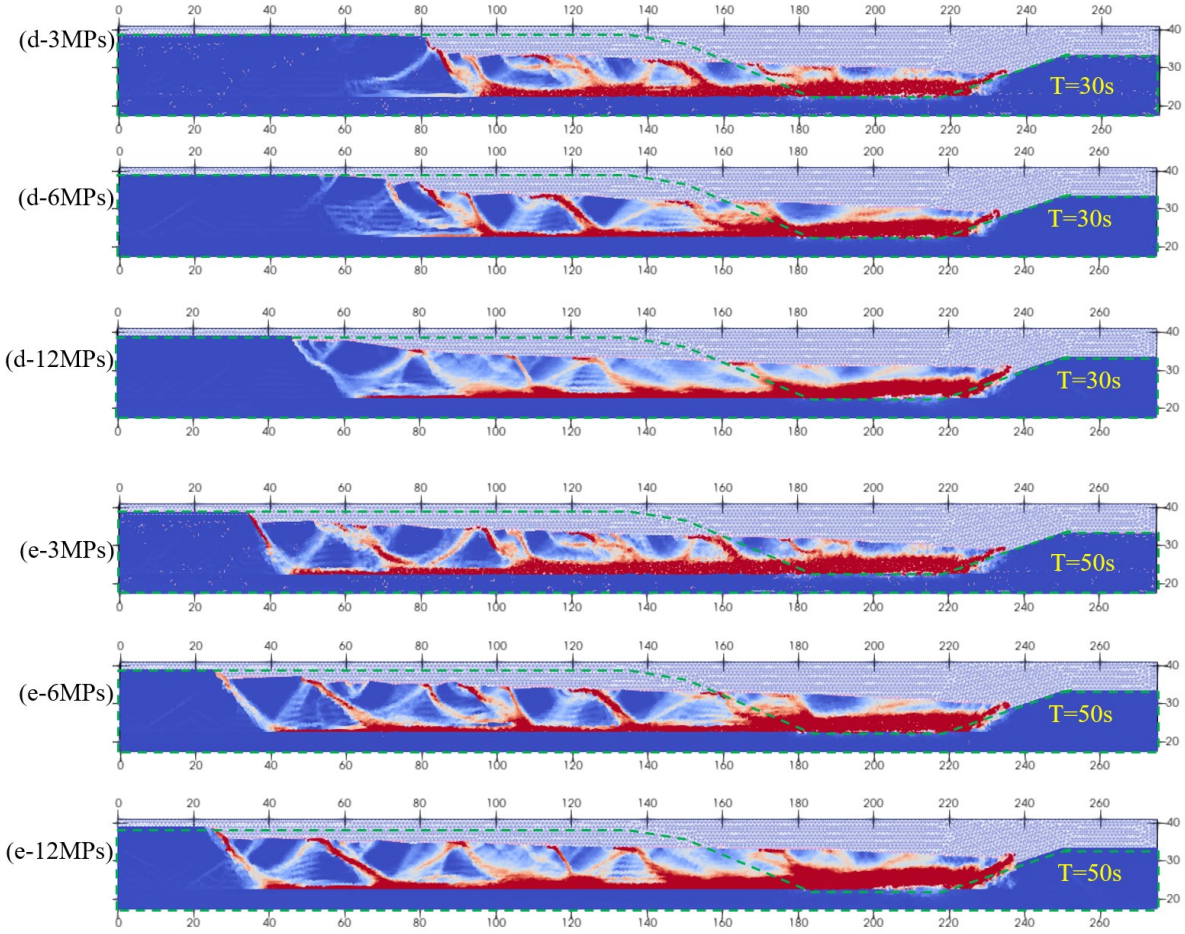

Figure 5-10: Comparison of the Post-failure behavior with 3, 6 and 12MPs per element.

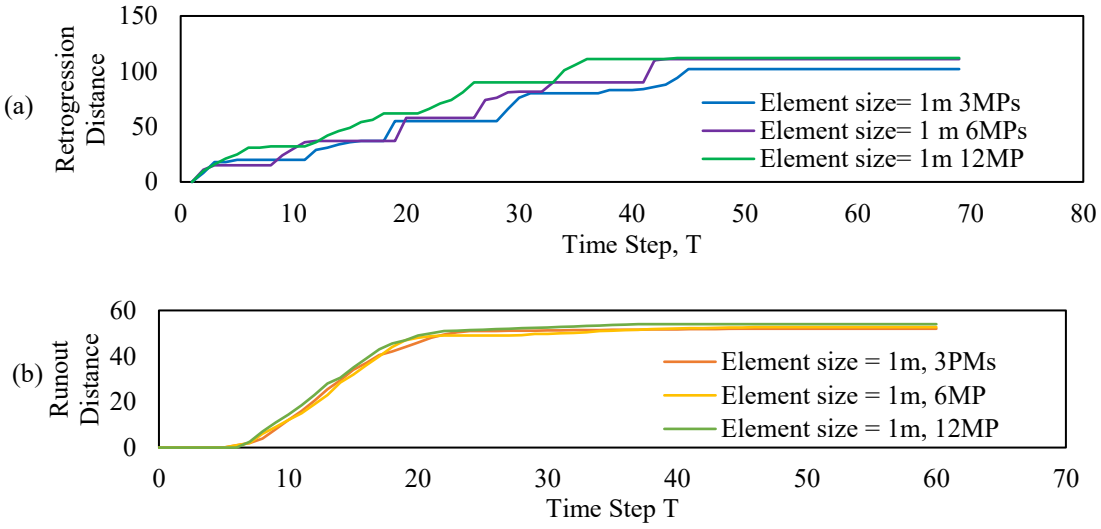

Figure 5-11: Progression of the landslide with time for different MPs per element, a) Retrogression, b) Runout.

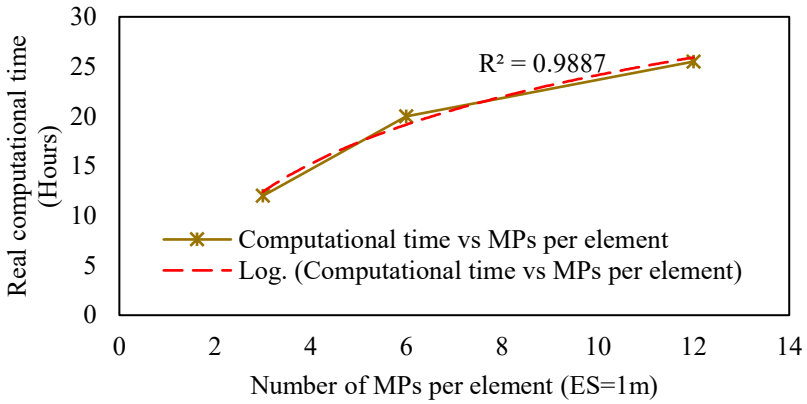

Figure 5-12: Real computational time vs. number of MPs per element.

5.5 GEOMETRICAL REPRESENTATION OF THE SLOPE

In studying complex landslides, such as retrogressive failures in sensitive clays, two-dimensional (2D) plane strain models are frequently employed. This preference arises from the simplicity of 2D analysis and the current lack of advanced three-dimensional (3D) modeling tools. While a 2D cross-section chosen for analysis typically aims to represent the slope's geometry closely, this method can sometimes overlook key geometric aspects critical to accurately predicting landslide dynamics.

For effective landslide prediction across diverse slope geometries, it's crucial to incorporate multiple representative cross-sections into the analysis. This approach facilitates the creation of a nuanced model that accurately reflects the potential behavior of a landslide over varied terrains. In this section, we employed a detailed comparative analysis of two distinct cross-sections from the Saint-Monique site, drawing from the work of Locat et al. [17]. Figure 5-13(a,b) delineates the geometric disparities between these cross-sections. By simulating landslides using these specific profiles, we intended to demonstrate if the numerical model is able to capture post-failure dynamics across different geometrical representations, particularly similar retrogression and runout distances as observed in the field investigation.

The simulation results (Figure 5-14) show that the runout and retrogression in section AA' are close to those in section BB', aligning with field observations. This highlights that the numerical model can capture realistic post-failure behavior across different cross-sections. In field observations, cross-section BB exhibited 5 meters less retrogression compared to cross-section AA, a difference well captured in the numerical model.

For predictive purposes, real-time landscape monitoring systems such as LiDAR can be utilized to obtain various cross-sections of the site. Conducting 2D analyses on these different cross-sections will enhance the overall reliability of the predictions.

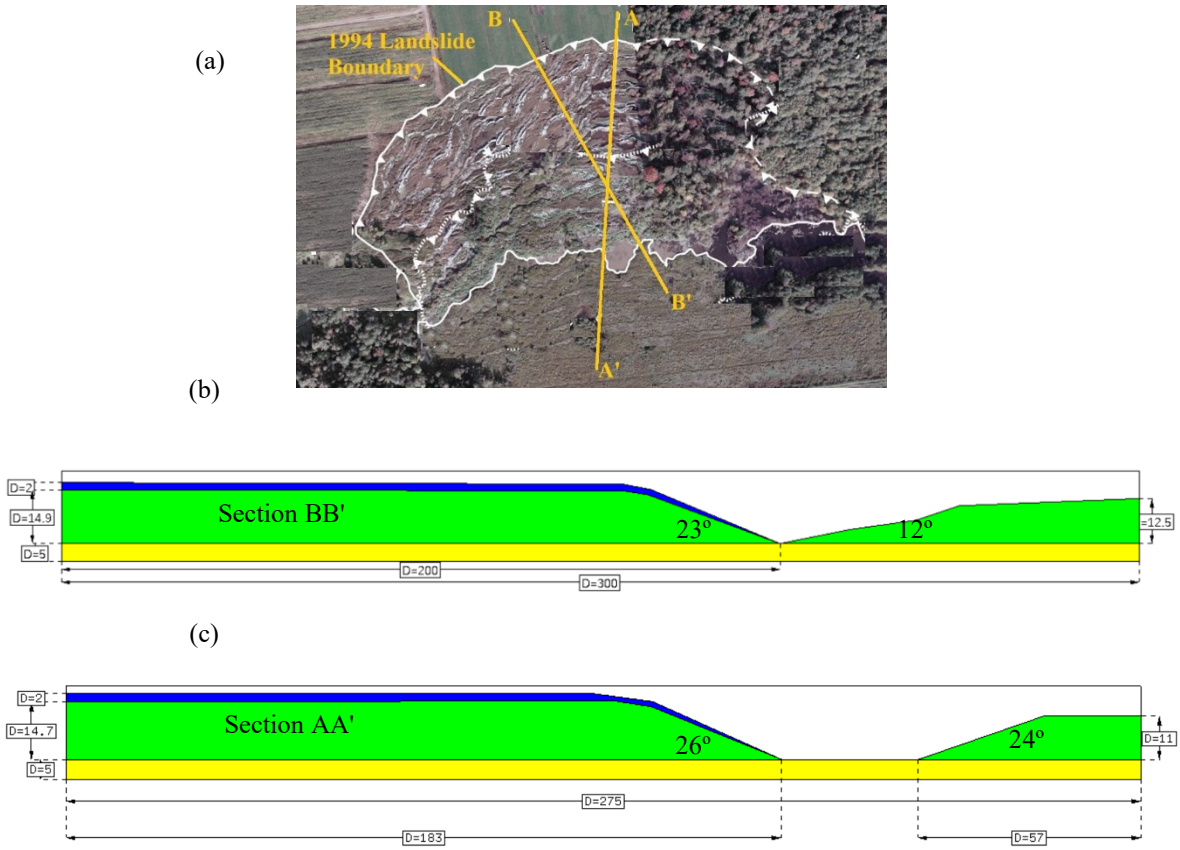

Figure 5-13: Geometrical representation of the Sainte-Monique slope with two different cross-sections

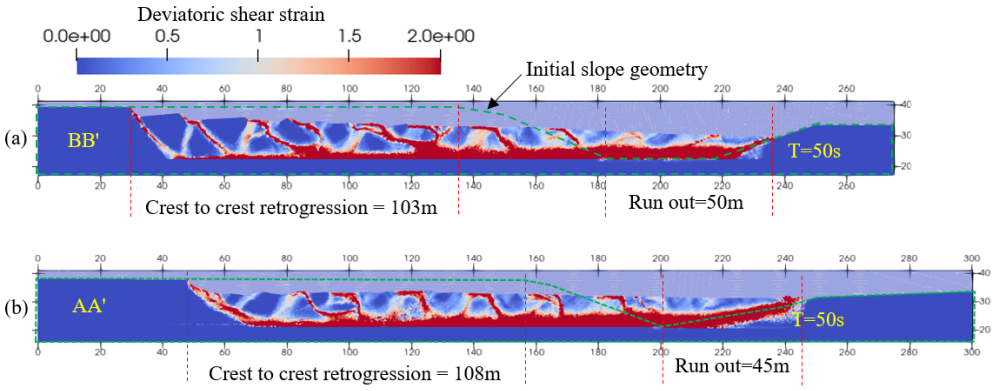

Figure 5-14: Post-failure retrogression and run-out of the Sainte-Monique slope with two different cross-sections

5.6 SELECTION OF THE TRIGGERING OF FAILURE IN THE NUMERICAL MODEL

To accurately replicate landslide triggering, it is crucial to consider the specific field conditions under analysis. The widely accepted hypothesis for retrogressive landslides induced by erosion posits that long-term erosion gradually reduces the stability of the slope to a marginal state. Continued erosion or additional stress—such as heavy rainfall—further deteriorates the slope's stability. This process of retrogressive failure typically unfolds over hours to days, resulting in slope failure under undrained conditions. The increase in pore water pressure triggers undrained strain-softening, leading to strain localization and the formation of shear bands. Consequently, the slope progressively fails in a retrogressive manner. The challenge for landslide analysts is to determine the state of failure initiation in the slope under consideration. Sometimes, undrained strain softening starts the strain localization process and the formation of the failure surface without any noticeable landslide movement. This study found that, after generating the initial stress condition with gravity loading, if the slope is stable with undrained strength parameters with strain-softening characteristics, additional excavation may be required to trigger slope failure and simulate further erosion in the model. However, if the failure surface begins to form under undrained conditions with strain-softening characteristics, further excavation is unnecessary to initiate failure. This will be clarified with a case study example.

As illustrated in Figure 5-15, for the Sainte-Monique case, after gravity loading, when undrained strain softening is activated with the undrained strength parameter mentioned for ES = 0.5m in Table 1, a shear band begins to form, and retrogressive failure progresses over calculation time steps without the need for additional excavation. For demonstration purposes, let us assume that the undrained peak shear strength of the sensitive clays was 50 kPa instead of 40.5 kPa while keeping all other parameters constant. In this scenario, the slope remains stable after the undrained softening parameters are assigned after the gravity loading stage, as illustrated in Figure 5-16. Additional excavation is necessary to initiate failure. Here, a small excavation initiates a local failure (Figure 5-16c). As the failed soil mass becomes remolded, the drag of the remolded debris triggers retrogressive failure (Figure 5-16d). For modeling the Sainte-Monique case, Shan et al. [95] and Urmi et al. [169] did not use any additional excavation; however, Tran and Solwoski [96] employed small excavation to facilitate landslide triggering. Is it wrong to use additional excavation, or does it significantly alter the result?

In this case, the answer is no. Our study found that even though additional excavation is redundant, its presence did not alter the progression of failure nor the final retrogression and runout, as illustrated in Figure 5-17.

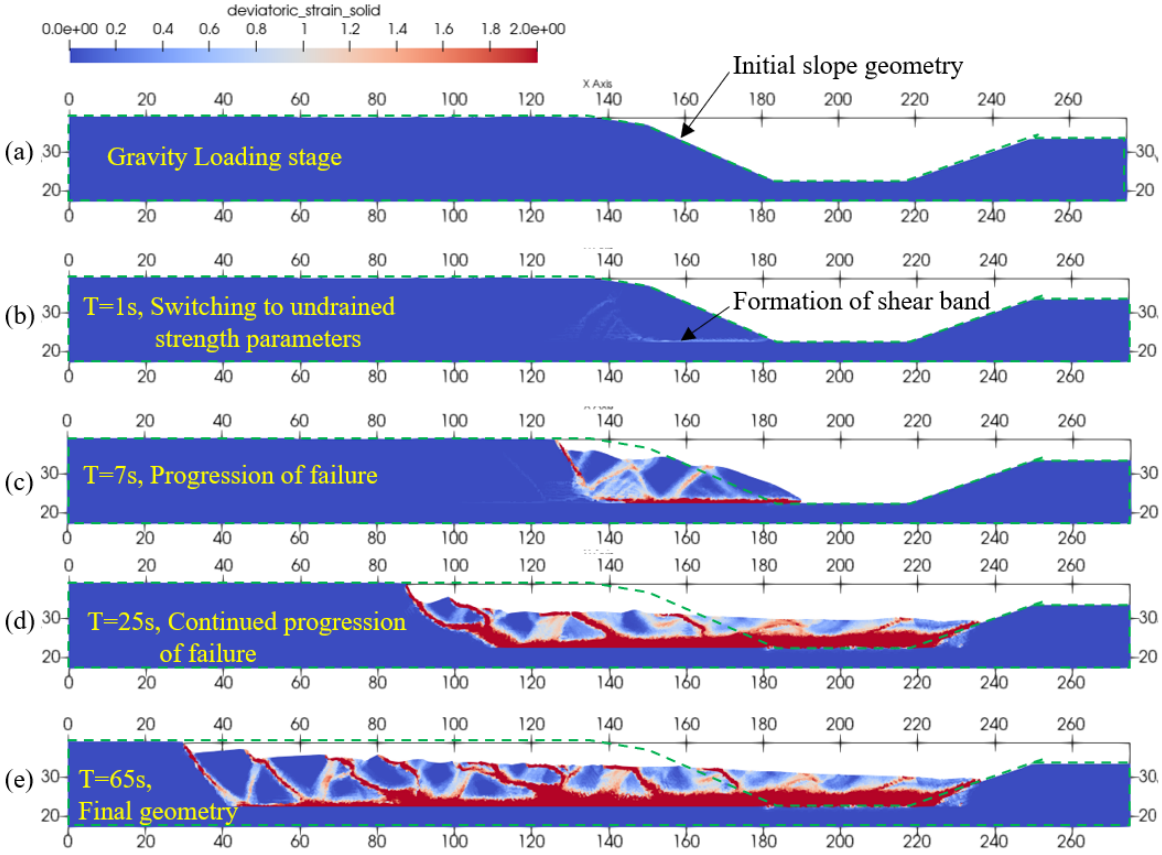

Figure 5-15: Failure initiation by activating undrained strain-softening

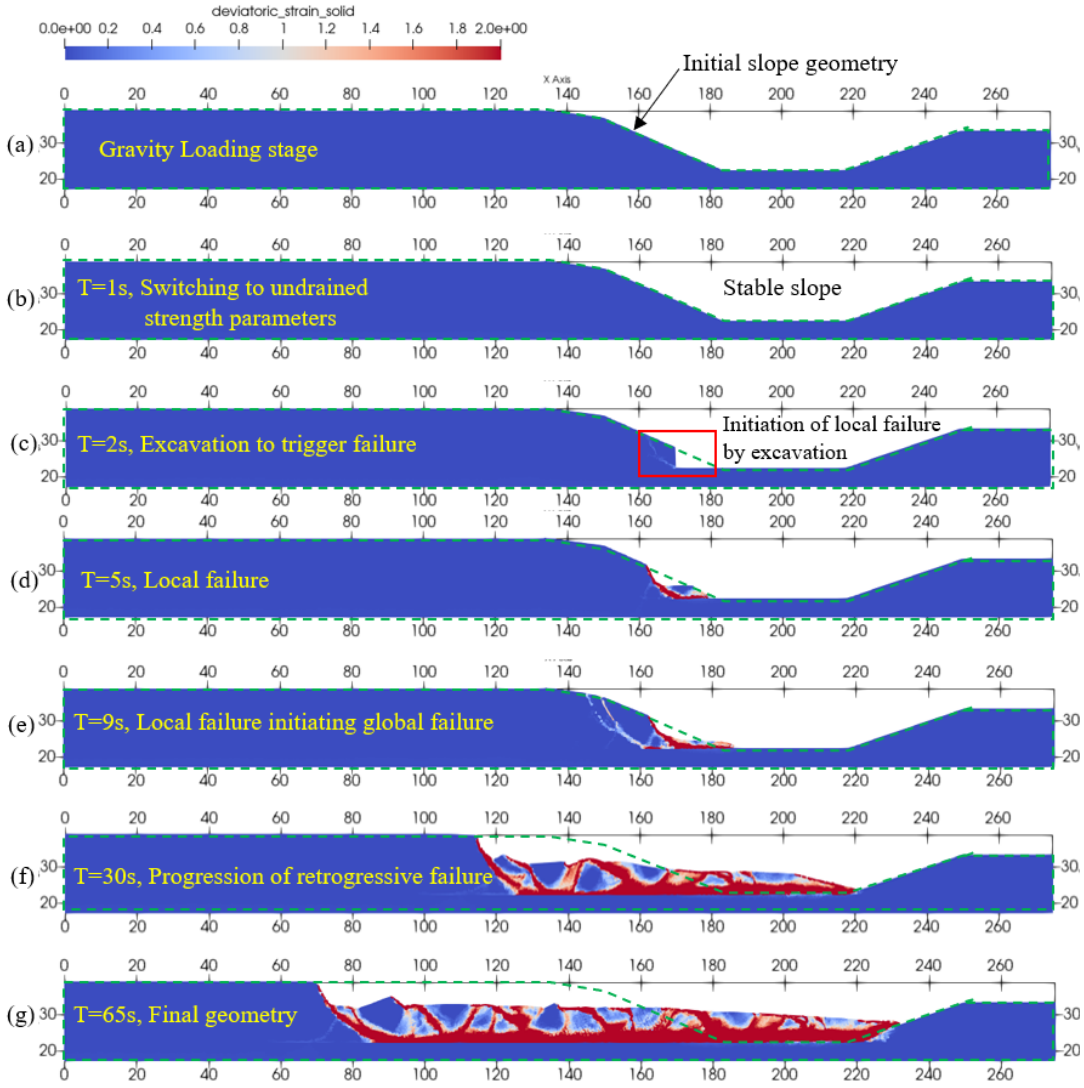

Figure 5-16: Failure initiation by excavation

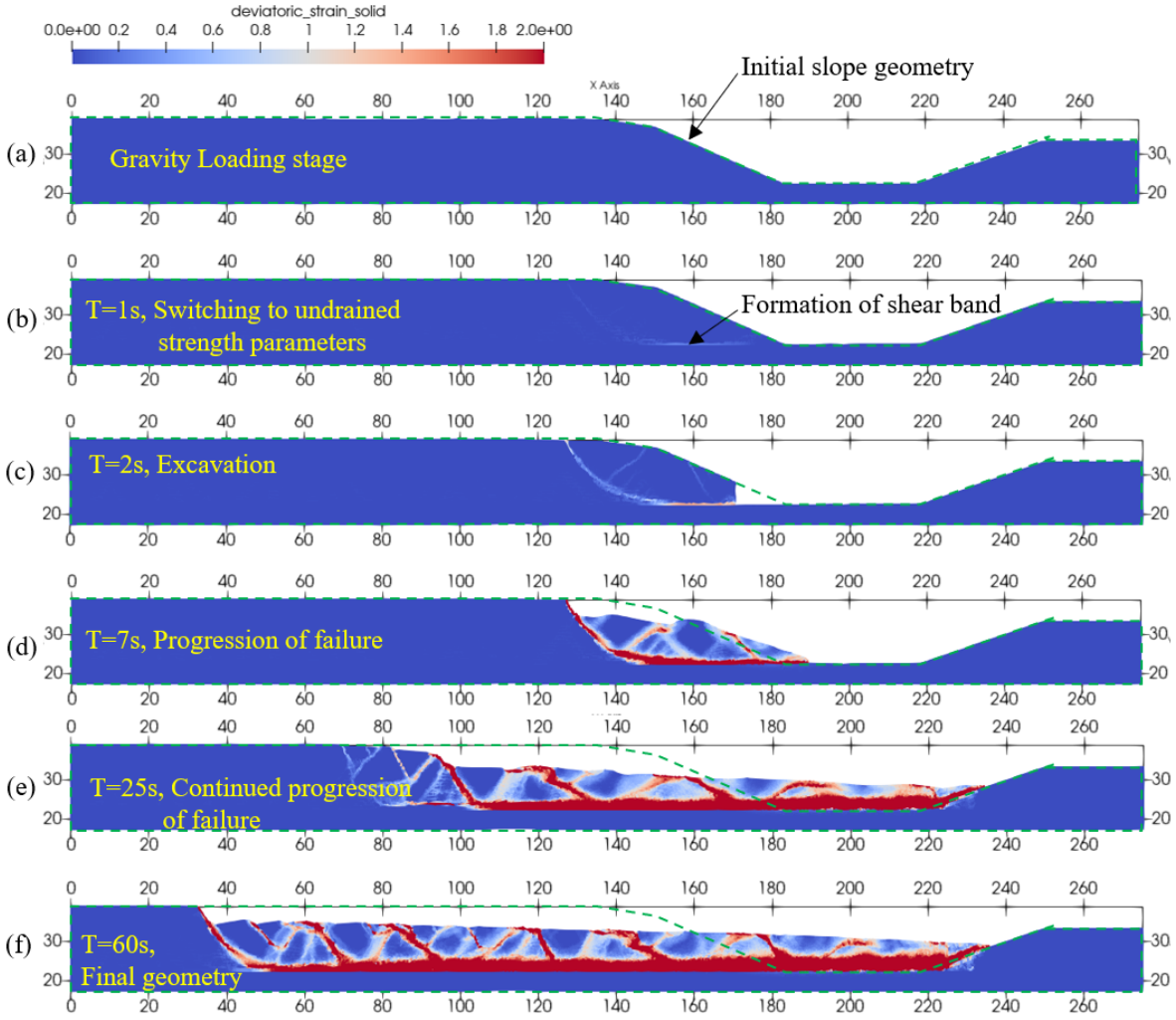

Figure 5-17: Additional excavation to facilitate failure initiation by undrained strain softening

5.7 THE 1993 LEMIEUX LANDSLIDE

In Section 5.6, the potential resolutions to issues in landslide analysis were discussed related to the impact of mesh size, the number of material points, 2D geometrical representation, and the triggering of failure. These aspects are crucial for accurately predicting the post-failure behavior of retrogressive landslides using numerical modeling, particularly the material point method. In this section, we will apply the discussed strategies to numerically simulate one of the most complex and most extensive retrogressive failures in eastern Canada, the 1993 Lemieux Landslide.

5.7.1 General description of the landslide (As per Evan And Brooks

On June 20, 1993, a significant landslide, estimated to involve 2.8 million cubic meters of earth, occurred in the Leda clay along the east bank of the South Nation River in Lemieux, Ontario (45.4°N, 75.06°W). This landslide, covering approximately 17 hectares, extended 680 meters from the riverbank, with 555 meters encroaching onto the flat plain above (Figure 5-18a). Although no fatalities were reported, one motorist sustained injuries after driving into the resultant crater. Initial assessments by the South Nation River Conservation Authority indicate that the total costs linked to the landslide, including both indirect expenses (such as the preemptive purchase of 28 homes) and direct expenses (immediate costs following the slide and river cleanup operations), amount to approximately 2.5 million Canadian dollars. Situated 4.5 kilometers downstream from the 1971 South Nation River landslide site, this area witnessed similar events in 1895 and 1910. Notably, a band of pre-existing slides, dating back to an undetermined time and ranging between 100 to 130 meters in width, was identified at the slope's base, potentially triggering the 1993 landslide through reactivation. Additionally, a gully was present on the upslope of the retrogressive slide complex. The erosion occurring in this gully might have weakened the slope in specific areas, setting the stage for the broader landslide event that followed.

The subsurface stratigraphical and geotechnical data analysis revealed a composition where a layer of soft marine clay is covered by a denser cap made of grey-blue laminated, interbedded sands and silts, topped with brown silty sand. Within the marine clay layer, particularly in its mid to lower sections, liquidity index values exceeding 1 signify a high sensitivity to remolding. Field vane testing, demonstrating sensitivities greater in the clay layer's upper portion near the landslide's base, supports the conclusion that the Lemieux landslide was triggered by a loss of strength in a highly sensitive clay zone situated 8 to 23 meters below the surface.

According to Varnes's classification [31], the Lemieux landslide is a highly rapid earthflow or a flow of quick clay involving lateral spreading of liquified remolded clay of the underlying layer, followed by disintegration or remolding of all or part of the sliding mass. They added that the landslide might have exhibited retrogressive rotational sliding during its initial and final phases. Moreover, straightforward translational movements might have also occurred, potentially in conjunction with rotational sliding, as noted in Odenstad’s

[78] study. The landslide's debris morphology suggested that a large part of the mass underwent fluidization, with the harder cap blocks subsiding, translating, and rotating. The calculated stability number for the site was approximately 9.6, indicating the landslide might have been caused by the extrusion of the underlying soft clay layer resulting from the undrained loading of the cap. This landslide temporarily dammed the South Nation River, leading to upstream flooding and negatively impacting the water quality downstream.

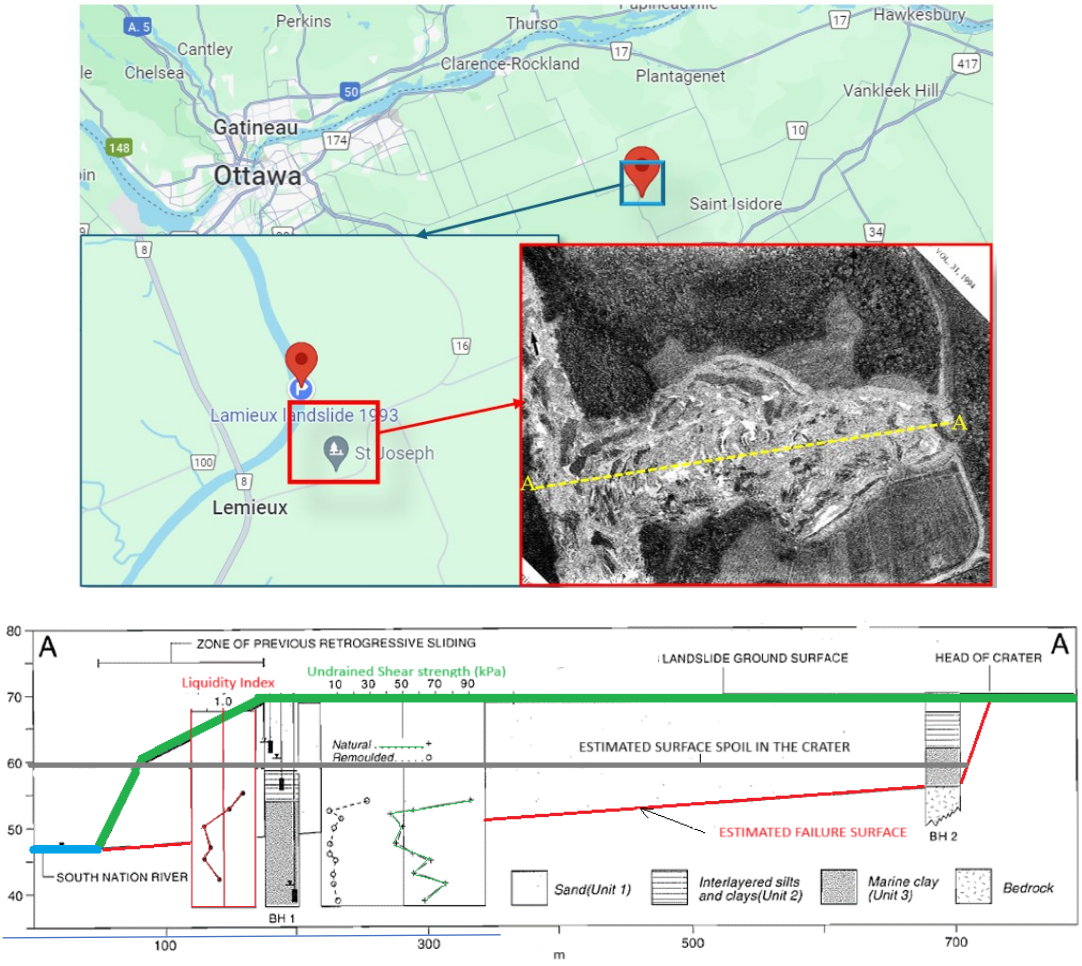

Figure 5-18. (a) Landslide location and (b) Cross-section AA (after [66])

5.8 DESCRIPTION OF THE NUMERICAL MODEL

5.8.1 Geometry and soil properties used in the numerical model

Figure 5-19 illustrates the two-dimensional plane strain model employed in the numerical analysis, with its dimensions tailored to match the topography depicted in Figure 5-18b. The riverbank stands at a height of

30m. It stretches over a length of 750m from the river. The primary slope is about 40 meters long with an inclination of 26.5 degrees, and the secondary slope is 90 meters long with an inclination of 6 degrees. The riverbed is extended on the left to allow space for debris movement. However, the river is at a transverse position in the field, which cannot be represented with a 2D plain strain model. The slope comprised of a 3m thick sand layer followed by a 6-18m thick sensitive clay layer followed by an 8-15m thick stiffer sensitive clay layer.

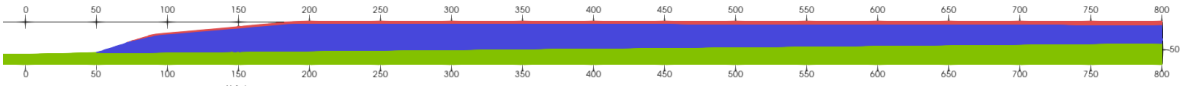

Figure 5-19. Slope geometry (after [66]).

To determine large deformation properties, the DSS test result of a sample taken from the South Nation river bed is 4.5km upstream of the Lemieux landslide location at an elevation of 42m [14]. The DSS shows a peak shear strength (s_{up}) of 87kPa, comparable to the shear strength of 80kPa of BH1 in Figure 1b at the same elevation. As per Urmi et al.'s [151] methodology, the large deformation parameters were obtained as follows,

1. From the partial stress-strain curve obtained from the DSS test, $\frac{s_u - s_{uR}}{s_{up} - s_{uR}}$ vs. γ is plotted to evaluate the value of α and β from the exponential trend of the plot, as shown in Figure 5-20. Here, s_{uR} = is obtained from equation 5-3.

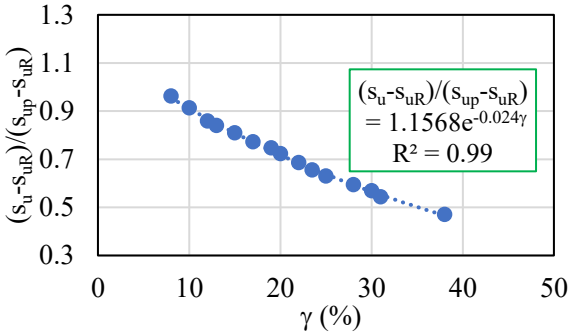

Figure 5-20. Determination of α and β

2. With the values of s_{up}, s_{uR} , α and β, the exponential part of Equation 5-2 was plotted as shown in Figure 5-21.

3. The strain value (γ_R) corresponding to the stress s_{uR} from the plotted curve is determined and γ_r from Equation 5-4 is estimated.

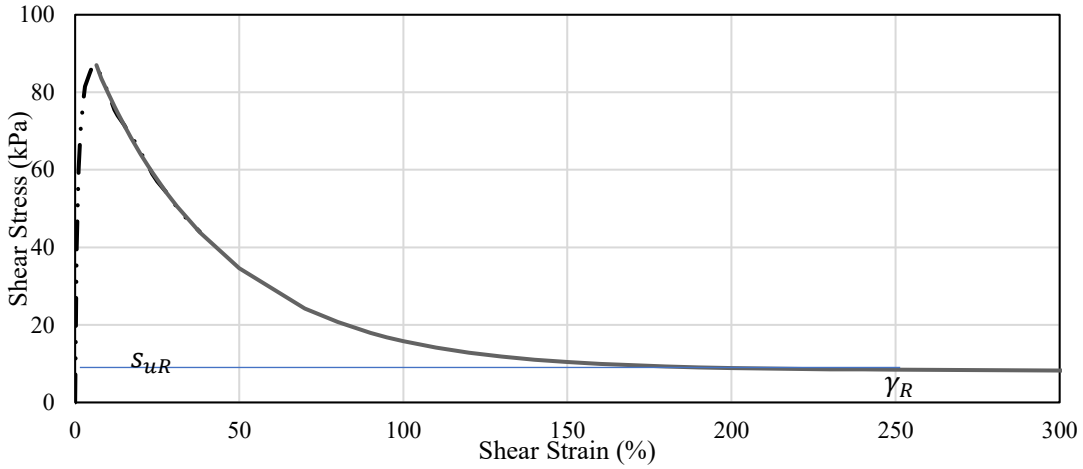

Figure 5-21. Determination of γ_R

A numerical simulation of the DSS test has been conducted to ensure that the constitutive soil model captures the exact stress-strain behavior depicted in the DSS results. In the laboratory shear test, a soil sample with a dimension of 14mm in height and 67.8mm in diameter was subjected to consolidation under a vertical stress level that closely matched the in-situ conditions corresponding to the sample's depth. The sample was placed inside plastic rings to prevent lateral deformation during consolidation. Shearing was conducted laterally by a motor, applying a horizontal strain rate of 0.7 mm/min at the top of the sample while the base remained fixed [14]. These conditions were replicated in Anura3D, considering loading and boundary conditions consistent with the laboratory tests, as shown in Figure 5-22a. In particular, plain strain conditions were considered, and an initial rectangular domain (with a height equal to the sample's height as measured in laboratory testing) was divided into triangular elements discretized with 46 MPs each (Figure 5-22b). A total stress analysis is performed in undrained conditions. A prescribed velocity, consistent with the horizontal strain rate used in the laboratory shear test, was applied at the top of the row of nodes to generate the DSS total stress path (Figure 5-22c). It can be observed that (Figure 5-22d) the constitutive equation has been well implemented in the numerical model to accurately depict the stress-strain behavior of sensitive clays up to the remolded strength. All material properties used in the numerical simulation of the DSS are presented in

Table 5-2.

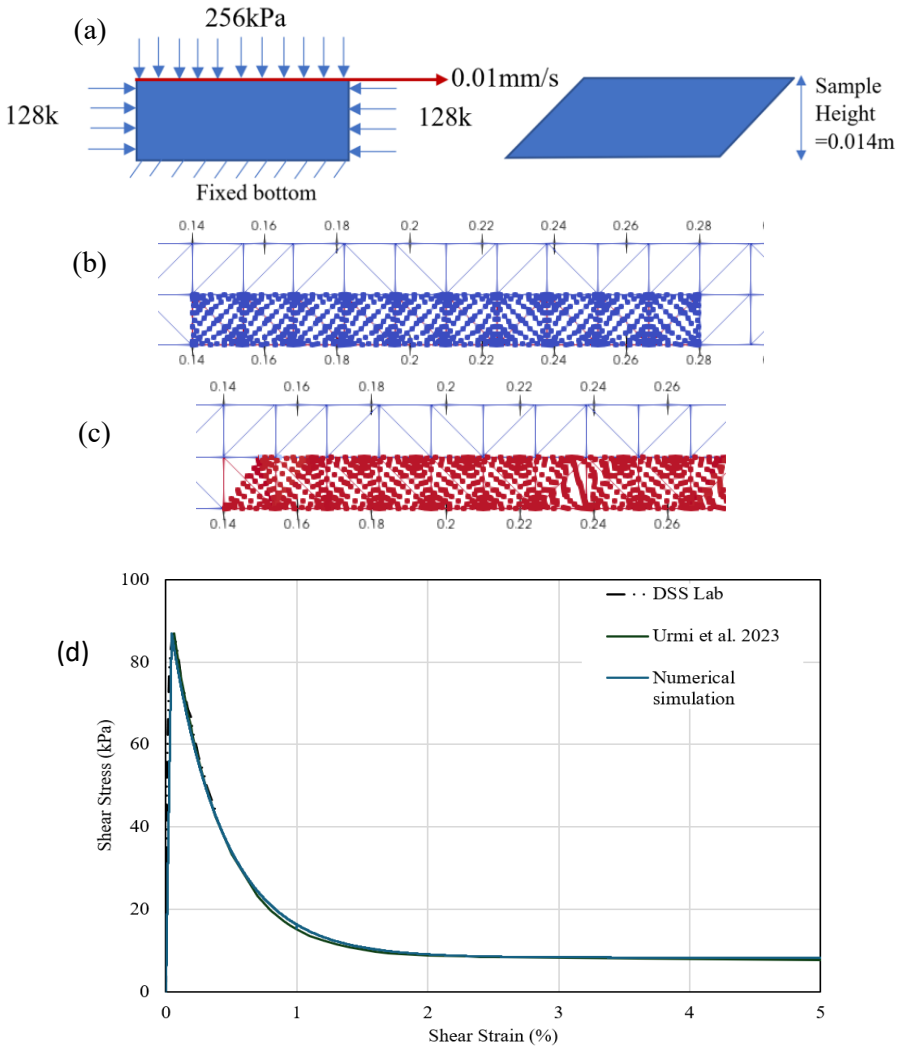

Figure 5-22. Simulation of DSS test. (a) Loading conditions; configuration of material points (b) initial and (c) final; (d) Stress-strain behavior

Table 5-2. Input parameters for the direct shear test simulation.

Parameter	Values
Natural weight of soil, m	17 kN/m^3
Effective vertical stress, $0.8\sigma_v'$	256 kPa
The coefficient of lateral earth pressure at rest, K_0	0.5
Shear Modulus, $G=\frac{s_{up}}{\gamma_p}$	4050kPa
Undrained Poisson's ratio, μ	0.45
Peak shear strength, s_{up}	87 kPa
Peak shear strain, γ_p	0.02
Remolded shear strength, s_{ur}	3 kPa

Residual strain, γ_R	2.5
Site-specific constant, α	1.16
Site-specific constant, β	2.8

As shown in Figure 5-19, the slope itself is 800m long, with additional spaces left on the left side of the model, so the total length of the model is 1.6km. Using a finer mesh would be computationally very expensive in this case. Therefore, for the landslide simulation, an element size of 1 meter was adopted; this size was selected because reducing it further would significantly increase computational time, while increasing it could affect the evolution and propagation of shear bands, thereby compromising overall simulation accuracy. To calibrate the β parameter to accommodate changes in element size, we conducted another Direct Simple Shear (DSS) test using a 1m element size. By carefully calibrating the β parameter in the softening equation, it is ensured that the areas under the stress-displacement curves are identical for both the standard and enlarged mesh sizes utilized in the DSS tests. This critical step assures that the soil demonstrates the same strain-softening response as depicted by experimental data, effectively standardizing the behavior across different element sizes and ensuring the reliability of the results in real-scale landslide simulation.

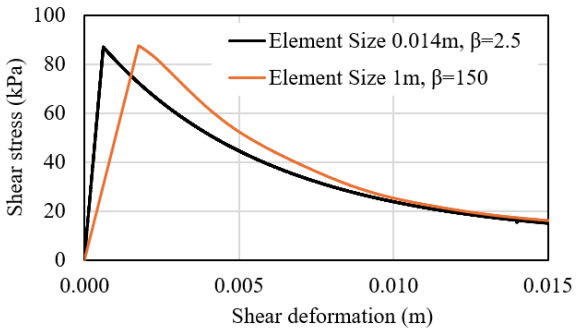

Figure 5-23. Calibration of β for element sizes as per smeared crack approach

All parameters used in the numerical simulation of the landslide are presented in Table 5-3. Apart from the large deformation parameters, most soil properties are taken based on the in-situ field investigation data provided by Evan and Brooks [66]. The Poisson's ratio is taken as 0.45 to represent undrained conditions similar to other studies simulating sensitive clay landslides in total stress undrained conditions [93, 94, 160].

Table 5-3. Input parameters for the numerical simulation of the landslide

Parameter	Crust	Sensitive clay layer1	Sensitive clay layer2
Natural weight of soil, m	18 kN/m^3	17 kN/m^3	17 kN/m^3
The coefficient of lateral earth pressure at rest, K_0	0.5	0.5	0.5
Shear Modulus, $G=\frac{s_{up}}{\gamma_p}$	4050kPa	4050kPa	4050kPa
Undrained Poisson's ratio, μ	0.45	0.45	0.45
Peak shear strength, s_{up}	90 kPa	60 kPa	87 kPa
Peak shear strain, γ_p	-	0.02	0.02
Remolded shear strength, s_{ur}	-	3 kPa	3 kPa
Residual strain, γ_R	-	2.5	2.5
Site-specific constant, α	-	1.16	1.16
Site-specific constant, β	-	150	150

5.8.2 Initial stress and the onset of failure

The initial stresses were induced by the force of gravity, as illustrated in the Figure 5-24. With the soil parameters as specified, the slope remains stable. As per Evans and Brooks [66], erosion in an upslope gully likely triggered localized slope failure, eventually leading to the 1993 landslide through the reactivation of a pre-existing band of slides. To replicate the erosion, a minor section near the slope's base was excavated (Figure 5-25). This excavation amplified stress within the weak sensitive clay layer, leading to localized failure. This, in turn, set off a chain reaction of retrogressive failure.

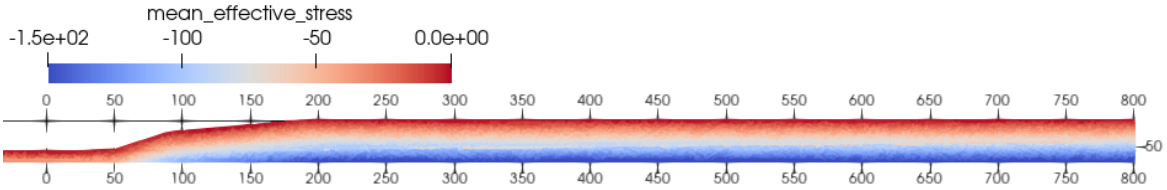

Figure 5-24. Initial stresses after gravity loading

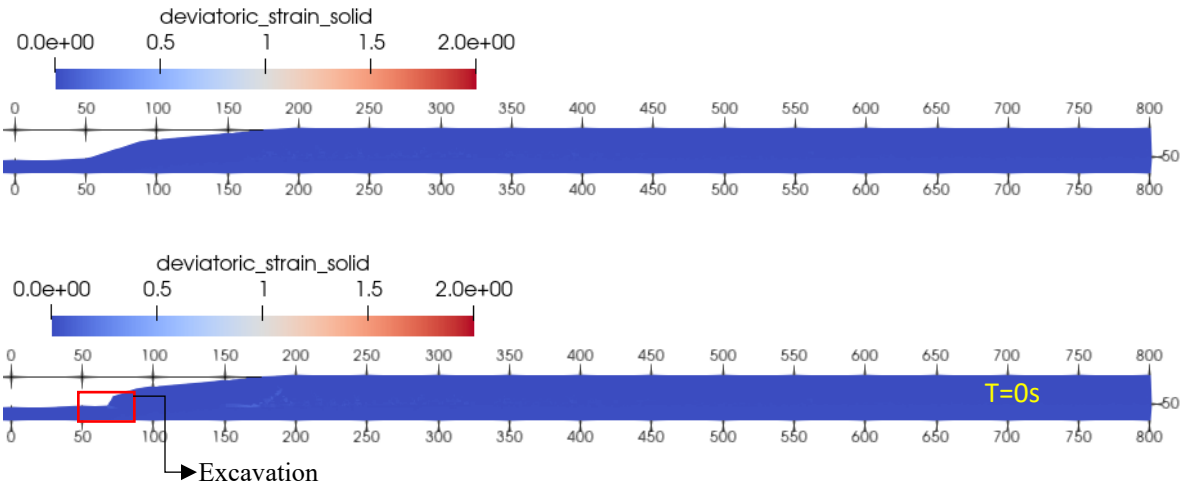

Figure 5-25. Failure initiation by replicating toe erosion

5.9 NUMERICAL RESULTS

5.9.1 Landslide mechanism

During excavation, the strain becomes localized within a narrow shear band in the most susceptible layer of sensitive clay Figure 5-26, manifesting within one second (T=1s). This strain concentration gives rise to forming a substantial shear band spanning 150 m, which is almost the length of a pre-existing band of slides, as mentioned by Evans and Brooks [66]. Almost simultaneously (T=5s), the excavation work triggers a minor slide at the slope's toe, resulting in the flow of remolded soil by eleven seconds (T=11s). This event, in turn, triggers the shear band spanning the pre-existing band of slides to fail, causing the soil mass within to initiate a forward translational movement.

As the soil progresses, it transforms into segmented blocks, flowing alongside the moving debris. This flow instigates a series of successive slides, with rapid sliding continuing until the debris movement slows down (T=100s). The pace of sliding then gradually reduces but persists over an extended period until the movement halts completely. However, slower successive sliding continues for a long time before the movement completely ceases (T=350s). The initial fifteen slides take place within the first 200 s (T=200s), while the final three slides unfold over the subsequent 150s (T=350s), resulting in a total retrogression distance of 480 m from the slope's crest.

This phenomenon aligns with the straightforward mechanism proposed by Bjerrum [74]. Yet, the development of each successive slide adheres to Odenstad's [78] mechanism, which involves the formation of alternating shear bands and prism-shaped soil blocks, creating structures resembling horsts and grabens. The rapid flow of debris leads to the eventual disappearance of these horst and graben structures, with only a few remaining near the crater, marking a stark contrast to the initial landscape.

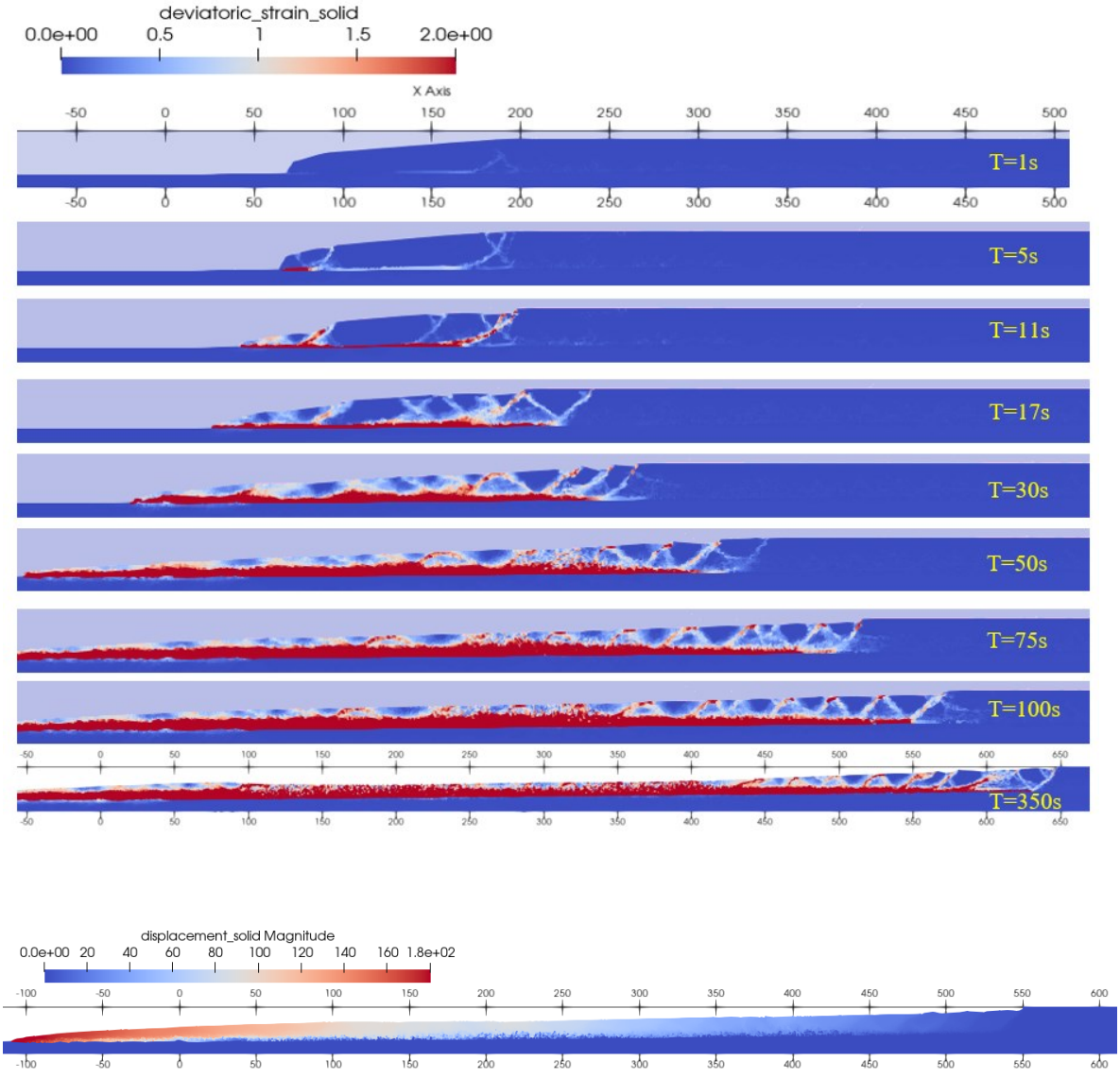

Figure 5-26. Failure mechanism and post-failure kinematics

5.9.2 Comparison with Field Observations

- The numerical simulation shows that the landslide occurred due to a loss of strength in an underlying sensitive clay zone beneath the surface, as identified by Evans and Brooks [66].
- The retrogression distance observed in the simulation reached 600m from the river itself and 475 meters from the headscarp of the prior retrogressive slides. In the field, the distances were 680 and 555m, respectively (Figure 5-27). The simulation predicted the post-failure retrogression 90% accurately.

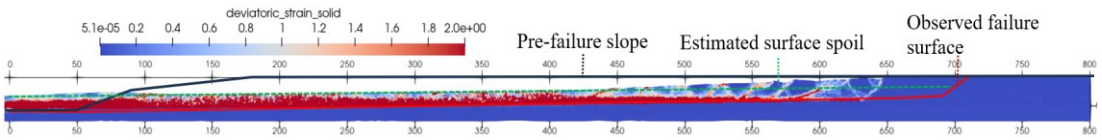

Figure 5-27. Comparison with field observations of Evans and Brooks [66].

- In the field observations within the crater, prismatic-shaped blocks were identified embedded in a mass of remolded spoil at multiple sites, notably near the crater's mouth. The simulation also highlighted the presence of prismatic-shaped ridges and valleys, a consequence of the formation of alternating shear bands (Figure 5-28).

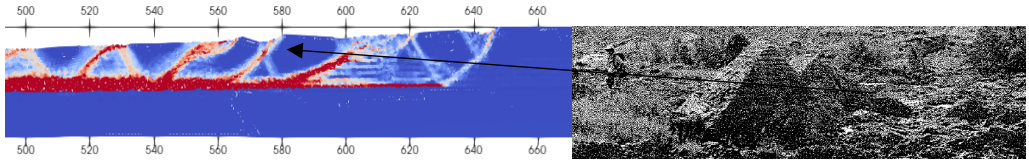

Figure 5-28. Prismatic blocks near the crest

- Upon the landslide's failure, the debris—comprising liquefied silts and clays, intact blocks of silt and sand, and rafts of sod, some bearing trees still upright in their natural growth position—surged into the basin of the South Nation Valley. This is due to the translational movements of material where the upper crust is intact, as observed in the simulation (Figure 5-29).

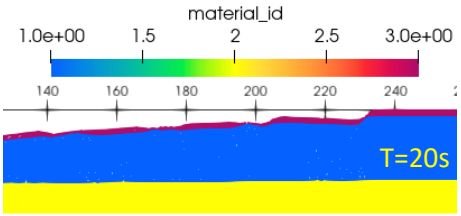

Figure 5-29. The intact upper layer after failure allows trees to remain upright in their natural growth position.

5.10 CONCLUSION

This study emphasizes the critical factors involved in using the Material Point Method (MPM) to predict retrogressive landslides in sensitive clays, detailing strategies to optimize simulation outcomes by carefully considering these factors. This study proposes a comprehensive methodology for selecting the optimal mesh size and material point density tailored to specific landslide scenarios, improving simulation accuracy and efficiency. Furthermore, the research explores the effectiveness of this numerical tool across various geometrical representations, a consideration vital for accurate modeling within a 2D plane strain framework, demonstrating that the simulated landslide kinematics corroborate the hypothesized behavior observed in the field across different cross-sections with varying element sizes and number of MPs per element. This study also discusses the scenarios of different landslide triggers for predictive purposes. The optimization strategies can be listed as follows,

- Using a smeared cracked approach as a mesh regularisation technique, retrogression and runout prediction accuracy is over 92% for a varying mesh size from 0.5m to 1.5m, while the landslide kinematics for each mesh size is not entirely the same but comparable. Coarser mesh size significantly reduces computational time.
- There is an optimal number of MPs per element for a particular element size beyond or below which the accuracy of prediction reduces. Sensitivity analysis shows that a minimal number of MPS per element capturing the post-failure kinematics properly should result in maximum accuracy. Increased MPs per element increase the computational time.

- The numerical model is capable of capturing the changes in the landslide retrogression and runout predictions for minor variations in different 2D cross-sections.
- If activating undrained conditions initiates failure in the model, additional excavation is redundant for replicating further erosion. However, adding further erosion doesn't alter the post-failure run-out or retrogression. For predictive purposes, if the slope is stable after activating undrained behavior, a small excavation is an effective way to trigger failure.

The strategies are considered for predicting the behavior of a complex real-case scenario with 90% prediction accuracy. This validation highlights the optimized simulation technique's reliability and need for detailed numerical analysis. The ability to predict landslides in sensitive clays holds significant promise for enhancing hazard mapping and risk analysis, potentially contributing to safer and more informed land-use planning and disaster preparedness.

CHAPTER 6

6.1 CONCLUSION

This comprehensive study contributes to advancing the understanding of retrogressive landslides in sensitive clays and offers practical tools for predicting and analyzing these critical events in geotechnical and geological contexts. The culmination of this research presents significant contributions and insights:

- A novel strain-softening equation was introduced, effectively replicating the nonlinear behavior observed in post-peak stress-strain curves. The equation adeptly addresses the challenge of accommodating the substantial stress-strain behavior of sensitive clays during large deformations, effectively surpassing limitations associated with conventional laboratory shear tests. By grounding the equation in the actual behavior of sensitive clays under large deformations, accurate predictions of post-peak stress-strain curves up to remolded shear stress levels were achieved.
- The comprehensive stress-strain curves generated by the newly developed equation offer a robust foundation for precise remolding energy calculations within sensitive clay slopes. Consequently, based on the remolding energy criterion, these calculations allow the accurate forecast of landslide vulnerability to retrogressive failure.
- The predicted retrogressive failures, using the newly developed strain softening equation alongside calibrated constitutive parameters, exhibited remarkable similarity with field observations. This validation not only affirms the applicability of the developed model for landslide prediction but also proves the effectiveness of the smeared crack approach in mitigating mesh dependency issues while incorporating strain-softening within continuum frameworks.
- The numerical model successfully captures the dynamics of shear band formation and showcases the progression of such bands during retrogressive landslide movements, enriching our understanding of these complex processes.

- Importantly, the predicted failure mechanisms generated by the numerical model align seamlessly with the theoretical assumptions established in previous literature, reinforcing the validity and reliability of the model's outcomes.

6.2 RECOMENDATION

Several avenues for future research emerge from this study's findings:

- **Preparation of sensitive clay landslide zonation maps:** Given that the input parameters are grounded in feasible soil investigation data, the model can readily be extended to landslide-prone areas with heightened risk factors to prepare landslide zonation maps in susceptible areas of eastern Canada, especially in Quebec. By employing the model, predictions of anticipated retrogression and runout can be generated, and these predictions can be further validated or fine-tuned based on future landslide occurrences.
- **Integrating the softening equation in other numerical frameworks:** The strain softening equation can be integrated into other numerical frameworks, which allows for increased flexibility in choosing between different numerical methods for modeling sensitive clays.
- **Transition to 3D Analysis**: The current implementation of the soil model in a 2D plane strain framework provides an initial understanding, but there is room for expansion into three-dimensional analysis. This extension would offer a more comprehensive depiction of the complexities of real-world scenarios, further enriching the model's capabilities.
- **Dynamic Loading Considerations:** The soil model, as it stands, does not account for dynamic loading parameters. To address this, future research could focus on adapting the model to dynamic loading conditions, enabling the assessment of retrogression potential in response to seismic events. This evolution would render the model even more versatile in predicting the behavior of sensitive clays under vary.

REFERENCES

1. NRCan: NRCan 2019, https://www.nrcan.gc.ca/science-and-data/science-and-research/natural-hazards/landslides/10661

2. Blais-Stevens, A.: Historical landslides in Canada resulting in fatalities (1771-2018). In: Geost.John's 2019, St.John's, Newfoundland and Labrador, Canada (2019)

3. Liu, Z., L'Heureux, J.S., Glimsdal, S., Lacasse, S.: Modelling of mobility of Rissa landslide and following tsunami. Comput Geotech. 140, (2021). https://doi.org/10.1016/j.compgeo.2021.104388

4. Pusch, R.: Recent quick-clay studies, an introduction. Eng Geol. 1, 413–414 (1966). https://doi.org/10.1016/0013-7952(66)90017-2

5. Lefebvre, G.: Sensitive clays of Eastern Canada: From geology to slope stability. In: Advances in Natural and Technological Hazards Research. pp. 15–34. Springer Netherlands (2017)

6. Rosenqvist, I.Th.: Norwegian research into the properties of quick clay—a review. Eng Geol. 1, 445–450 (1966). https://doi.org/10.1016/0013-7952(66)90020-2

7. Mitchell, R.J., Markell, A.R.: Flowsliding in Sensitive Soils. Canadian Geotechnical Journal. 11, 11–31 (1974)

8. Rødvand, L.A., Jostad, H.P., Grimstad, G., Andresen, L.: Strain localisation in sensitive clays: can rate dependency provide mesh independent results? Comput Geotech. 145, 104678 (2022). https://doi.org/10.1016/j.compgeo.2022.104678

9. Tran, Q.A., Sołowski, W.: Generalized Interpolation Material Point Method modelling of large deformation problems including strain-rate effects – Application to penetration and progressive failure problems. Comput Geotech. 106, 249–265 (2019). https://doi.org/10.1016/j.compgeo.2018.10.020

10. Wang, C., Hawlader, B., Perret, D., Soga, K.: Effects of geometry and soil properties on type and retrogression of landslides in sensitive clays. Géotechnique. 72, 322–336 (2022). https://doi.org/10.1680/jgeot.20.P.046

11. Zhang, X., Sloan, S.W., Oñate, E.: Dynamic modelling of retrogressive landslides with emphasis on the role of clay sensitivity. Int J Numer Anal Methods Geomech. 42, 1806–1822 (2018). https://doi.org/10.1002/nag.2815

12. Stark, T.D., Contreras, I.A.: Constant volume ring shear apparatus. Geotechnical Testing Journal. 19, 3–11 (1996). https://doi.org/10.1520/gtj11402j

13. Thakur, V., Jostad, H.P., Kornbrekke, H.A., Degago, S.A.: How well do we understand the undrained strain softening response in soft sensitive clays? In: Advances in Natural and Technological Hazards Research. pp. 291–303. Springer Netherlands (2014)

14. Durand, A.: Contribution à l'étude des étalements dans les argiles sensibles de la mer de Champlain, https://corpus.ulaval.ca/jspui/handle/20.500.11794/27148, (2016)

15. Locat, A.: Étude d'un Étalement Latéral dans Les Argiles de L'est du Canada et de la Rupture Progressive le Cas du Glissement de Saint-Barnabé-Nord, (2007)

16. Locat, A., Jostad, H.P., Leroueil, S.: Numerical modeling of progressive failure and its implications for spreads in sensitive clays. Canadian Geotechnical Journal. 50, 961–978 (2013). https://doi.org/10.1139/cgj-2012-0390

17. Locat, A., Leroueil, S., Fortin, A., Demers, D., Jostad, H.P.: The 1994 landslide at Sainte-Monique, Quebec: Geotechnical investigation and application of progressive failure analysis. Canadian Geotechnical Journal. 52, 490–504 (2015). https://doi.org/10.1139/cgj-2013-0344

18. Locat, A., Locat, P., Demers, D., Leroueil, S., Robitaille, D., Lefebvre, G.: The saint-jude landslide of 10 May 2010, Quebec, Canada: Investigation and characterization of the landslide and its failure mechanism. Canadian Geotechnical Journal. 54, 1357–1374 (2017). https://doi.org/10.1139/cgj-2017-0085

19. Thakur, V., Degago, S., Gylland, A.S., Sandven, R.: In-situ determination of disintegration energy for soft sensitive clays. In: GEOQuebec 2015, 68th Annual Canadian Geotechnical Conference. , Québec (2015)

20. Gylland, A.S., Thakur, V., Emdal, A.: Extended interpretation basis for the vane shear test. In: NGM 2016 Reykjavik, Proceedings of the 17th Nordic Geotechnical Meeting Challenges in Nordic Geotechnic . pp. 233–240 (2016)

21. Mohammadi, S., Taiebat, H.A.: A large deformation analysis for the assessment of failure induced deformations of slopes in strain softening materials. Comput Geotech. 49, 279–288 (2013). https://doi.org/10.1016/j.compgeo.2012.08.006

22. Thakur, V.: Numerically observed shear bands in soft sensitive clays. Geomechanics and Geoengineering. 6, 131–146 (2011). https://doi.org/10.1080/17486025.2010.546434

23. Einav, I., Randolph, M.F.: Combining upper bound and strain path methods for evaluating penetration resistance. Int J Numer Methods Eng. 63, 1991–2016 (2005). https://doi.org/10.1002/nme.1350

24. Rots, J., Natua, P., Kuster, G., Blaauwendraad, J.: Smeared crack approach and fracture localization in concrete. HERON 30. 1, 3–48 (1985)

25. Skempton, A.W., Northey, R.D.: The sensitivity of clays. Géotechnique. 3, 30–52 (1952). https://doi.org/10.1680/geot.1952.3.1.30

26. Crawford, C.B.: Quick clays of eastern Canada. Eng Geol. 2, 239–265 (1968). https://doi.org/10.1016/0013-7952(68)90002-1

27. Lefebvre, G.: Soft sensitive clays. , Washington, DC (1996)

28. Rosenqvist, I.T.: Considerations on the sensitivity of norwegian quick-clays. Géotechnique. 3, 195–200 (1953)

29. Norweigian Geotechnical Socieity: Retlingslinjer for Presentasjon av Geotekniske Unders ö kelser. (1974)

30. Bjrrum, L.: Stability of Natural Slopes in Quick Clay. Géotechnique. 5, 101–119 (1955). https://doi.org/10.1680/geot.1955.5.1.101

31. Varnes, D.J.: Landslide Types and Processes. , Washington, DC. (1978)

32. Dey, R., Hawlader, B., Phillips, R., Soga, K.: Large deformation finite-element modelling of progressive failure leading to spread in sensitive clay slopes. Geotechnique. 65, 657–668 (2015). https://doi.org/10.1680/geot.14.P.193

33. Wang, C., Hawlader, B., Perret, D., Soga, K.: Effects of geometry and soil properties on type and retrogression of landslides in sensitive clays. Géotechnique. 1–15 (2020). https://doi.org/10.1680/jgeot.20.p.046

34. Singh, V., Stanier, S., Bienen, B., Randolph, M.F.: Modelling the behaviour of sensitive clays experiencing large deformations using non-local regularisation techniques. Comput Geotech. 133, 104025 (2021). https://doi.org/10.1016/j.compgeo.2021.104025

35. Sulsky, D., Chenb, Z., Schreyer, H.L.: A particle method for history-dependent materials. Comput Methods Appl Mech Eng. 118, 179–196 (1994). https://doi.org/10.1016/0045-7825(94)90112-0

36. Enyang, Z., Wang, S., Wang, Y.: Modelling strain softening of structured soils. IOP Conf Ser Earth Environ Sci. 371, 022090 (2019). https://doi.org/10.1088/1755-1315/371/2/022090

37. Lefebvre, G.: Fourth Canadian Geotechnical Colloquium: Strength and slope stability in Canadian soft clay deposits. Canadian Geotechnical Journal. 18, 420–442 (1981). https://doi.org/10.1139/t81-047

38. Skempton, A.W.: Long-term stability of clay slopes. Géotechnique. 14, 77–102 (1964)

39. Bjerrum, L., Landva, A.: Direct Simple-Shear Tests on a Norwegian Quick Clay. Géotechnique. 16, 1–20 (1966). https://doi.org/10.1680/geot.1966.16.1.1

40. Bernander, S.: Progressive Landslides in Long Natural Slopes, (2000)

41. Gylland, A.S., Jostad, H.P., Nordal, S.: Failure geometry around a shear vane in sensitive clay. In: Proceedings of the 16th Nordic Geotechnical Meeting. , Copenhegen (2012)

42. Stark, T.D., Eid, H.T.: Drained Residual Strength of Cohesive Soils. Journal of Geotechnical Engineering. 120, 856–871 (1994). https://doi.org/10.1061/(ASCE)0733-9410(1994)120:5(856)

43. Demers, D., Robitaille, D., Locat, P., Potvin, J.: Inventory of large landslides in sensitive clay in the province of Québec, Canada: Preliminary analysis. In: Advances in Natural and Technological Hazards Research. pp. 77–89. Springer Netherlands (2014)

44. Tavenas, F., Flon, P., Leroueil, S., Lebuis, J.: Remolding energy and risk of retrogression in sensitive clays. In: Proceedings of the symposium on slopes on soft clays. pp. 423–454. , Linköping, Sweden, SGI Report No. 17 (1983)

45. Quinn, P.E., Diederichs, M.S., Rowe, R.K., Hutchinson, D.J.: A new model for large landslides in sensitive clay using a fracture mechanics approach. Canadian Geotechnical Journal. 48, 1151–1162 (2011). https://doi.org/10.1139/t11-025

46. Locat, A., et, Leroueil, S., Demers, D., Robitaille, D.: Investivation géotechnique de l'étalement de 1986 à Saint-Luc-de-Vicennnes. In: 66th Canadian Conference of Geotechinque. Montréal. , Montreal, Quebec (2013)

47. Urmi, Z.A., Chavali, R.V.P., Saeidi, A., Yerro, A.: Prediction of remolded shear strain for eastern Canadian sensitive clays. In: Cloutier, C., Turmel, D., Maghoul, P., and Locat, A. (eds.) 8th Canadian

Conference on Geotechnique and Natural Hazards : Geohazards 8. pp. 239–244. Canadian Geotechnical Scociety (CGS), Quebec (2022)

48. Vaid, Y.P., Robertson, P.K., Campanella, R.G.: Strain rate behaviour of Saint-Jean-Vianney clay. Canadian Geotechnical Journal. 16, 34–42 (1979). https://doi.org/10.1139/t79-004

49. Yin, Z.-Y., Karstunen, M., Chang, C.S., Koskinen, M., Lojander, M.: Modeling Time-Dependent Behavior of Soft Sensitive Clay. Journal of Geotechnical and Geoenvironmental Engineering. 137, 1103–1113 (2011). https://doi.org/10.1061/(ASCE)GT.1943-5606.0000527

50. Leroueil, S., Kabbaj, M., Tavenas, F., Bouchard, R.: Stress–strain–strain rate relation for the compressibility of sensitive natural clays. Géotechnique. 35, 159–180 (1985). https://doi.org/10.1680/geot.1985.35.2.159

51. Graham, J., Crooks, J.H.A., Bell, A.L.: Time effects on the stress-strain behaviour of natural soft clays. Géotechnique. 33, 327–340 (1983). https://doi.org/10.1680/geot.1983.33.3.327

52. Lefebvre, G., Leboeuf, D.: Rate effects and cyclic loading of sensitive clays. Journal of Geotechnical Engineering. 113, 476–489 (1987). https://doi.org/10.1061/(ASCE)0733-9410(1987)113:5(476)

53. Okamoto, T., Larsen, J.O., Matsuura, S., Asano, S., Takeuchi, Y., Grande, L.: Displacement properties of landslide masses at the initiation of failure in quick clay deposits and the effects of meteorological and hydrological factors. Eng Geol. 72, 233–251 (2004). https://doi.org/10.1016/j.enggeo.2003.09.004

54. Zhang, W., Wang, D.: Stability analysis of cut slope with shear band propagation along a weak layer. Comput Geotech. 125, (2020). https://doi.org/10.1016/j.compgeo.2020.103676

55. Puzrin, A.M., Germanovich, L.N.: The growth of shear bands in the catastrophic failure of soils. Proceedings of the Royal Society A: Mathematical, Physical and Engineering Sciences. 461, 1199–1228 (2005). https://doi.org/10.1098/rspa.2004.1378

56. Quinn, P.E., Diederichs, M.S., Rowe, R.K., Hutchinson, D.J.: Development of progressive failure in sensitive clay slopes. Canadian Geotechnical Journal. 49, 782–795 (2012). https://doi.org/10.1139/T2012-034

57. Zhang, W., Wang, D., Randolph, M.F., Puzrin, A.M.: Catastrophic failure in planar landslides with a fully softened weak zone. Geotechnique. 65, 755–769 (2015). https://doi.org/10.1680/geot14.P.218

58. Locat, A., Leroueil, S., Bernander, S., Demers, D., Jostad, H.P., Ouehb, L.: Progressive failures in eastern canadian and scandinavian sensitive clays. Canadian Geotechnical Journal. 48, 1696–1712 (2011). https://doi.org/10.1139/t11-059

59. Torrance, J.K.: Towards a general model of quick clay development. Sedimentology. 30, 547–555 (1983)

60. Hillaire-Marcel, L.: The fauna of the post glacial seas of Quebec: some palaeoecological aspects. Geographie Physique et Quaternaire. 34, 3–59 (1980). https://doi.org/10.7202/1000383ar

61. Lefebvre, G.: Slope instability and valley formation in Canadian soft clay deposits. Canadian Geotechnical Journal. 23, 261–270 (1986). https://doi.org/10.1139/t86-039

62. Urmi, Z.A., Chavali, R.V.P., Saeidi, A., Yerro, A.: Analytical and numerical assessment of the effect of erosion in sensitive clay landslide: A case study of Saint-Jude Landslide . In: Geo Calgary 2022. , Calgary (2022)

63. Eden, W.J., Mitchell, R.J.: The mechanics of landslides in Leda clay. Canadian Geotechnical Journal. 7, 285–296 (1970). https://doi.org/10.1139/t70-035

64. Donovan, J.J.: On the retrogression of landslides in sensitive muddy sediments: Discussion. Canadian Geotechnical Journal. 15, 441–446 (1978). https://doi.org/10.1139/t78-046

65. Karrow, P.F.: Earthflows in the Grondines and Trois Rivieres Areas, Quebec. Can J Earth Sci. 9, 561–573 (1972). https://doi.org/10.1139/e72-045

66. Evans, S.G., Brooks, G.R.: An earthflow in sensitive Champlain Sea sediments at Lemieux, Ontario, June 20, 1993, and its impact on the South Nation River. Canadian Geotechnical Journal. 31, 384–394 (1994). https://doi.org/10.1139/t94-046

67. Carson, M.A., Lajoie, G.: Some constraints on the severity of landslide penetration in sensitive deposits. Geographie Physique et Quaternaire. 35, 301–316 (1981). https://doi.org/10.7202/1000541ar

68. Tavenas, F.: Landslides in Canadian sensitive clays — a state-of-the-art. In: Proceedings of the 4th International Symposium on Landslides. pp. 141–153. University of Toronto Press, Torronto (1984)

69. Hungr, O., Leroueil, S., Picarelli, L.: The Varnes classification of landslide types, an update. Landslides. 11, 167–194 (2014). https://doi.org/10.1007/s10346-013-0436-y

70. Carson, M.A.: On the retrogression of landslides in sensitive muddy sediments. Canadian Geotechnical Journal. 14, 582–602 (1977). https://doi.org/10.1139/t77-059

71. Locat, A., Leroueil, S., Bernander, S., Demers, D., Locat, J., Ouehb, L.: Study of a lateral spread faiulre in an eastern Canada clay deposit in relation with progressive failure : The Saint-Barnabé-Nord slide. In: Proceedings of the 4th Canadian Conference on Geohazards: From Causes to Management, Québec, Que., 20–24 may (2008)

72. Demers, D., Robitaille, D., Locat, P., Potvin, J.: Inventory of large landslides in sensitive clay in the province of Québec, Canada: Preliminary analysis. In: Advances in Natural and Technological Hazards Research. pp. 77–89. Springer Netherlands (2014)

73. Quinn, P., Diederichs, M.S., Hutchinson, D.J., Rowe, R.K.: An exploration of the mechanics of retrogressive landslides in sensitive clay. In: 60th Canadian Geotechnical Conference and 8th Joint CGS/IAH-CNC Groundwater Conference, Ottawa, Ontario, Canada, October 21-24 (2007)

74. Bjerrum, L.: Stability of Natural Slopes in Quick Clay. Géotechnique. 5, 101–119 (1955). https://doi.org/10.1680/geot.1955.5.1.101

75. Mitchell, R.J., Markell, A.R.: Flowsliding in Sensitive Soils. Canadian Geotechnical Journal. 11, 11–31 (1974)

76. Lebuis, J., Rissman, P.: Earthflows in the Quebec and Shawnigan areas. Springer Netherlands, Quebec (1979)

77. Thakur, V., Degago, S.A.: Quickness of sensitive clays. Geotechnique Letters. 2, 87–95 (2012). https://doi.org/10.1680/geolett.12.0008

78. Odenstad, S.: The landslide in Skoptrop on the Lidan river. In: Royal Swedish Geotechnical Institute Proceedings No. 4 (1951)

79. Mollard, J.D., Hughes, G.T.: Earthflows in the Grondines and Trois Rivikres Areas, Quebec: Discussion. Canadian Geotechnical Journal. 10, 324–326 (1973). https://doi.org/10.1139/e73-029

80. Grondin, G., Demers, D.: The Saint-Liguori flakeslide: Characterisation and remedial works. In: In Proceedings of the 7th International Symposium on Landslides. pp. 743–748. , Trondheim (1996)

81. Zhang, X., Wang, L., Krabbenhoft, K., Tinti, S.: A case study and implication: particle finite element modelling of the 2010 Saint-Jude sensitive clay landslide. Landslides. 17, 1117–1127 (2020). https://doi.org/10.1007/s10346-019-01330-4

82. Wang, B., Hicks, M.A., Vardon, P.J.: Slope failure analysis using the random material point method. Geotechnique Letters. 6, 113–118 (2016). https://doi.org/10.1680/jgele.16.00019

83. Wang, B., Vardon, P.J., Hicks, M.A.: Investigation of retrogressive and progressive slope failure mechanisms using the material point method. Comput Geotech. 78, 88–98 (2016). https://doi.org/10.1016/j.compgeo.2016.04.016

84. Wang, B., Vardon, P.J., Hicks, M.A.: Investigation of retrogressive and progressive slope failure mechanisms using the material point method. Comput Geotech. 78, 88–98 (2016). https://doi.org/10.1016/j.compgeo.2016.04.016

85. Wang, B., Hicks, M.A., Vardon, P.J.: Slope failure analysis using the random material point method. Geotechnique Letters. 6, 113–118 (2016). https://doi.org/10.1680/jgele.16.00019

86. Dey, R., Hawlader, B., Phillips, R., Soga, K.: Numerical modeling of combined effects of upward and downward propagation of shear bands on stability of slopes with sensitive clay. Int J Numer Anal Methods Geomech. 40, 2076–2099 (2016). https://doi.org/10.1002/nag.2522

87. Dey, R., Hawlader, B.C., Phillips, R., Soga, K.: Numerical modelling of submarine landslides with sensitive clay layers. Geotechnique. 66, 454–468 (2016). https://doi.org/10.1680/jgeot.15.P.111

88. Islam, N., Hawlader, B., Wang, C., Soga, K.: Large-deformation finite-element modelling of earthquake-induced landslides considering strain-softening behaviour of sensitive clay. Canadian Geotechnical Journal. 56, 1003–1018 (2019). https://doi.org/10.1139/cgj-2018-0250

89. Wang, C., Hawlader, B., Perret, D., Soga, K., Chen, J.: Modeling of Initial Stresses and Seepage for Large Deformation Finite-Element Simulation of Sensitive Clay Landslides. Journal of Geotechnical and Geoenvironmental Engineering. 147, 04021111 (2021). https://doi.org/10.1061/(asce)gt.1943-5606.0002626

90. Zhou, H., Randolph, M.F.: Numerical investigations into cycling of full-flow penetrometers in soft clay. Géotechnique. 59, 801–812 (2009). https://doi.org/10.1680/geot.7.00200

91. Deglo De Besses, B., Magnin, A., Jay, P.: Viscoplastic flow around a cylinder in an infinite medium. J Nonnewton Fluid Mech. 115, 27–49 (2003). https://doi.org/10.1016/S0377-0257(03)00169-1

92. Zhu, H., Randolph, M.F.: Numerical analysis of a cylinder moving through rate-dependent undrained soil. Ocean Engineering. 38, 943–953 (2011). https://doi.org/10.1016/j.oceaneng.2010.08.005

93. Yuan, W.H., Liu, K., Zhang, W., Dai, B., Wang, Y.: Dynamic modeling of large deformation slope failure using smoothed particle finite element method. Landslides. 17, 1591–1603 (2020). https://doi.org/10.1007/s10346-020-01375-w

94. Shan, Z., Zhang, W., Wang, D., Wang, L.: Numerical investigations of retrogressive failure in sensitive clays: revisiting 1994 Sainte-Monique slide, Quebec. Landslides. 18, 1327–1336 (2021). https://doi.org/10.1007/s10346-020-01567-4

95. Shan, Z., Zhang, W., Wang, D., Wang, L.: Numerical investigations of retrogressive failure in sensitive clays: revisiting 1994 Sainte-Monique slide, Quebec. Landslides. 18, 1327–1336 (2021). https://doi.org/10.1007/s10346-020-01567-4

96. Tran, Q.A., Sołowski, W.: Generalized Interpolation Material Point Method modelling of large deformation problems including strain-rate effects – Application to penetration and progressive failure problems. Comput Geotech. 106, 249–265 (2019). https://doi.org/10.1016/j.compgeo.2018.10.020

97. Jin, Y.F., Yin, Z.Y., Yuan, W.H.: Simulating retrogressive slope failure using two different smoothed particle finite element methods: A comparative study. Eng Geol. 279, (2020). https://doi.org/10.1016/j.enggeo.2020.105870

98. Imran, J., Harff, P., Parker, G.: A numerical model of submarine debris flow with graphical user interface. Comput Geosci. 27, 717–729 (2001). https://doi.org/10.1016/S0098-3004(00)00124-2

99. Turmel, D., Locat, J.: Propagation of sensitive clay flowslides: a new approach Second JTC1 Workshop 3-5 December 2018, Hong Kong Triggering and Propagation of Rapid Flow-like Landslides. (2018)

100. Turmel, D., Locat, P., Locat, J., Locat, A., Leroueil, S.: The energy reduction factor (FER) to model sensitive clay flowslides using in situ geotechnical and rheological data. Landslides. 17, 839–853 (2020). https://doi.org/10.1007/s10346-019-01321-5

101. Zhang, X., Sheng, D., Sloan, S.W., Bleyer, J.: Lagrangian modelling of large deformation induced by progressive failure of sensitive clays with elastoviscoplasticity. Int J Numer Methods Eng. 112, 963–989 (2017). https://doi.org/10.1002/nme.5539

102. Prime, N., Dufour, F., Darve, F.: Solid-fluid transition modelling in geomaterials and application to a mudflow interacting with an obstacle. Int J Numer Anal Methods Geomech. 38, 1341–1361 (2014). https://doi.org/10.1002/nag.2260

103. Augarde, C.E., Lee, S.J., Loukidis, D.: Numerical modelling of large deformation problems in geotechnical engineering: A state-of-the-art review. Soils and Foundations. 61, 1718–1735 (2021). https://doi.org/10.1016/j.sandf.2021.08.007

104. Soga, K., Alonso, E., Yerro, A., Kumar, K., Bandara, S.: Trends in large-deformation analysis of landslide mass movements with particular emphasis on the material point method. Geotechnique. 66, 248–273 (2016). https://doi.org/10.1680/jgeot.15.LM.005

105. Wang, D., Bienen, B., Nazem, M., Tian, Y., Zheng, J., Pucker, T., Randolph, M.F.: Large deformation finite element analyses in geotechnical engineering, (2015)

106. Bathe, K.-J.: Finite Element Procedures in Engineering Analysis. Prentice hall, New Jersey (1996)

107. Hu, Y., Randolph, M.F.: A practical numerical approach for large deformation problems in soil. International Journal for Numerical And Analytical Methods in Geomechanics. 22, 327–350 (1996). https://doi.org/10.1002/(SICI)1096-9853(199805)22:5%3C327::AID-NAG920%3E3.0.CO;2-X

108. Ullah, S.N., Hou, L.F., Satchithananthan, U., Chen, Z., Gu, H.: A 3D RITSS approach for total stress and coupled-flow large deformation problems using ABAQUS. Comput Geotech. 99, 203–215 (2018). https://doi.org/10.1016/j.compgeo.2018.01.018

109. Tian, Y., Cassidy, M.J., Randolph, M.F., Wang, D., Gaudin, C.: A simple implementation of RITSS and its application in large deformation analysis. Comput Geotech. 56, 160–167 (2014). https://doi.org/10.1016/j.compgeo.2013.12.001

110. Zhang, W., Puzrin, A.M., Wang, D.: Transition from shear band propagation to global slab failure in submarine landslides. Canadian Geotechnical Journal. 56, 564–569 (2019). https://doi.org/10.1139/cgj-2017-0648

111. Qiu, G., Henke, S., Grabe, J.: Application of a Coupled Eulerian–Lagrangian approach on geomechanical problems involving large deformations. Comput Geotech. 38, 30–39 (2011). https://doi.org/10.1016/j.compgeo.2010.09.002

112. Dey, R., Hawlader, B., Phillips, R., Soga, K.: Progressive failure of slopes with sensitive clay layers. In: Proceedings of the 18th International Conference on Soil Mechanics and Geotechnical Engineering, Paris 2013 (2013)

113. Zhang, X., Sloan, S.W., Oñate, E.: Dynamic modelling of retrogressive landslides with emphasis on the role of clay sensitivity. Int J Numer Anal Methods Geomech. 42, 1806–1822 (2018). https://doi.org/10.1002/nag.2815

114. Zhang, W., Yuan, W., Dai, B.: Smoothed Particle Finite-Element Method for Large-Deformation Problems in Geomechanics. International Journal of Geomechanics. 18, 04018010 (2018). https://doi.org/10.1061/(asce)gm.1943-5622.0001079

115. Fern, J., Rohe, A., Soga, K., Alonso, E. eds: The Material Point Method for Geotechnical Engineering. CRC Press, Boca Raton : CRC Press, Taylor & Francis Group, [2019] (2019)

116. Dey, R., Hawlader, B., Phillips, R., Soga, K.: Numerical modeling of combined effects of upward and downward propagation of shear bands on stability of slopes with sensitive clay. Int J Numer Anal Methods Geomech. 40, 2076–2099 (2016). https://doi.org/10.1002/nag.2522

117. Lo, K.Y., Lee, C.F.: Stress analysis and slope stability in strain-softening materials. Géotechnique. 23, 1–11 (1973)

118. Bishop, A.W.: The Influence of Progressive Failure on the Choice of the Method of Stability Analysis. Géotechnique. 21, 168–172 (1971). https://doi.org/10.1680/geot.1971.21.2.168

119. Dey, R., Hawlader, B., Phillips, R., Soga, K.: Large deformation finite-element modelling of progressive failure leading to spread in sensitive clay slopes. Geotechnique. 65, 657–668 (2015). https://doi.org/10.1680/geot.14.P.193

120. Cloutier, C., Locat, J., Greetsema, M., Jacob, M., Schnorbus, M.: Potential impacts of climate change on landslides occurrence in Canada. In: Ho, K., Lacasse, S., and Picarelli, L. (eds.) Slope safety preparedness for impact of climate change. CRC Press, London (2016)

121. Wang, C., Hawlader, B., Perret, D., Soga, K., Chen, J.: Modeling of Initial Stresses and Seepage for Large Deformation Finite-Element Simulation of Sensitive Clay Landslides. Journal of Geotechnical and Geoenvironmental Engineering. 147, (2021). https://doi.org/10.1061/(ASCE)GT.1943-5606.0002626

122. Li, Y., Dijkstra, J., Karstunen, M.: Thermomechanical Creep in Sensitive Clays. Journal of Geotechnical and Geoenvironmental Engineering. 144, (2018). https://doi.org/10.1061/(ASCE)GT.1943-5606.0001965

123. Pinyol, N.M., Alvarado, M., Alonso, E.E., Zabala, F.: Thermal effects in landslide mobility. Géotechnique. 68, 528–545 (2018). https://doi.org/10.1680/jgeot.17.P.054

124. Dey, R., Hawlader, B., Phillips, R., Soga, K.: Modeling of large-deformation behaviour of marine sensitive clays and its application to submarine slope stability analysis. Canadian Geotechnical Journal. 53, 1138–1155 (2016). https://doi.org/10.1139/cgj-2015-0176

125. Bjerrum, L.: The Third Terzaghi Lectures; Progressive Failure in Slopes of Overconsolidated Plastic Clay and Clay Shales. Journal of the Soil Mechanics and Foundations Division. 93, 1–49 (1967). https://doi.org/10.1061/JSFEAQ.0001017

126. Gylland, A.S., Jostad, H.P., Nordal, S.: Experimental study of strain localization in sensitive clays. Acta Geotech. 9, 227–240 (2014). https://doi.org/10.1007/s11440-013-0217-8

127. Wang, C., Hawlader, B., Perret, D., Soga, K.: Effects of geometry and soil properties on type and retrogression of landslides in sensitive clays. Géotechnique. 1–15 (2020). https://doi.org/10.1680/jgeot.20.p.046

128. Thakur, V., Degago, S.A., Selänpää, J., Länsivaara, T.: Determination of Remoulding Energy of Sensitive Clays. Presented at the (2017)

129. Lebuis, J., Robert, J.M., Rissman, P.: Regional Mapping of Landslide Hazard in Quebec. In: Proceedings of the Symposium on slopes on soft clays. Swedish geotechnical Institute, Report no.17. pp. 205–262 (1983)

130. Tavenas, F., Des Rosiers, J.-P., Leroueil, S., La Rochelle, P., Roy, M.: The use of strain energy as a yield and creep criterion for lightly overconsolidated clays. Géotechnique. 29, 285–303 (1979). https://doi.org/10.1680/geot.1979.29.3.285

131. Mohammadi, S., Taiebat, H.A.: A large deformation analysis for the assessment of failure induced deformations of slopes in strain softening materials. Comput Geotech. 49, 279–288 (2013). https://doi.org/10.1016/j.compgeo.2012.08.006

132. Thakur, V.: Numerically observed shear bands in soft sensitive clays. Geomechanics and Geoengineering. 6, 131–146 (2011). https://doi.org/10.1080/17486025.2010.546434

133. Urmi, Z.A., Saeidi, A., Yerro, A., Chavali, R.V.P.: Effect of strain softening on the prediction of post-failure runout in sensitive clay landslide . In: NUMGE 2023: 10th European Conference on Numerical Methods in Geotechnical Engineering . , London (2023)

134. Thakur, V., Degago, S.A.: Quickness of sensitive clays. Geotechnique Letters. 2, 87–95 (2012). https://doi.org/10.1680/geolett.12.0008

135. Leroueil, S., Vaunat, J., Picarelli, L., Locat, J., Faure, R., Lee, H.: A geotechnical characterisation of slope movements. In: Proceedings of the 7th symposium on landslides. pp. 53–74. , Trondheim (1996)

136. Locat, P., Leroueil, S., Locat, J.: Remaniement et mobilité des débris de glissements de terrain dans les argiles sensibles de l'est du Canada. In: Proceedings of the 4th Canadian conference on Geohazards : From causes to management. p. 594. Presse de l'Université Laval, Québec (2008)

137. Mitchell, R.J.: Landslides at Breckenridge, Pineview Golf Club, and Rockcliffe. , Internal Report, National Research Council of Canada, Division of Building Research, Ottawa (1969)

138. Burn, K.N.: Direct simple shear tests on Leda clay. , Internal Report 363, Division of Building Research, National Research Council of Canada, Ottawa (1968)

139. Eide, O., Bjerrum, L.: The Slide at Bekkelaget. Géotechnique. 5, 88–100 (1955). https://doi.org/10.1680/geot.1955.5.1.88

140. Lefebvre, G., Poulin, C.: A new method of sampling in sensitive clay. Canadian Geotechnical Journal. 16, 226–233 (1979). https://doi.org/10.1139/t79-019

141. Rochelle, P. La, Sarrailh, J., Tavenas, F., Roy, M., Leroueil, S.: Causes of sampling disturbance and design of a new sampler for sensitive soils. Canadian Geotechnical Journal. 18, 52–66 (1981). https://doi.org/10.1139/t81-006

142. Leroueil, S., Tavenas, F., Bihan, J.-P. Le: Propriétés caractéristiques des argiles de l'est du Canada. Canadian Geotechnical Journal. 20, 681–705 (1983). https://doi.org/10.1139/t83-076

143. D'Ignazio, M., Jostad, H.P., Länsivaara, T., Lehtonen, V., Mansikkamäki, J., Meehan, C.: Effects of Sample Disturbance in the Determination of Soil Parameters for Advanced Finite Element Modelling of Sensitive Clays. Presented at the (2017)

144. Lunne, T., Berre, T., Andersen, K.H., Strandvik, S., Sjursen, M.: Effects of sample disturbance and consolidation procedures on measured shear strength of soft marine Norwegian clays. Canadian Geotechnical Journal. 43, 726–750 (2006). https://doi.org/10.1139/t06-040

145. Locat, A., Locat, P., Michaud, H., Hébert, K., Leroueil, S., Demers, D.: Geotechnical characterization of the Saint-Jude clay, Quebec, Canada. AIMS Geosci. 5, 273–302 (2019). https://doi.org/10.3934/geosci.2019.2.273

146. Carson, M.A., Lajoie, G.: Some constraints on the severity of landslide penetration in sensitive deposits. Géographie physique et Quaternaire. 35, 301–316 (1981). https://doi.org/10.7202/1000541ar

147. L'heureux, J.-S.: A study of the retrogressive behavior and mobility of Norwegian quick clay landslides. In: Proceedings of the 11th International & 2nd North American Symposium on Landslides, Banff, Canada (2012)

148. Turmel, D., Potvin, J., Demers, D., Locat, P., Locat, A., Locat, J., Leroueil, S.: Empirical estimation of the retrogression and the runout distance of sensitive clay flowslides. In: 7th Canadian Geohazards Conference – Geohazards 7. , Canmore, Alberta (2018)

149. Locat, J., Demers, D.: Viscosity, yield stress, remolded strength, and liquidity index relationships for sensitive clays. Canadian Geotechnical Journal. 25, 799–806 (1988). https://doi.org/10.1139/t88-088

150. Urmi, Z.A., Saeidi, A., Chavali, R.V.P., Yerro, A.: Failure mechanism, existing constitutive models and numerical modeling of landslides in sensitive clay: a review. Geoenvironmental Disasters. 10, 14 (2023). https://doi.org/10.1186/s40677-023-00242-9

151. Urmi, Z.A., Saeidi, A., Yerro, A., Chavali, R.V.P.: Prediction of post-peak stress-strain behavior for sensitive clays. Eng Geol. 323, 107221 (2023). https://doi.org/10.1016/j.enggeo.2023.107221

152. Urmi, Z.A., Saeidi, A., Yerro, A., Chavalli, R.V.P.: Implementation of a New Strain Softening Constitutive Model in the Material Point Method for the Simulation of Retrogressive Failure in Sensitive Clays. In: Geo-Congress 2024. pp. 286–296. American Society of Civil Engineers, Reston, VA (2024)

153. Anura3D MPM Research Community: <www.anura3d.com>

154. York Ii, A.R., Sulsky, D., Schreyer, H.L.: The material point method for simulation of thin membranes. INTERNATIONAL JOURNAL FOR NUMERICAL METHODS IN ENGINEERING Int. J. Numer. Meth. Engng. 44, 1429–1456 (1999)

155. de Vaucorbeil, A., Nguyen, V.P., Sinaie, S., Wu, J.Y.: Material point method after 25 years: Theory, implementation, and applications. Presented at the (2020)

156. Yost, K.M., Yerro, A., Green, R.A., Martin, E., Cooper, J.: MPM Modeling of Cone Penetrometer Testing for Multiple Thin-Layer Effects in Complex Soil Stratigraphy. Journal of Geotechnical and Geoenvironmental Engineering. 148, (2022). https://doi.org/10.1061/(ASCE)GT.1943-5606.0002730

157. Yerro, A., Alonso, E.E., Pinyol, N.M.: Run-out of landslides in brittle soils. Comput Geotech. 80, 427–439 (2016). https://doi.org/10.1016/j.compgeo.2016.03.001

158. Alsardi, A., Yerro, A.: Coseismic site response and slope instability using periodic boundary conditions in the material point method. Journal of Rock Mechanics and Geotechnical Engineering. 15, 641–658 (2023). https://doi.org/10.1016/j.jrmge.2022.09.016

159. Soga, K., Alonso, E., Yerro, A., Kumar, K., Bandara, S.: Trends in large-deformation analysis of landslide mass movements with particular emphasis on the material point method. Géotechnique. 66, 248–273 (2016). https://doi.org/10.1680/jgeot.15.LM.005

160. Troncone, A., Pugliese, L., Parise, A., Conte, E.: Analysis of a landslide in sensitive clays using the material point method. Geotechnical Research. 10, 67–77 (2023). https://doi.org/10.1680/jgere.22.00060

161. Tremblay-Auger, F., Locat, A., Leroueil, S., Locat, P., Demers, D., Therrien, J., Mompin, R.: The 2016 landslide at Saint-Luc-de-Vincennes, Quebec: geotechnical and morphological analysis of a combined flowslide and spread. Canadian Geotechnical Journal. 58, 295–304 (2021). https://doi.org/10.1139/cgj-2019-0671

162. Oliver, J., Huespe, A.E.: Continuum approach to material failure in strong discontinuity settings. Comput Methods Appl Mech Eng. 193, 3195–3220 (2004). https://doi.org/10.1016/j.cma.2003.07.013

163. Alsardi, A., Copana, J., Yerro, A.: Modelling earthquake-triggered landslide runout with the material point method. Proceedings of the Institution of Civil Engineers - Geotechnical Engineering. 174, 563–576 (2021). https://doi.org/10.1680/jgeen.20.00235

164. Zambrano-Cruzatty, L., Yerro, A.: Numerical simulation of a free fall penetrometer deployment using the material point method. Soils and Foundations. 60, 668–682 (2020). https://doi.org/10.1016/j.sandf.2020.04.002

165. Ceccato, F., Simonini, P.: Numerical features used in simulations. In: Fern, J., Rohe, A., Soga, K., and Alonso, E. (eds.) The Material Point Method for Geotechnical Engineering. . pp. 101–124. CRC Press (2019)

166. Shen, J., Chen, Q., Wang, L., Wang, D.: Numerical investigations of the failure mechanism of spreading landslides. Canadian Geotechnical Journal. 61, 228–240 (2024). https://doi.org/10.1139/cgj-2022-0533

167. Urmi, Z.A., Saeidi, A., Chavali, R.V.P., Yerro, A.: Failure mechanism, existing constitutive models and numerical modeling of landslides in sensitive clay: a review. Geoenvironmental Disasters. 10, 14 (2023). https://doi.org/10.1186/s40677-023-00242-9

168. Thakur, V., Nordal, S., Viggiani, G., Charrier, P.: Shear bands in undrained plane strain compression of Norwegian quick clays. Canadian Geotechnical Journal. 55, 45–56 (2018). https://doi.org/10.1139/cgj-2016-0443

169. Urmi, Z.A., Yerro, A., Saeidi, A., Chavali, R.V.P.: Prediction of retrogressive landslide in sensitive clays by incorporating a novel strain softening law into the Material Point Method. Eng Geol. 340, 107669 (2024). https://doi.org/10.1016/j.enggeo.2024.107669

170. Yost, K.M., Yerro, A., Green, R.A., Martin, E., Cooper, J.: MPM Modeling of Cone Penetrometer Testing for Multiple Thin-Layer Effects in Complex Soil Stratigraphy. Journal of Geotechnical and Geoenvironmental Engineering. 148, (2022). https://doi.org/10.1061/(ASCE)GT.1943-5606.0002730

171. Yerro, A., Alonso, E.E., Pinyol, N.M.: Run-out of landslides in brittle soils. Comput Geotech. 80, 427–439 (2016). https://doi.org/10.1016/j.compgeo.2016.03.001

172. Alsardi, A., Yerro, A.: Coseismic site response and slope instability using periodic boundary conditions in the material point method. Journal of Rock Mechanics and Geotechnical Engineering. 15, 641–658 (2023). https://doi.org/10.1016/j.jrmge.2022.09.016

173. Troncone, A., Pugliese, L., Parise, A., Conte, E.: A simple method to reduce mesh dependency in modelling landslides involving brittle soils. Géotechnique Letters. 12, 167–173 (2022). https://doi.org/10.1680/jgele.22.00023

174. Ceccato, F., Yerro, A., Martinelli, M.: Modelling soil-water interaction with the material point method. Evaluation of single-point and double-point formulations. In: Numerical methods in geotechnical engineering IX. pp. 351–358. CRC Press (2018)

PUBLICATIONS

JOURNALS

1. Urmi, Z. A., Saeidi, A., Yerro, A., and Chavali, R. V. P. 2023. Prediction of post-peak stress-strain behavior for sensitive clays. Engineering Geology, Volume 323. https://doi.org/10.1016/j.enggeo.2023.107221
2. Urmi, Z. A., Saeidi, A., Chavali, R. V. P., and Yerro, A. 2023. Failure mechanism, existing constitutive models and numerical modeling of landslides in sensitive clay: a review. Geoenvironmental Disasters, 10(14). https://doi.org/10.1186/s40677-023-00242-9
3. Urmi, Z. A., Saeidi, A., Yerro, A., and Chavali, R. V. P. 2023. Prediction of retrogressive landslide in the sensitive clays: Incorporating a novel Strain Softening Constitutive Model into the Material Point Method. Engineering Geology, Volume 340. https://doi.org/10.1016/j.enggeo.2024.107669
4. Urmi, Z. A., Saeidi, A., Yerro, A., and Chavali, R. V. P. 2023. Balancing Advanced Numerical Techniques and Engineering Judgment in Predicting Retrogressive Landslides in Sensitive Clays for Increased Reliability. Submitted.

CONFERENCES

1. Urmi, Z. A., Saeidi, A., Yerro, A., and Chavali, R. V. P. 2024. Implementation of a New Strain Softening Constitutive Model in the Material Point Method for the Simulation of Retrogressive Failure in Sensitive Clays. In: Geo Congress 2024 .25th-28th February 2024, Vancouver, Canada.
2. Urmi, Z. A., Saeidi, A., Yerro, A., and Chavali, R. V. P. 2023. Effect of strain softening on predicting post-failure runout in sensitive clay landslide. In: The 10th European Conference on Numerical Methods in Geotechnical Engineering (NUMGE 2023).25th-28th June 2023, London, United Kingdom.
3. Urmi, Z. A., Chavali, R. V. P., Saeidi, A., and Yerro, A. 2022. Analytical and numerical assessment of the effect of erosion in sensitive clay landslide: a case study of Saint-Jude Landslide. In: The 75th Canadian Geotechnical Conference – Geo Calgary 2022, 2nd-5th October 2022, Calgary, Canada.

4. Urmi, Z. A., Chavali, R. V. P., Saeidi, A. and Yerro, A. 2022. Prediction of Remolded Shear Strain for Eastern Canadian Sensitive Clays. Proceedings of the 8th Canadian Conference on Geotechnique and Natural Hazards – Geohazard 2022, 12th – 15th June 2022, Quebec, Canada.
5. Urmi, Z. A., Saeidi, A., Chavali, R. V. P. 2021. Evaluation of the applicability of numerical methods for landslide analysis in sensitive clays. The 1971 Saint Jean Vianney disaster: 50 years of advancing geotechnical knowledge, 13th – 14th May 2021, Quebec, Canada.

APPENDIX: CONFERERENCE PUBLICATIONS

Prediction of remolded shear strain for eastern Canadian sensitive clays

Zinan Ara Urmi, Rama Vara Prasad Chavali & Ali Saeidi
Department of Applied Science – University of Quebec at Chicoutimi, Saguenay, Quebec, Canada
Alba Yerro
Department of Geotechnical Engineering – Virginia Tech, Blacksburg, Virginia, USA

ABSTRACT
Remolded shear strain is one of the key components for the post-failure analysis of sensitive clay landslides. This is the strain at which sensitive clays almost reach their remolded shear strength and start to transform to a liquid-like mass from a solid state. The velocity of liquified debris and the final runout are significantly dependent on the strain energy, and remolded shear strain is one of the most important factors controlling the strain energy. However, the remolded strain of sensitive clays is very large, and it is practically impossible to determine using conventional laboratory testing. This paper presents an indirect method for obtaining remolded shear strain with a strain-softening equation combined with laboratory test results. The method is then validated against two well-known previously occurred landslide sites in Quebec.

RÉSUMÉ
La déformation résiduelle est l'un des éléments clés de l'analyse post-rupture des glissements de terrain dans les argiles sensibles. C'est le seuil où les argiles sensibles commencent à se transformer en une masse liquide à partir d'un état solide intact. La vitesse des débris liquéfiés et leurs distances parcourus final dépendent de de l'énergie de déformation, et la déformation résiduelle est l'un des composants les plus importants de la mesure de l'énergie de déformation. Cependant, la déformation résiduelle est un paramètre important pour les argiles sensibles qu'il est pratiquement impossible de la déterminer au moyen d'essais conventionnels en laboratoire. Cet article présente une méthode indirecte pour déterminer la déformation de cisaillement résiduelle avec une équation pour le partie anti-écrouissage combinée à des résultats d'essais en laboratoire. La méthode est ensuite validée à l'aide des résultats de deux sites de glissements de terrain bien connus au Québec.

INTRODUCTION

Landslides in sensitive clays are regarded as the major hazard in Canada (Lefebvre et al. 2017). Natural resources Canada has reported that the annual damages by landslides in Canada are worth $200 to $400 million (NRCan 2019). A total of 778 people has died in the landslide events all over Canada from 1771 to 2018 (Stevens 2019). The unique nature of sensitive clay is that it experiences extensive strength degradation at large strains and completely loses its strength to retain the intact solid state. With appreciable displacement, the clays transform to a liquid-like substance and start to flow under increasing stress. This characteristic significantly affects the mechanism of landslides in this type of clays. Due to the clay being fluidized, the retrogression (i.e., the distance between the toe of the slope before and after landslide) and runout (i.e., the total displacement of the fluidized soil mass from the toe of the slope) of these landslides are extremely high, over 1000m in Canadian sensitive clays (Demers et al. 2014). The highest retrogression and runout recorded in Norway in sensitive clays are over 2000m and 5000m, respectively (Thakur et al. 2014). The strain at which the soil starts to transform from solid to liquid (i.e., remolded strain) is vital for analyzing the post-failure behavior of sensitive clays landslides. However, it is practically impossible to reach such a large strain with conventional shear testing such as Direct Simple Shear (DSS) or Triaxial Shear Testing. For measuring large strain, DSS is preferred, which is in general limited to 30-40% maximum shear strain.

Quinn et al. (2011) attempted to determine remolded shear displacement for eastern Canadian sensitive clays. He interpreted stress-displacement curves from the remolding index vs. strain energy curves of Tavenas et al. (1983) to estimate remolded shear displacement. Later on, Dey et al. (2016a) worked with the interpreted curves from Quinn et al. (2011) and tried to fit the curves with an exponential strain-softening equation provided by Einav and Randolph (2005). He concluded that the remolded shear displacement is so large that it can not be estimated from the exponential equation. He defined a residual shear displacement at the end of the exponential curve and incorporated a linear degradation connecting the residual and remolded

displacements. Thakur and Degago (2013) provided a value of remolded shear strain for Norwegian clays as 300, but no site-specific approach was made. All the recent studies in the simulation of sensitive clay landslides in Canada (Dey et al. 2015, 2016b; Tran and Solowski 2018; Wang et al. 2020, 2021; Zhang and Wang 2020) have been done with an assumed value of remolded shear strain, and the values have been adjusted through a back analysis of known post-failure conditions. Nevertheless, Turmel et al. (2019) introduced a new concept, energy reduction factor (F_{ER}), to assess the runout distance of Rivière Saint-Jean flow slide. The energy reduction factor, defined as the ratio of the potential energy to the energy available for the mobility of the remolded sensitive clay, is believed to be a realistic approach in modeling runout distance. This approach warrants a need for the estimation of the strain energy required to completely remold the soil (remolding energy) which is a direct function of remolded shear strain. Due to the unavailability of the complete stress-strain curve, the authors had to use an empirical equation to obtain the remolding energy. In a nutshell, even though the remolded shear strain of sensitive clays is vitally important, the work related to the estimation of this parameter is limited. This study seeks to provide a methodology to estimate the remolded shear strain for eastern Canadian sensitive clays.

1 ESTIMATION OF REMOLDED STRAIN

In this study, for the estimation of the remolded shear strain, firstly, the remolding index-strain energy curves (Tavenas et al. 1983) are converted to stress-strain curves. Then, remolded strains are estimated from the interpreted curves. Next, the stress-strain curves are fitted to Einav and Randolph's (2005) strain-softening equation, and a relationship between γ_{95} and γ_r is established. Finally, a methodology is provided to estimate γ_r from laboratory test results combined with the softening equation.

1.1 Interpretation of stress-strain curve from remolding index-strain energy curve

Quinn et al. (2011) first interpreted the energy curves from Tavenas et al. (1983) to stress-strain and stress-displacement curves considering some simple assumptions. The authors of this paper reinterpreted those curves, and the reasons behind them will be clarified further through this section.

From Tavenas et al. (1983), the values of remolding index I_r are defined as

$$I_r = \frac{\tau_p - \tau_x}{\tau_p - \tau_r} \times 100\% \qquad [1]$$

where, τ_p, τ_x, and τ_r are the peak shear strength, shear strength at any point after the peak, and remolded shear strength. Additionally, the normalized strain energy (w_N) corresponding to a particular I_r is defined as

$$w_N = \frac{Wx}{0.013\acute{\sigma}_p} \times 100\% \qquad [2]$$

where w_x is the energy per unit volume (kN-m/m^3) and $\acute{\sigma}_p$ is the pre-consolidation pressure.

A stress-strain curve has been considered for sensitive clays, as shown in Figure 1.

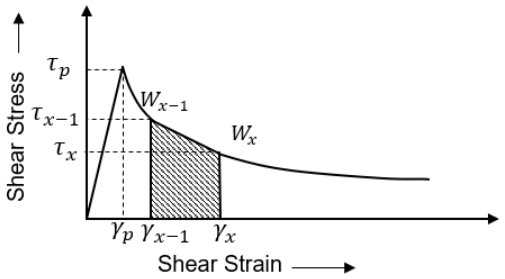

Figure 1. Stress-strain curve of a sensitive clay.

It is assumed that the soil is perfectly elastic up to the peak (i.e., no energy dissipation during this part of the curve). Consider two points in the curve after the peak at a stress τ_{x-1} and τ_x having strains γ_{x-1} and γ_x, respectively. Therefore, the strain energy required for the reduction of the stress from τ_{x-1} to τ_x is the shaded area under the stress-strain curve in Figure 1. This energy is the difference between the energies at these two points (i.e., w_{x-1} and w_x), and it can be approximated as such,

$$\frac{1}{2}(\tau_{x-1} + \tau_x)(\gamma_x - \gamma_{x-1}) = w_x - w_{x-1}$$
$$\gamma_x = \frac{2(w_x - w_{x-1})}{(\tau_{x-1} + \tau_x)} + \gamma_{x-1} \qquad [3]$$

The very first τ_{x-1}, γ_{x-1}, and w_{x-1} are the peak stress (τ_p), peak strain (γ_p), and the energy required to reach the peak stress (w_{LS}). As per Tavenas et al. (1979) the energy required to reach the peak stress (Limit state energy) can be expressed as,

$$w_{LS} = 0.013\acute{\sigma}_p \qquad [4]$$

Again, assuming an elastic behavior up to the peak, one can determine,

$$\gamma_p = \frac{2 \times w_{LS}}{\tau_p} \qquad [5]$$

While τ_x can be determined from Equation 1. Using Equation 1-5, I_r vs w_N curves can be converted to stress-strain curves. Figure 2 and Figure 3 show the

remolding index vs. normalized strain energy curve (Tavenas et al. 1983) and the interpreted stress-strain curves.

For the interpretation of strains (γ_x), Quinn et al. (2011) proposed the following equation,

$$\gamma_x = \frac{2w_N}{(\tau_{x-1}+\tau_x)} + \gamma_{x-1} \quad [6]$$

It can be noted that instead of using the difference of energies between two incremental stresses $w_x - w_{x-1}$ Equation 6 considers the normalized strain energy of the current step. Moreover, in Equation 6, normalized strain energy is taken instead of energy per unit volume, which ignores the limit state energy (w_{LS}). Furthermore, γ_p =1 is assumed for interpretation of shear strain (γ_x) from Equation 6, which gives a peak shear strength (τ_p)= 200kPa for all the soil samples as per Equation 5. It contradicts taking the value of peak strength of respective sites from fall cone test results of Tavenas et al. (1983) for the interpretation.

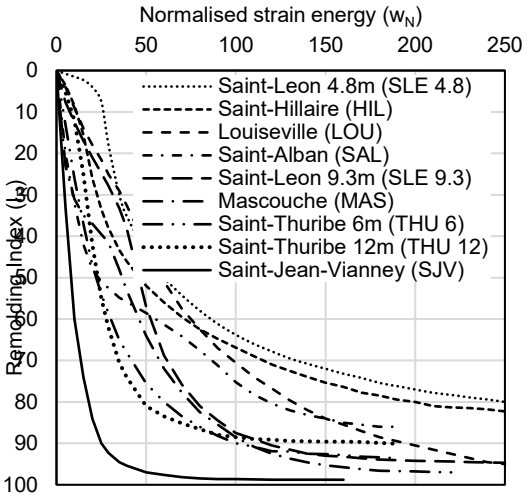

Figure 2. Relationship between normalized energy and remolding index for Champlain clay samples (replotted from Tavenas et al. 1983).

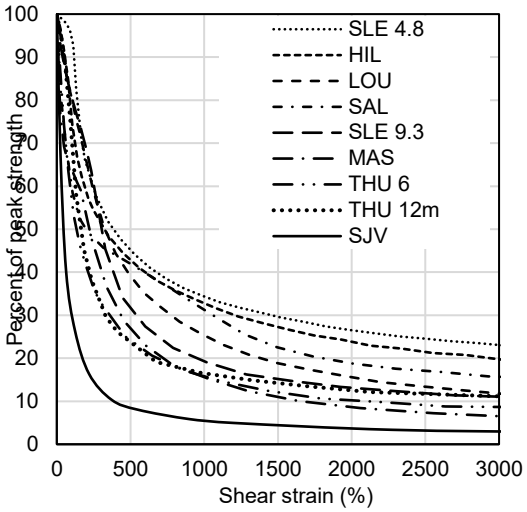

Figure 3. Strength-reduction curves interpreted from Tavenas et al. (1983).

A comparison between the interpreted curves using Equation 3 and Equation 6 (Quinn et al., 2011) has been illustrated in Figure 4 and Figure 5. It can be seen that the variation of the curves is significant. From the interpretation of Quinn et al. (2011), the strains are considerably high. Tavenals et al. (1983) determined the strain energy from four methods, one of which was simple shearing. The description of these tests can be found in Flon (1982). Each cycle of simple shearing was equivalent to a displacement of 16cm, and the highest number of cycles for each sample varied between 60 to 90. The sample size was 12x12x10cm. Therefore, the highest strain for each sample could be in the range of 8000-12000%, if not exact but somewhat near. From this study, the highest values of interpreted strains from the last point of strain energy curves are in the range of 3200-12000%, whereas the interpreted strains by Quinn et al. (2011) for the last points are in the range of 14000-55000%. That is why the re-interpretation of the strains was considered important in this study.

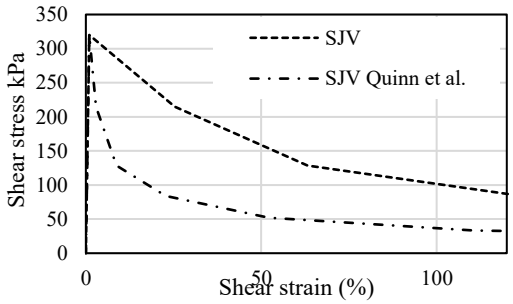

Figure 4. Comparison of the Stress-strain curve for the site Saint-Jean-Vianney interpreted by this study with Quinn et al. (2011)

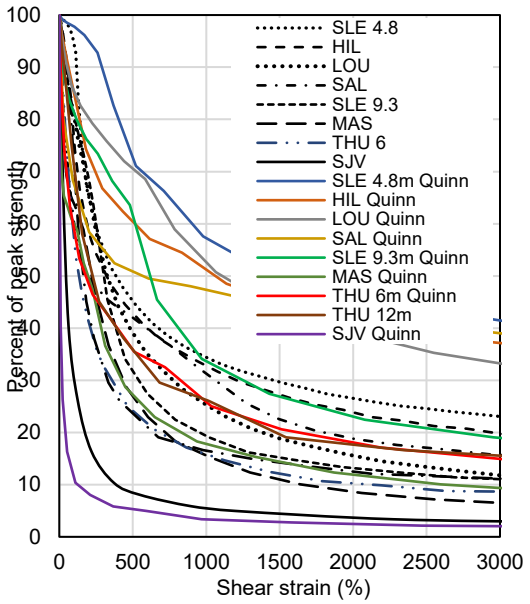

Figure 5. Comparison of the strength reduction curves interpreted by this study with Quinn et al. (1983)

1.2 Determination of the remolded strain from the interpreted curves

From the newly interpreted curves, it can be observed that at some point during the softening, the rate of strength reduction is very low, as the curve tends to be almost a horizontal straight line. The strain at which the rate of strength reduction is less than 0.5% (beyond this point, reduction of stress by 0.005kPa requires a minimum of 500% of strain increase) is taken as the remolded strain, as illustrated in Figure 6. Based on this, the remolded strains obtained for all the reference sites are presented in Table 1.

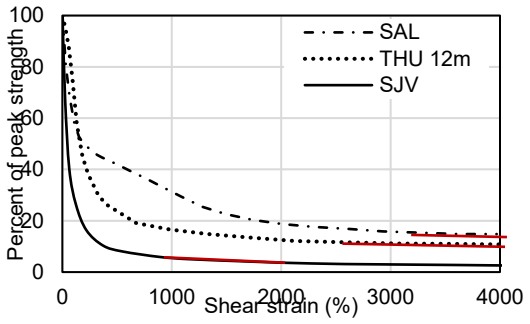

Figure 6. Determination of the remolded shear strain from the interpreted stress-strain curve

Table 1. Remolded strain for the sensitive clays of different Champlain-Sea clays

Sites	Remolded strain γ_r(%)
Saint- Léon 4.8m	3044
Saint- Léon 9.3m	3114
Saint-Hillaire	3242
Louiseville	4685
Saint-Alban	3265
Maschouche	4486
Saint-Thuribe 6m	2636
Saint-Thuribe 12m	2583
Saint-Jean-Vianney	899

1.3 Relationship between γ_{95} and γ_r

The use of exponential strain-softening laws is relatively common for predicting the stress-strain behavior of sensitive clays (Dey et al. 2015, 2016; Wang et al. 2018, 2020; Zhang et al. 2020; Tran and Solowoski 2021). These are based on an exponential law provided by Einav and Randolph (2005) as follows

$$\frac{s_u}{s_{up}} = \left[\frac{1}{s_t} + \left(1 - \frac{1}{s_t}\right) e^{-3\frac{\gamma}{\gamma_{95}}}\right] \quad [7]$$

Where s_{up} is the peak shear strength, s_u is the degraded shear strength after the peak, s_t is the clay sensitivity, which is understood as the ratio between the peak and the remolded shear strength ($\frac{s_{up}}{s_{ur}}$) of the clay, γ is the strain corresponding to s_u, and γ_{95} is the strain when the strength is reduced 95% of the supposed total reduction (s_{up}-s_{ur}).

To assess the compatibility of Equation 7, particularly for Canadian sensitive clays, previous curves based on Einav and Randolph (2005) are compared with the reinterpreted curves based on Tavenas et al. (1983). For plotting the curves as per Equation 7, the value of sensitivity and γ_{95} is required. For determination of the sensitivity, the remolded stress has been taken as the stress corresponding to remolded strain from the curves (Figure 3), and γ_{95} is taken as the 95% degradation of peak strength to remolded strength. It can be observed from Figure 7 that the initial portion of the interpreted curves from Equation 7 doesn't exactly match with that of the curves interpreted from the data of Tavenas et al. (1983), but the area under the curves appears to be similar. The final portion of the curves fits well.

Dey et al. (2016a) provided an indirect method to estimate γ_{95} by rearranging Einav and Randolph's equation (Equation 7) because in most cases obtaining such high strain by conventional shear testing (DSS or Triaxial) is not possible. By rearranging Equation 7, one can get,

$$\gamma_{95} = -3\frac{\gamma}{\ln\left[\left(\frac{s_u}{s_{up}} - \frac{1}{s_t}\right)/\left(1 - \frac{1}{s_t}\right)\right]} \quad [8]$$

The problem with Equation 8 is that for each pair of stress and strain (s_u and γ) values, there could be a different value of γ_{95}. Dey et al. (2016a) suggested estimating γ_{95} from 50% degraded stress and strain (s_{u50} and γ_{50}) assuming that 50% reduction of stress is attainable by laboratory testing. Therefore, γ_{95} is re-evaluated from Equation 8 using the respective sensitivities of the sites provided by Tavenal et al. (1983). Tables 2 and 3 are the estimation and comparison for estimated γ_{95} directly from Figure 3 and Equation 8. It can be observed from Tables 2 and 3 that the estimated values of γ_{95} from equation 8 with 50% degraded stress and strains are very close to the ones obtained from the interpreted curves of Figure 3 other than Saint-Thuribe 6m and Saint-Jean-Vianney.

Table 2. Estimation of γ_{95} (%) from Equation 8.

Sites	s_t	s_{u50}/s_{up}	γ_{50}(%)	γ_{95} (%)
Saint- Léon 4.8m	60	0.492	415	1711
Saint- Léon 9.3m	24	0.497	324	1240
Saint-Hillaire	106	0.495	340	1432
Louiseville	30	0.483	360	1413
Saint-Alban	105	0.495	215	905
Maschouche	104	0.495	245	1031
Saint-Thuribe 6m	137	0.496	140	593
Saint-Thuribe 12m	600	0.499	176	758
Saint-Jean-Vianney	260	0.498	52	223

.

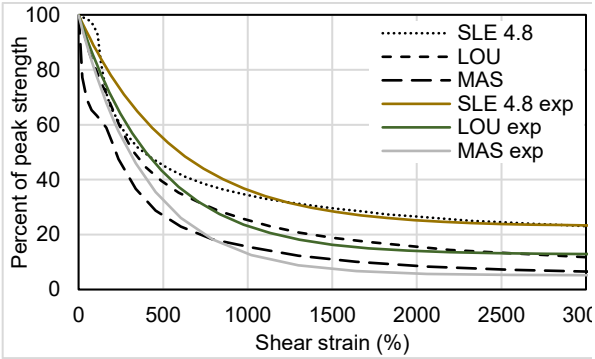

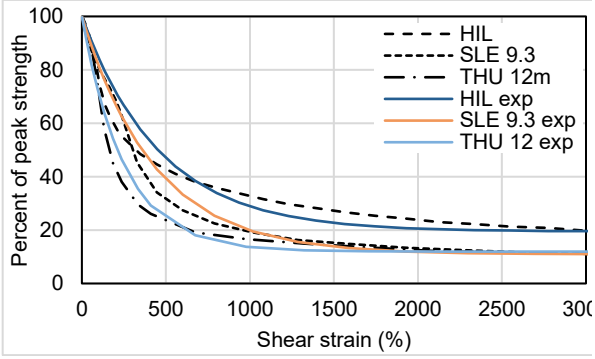

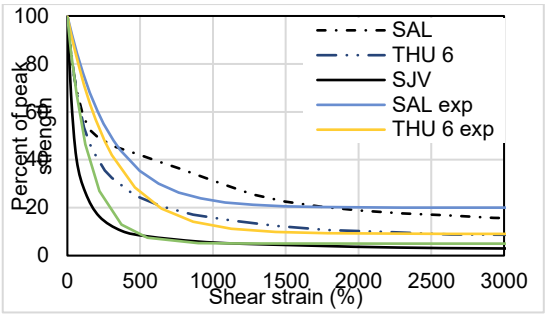

Figure 7. Comparison of the interpreted curves from Tavenas et al. (1983) and Einav and Randolph's (2005) equation

Table 3. Comparison of estimated γ_{95} for the sensitive clays of different Champlain-Sea clay.

Sites	γ_{95} (%) from curve	γ_{95} (%) from Equation
Saint- Léon 4.8m	1700	1711
Saint- Léon 9.3m	1300	1240
Saint-Hillaire	1500	1432
Louiseville	1400	1413
Saint-Alban	1000	905
Maschouche	1200	1031
Saint-Thuribe 6m	900	593
Saint-Thuribe 12m	800	758
Saint-Jean-Vianney	450	223

Table 4. Comparison of estimated γ_{95} for the sensitive clays of different Chaplain-Sea clay

Sites	γ_r (%)	γ_{95} (%)	$\frac{\gamma_r}{\gamma_{95}}$	Average
Saint- Léon 4.8m	3044	1711	1.8	
Saint- Léon 9.3m	3114	1240	2.4	
Saint-Hillaire	3242	1432	2.2	
Louiseville	4685	1413	3.6	
Saint-Alban	3265	905	3.3	
Maschouche	4486	1031	3.7	2.8
Saint-Thuribe 6m	2636	593	2.9	
Saint-Thuribe 12m	2583	758	3.2	
Saint-Jean-Vianney	899	223	2.0	

For the correlation between γ_{95} and γ_r the ratio between these two parameters has been obtained as per Table 4.

It is observed from Table 4 that the remolded strain (γ_r) is about 2-4 times greater than γ_{95}. Therefore, the following correlation between γ_{95} and γ_r is reasonable:

$$\gamma_r = 3 \times \gamma_{95} \quad [9]$$

1.4 Proposed methodology for indirect measurement of the remolded strain

For the indirect measurement of γ_r The following steps are proposed (Figure 8):

1. Determine s_{up} , s_{u50} and γ_{50} from the partial post-peak curve obtained from the DSS test result
2. Estimate γ_{95} (%) with Equation 8 for a known sensitivity
3. Determine γ_r from Equation 9.

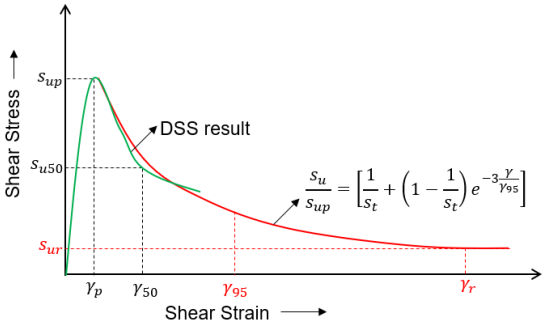

Figure 8. Determination of remolded shear strain

2 APPLICATION TO PREVIOUS LANDSLIDES

For the implementation of the proposed method (Figure 6), the DSS test results from the Saint-Jude landslide (Locat et al. 2017) and Sainte-Monique landslide (Locat et al. 2015) have been considered (Figure 9). For Saint-Jude, the sensitivity value varied from 40 to 80 (Locat et al. 2017), and Sainte-Monique clay has an average sensitivity of 55 (Locat et al. 2015). So, for the estimation of s_{u50} and γ_{95} a sensitivity value of 60 was considered for Saint-Jude, and 55 was taken for Sainte-Monique. The peak stress and strain are 55 kPa and 3% respectively for Saint-Jude, and 40.5kPa and 2.4% for Sainte-Monique. The values of s_{u50} for Saint-Jude is slightly lower than the last point of the curve, therefore, γ_{95} has been estimated with the last degraded point using Equation 8.

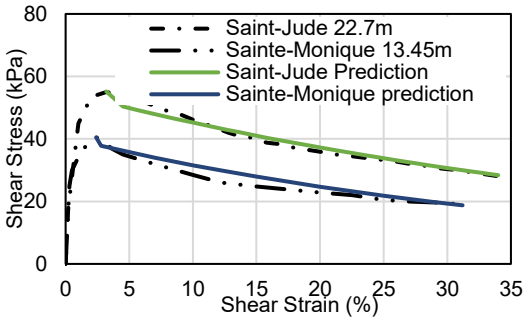

Figure 9. Stress-strain curve from DSS test results of Saint-Jude and Sainte-Monique sensitive clay (as per Locat et al. 2017 and 2015)

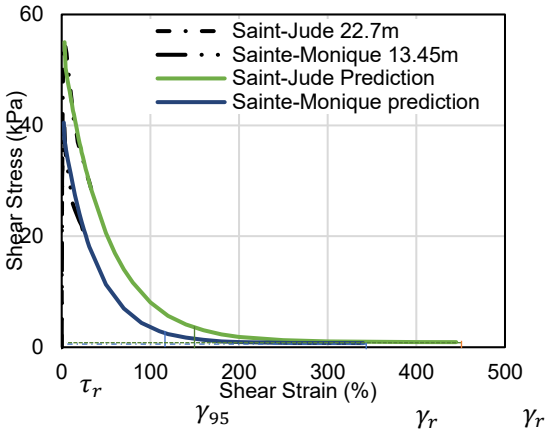

Figure 10. Determination of remolded shear strain for Saint-Jude and Sainte-Monique.

γ_{95} is found to be 148% for Saint-Jude and 113% for Sainte-Monique, thus γ_r for the sites are 445% and 340%, respectively, using Equation 9. Findings are illustrated in Figure 10. It should be noted that at the estimated remolded strains for both the sites, the strengths reduce exactly to their remolded shear strengths. Tran and Solowski (2018) numerically modeled the Sainte-Monique landslide with an assumed γ_{95}= 120% to achieve the post-failure runout. The estimated value in the proposed method of this paper came close to the assumed value of their numerical simulation.

3 CONCLUSION

This paper presented a new approach to obtain the remolded shear strain for eastern Canadian sensitive clays and validated the approach by two case studies. With the estimated remolded strain and the softening curve, it is also possible to estimate the remolding energy, which is a key factor for the initiation of retrogressive landslides.

4 REFERENCES

Demers, D., Robitaille, D., Locat and P. Potvin, J. 2014. Inventory of Large Landslides in Sensitive Clay in the Province of Québec, Canada: Preliminary Analysis, Landslides in Sensitive Clays: From Geosciences to Risk Management, Advances in Natural Technological Hazards Research, 36: 78-89.

Dey, R., Hawlader, B., Phillips, R. and Soga, K. 2016a. Modeling of large displacement behavior of marine sensitive clays and its application to submarine slope stability analysis. Canadian Geotechnical Journal, 53:1-18.

Dey, R., Hawlader, B., Phillips, R. and Soga, K. 2015. Large displacement finite element modeling of progressive failure leading to spread in sensitive clay slopes. Géotechnique, 65(8): 657-668.

Dey, R., Hawlader, B., Phillips, R. and Soga, K. 2016b. Numerical modeling of submarine landslides with sensitive clay layers. Géotechnique, 66(6): 454-468.

Einav, I., and Randolph, M.F. 2005. Combining upper bound and strain path methods for evaluating penetration resistance. International Journal for Numerical Methods in Engineering, 63(14): 1991–2016.

Flon, P. 1982. Energie de remaniement et regression des coulees d'argile, MSc thesis., Department of Civil Engineering, Laval University, Quebec, Canada.

Lefebvre, G. 2017. Sensitive Clays of Eastern Canada: From Geology to Slope Stability, Landslides in Sensitive Clays, Advances in Natural Technological Hazards Research, 46: 15-33.

Locat, A., Leroueil, S., Fortin, A., Demers, D and Jostad, H.P. 2015. The 1994 landslide at Sainte-Monique, Quebec: geotechnical investigation and application of progressive failure analysis. Canadian Geotechnical Journal, 52: 490-504.

Locat, A., Locat, P., Demers, D., Leroueil, S., Robitaille, D. and Lefebvre, G. 2017. The Saint-Jude landslide of 10 May 2010, Quebec, Canada: Investigation and characterization of the landslide and its failure mechanism. Canadian Geotechnical Journal, 54: 1357–1374.

Natural Resources Canada. 2019. https://www.nrcan.gc.ca/hazards/landslides

Quinn, P.E., Diederichs, M.S., Rowe, R.K., and Hutchinson, D.J. 2011. A new model for large landslides in sensitive clay using a fracture mechanics approach. Canadian Geotechnical Journal, 48(8): 1151–1162.

Stevens, A.B. 2019. Historical landslides in Canada resulting in fatalities (1771-2018), Geo-st.John's 2019, St.John's, Newfoundland and Labrador, Canada.

Tavenas, F., Flon, P., Leroueil, S., and Lebuis, J. 1983. Remolding energy and risk of slide retrogression in sensitive clays. In Proceedings of the Symposium on Slopes on Soft Clays, SGI Report, Linköping, Sweden., 17: 423–454

Thakur, V., Degago, S.A., Oset, F., Aabøe, R., Dolva, B.K., Aunaas, K., Nyheim, T., Lyche, E., Jensen, O.A., Sæter, M.B., Robsrud, A., Viklund, M., Nigussie, D. and L'Heureux, J.S. 2014. Characterization of Post-failure Movements of Landslides in Soft Sensitive Clays, Landslides in Sensitive Clays: From Geosciences to Risk Management, Advances in Natural Technological Hazards Research, 36: 91-104.

Thakur, V. and Degago, S. A. 2013. Disintegration energy of sensitive clays. Ge´otechnique Letters, 3: 20–25.

Tran, Q. and Solowski, W. 2018. Generalized Interpolation Material Point Method modeling of large displacement problems including strain-rate effects – Application to penetration and progressive failure problems. Computers and Geotechnics, 106: 249-265.

Turmel, D., Locat, P., Locat, J., Locat, A. and Leroueil, S. 2019. The energy reduction factor (FER) to model sensitive clay flowslides using in situ geotechnical and rheological data. Landslides, 17: 839-853.

Wang, C., Hawlader, B. and Perret, D. 2020. Effects of geometry and soil properties on type and retrogression of landslides in sensitive clays. Géotechnique.

Wang, C., Hawlader, B., Perret, D and Soga, K. 2021. Modeling of Initial Stresses and Seepage for Large Displacement Finite-Element Simulation of Sensitive Clay Landslides. Journal of Geotechnical and Geoenvironmental Engineering, ASCE. 147(11).

Analytical and numerical assessment of the effect of erosion in sensitive clay landslide: A case study of Saint-Jude Landslide

Zinan Ara Urmi, Rama Vara Prasad Chavali & Ali Saeidi
Department of Applied Science – Université du Québec à Chicoutimi,
Saguenay, Quebec, Canada
Alba Yerro
Department of Geotechnical Engineering – Virginia Tech,
Blacksburg, Virginia, USA

ABSTRACT
Erosion is regarded as the triggering factor of the majority of the retrogressive landslides in sensitive clays of eastern Canada. Due to the process of valley formation, the soils on the banks of water bodies of eastern Canada are getting eroded over the decades, and the shear strength of the soils near the valleys reduces. This strength reduction is owing to the change in salinity of these soils during the erosion process by leaching salt from the soil to the water bodies. When the slope is marginally stable, a very small increase in stress can trigger large retrogressive failure in sensitive clays. Saint-Jude Landslide that occurred in Quebec in 2010 can be considered a classic example of a landslide triggered by erosion. This study attempts to evaluate the effect of erosion in initiating the failure in a marginally stable slope. The stability of the slope has been determined with limit equilibrium methods and finite element analysis using strength reduction factor prior to the failure, and it has been demonstrated how small stress increase in a marginally stable can initiate failure.

RÉSUMÉ
L'érosion est considérée comme le facteur déclenchant de la majorité des glissements de terrain régressifs dans les argiles sensibles de l'est du Canada. En raison du processus de formation des vallées, les sols des rives des plans d'eau de l'est du Canada s'érodent au fil des décennies, et la résistance au cisaillement des sols près des vallées diminue. Cette réduction de résistance est due au changement de salinité de ces sols au cours du processus d'érosion par lessivage du sel du sol vers les plans d'eau. Lorsque la pente est marginalement stable, une très faible augmentation de la contrainte peut déclencher une rupture régressive importante dans les argiles sensibles. Le glissement de terrain de Saint-Jude survenu au Québec en 2010 peut être considéré comme un exemple classique de glissement de terrain déclenché par l'érosion. Cette étude tente d'évaluer l'effet de l'érosion dans l'initiation de la rupture dans une pente légèrement stable. La stabilité de la pente a été déterminée avec des méthodes d'équilibre limite et une analyse par éléments finis en utilisant le facteur de réduction de résistance avant la rupture, et il a été démontré comment une petite augmentation de contrainte dans une stabilité marginale peut déclencher une rupture.

1. INTRODUCTION

Landslides in sensitive clays are considered one of the major hazards in the northern countries of the world, especially in Canada and Norway. The impact of landslides is catastrophic to both population and economy. Natural resources Canada (NRCan) has reported that in Canada, the annual damages by landslides are worth $200 to $400 million (NRCan 2019). A total of 778 people have died in the landslide events all over the country from 1771 to 2018, among which 134 fatalities are recorded solely in Québec region due to the glaciomarine sensitive clay failures in the St. Lawrence Lowlands (Blais-Stevens 2019). The devastating aftermath of landslides in sensitive clays intrigued researchers to extensively investigate the triggering factors and mechanism of such landslides, most importantly, the behavior of sensitive clays that leads to the initiation and progress of extremely large landslides under different loading conditions. The post-failure behavior of sensitive clays is attributed to the post-peak strength reduction under shear loading. Sensitive clays generally have high intact shear strength, but the shear strength reduces to a significantly low value (remolded shear strength) when subjected to disturbance and the clay completely loses its intact structure and disintegrates to a liquid-like mass (remolded clay) that can flow. Thus, the soil is referred to as “sensitive” because its strength is sensitive to disturbance. The sensitivity (S_t) of soil is quantified by the ratio between the peak and remolded shear strength. Once the slope failure starts in sensitive clays, the clay layer gets remolded to a liquid form and keeps moving away from its original position. The drag of this liquified soil results in subsequent failures (progressive or retrogressive)

until the flow of this liquified clay stops or is unable to initiate another failure. Thus, the extent of the failure of sensitive clay slopes is enormous compared to slope failure in non-sensitive soil. For example, recently in the highly sensitive clays of Norway the Gjerdrum landslide (2020), spanned a flow-off area of 210000 m^2 and additionally affected 90000m^2 by debris flow (Liu et al. 2021).

The development of sensitivity (high intact strength with low remolded shear strength) of the clays is attributed to the depositional features of sensitive clays as well as the ongoing weathering effect on embankment soils. Sensitive clays are believed to be deposited in marine environment depressions left by the Laurentian ice sheet around 14000 to 6000 years ago from the present time (Quigley 1980, Lefebvre 1996, 2017). Due to the exposure to the seawater with high salt concentration, the clays formed a flocculated structure with high undisturbed shear strength. With the deglaciation of the ice sheets over time, the lands which were once depressed by the huge weight of the ice sheets rose above the sea level (iso-static rebound). Due to this uplift of the clay deposition above the seawater, the clays got exposed to freshwater. When the freshwater flows through the soil, the salt concentration within the soil mass reduces due to the leaching out of salt into the freshwater. As a result, even though the clays retain their flocculated structure, they do not have the salt ions that were keeping the structure stable. This structure is called meta-stable, which is highly susceptible to disturbance and leads to very low remolded strength. This is why the vast majority of sensitive clay landslides have occurred along watercourses (Figure 1) with active erosion at the toe of the slopes (Lebuis et al. 1983).

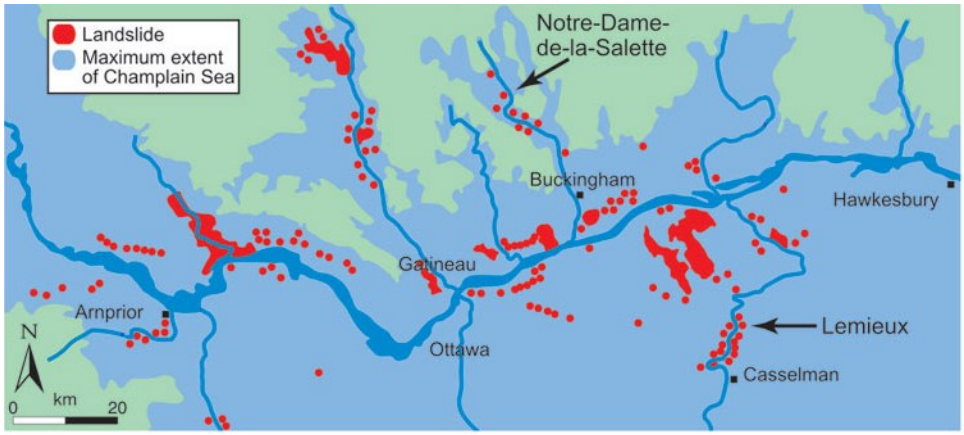

Figure 1. Landslides in sensitive clays in the Champlain sea region (Canadian Geoscience Education Network archive 2019).

Apart from erosion, seismic activity, sudden increase of pore water pressure due to heavy rainfall or melting of snow, or other man-made activities may trigger landslides in a marginally stable slope (marginally stable refers to the factor of safety being slightly over 1). Whatever the final triggering factor for a landslide in sensitive clays is, the pre-failure condition of the slope (marginal stability) is always attributed to the long-term erosion (Lefebvre 1996). That is why It is widely agreed upon that the stability of a sensitive clay slope against the initial slide or the assessment of initial stresses in a sensitive clay slope before retrogressive/progressive failure should be done against drained soil parameters (Bjrum 1955, Michell and Markle 1974, Tavenas et al. 1983, Locat et al. 2013, Lefebvre 2017). Thus, the behavior of sensitive clays in the drained condition is particularly important. While over-consolidated sensitive clays show softening behavior in both drained and undrained conditions (Lefevre 2017), normally consolidated or slightly over-consolidated sensitive clays (Over Consolidation Ratio, OCR < 2) do not show softening behavior in drained condition (Locat et al. 2019) as illustrated in Figure 2. OCR for Norwegian sensitive clays is reported between 1-6 based on 61 samples from 17 different locations among which 12 locations with 39 samples had OCR ≤ 2 (Paniagua et al. 2019). Again Demers et al. 2002 reported OCR values for 31 different locations of Canadian sensitive clays where 17 locations had OCR ≤ 2 and 29 locations had OCR ≤ 5. Therefore, it can be said that a large number of sensitive clay sites are normally consolidated and stability analysis in these sites against long-term erosion does not require the consideration of the drained strain softening. However, once the first slide has taken place, subsequent failures happen within a very short time and retrogression or progression of the failure takes place in undrained condition and large retrogressive failures occur due to undrained strain-softening even though the failure was initiated in drained condition. This information is important in the initial stability analysis of sensitive clay slopes with ongoing erosion in normally/lightly consolidated clays.

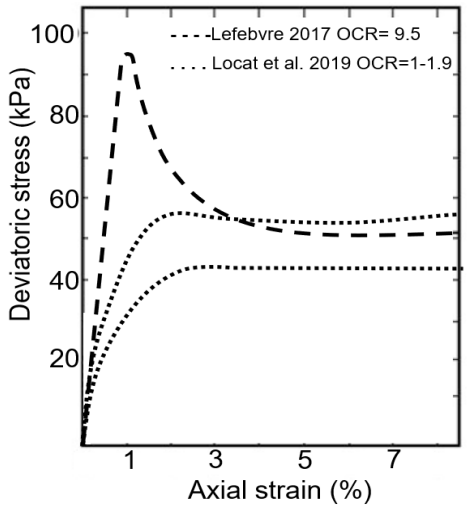

Figure 2: Behavior of sensitive clay under consolidated drained triaxial test

Demers et al. (2014) studied 108 large retrogressive landslides that previously occurred in Quebec and suggested that in 90% of the cases, erosion played an active role in triggering the landslides. Therefore, it is imperative to understand the role of erosion in the instability of sensitive clay slopes for disaster risk mitigation. The objective of this study is to explain the effect of erosion in slope stability analysis in sensitive clay deposits. Firstly, the role of erosion on previously occurred sensitive clay landslides have been presented, and finally a case study of erosion-induced sensitive clay landslide has been investigated analytically and numerically to provide insights on the effect of erosion on the failure initiation of sensitive clay slopes.

2. HISTORY OF LARGE LANDSLIDES ON ERODED MARGINALLY STABLE SLOPES

A detailed record of sensitive clay landslides is available in the literature from the early eighteenth century to the present time. This section discusses the pre-failure conditions of the slopes before the occurrence of large landslides and the contribution of erosion in making the slope susceptible to failure.

Brzezinski (1971) reported that in the Kenogemi landslide (1924), Quebec, Canada, the clay slope was being eroded at an alarming rate due to the high amount of wastewater disposal into a natural clay gully. Noticeable effects of these erosions were observed three months before the catastrophic landslide through smaller slides in the valley. In addition, significantly high rainfall intensity was recorded two days before the landslide, and just the day before the event, a magnitude VII-VIII (modified Mercalli scale) earthquake having an epicenter very close to the landslide location was recorded. After the disaster took place, as mitigation measures, immediate backfilling was done, drainage valves were opened to reduce the pore water pressure on the slope, and other measures of waste disposal were introduced. As a result of such actions, erosion was prevented in the new backfill. Interestingly, another earthquake took place with greater intensity (magnitude IX) with the same epicenter four months later no damaging effect was observed on the slope.

Odenstad (1951) discussed the Skottorp landslide (1946) near the Lidan River in the Norweigian quick clays (highly sensitive clays) and illustrated that the pre-failure slope stability was found to be 0.77-1.34 by the slip circle method. He conferred that the frequent erosion of the river bed and strength reduction due to the leaching out of salt, overall, the process of valley formation could be the reasons for this reduced slope stability and reasoned that such slopes are susceptible to retrogressive failure with a sudden increase of pore water pressure due to rainfall. South Nation River landslide (1971) was believed to be triggered by the increase of the pore water pressure due to snowmelt and spring flood. However, a geotechnical investigation of a county road crossing about 460m south of the landslide location revealed that the slope was marginally stable due to embankment erosion over the years and unfit for a crossing (Eden et al. 1971). The devastating Rissa landslide (1978) initially started from a small excavation activity (Gregersen 1981), but the stability of the slope before failure was found to be marginal due to prolonged erosion. This also highlights that landslides are more likely to occur for a small increase in stresses (heavy rainfall, small excavation, or other reasons) on slopes already at reduced stability due to ongoing erosion over the years.

Crawford and Eden (1964) suggested that sensitive clay slopes become potentially unstable due to the long-term natural process while discussing the causes of the Nicolet landslide (1955). Furre landslide in the quick clays of central Norway (1959) also occurred due to the unloading at the toe of the slope owing to lateral erosion (Hutchinson 1961). Toulnosac (1962), Saint-Jean-Vianney (1971), Basstaad (1974), La Grande River landslide (1987), Lameux Landslide (1993), Sainte-Monique landslide (1994), Saint-Jude landslide (2010), and Saint-Luc landslide (2016) are some other landslides where active stream erosion gradually increased the shear stress at the slope leading to an eventual failure in highly sensitive clays (Colon 1966, Tavenas et al. 1971, Gregersen and Loken 1978, Lefebvre et al. 1990, Evans and Brooks 1994, Locat et al. 2015, 2017, Tremblay- Auger et al. 2021).

Therefore, it can be concluded that the process of valley formation and active erosion of the highly sensitive embankment clays play the primary role in the initiation of large retrogressive failure. Another important aspect to be noted from the above discussion for stability analysis is that these landslides are occurring in the zones of active erosions, that is, landslides keep occurring in the vicinity of the location where previous landslides have been recorded. Therefore, if these zones with active erosion and slopes with marginal stabilities are identified and measures are taken for slope stability improvement,

the risk for large retrogressive landslides can be significantly reduced.

3. CASE STUDY OF STABILITY ANALYSIS ON MARGINALLY STABLE SLOPE

From the previous section, it is clear that to assess the risk of retrogressive failure, the slope has to be marginally stable against long-term stability (drained condition). With reduced stability, a small increase in stresses can induce failure of the slope. To further analyze the phenomenon of reduced stability due to erosion in pre-failure conditions and initiation of failure with further small erosion, the Saint-Jude landslide (2010) is selected because a detailed geotechnical investigation of this landslide is available in the literature (Locat et al. 2011, 2017, 2019). The Saint-Jude landslide occurred in the municipality of Saint-Jude, Quebec, about 50 km northeast of Montréal, in a sensitive
Champlain Sea clay deposit along the Salvail River (Figure 2). Sixteen similar landslide scars were found on the same location of the landslide from aerial light detection and ranging (LIDAR) surveys (Locat et al. 2017).

The stability of the slope in a drained condition has been studied with the limit equilibrium and finite element methods considering effective strength parameters. The slope geometry and geotechnical properties used in the analysis are presented in Figure 3 and Table 1. This should be noted that triaxial tests for effective strength parameters (i.e., effective cohesion (c') and friction angle (Φ')) are only available for the sensitive clay layer (Locat et al. 2019). The drained soil strength parameters for other layers are reasonably assumed as per Locat et al. (2017). The sensitive clay layer was normally to slightly overconsolidated and showed no strain-softening in drained condition.

Table 1: Soil properties used in modeling

Layers	Unit weight γ (kN/m^3)	Strength Parameters c'	Φ'
Sandy crust	18.6	0.0	35.0
Sensitive clay	16.0	6.0	31.0
Silty clay	16.8	7.7	40.0
Clayey silt	19.3	0.0	35.0
Sandy silt	20.7	0.0	40.0

3.1. Limit equilibrium methods

The slope pre-failure state has been modeled using SLIDE/W software in a drained condition to assess whether the slope was marginally stable before failure. In general, the long-term erosion that leads to marginal stability should always be an instability against soil parameters in effective stress conditions. Therefore, stability analysis has been done in drained condition. Safety factor has been obtained with three different methods, Bishop Simplified, Spencer, and Morgenstern-Price, and found to be 1.00, 1.015, and 1.01, respectively. It is observed that in the pre-failure condition, the factor of safety of the slope against long-term stability was very marginal (Figure 4).

After that, a small excavation (about 2m^2) was carried out to replicate further erosion. The safety factor was significantly reduced below 1 (FS= 0.85, Figure 5) indicating failure. This initial sliding may trigger retrogressive failure with subsequent sliding.

3.2. Numerical modeling

It is well known that limit equilibrium analysis has a number of assumptions that may oversimplify the problem and provide inaccurate results (e.g., limitations regarding the interslice forces, deformation compatibility, convergence, accurate estimation of ground stresses, soil-structure interaction, etc.) (Krahn 2003). A similar analysis has been carried out with the Finite Element Method (FEM), which provides a more robust and accurate framework to evaluate boundary value problems. For this study, Slope stability software RS2 from the Rocscience software suite (https://www.rocscience.com/software) has been used. The Stress Reduction Factor method (SRF method) has been used to assess the stability of the Saint-Jude sensitive clay slope. The 2D plane-strain geometry was modeled with 3000 three noded triangular elements. Bottom and Lateral boundaries were fixed in both directions. The soil was defined as an elastoplastic material with the Mohr-Coulomb failure criterion. The porosity value was set to 0.5. The drained Poisson's ratio is considered to be 0.3, and Young's modulus is taken to be 10,000kPa for sensitive clay layer and 50,000kPa for other layers.

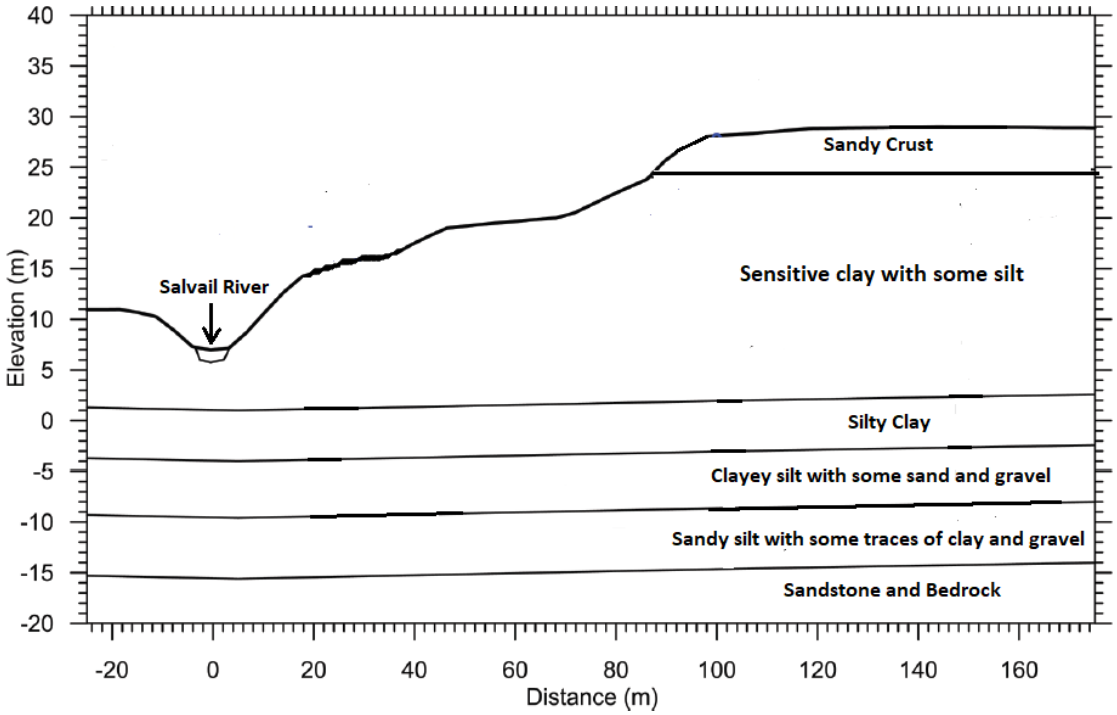

Figure 3: Slope Geometry (Locat et al. 2017).

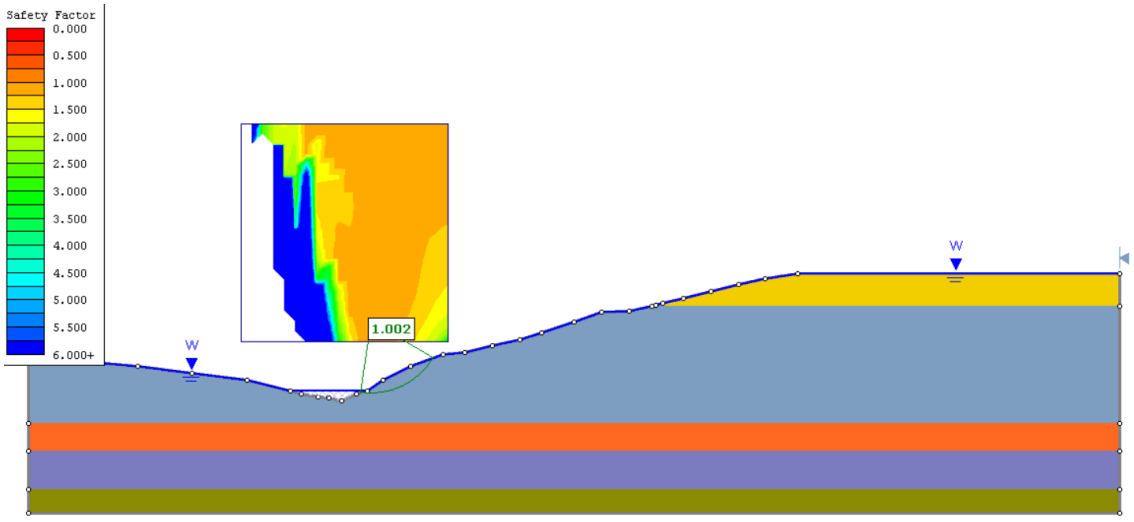

Figure 4: Slope stability for drained condition before failure (Using Bishop Simplified method)

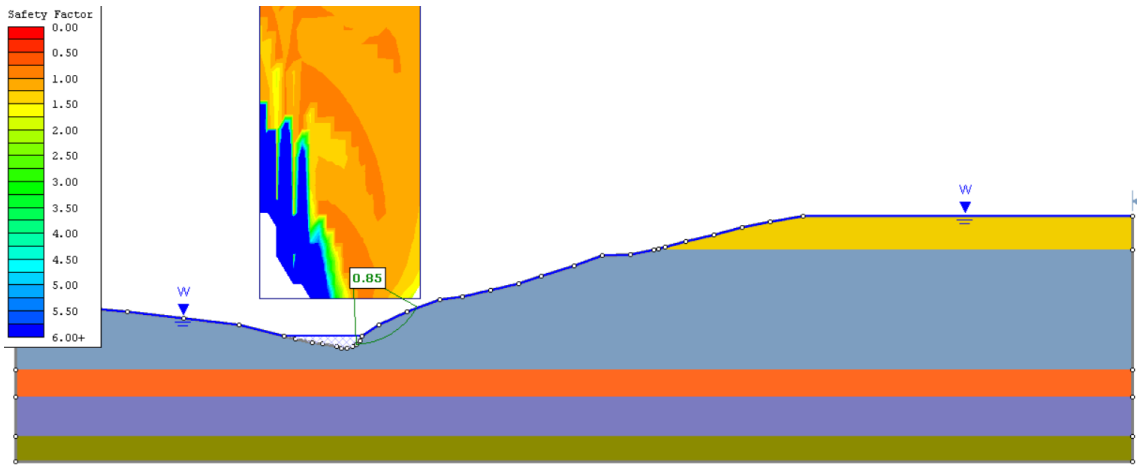

Figure 5: Further reduction of stability with a small excavation (Using Bishop Simplified method)

The FEM safety factors using the SRF method were found to be consistent with the results from the limit equilibrium analysis before excavation (FS=1.01) and slightly higher after excavation (FS= 0.94) as shown in Figure 6 and Figure 7. Unlike LEM, FEM results provide the stress-strain distribution throughout the slope. Moreover, FEM analysis considers important factors like boundary conditions, stiffness parameters, the porosity of the soil, constitutive soil models to capture real soil behavior, etc., which makes the stability analysis more realistic. Nevertheless, for preliminary stability analysis where the main goal is to determine the factor of safety as in this study, LEM is the easiest and most convenient method to execute to obtain satisfactory preliminary results that are comparable to FEM.

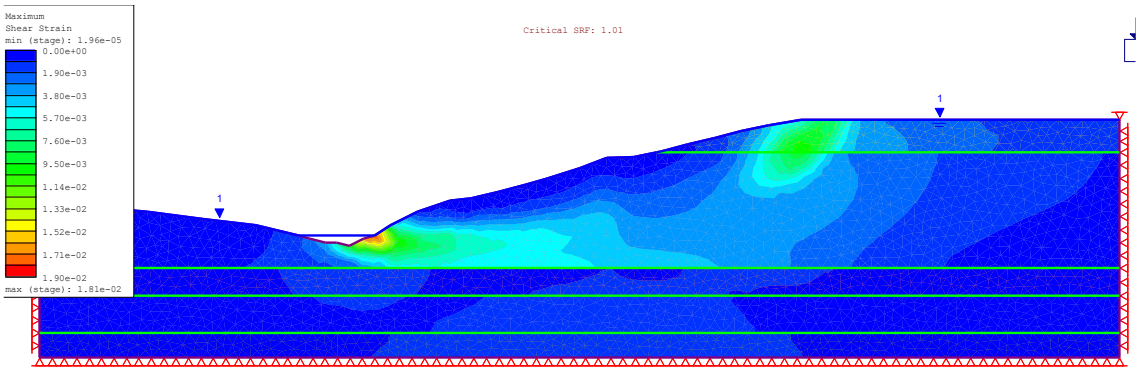

Figure 6: Slope stability for drained condition before failure using FEM (SRF method).

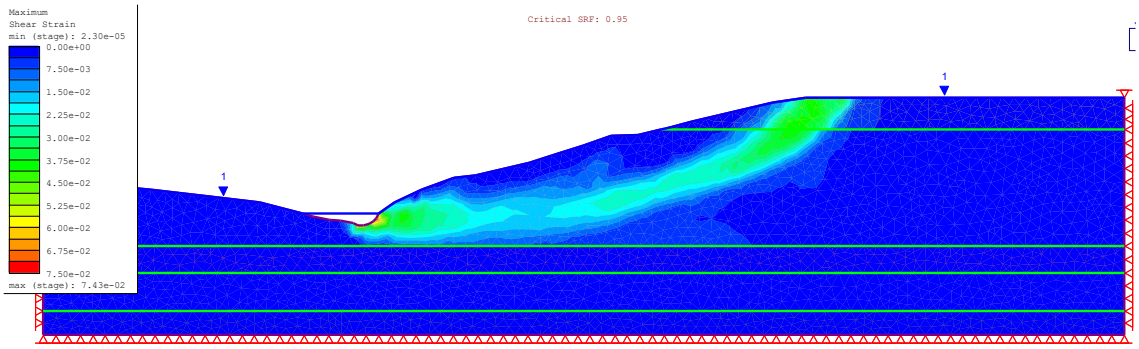

Figure 7: Initiation of failure with a small excavation using FEM (SRF method).

4. CONCLUSION

The stability of the slopes in sensitive clays before retrogressive failure has been investigated. It is concluded that the factor of safety of such slopes just before the final trigger is extremely marginal due to ongoing embankment erosion. Having marginally stable slopes on sensitive clays is a major warning sign for future landslide occurrences because a minor stress increase can trigger a massive catastrophic event. LEM methods are comparable to FEM results in normally to slightly overconsolidated sensitive clays for assessing the pre-failure slope stability. Large landslides can be prevented by regularly monitoring the erosion activities at the locations of previous large landslides and taking adequate measures for slope stability improvement.

5. REFERENCES

Bjrrum, L. 1955. Stability of Natural Slopes in Quick Clay. Géotechnique, 5(1): 101–119

Blais-Stevens, A. 2019. Historical landslides in Canada resulting in fatalities (1771-2018), Geo-st.John's 2019, St.John's, Newfoundland and Labrador, Canada.

Brzezinski, L.S. 1971. A Review of the 1924 Kenogami Landslide. Canadian Geotechnical Journal, 8: 1-6

Colon, R. J. 1966. Landslide on the Toulnustouc River, Quebec. Canadian Geotechnical Journal, 3: 113-144.

Crawford, C. B., and Eden, W. J. 1964. Nicolet landslide of November 1955, Quebec, Canada. Engineering Geology Case Histories, 4: 45-50

Demers, D., Robitaille, D., Locat and P. Potvin, J. 2014. Inventory of Large Landslides in Sensitive Clay in the Province of Québec, Canada: Preliminary Analysis, Landslides in Sensitive Clays: From Geosciences to Risk Management, Advances in Natural Technological Hazards Research, 36: 78-89.

Eden, W. J., Flecher, E. B. and Mitchell R. J. 1971. South Nation River Landslide, 16 May 1971. Canadian Geotechnical Journal, 8: 446-451

Gregersen, O. 1981. The Quick Clay Landslide in Rissa Norway. The Sliding Procedure and Discussion on Failure Mode. Norwegian Geotechnical Institute. Publication no 135, Oslo, Norway.

Gregersen, O. and Loken, T., 1979. The quick-clay slide at Baastad, Norway, 1974. Engineering Geology, 14: 183--196.

Hutchinson, J. N. 1961. A Landslide on a Thin Layer of Quick Clay at Furre, Centralnorway. Géotechnique, 11(2): 69-94.

Krahn, J. 2003. The 2001 R.M. Hardy Lecture: The limits of limit equilibrium analyses. Canadian Geotechnical Journal. 40: 643-660.

Lebuis, J., Robert, J.M., and Rissman, P. 1983. Regional Mapping of Landslide Hazard in Quebec. In Proceedings of the Symposium on slopes on soft clays. Swedish Geotechnical Institute, Report no.17. pp. 205–262.

Lefebvre, G., Rosenberg, P., Paquette, J. and Lavallée, J. G. 1990. The September 5, 1987, landslide on the La Grande River, James Bay, Quebec, Canada. Canadian Geotechnical Journal. 28(2): 263-275

Lefebvre, G. 1996. Soft Sensitive Clays. In Landslides: investigation and mitigation, Special report 247, Transportation Research Board. National Academy Press, Washington, DC, pp 607–619. Washington, DC.

Lefebvre, G. 2017. Sensitive Clays of Eastern Canada: From Geology to Slope Stability, Landslides in Sensitive Clays, Advances in Natural Technological Hazards Research, 46: 15-33.

Liu, Z., Heureux, J. S., Glimsdal, S. and Lacasse, S. 2021. Modeling of mobility of Rissa landslide and following tsunami. Computers and Geotechnics, 140: 104388

Locat, P., Fournier, T., Robitaille, D., and Locat, A. 2011. Glissement de terrain du 10 mai 2010, Saint-Jude, Montérégie, Rapport sur les caractéristiques et les causes. Rapport MT11-01. Section des mouvements de terrain, Services de la géotechnique et de la géologie, Ministère des transports du Québec. Bibliothèque et Archives nationales du Québec, Gouvernement du Québec.

Locat, A., Jostad, H.P., and Leroueil, S. 2013. Numerical modeling of progressive failure and its implications for spreads in sensitive clays. Canadian Geotechnical Journal, 50(9): 961–978

Locat, A., Leroueil, S., Fortin, A., Demers, D and Jostad, H.P. 2015. The 1994 landslide at Sainte-Monique, Quebec: geotechnical investigation and application of progressive failure analysis. Canadian Geotechnical Journal, 52: 490-504.

Locat, A., Locat, P., Demers, D., Leroueil, S., Robitaille, D. and Lefebvre, G. 2017. The Saint-Jude landslide of 10 May 2010, Quebec, Canada: Investigation and characterization of the landslide and its failure

mechanism. Canadian Geotechnical Journal, 54: 1357–1374.

Locat, A., Locat, P., Michaud, H., Hébert, K., Leroueil, S. and Demers, D. 2019. Geotechnical characterization of the Saint-Jude clay, Quebec, Canada. AIMS Geosciences, 5(2): 273-302.

Mitchell, R.J., and Markell, A.R. 1974. Flowsliding in Sensitive Soils. Canadian Geotechnical Journal, 11: 11–31.

Natural Resources Canada. 2019. https://www.nrcan.gc.ca/hazards/landslides

Odenstad, S. 1951. The Landslide At Scottorp on the Lidan River, Royal Swedish Geotechnical Engineering Proceeding 4, Stockhome, Switzerland.

Evans, S.G. and Brooks, G.R.1994. An earthflow in sensitive Champlain Sea sediments at Lemieux, Ontario, June 20, 1993, and its impact on the South Nation River. Canadian Geotechnical Journal. 31(3): 384-394.

Tavenas, F., Chagnon, J. Y. and La Rochelle, P. 1971. The Saint-Jean-Vianney Landslide: Observations and Eyewitnesses Accounts. Canadian Geotechnical Journal, 8: 463-478.

Tavenas, F., Flon, P., Leroueil, S., and Lebuis, J. 1983. Remolding energy and risk of retrogression in sensitive clays. In Proceedings of the symposium on slopes on soft clays.

Tremblay-Auger, F., Locat, A., Leroueil, S., Locat, P., Demers, D., Therrien, J. and Mompin, R. 2021. The 2016 landslide at Saint-Luc-de-Vincennes, Quebec: geotechnical and morphological analysis of a combined flowslide and spread. Canadian Geotechnical Journal. 58(2): 295-304.

Quigley, R. M. 1980. Geology, mineralogy, and geochemistry of Canadian soft soils: a geotechnical perspective. Canadian Geotechnical Journal, 17: 261-285.

Proceedings 10th NUMGE 2023
10th European Conference on Numerical Methods in Geotechnical Engineering
Zdravković L, Konte S, Taborda DMG, Tsiampousi A (eds)
ISSN

doi: https://doi.org/10.53243/NUMGE2023-369

Effect of strain softening on the prediction of post-failure runout in sensitive clay landslide

Z.A. Urmi[1] , A. Saeidi[1] , R.V.P Chavali[1] , A. Yerro[2]

[1]Department of Applied Science, Université du Québec à Chicoutimi, Québec, Canada
[2] Department of Geotechnical Engineering – Virginia Tech, Blacksburg, Virginia, USA

ABSTRACT: Due to extensive post-peak strain softening and subsequent remolding of sensitive clays, landslides in these soils result in catastrophic progressive or retrogressive failures. Analysis and prediction of failure initiation and runout of sensitive clay landslides are crucial to reducing their impact; however, the post-failure behavior of such landslides is very complex. The use of advanced numerical techniques capable of accounting for large deformations and the strain-softening of the material is vital to accurately predicting post-failure movements. This study uses the material point method (MPM) to evaluate the influence of strain-softening behavior on the post-failure mechanism and runout of sensitive clay landslides. The simulation has been performed using Anura3D software with a strain-softening Mohr-Coulomb constitutive soil model. In particular, parametric studies are performed on the controlling parameters of the strength-degradation equation to assess strain-softening effects on retrogression and runout distances. The results showed that an increased rate of softening increases post-failure movement. For a fixed peak and remolded shear strength, there is a limiting value of strain-softening factor below which retrogressive failure does not occur.

Keywords: Sensitive clay; strain-softening; retrogressive failure; large-deformation; MPM.

1) INTRODUCTION

Large retrogressive landslides in sensitive clays frequently occur in Scandinavia and eastern Canada. Extensive post-peak strength reduction (Figure 1), generally referred to as "strain softening" in these soils, is considered to be the primary reason for such large-scale landslide occurrences (Locat et al. 2011).

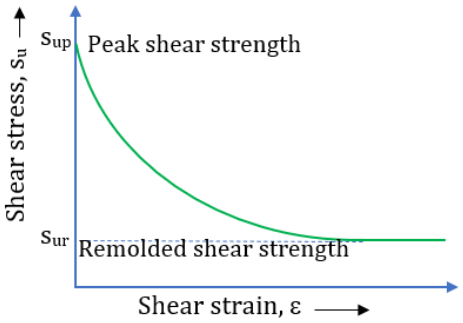

Figure 1. Strain-softening in sensitive clays

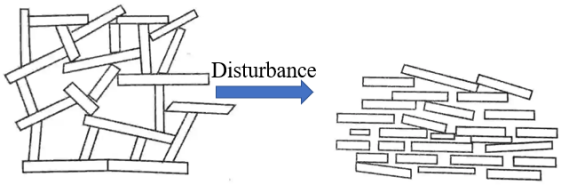

Figure 2. Structural susceptibility of sensitive clays to disturbance

The strain-softening nature of sensitive clays of eastern Canada can be better understood from their depositional features. These soils were deposited in the marine environment on the depressions left by the Laurentian ice sheet around 14000 to 6000 years ago (Lefebvre 1996). Due to the salt ions exposure, the clays formed a flocculated structure with high undisturbed shear strength. After the iso-static rebound, the clays rose above the seawater, and the salt ions leached into the fresh water. As a result, the clay formed a meta-stable structure highly susceptible to disturbance (Figure 2), eventually leading to a substantial loss of shear strength at large strains (Lefebvre 1996). Sensitive clays are thus named after

their sensitivity towards the disturbance, and the term sensitivity (S_t) is quantified as the ratio of the peak shear strength (s_{up}) to the reduced (remolded) shear strength (s_{ur}) (Skempton and Northey 1952). When slopes containing sensitive clay layers are subjected to stresses beyond their peak shear strength, strain is localized in the weak soil layers forming narrow shear bands where strength reduces nearly to zero. Failure surfaces are formed along the shear bands, and soil within them loses its intact structure and transforms into a liquid-like mass (remolded soil) that flows (Rosenqvist 1953). These liquified soils either laterally spread or drift away from their original location, resulting in a series of failures proceeding rapidly in a progressive or retrogressive manner (Locat et al. 2011) and eventually destroying areas far away from the site of the initial failure. Thus, the extent of the failure of sensitive clay landslides is enormous, with devastating aftermath compared to slope failure in non-sensitive soil (Figure 3).

Figure 3. Retrogressive landslide in the sensitive clays of Gjerdrum in Eastern Norway on December 30, 2020 (Photo: Anders Martinsen)

The landslide mechanism in a retrogressive failure in sensitive soil involves several complex features such as the landslide trigger, formation of shear bands or multiple failure surfaces, movement of the remolded soil, progression of the landslide, etc. These issues make the numerical analysis of sensitive clay landslides exceptionally challenging. The conventional methods like limit equilibrium or finite element strength reduction used in slope stability analyses suffer from two problems that make them unsuitable for application in sensitive clay slopes. Firstly, these approaches can barely predict the landslide initiation, let alone estimate the subsequent failures or runouts resulting in retrogressive landslides. Secondly, these landslides involve large deformations, which result in mesh tangling in conventional FEM techniques. The strain-softening behavior of sensitive clays responsible for the complex failure mechanism requires a sophisticated constitutive soil model and an advanced numerical tool to handle large deformation problems.

In the last two decades, significant development has been made in the numerical tools to accommodate large deformation problems in geotechnical engineering. Several mesh-based and meshless numerical frameworks like arbitrary lagrangian finite element method, particle finite element method, material point method, etc., have successfully been implemented to model some key characteristics of large retrogressive failures (Wang et al. 2022, Zhang et al. 2018, Tran and Solowski 2019). In this study, the material point method (MPM) is the preferred method for modeling landslide problems. MPM has previously been used to demonstrate the formation of shear bands in retrogressive and sensitive clay spread failure (Wang et al. 2016, Tran and Solowski 2019). The MPM uses a combined Eulerian and Lagrangian framework where particles are described with a collection of Lagrangian material points and governing equations are solved at the computational nodes of a fixed Eulerian background mesh (Sulsky et al. 1994). The movement of material points is free but confined within the background mesh. There are several reasons for choosing MPM; firstly, this method is based on a continuum description of material flow using an Eulerian-Lagrangian approach which makes it well suited for large deformation failure analyses; secondly, the governing equations of MPM and FEM are generally the same which makes its implementation easier for the FEM users; thirdly, Lagrangian description of soil particles makes it capable of working with advanced history-dependent soil constitutive models and; finally, the background mesh makes the application of the boundary conditions easier compare to other mesh-free methods. Although it can be argued that other mesh-free methods have similar features, the study aims to show that MPM is a very suitable framework for serving the purpose of the study.

The most crucial component for modeling sensitive clay slopes is the constitutive soil

model, which represents the stress-strain behavior of the soil. The capability to reproduce realistic strain-softening characteristics in the material model is necessary for more accurate numerical analyses (Rødvand et al., 2022). Some strain-softening constitutive soil models for sensitive clays have also been developed to aid the purpose (Dey et al. 2015, Zhang et al. 2018). In recent studies, highly non-linear post-peak strain-softening of sensitive clays has inspired the implementation of an exponential strength degradation equation (Equation 1) to capture the post-peak soil behavior (Wang et al. 2022, Tran and Solowski 2019).

$$s_u = s_{ur} + (s_{up} - s_{ur})e^{-\eta\varepsilon_d^p} \quad (1)$$

where ε_d^p is the deviatoric part of the plastic strain tensor, s_{up} and s_{ur} are the peak and remolded undrained shear strength, respectively, and η is a shape factor controlling the strength degradation rate. A similar constitutive model has been used in this study. The shape factor (η) is required to calibrate the exponential functional form of this softening law against experimental data. Large values of η correspond to greater strength decrease with plastic strain accumulation (i.e., more brittle nature).

Including strain-softening features in numerical methods can lead to strain localization issues. To address this, Rots et al. (1985) proposed a smeared crack approach as a regularization technique. This method assumes that the total work dissipated by a shear band is equivalent to the fracture energy dissipated in a discrete crack. By calibrating the parameter η through numerical shear tests, where the thickness of a shear band is approximately equal to the size of mesh elements, a specific relationship between shear stress and displacement can be obtained. The goal is to ensure that the areas under the stress-strain curve, representing fracture energy, are equal for each element size, thus minimizing mesh dependency in the numerical solution.

This study focuses on the effects of changes in peak strength, remolded strength, and shape factor on the final retrogression and runout when a failure occurs in a sensitive clay slope. For this, stress distribution and the progression of failure in a simple, sensitive clay slope have been illustrated. Afterward, parametric studies were performed on the strain-softening parameters of sensitive clays, the peak shear strength, remolded shear strength, and shape factor. It then discusses how these factors control retrogressive failure and post-failure slope response.

2) BASIS OF MPM FRAMEWORK

In MPM, the continuum is discretized into a set of subdomains, and the mass of each sub-domain is carried by a certain number of material points (Figure 4).

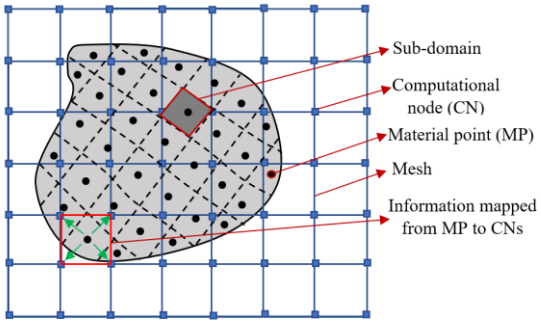

Figure 4. Spacial formulation of MPM framework

Material points (MPs) also carry properties like stresses, strains, velocities, accelerations, etc. The information is then mapped from MPs to the computational nodes of the background mesh. Governing equations are solved on the nodes, and updated information is mapped back to the MPs. The relationship between the MPs and the nodes at any domain point is defined with linear interpolation shape functions. The slope presented below is modeled using the two-phase single-point formulation executed in the MPM code Anura3D (www.anura3d.com). In the two-phase single-point approach (Ceccato et al. 2018), the saturated porous media is discretized by a single set of MPs which moves according to the solid velocity field. Each MP describes a representative volume element of fully saturated soil, carrying the information of both phases, solid and liquid. Displacements and velocities are updated based on calculated acceleration using an explicit Euler-Cromer scheme. A damping force is employed to avoid non-physical vibrations. This force is proportional to the out-of-balance force, and the proportion should be chosen wisely (very low for dynamic problems) to obtain an accurate solution.

3) DESCRIPTION OF THE NUMERICAL MODEL

A simple 5m high, 25m long single layered sensitive clay slope is taken, inclined at 45° to the horizontal from crest to toe (Figure 5). The slope rests on a firm base restricted for horizontal and vertical movement, whereas only horizontal movement is allowed at the left boundary. As the slope is expected to experience retrogressive failure, the length of the background mesh is extended up to 55m from the left slope boundary, and the height is 6m so that the soil particles have sufficient space for movement after failure. The computational mesh is discretized with three noded triangular elements with an average size of 0.3m. This size was determined through trial and error, considering larger and smaller sizes to achieve minimal mesh dependency while maintaining reasonable computational time. The analysis is performed in plane strain condition, and gravity loading is applied to generate the initial stress state of the slope. This non-physical stage involves instantaneously applying the full gravity load to the slope. To prevent any abrupt blasting effects of the sudden load on the material points, it is imposed that the material behaves elastically during this stage. Failure has been initiated by introducing the strain-softening behavior of sensitive clays in the subsequent calculation step after gravity loading.

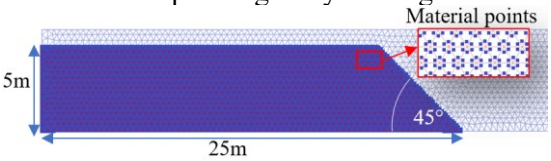

Figure 5. Slope geometry, meshing, and material points description of the numerical model

The undrained shear strength of sensitive clays can be as high as 100kPa or more. However, for different retrogressive landslide locations of eastern Canada, 7 out of 9 sites had an undrained shear strength from 20kPa-50kPa (Tavenas et al. 1983), and this parameter varied from 15-35kPa for 10 out of 14 previous landslide locations of Norwegian quick clays (Thakur and Degago 2012). The remolded shear strength for these sites was 0.2-2.1kPa for Canadian soils and 0.15-0.8kPa for Norwegian locations. Therefore, to demonstrate the process of retrogressive failure, peak, and remolded undrained shear strengths were taken to be 30kPa and 2kPa, respectively. And the post-peak degradation is exponential, as described in Equation 1. The rate of strength decrease depends on the shape factor η.

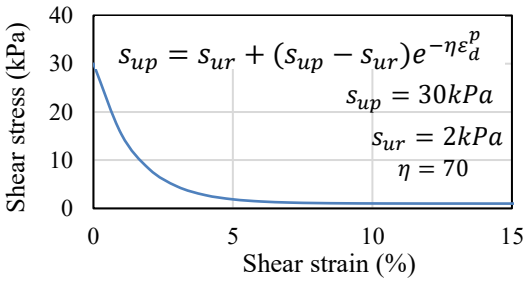

Figure 6. Strain-softening behavior was adopted for the demonstration of retrogressive failure.

For the taken strength values (30kPa and 2kPa), retrogressive failure doesn't occur in the simulated model for a shape factor <60. Therefore, the shape factor is assumed to be 70. The stress-strain curve adopted for the numerical model is illustrated in Figure 6. The elastic modulus is 5Mpa for soft sensitive clays, and the Poisson's ratio is 0.45 to replicate undrained conditions.

The effect of post-failure retrogression and runout has been analyzed for parametric studies. The range for the soil parameters is primarily based on the soil properties of historical sensitive clay landslide locations (Tavenas et al. 1983, Thakur and Degago 2012). However, for the taken slope geometry of the simulated model, failure doesn't occur beyond an undrained shear strength of 30kPa. Additionally, for a fixed shape factor, there is a range for the shear strength values (both peak and remolded) below which retrogression doesn't stop (slope remains unstable) and beyond which retrogressive failure doesn't occur and vise-versa. Therefore, parametric studies have been performed considering all the factors mentioned above.

Table 0-1. Parametric studies

S_{up} (kPa)	S_{ur} (kPa)	η	S_t	L_R (m)	L_O (m)
30	1.0	65	30	>20	>35
30	1.3	65	23	16.2	33.5
30	1.8	65	17	15.8	31.0
30	2.5	65	12	13.5	27.9
30	3.2	65	9	10.8	24.5
19	2.8	45	7	17.5	26.8
22	2.8	45	8	15.5	25.2
25	2.8	45	9	16.1	25.6
28	2.8	45	10	10.7	24.6
20	2.0	65	10	18.2	32.6
25	2.5	65	10	13.6	28.1
30	3.0	65	10	14.5	25.3

25	3.0	20	8	4.0	23.8
25	3.0	40	8	11.2	25
25	3.0	60	8	13.3	26.5
25	3.0	80	8	17.8	26.2
25	3.0	90	8	18.4	28.0

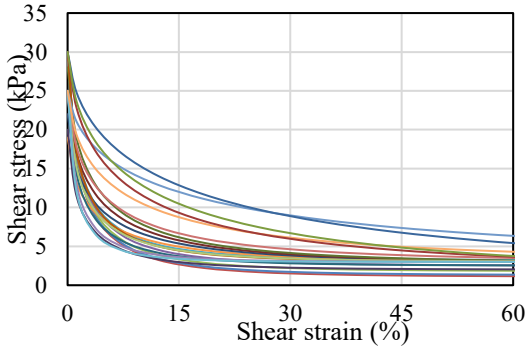

Figure 7. Strain-softening behavior adopted for the parametric studies.

Studies have been carried out, firstly, for a variation of remolded shear strength from 1.0 to 3.0 kPa, keeping the peak shear strength and shape factor constant; secondly, for a variation of peak shear strength from 15kPa to 30kPa keeping the other parameters unchanged, for a variation of both peak and remolded shear strength keeping the sensitivity constant and finally, changing the shape factor from 20 to 90 keeping other parameters the same. The material parameters for each trial are listed below, along with the final retrogression and runout in Table 1. Strain-softening curves adopted for the parametric studies are presented in Figure 7.

4) RESULTS

a) Mechanism of retrogressive failure

After the gravity loading in the first calculation step (Figure 8), the soil is stable with an undrained shear strength of 30kPa, and the strain starts to localize in a shear band as soon as strain softening is activated. When the failed soil mass starts to move forward as the first rotational slide happens, the drag of the liquified clay creates a shear band at a 45° angle to the horizontal. This process of strain localization can be found in Odenstad's (1951) hypothesis of the retrogressive spread failure mechanism, which later on was mathematically explained by Carson (1977). As failed soil mass continues progressing, consecutive 2nd, 3rd, and 4th slides occur. After the 4th slide, no new shear band is formed, and the failure stops after the failed soil mass from the 4th slide moves forward until the kinetic energy runs out. The final retrogression distance is (L_R)=15.8m, and the runout distance (L_O) is= 29.5m.

b) Effect of material parameters on post-failure movement

The peak and remolded shear strength both play a significant role in controlling the post-failure movement. However, it has been observed that runout in brittle soils has a significant impact and is primarily determined by remolded strength (Yerro et al. 2016). Zhang et al. 2018 illustrated that when the remolded shear strength approaches zero, both the final runout distance and retrogression distance become very large. Additionally, an increase in sensitivity leads to greater final runout and retrogression distances. Therefore, it is tough to assess the effect of varying peak or remolded shear strength on runout and retrogression because changing either of them and keeping the other constant changes the sensitivity of the soil, and sensitivity also affects the post-failure movement. Moreover, the overall effect of the shear strength parameters on the post-failure movement is highly influenced by the rate of strength decrease of the sensitive clay (Zhang et al. 2018, Wang et al. 2022), which makes it even more challenging.

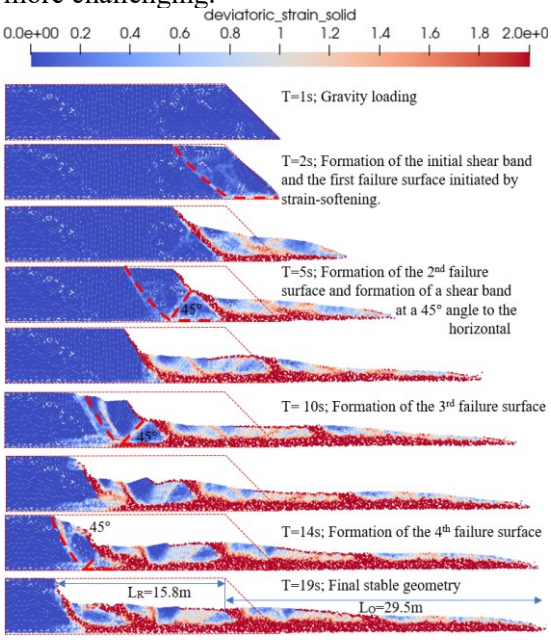

Figure 8. Mechanism of retrogressive failure

Increasing the remolded shear strength decreases the sensitivity, and as a result, the retrogression and runout distance substantially reduce (Figure 9). For an increase of remolded shear strength just by 0.9kPa, the retrogression distance reduces by 5.4m, and the runout reduces by 9m. If remolded shear strength keeps increasing, it reaches a specific value at which the failure stops at the first slide, and retrogression does not occur. The limiting value of remolded strength depends on the peak-shear strength and shape factor. For example, for 30kPa peak strength with a shape factor of 65, retrogressive failure doesn't occur beyond a remolded strength of 3.3kPa. Therefore, for a particular geometry and stress-strain profile, there is a unique value of remolded shear strength above which the failure would no longer be retrogressive.

The effect of varying peak-shear strength on the post-failure movement is not as straightforward as for remolded shear strength because sensitivity also increases with increasing peak shear strength. It is observed that retrogression and runout decrease with increasing peak strength (Wang et al., 2022). At the same time, retrogression increases with increased sensitivity (Zhang et al. 2018). These two factors are counterproductive. Therefore, to assess the effect of varying peak strength on the final runout, the change in sensitivity is kept as low as possible. An increase in peak strength decreases the retrogression and runout in most cases but doesn't have as significant an impact as the remolded shear strength. For a peak strength variation of 9kPa and sensitivity by 3, the retrogression reduces by 6.8m, and the runout reduces by only 2m. This effect is reflected in the MPM results presented in Figure 10. With the increase of peak-shear strength and simultaneous increase of sensitivity, there is a minimal change in post-failure runout. It could be because increased peak strength counters the effect of increased sensitivity.

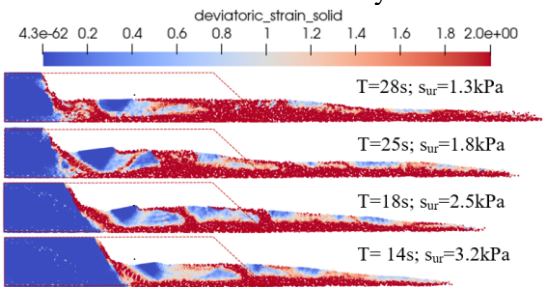

Figure 9. Effect of remolded shear strength on post-failure movement

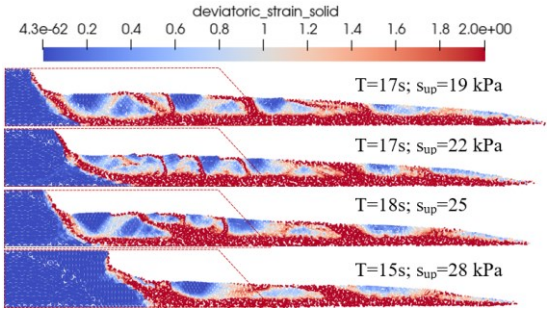

Figure 10. Effect of peak shear strength on post-failure movement

Another study has assessed the impact of the varying peak and remolded strength when the sensitivity is kept constant. It is observed that an increase in both peak and remolded shear strength decreases the post-failure movement (Figure 11).

The shape factor (η) controls the rate of strength reduction. It has been observed that, for a fixed pair of peak and remolded strength values, an increase in shape factor increases significantly increases retrogression distance (number of successive slides). Runout distance also increases with an increasing shape factor.

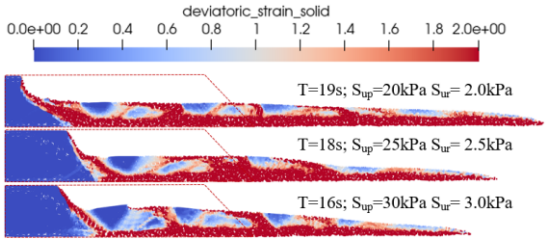

Figure 11. Effect of changing peak and remolded shear strength on post-failure movement with constant sensitivity

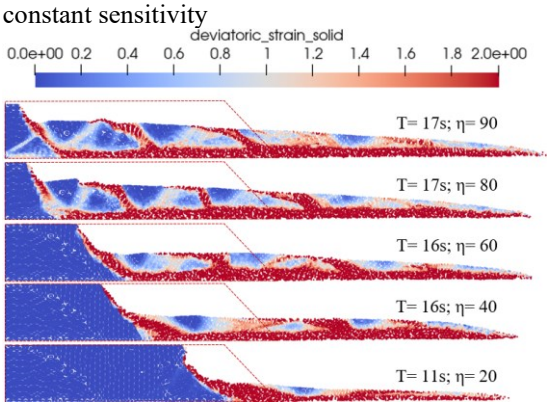

Figure 12. Effect of the shape factor on post-failure movement with constant sensitivity

5) CONCLUSION

This study has thoroughly assessed the effect of strain softening for retrogressive failure and associated post-failure movements. It can be concluded that,

- Strain-softening causes strain localization forming narrow shear bands, which create subsequent failure surfaces, eventually leading to retrogressive failure
- The occurrence of retrogressive failure significantly depends on a low value of remolded shear strength. The remolded shear strength should be low enough to cause strain localization within a narrow shear band.
- For a fixed sensitivity, higher values of peak and remolded shear strength results in lower post-failure movement.
- For a fixed value of peak and remolded shear strength, the rate of strength reduction factor/ shape factor has a marginal value; less than this value will not cause retrogressive failure
- The effect of sensitivity and peak shear strength on the occurrence of retrogressive failure vastly depends on the remolded shear strength and the shape factor. A set of particular peak shear strengths and sensitivity may not cause a retrogressive failure if the shape factor is too low or the remolded strength is too high.

6) REFERENCES

Carson, M.A., 1977. On the retrogression of landslides in sensitive muddy sediments. Canadian Geotechnical Journal **14**, 582–602.

Ceccato, F., Yerro, A., Martinelli, M.2018. Modelling soil-water interaction with the material point method. Evaluation of Single-Point and Double-Point Formulations. NUMGE IX. Volume 1, CRC Press; 2018: 351.

Dey, R., Hawlader, B., Phillips, R., Soga, K., 2015. Large deformation finite-element modelling of progressive failure leading to spread in sensitive clay slopes. Geotechnique **65**, 657–668.

Lefebvre, G. 1996. Soft Sensitive Clays. Landslides: investigation and mitigation, Special report 247, Transportation Research Board. National Academy Press, Washington, DC, pp 607–619. Washington, DC.

Locat A., Leroueil S., Bernander S., Demers D., Jostad H.P., and Ouehb L. 2011. Progressive failures in eastern Canadian and Scandinavian sensitive clays. Canadian Geotechnical Journal, **48**(11): 1696–1712

Locat, A., Jostad, H.P., Leroueil, S., 2013. Numerical modeling of progressive failure and its implications for spreads in sensitive clays. Canadian Geotechnical Journal **50**, 961–978.

Odenstad, S., 1951. The landslide in Skoptrop on the Lidan river, in: Royal Swedish Geotechnical Institute Proceedings No. 4.

Rødvand, L.A., Jostad, H.P., Grimstad, G., Andresen, L., 2022. Strain localisation in sensitive clays: can rate dependency provide mesh independent results? Computers and Geotechnics **145.**

Rots, J., Nauta, P., Kuster, G., Blaauwendraad, J. 1985. Smeared crack approach and fracture localization in concrete. HERON 30, **1**, 3–48.

Rosenqvist, I.T. 1953. Considerations on the sensitivity of norwegian quick-clays. Géotechnique **3**, 195–200.

Skempton, A.W., Northey, R.D. 1952. The sensitivity of clays. Géotechnique **3**, 30–52.

Sulsky, D., Chen, Z., Schreyer, H.L. 1994. A particle method for history-dependent materials. Computer Methods in Applied Mechanics and Engineering **118**, 179–96.

Tavenas, F., Flon, P., Leroueil, S., Lebuis, J., 1983. Remolding energy and risk of retrogression in sensitive clays, in: Proceedings of the Symposium on Slopes on Soft Clays.

Thakur, V., Degago, S.A., 2012. Quickness of sensitive clays. Geotechnique Letters **2**, 87–95.

Tran, Q.A., Sołowski, W., 2019. Generalized InterpolationMaterial Point Method modelling of large deformation problems including strain-rate effects – Application topenetration and progressive failure problems. Computers and geotechniques **106**, 249–265.

Wang, C., Hawlader, B., Perret, D., Soga, K. 2022. Effects of geometry and soil properties on type and retrogression of landslides in sensitive clays. Géotechnique **72**, 322-336.

Wang, B., Vardon, P.J., Hicks, M.A. 2016. Investigation of retrogressive and progressive slope failure mechanisms using the material point method. Computers and Geotechnics **78**, 88–98.

Yerro, A., Alonso, E.E., Pinyol, N.M. 2016. Runout of landslides in brittle soils. Computers and Geotechnics **80**, 427-439.

Zhang, X., Sloan, S.W., Oñate, E., 2018. Dynamic modelling of retrogressive landslides with emphasis on the role of clay sensitivity. International Journal for Numerical and

Analytical Methods in Geomechanics **42**, 1806–1822.

Proceedings 10th NUMGE 2023
10th European Conference on Numerical Methods in Geotechnical Engineering
Zdravković L, Konte S, Taborda DMG, Tsiampousi A (eds)
ISSN

doi: https://doi.org/10.53243/NUMGE2023-369

Implementation of a New Strain Softening Constitutive Model in the Material Point Method for the Simulation of Retrogressive Failure in Sensitive Clays

Zinan A. Urmi,[1] Ali Saeidi, Ph.D., M.ASCE.,[1] Alba Yerro, Ph.D., M.ASCE.,[2] and Rama V. P. Chavalli, Ph.D. [1]

[1]Department of Applied Science, Université du Québec à Chicoutimi, 555 Bd de l'Université, Chicoutimi, G7H 2B1 Saguenay, Quebec, Canada. E-mail: zaurmi@uqac.ca
[2]Department of Civil and Environmental Engineering, Virginia Tech, Blacksburg, Blacksburg, VA 24061, United States; E-mail: ayerro@vt.edu

ABSTRACT

Sensitive clays experience significant strain-softening behavior, i.e., when subjected to large strains. They disintegrate into a remolded liquid with diminutive shear strength. When a slope begins to fail, the remolded clay keeps moving away from its original position causing subsequent failures, resulting in catastrophic aftermath. The capability to reproduce realistic strain-softening characteristics in the constitutive soil model is necessary for more accurate numerical slope analyses in sensitive clays. This paper illustrates a simple yet practical constitutive model specially developed for simulating the strain-softening behavior of sensitive clays. The model is then implemented in Anura3D, an open-source software that uses the Material Point Method to simulate large deformations. The model is tested using the failure of a previously occurred retrogressive failure in sensitive clay. Finally, the model's predictions have been compared with the actual post-failure run out of the landslide, and the results show that the model is reasonable and practical.

INTRODUCTION

Scandinavia and eastern Canada experience a high frequency of large retrogressive landslides in sensitive clays. The primary cause of large-scale retrogressive landslides in sensitive clays, as indicated by previous studies [7, 74, 78], is the significant reduction in post-peak shear strength, commonly known as "strain-softening" in these soils. Originating from marine environments, these clays initially possess a flocculated structure with high shear strength due to salt ion exposure. However, after the iso-static rebound and leaching of salt ions, they adopt a meta-stable structure that undergoes significant strength loss upon disturbance. (Lefebvre 1996). This loss of shear strength is quantified with the term sensitivity (S_t) as the ratio of the peak shear strength (s_{up}) to the reduced (remolded) shear strength (s_{ur}) [25]. Due to strain-softening, sensitive clay slopes that experience excessive stress beyond their peak shear strength form narrow shear bands with localized strain. The soil within these shear bands undergoes significant

strength loss, transforming into a liquid-like mass known as remolded soil that flows [28]. The liquified soil either spreads laterally or drifts away from its original location, leading to a rapid series of failures that progress in a progressive or retrogressive manner [7], destroying kilometers of areas with devastating consequences (Figure 0-1).

Figure 0-1. The devastating aftermath of Gjerdrum landslide (2020) in Norway

Retrogressive failure involves several complex features that make it challenging to model using conventional numerical methods. The strain-softening behavior of sensitive clays requires a suitable constitutive soil model and an advanced numerical tool capable of handling large deformation. In the last two decades, significant development has been made to accommodate large deformation problems in geotechnical engineering. Several mesh-based and meshless numerical frameworks like arbitrary lagrangian finite element method, particle finite element method, material point method, etc., have successfully been implemented to model some key characteristics of large retrogressive failures [9, 11, 127]. In these studies, the highly non-linear post-peak strain-softening of sensitive clays has inspired the implementation of an exponential strength degradation equation (Eq. 5) to capture the post-peak soil behavior [9, 93].

$$s_u = s_{ur} + (s_{up} - s_{ur})e^{-3\gamma/\gamma_{95}} \qquad \text{Eq. 5}$$

where s_u is the degraded shear strength after the peak, γ is the strain corresponding to s_u, and γ_{95} is the strain when the strength is reduced by 95% of the supposed total reduction ($s_{up} - s_{ur}$). Even though 95% strength reduction does not correspond to a wholly remolded state, the strain value at 95% strength reduction is so large that it cannot be attained with conventional laboratory shear tests (Tavenas et al. 1983). Urmi et al. (2023c) showed that the generalized application of this equation might result in erroneous outcomes. They developed the following site-specific strain-softening equation based on the strain-softening pattern observed in the sensitive clays of several Canadian sites.

$$s_u = \begin{cases} s_{uR} + (s_{up} - s_{uR})\alpha e^{-\beta\gamma}, & s_u \geq s_{uR} \\ s_{uR} - (s_{uR} - s_{ur})\,(\gamma - \gamma_R)/(\gamma_r - \gamma_R), & s_{uR} > s_u \geq s_{ur} \end{cases} \qquad \text{Eq. 6}$$

Where, s_{uR} is the residual strength defined as the degraded strength up to which the strength reduction is exponential and can be determined by

$$s_{uR} = 0.095 s_{up} \qquad \text{Eq. 7}$$

γ_R is the corresponding residual strain at s_{uR}, α and β are site-specific parameters that can be determined from a direct shear test result of a specific site. γ_r is the strain at the remolded shear strength s_{ur} that can be estimated as,

$$\gamma_r = 0.13 s_{up} \gamma_R \quad \text{Eq. 8}$$

For this study, Eq. 6 has been employed on an elastoplastic constitutive model obeying the Tresca failure criterion, which considers the undrained shear strength (s_u) of the material as an input parameter. Although this is a basic constitutive model, the incorporation of strain softening based on the Tresca or Von Mises criteria has been frequently used in simulating sensitive clay landslides under undrained conditions [150].

The primary objective of this paper is to validate the effectiveness of this new strain-softening equation by implementing it in an MPM framework such as the Anura 3D software [153] for simulating a sensitive clay landslide. Firstly, a direct shear test was simulated to assess the reliability of the numerical model in predicting the post-peak stress-strain behavior. Then, the constitutive strain-softening model was employed to simulate the 1994 Sainte-Monique landslide in Quebec, Canada. To validate the model's predictions, a comparison was made between the predicted post-failure behavior and observed behavior in the field. This landslide was chosen for analysis because it has been previously modeled in various numerical frameworks and with different constitutive models, allowing for practical comparative analysis.

BASIS OF MPM FRAMEWORK

The Material Point Method (MPM) is a computational technique that divides a continuum into subdomains, each represented by a set of material points (Figure 0-2). These material points carry information such as stresses, strains, velocities, and accelerations. The data is then transferred from the material points to the background mesh's computational nodes, where governing equations are solved. The updated information is transferred back to the material points. Interpolation shape functions define the relationship between the material points and the nodes. Initially developed by Sulsky et al. (1994) for mechanical problems, MPM has since been extended by several researchers to solve hydro-mechanical problems. Anura3D, an MPM code, models slopes using the two-phase single-point formulation. In particular, the 2-phase single-point formulation discretizes saturated porous media with a single set of material points that carry solid and liquid phase information [174]. The material points' displacements and velocities are updated using an explicit Euler-Cromer scheme based on calculated acceleration, with a damping force employed to prevent non-physical vibrations. The proportion of the damping force to the out-of-balance force is carefully selected to ensure accurate solutions, particularly in dynamic problems. This study uses an MPM-mixed integration, which means that state variables are averaged within each element. There are other numerical integration schemes, and the sensitivity of the results on this aspect has not been analyzed in this paper.

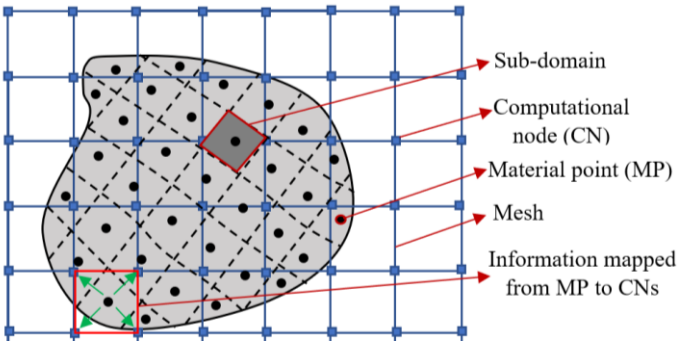

Figure 0-2. Spatial formulation of MPM framework after Urmi et al. (2023b)

SIMULATION OF DIRECT SIMPLE SHEAR (DSS) TEST

Locat et al. (2015) conducted multiple direct simple shear tests using soil samples taken from the sensitive clay layer at the Sainte-Monique site to study the shear behavior of the clay involved in the landslide. Soil samples with a height of 15mm and a diameter of 67.8mm were consolidated under 93kPa, and the sample was placed inside plastic rings to prevent lateral deformation during consolidation. Shearing was conducted laterally by a motor, applying a horizontal strain rate of 0.013mm/min at the top of the sample while the base remained fixed. Similar conditions were replicated in the numerical model, as shown in Figure 4-3. In particular, plain strain conditions were considered, and an initial rectangular domain (with a height equal to the sample's height as measured in laboratory testing) was divided into triangular elements discretized with 46 material points each. A total stress analysis is performed in undrained conditions. A damping factor is assumed as 2%. Input parameters for the simulation are listed in
Table **0-2**. Parameters for the softening equation are based on laboratory test results obtained with a detailed methodology described in Urmi et al. (2023c). The simulation result shows that (Figure 0-4) the constitutive equation has been well implemented in the numerical model to accurately depict the stress-strain behavior of sensitive clays up to the remolded strength. The simulated direct shear test results closely resemble those obtained from laboratory tests, particularly within the laboratory's maximum strain range. These observations suggest that this constitutive model is a reliable tool for predicting the material behavior of sensitive clays under undrained shear loading. To further validate and enhance the model's predictive credibility, a real-scale sensitive clay landslide has been modeled.

Table 0-2. Input parameters for the numerical simulations

Parameter	Value
Natural weight of soil, m	16 kN/m3
Shear Modulus, G	5000 kPa
Poisson's ratio, μ	0.45
Earth Pressure coefficient Ko	0.5
Peak shear strength, s_{up}	40.5 kPa
Remolded shear strength, s_{ur}	1 kPa
Residual strain, γ_R	1.8
Site-specific constant (Element Size=0.014m & 0.5m), α	0.95 & 0.95
Site-specific constant (Element Size=0.014m & 0.5m), β	2.9 & 105

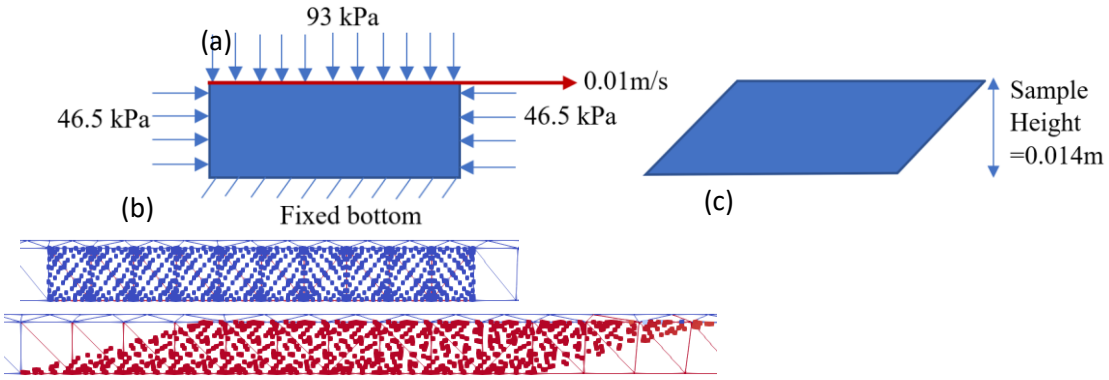

Figure 0-3. (a) Loading conditions; configuration of material points (b) initial and (c) final.

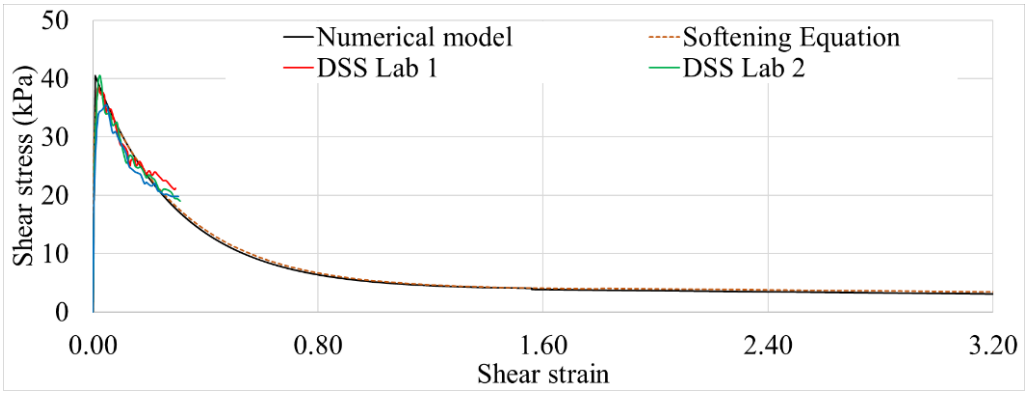

Figure 0-4. Assessment of the stress-strain behavior depicted by the numerical simulation of the direct shear test

SIMULATION OF THE SAINTE-MONIQUE LANDSLIDE

Description of the Model. Figure 4-5 illustrates a two-dimensional plane strain model for the numerical simulation of the Sainte-Monique landslide. The model's dimensions are determined based on the in-situ topography, as detailed in a study by Locat et al. (2015). The dimensions of the left-hand riverbank in the studied area are 16.6 meters in height and 200 meters in length. The right-hand embankment, which prevents further sliding, is 12 meters high and 50 meters long. The length of the slope at the left side of the brook is 37 m with a slope angle of 24°, while the right-hand slope is 25 m in length with a slope angle of 26°. In the numerical model, the computational mesh is discretized with three-noded 50,000 triangular elements with an average element size of 0.5m., each element having three material points leading to the total number of material points of approximately 150,000.

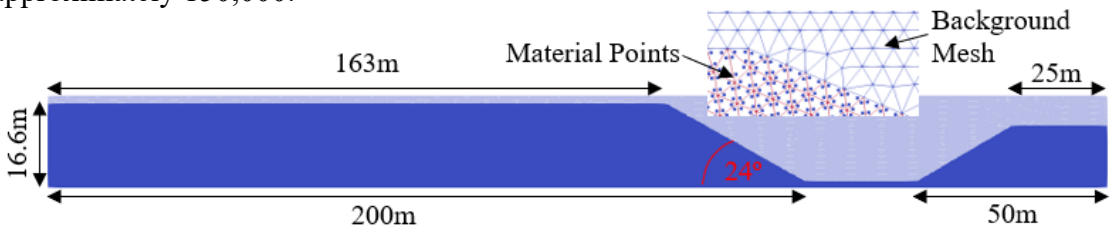

Figure 0-5. The geometry of the slope used in the numerical model

Including strain-softening features in continuum numerical methods can cause strain localization problems [162]. A smeared crack approach is used to address this, treating energy dissipation in a shear band as equivalent to the fracture energy in a discrete

crack [24]. In the Material Point Method (MPM), the thickness of the shear band is estimated based on the mesh element size. To ensure uniform work dissipation and avoid mesh size dependence, the constitutive modulus (α and β) of the material is adjusted according to the element size. This calibration is achieved through numerical shear tests with different element sizes, aiming for consistent areas under the stress-strain curves up to the remolded strength. Further details can be found in Soga et al.'s (2016) work. In the simulation of retrogressive failure, another direct shear test was conducted using a sample and element thickness of 0.5m. Keeping α constant, β was calibrated to guarantee that the area under the stress-strain curve is equal for both DSS tests.

The numerical analysis assumed that simulating only 1 meter below the failure surface of the thick in-situ sensitive clay layer was adequate. Additional thickness did not significantly influence the results but increased the number of material points. The left and right boundaries were fixed horizontally, and the bottom boundary was fixed vertically. The initial stress condition was created in the drained condition using drained shear strength, while the undrained shear strength was used for the undrained condition during the slope failure, both obtained from soil investigations. The stresses are initialized under a gravity loading, and in the process of reaching the initial quasistatic equilibrium, a damping factor of 75% is used to converge to the quasi-static solution while avoiding dynamic oscillations. The mean effective vertical stress before failure after the gravity loading stage is shown in Figure 4-8. Failure was then initiated by implementing undrained strain-softening. At this stage, the damping factor is reduced down to 2% to allow for the dynamic post-failure response. Model parameters for the retrogressive failure analysis are the same as the DSS simulation except for β, presented in

Table **0-2**. The model did not account for anisotropy and creep, nor did it consider the long-term effects of clay behavior, such as fatigue, weathering, and chemical effects. Further research may consider these complexities for a more accurate simulation. This study considers a single-phase total stress MPM formulation; hence, excess pore pressure is not calculated.

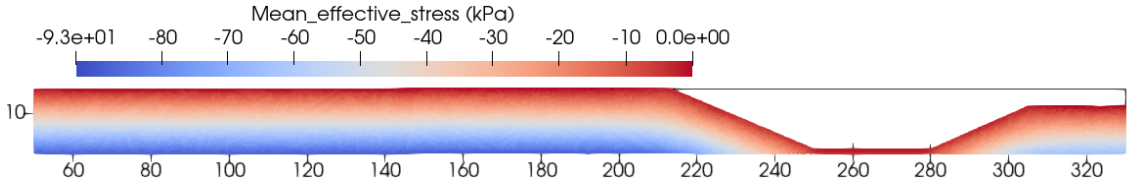

Figure 0-6. Initial vertical stress of the slope

Failure mechanism observed in the simulation. After the gravity loading in the first calculation step (Figure 4-9), the soil is stable with an undrained shear strength of 40 kPa, and the strain starts to localize in a thin shear band as soon as strain softening is activated from step 2. Failure propagates horizontally through the layer opposite to the river producing a slide bottom "ba"; simultaneously, a slip surface "bc" is formed at an angle of 55° parallel to the slide bottom (Figure 4-9a). When stresses along "bc" reach near zero, it starts to slip, forming a wedge "abcd" (Figure 4-9b). When "abcd" slips from position 1 to 2, the drag of this slip causes a rupture "de" parallel to "bc." By this time, the slide bottom has already reached point "d" (Figure 4-9c), and a secondary failure surface along "cd" creates a wedge "cde" (Figure 4-9d). The wedge "cde" sinks from its original position creating a graben which leaves a horst at "bcd" (Figure 4-9e). Thus the whole strip "AA'" forms in a retrogressive and discontinuous manner (Figure 4-9f) and slips into the river with an almost horizontal (slightly inclined towards the bottom) translatory movement.

During the movement, tension cracks are formed within the wedges that also contribute to the formation of horst and graben-like structures.

Similarly, strips BB, CC, and DD are formed. During the movement of CC, the front portion of the moving debris is arrested on the other side of the river, and the landslide movement starts to cease. The landslide completely stops by the time when strip DD propagates about 6m from its original position. The failure observed mechanism perfectly complies with Urmi et al. (2023a) description of the spread mechanism based on previous literature [70, 78]. The final retrogression distance is =140 m.

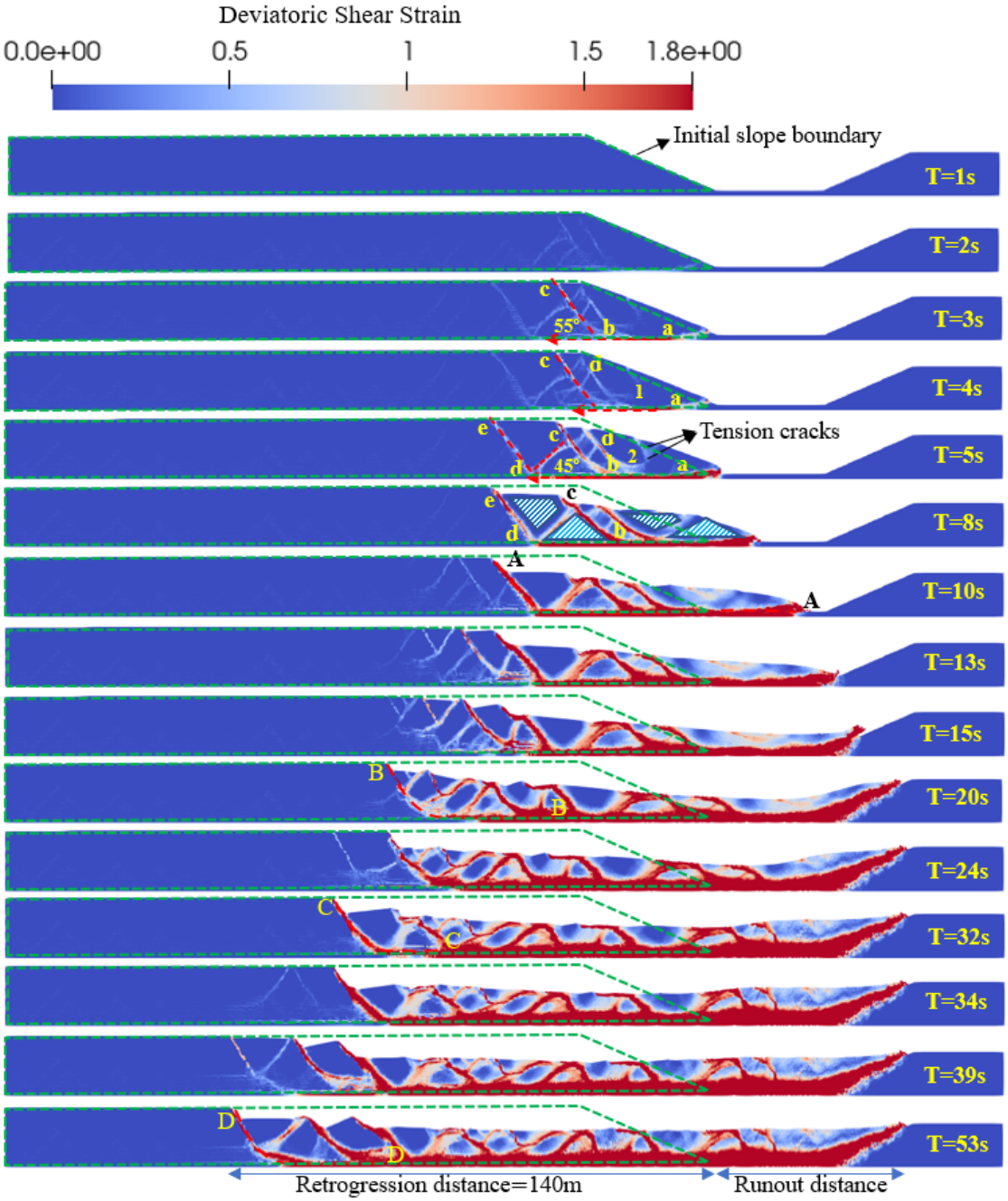

Figure 0-7. The failure mechanism of simulated retrogressive landslide

Comparison of the simulation results with the observed in situ post-failure movement.

The numerical simulation accurately captured the retrogression observed in the field, resulting in a similar retrogression distance and post-failure geometry (Figure 4-9). A

comparison of the simulation's post-failure features with the field observation by Locat et al. (2015) reveals several similarities.

- Firstly, the landslide debris remained inside the crater, with the opposite side of the brook obstructing the flow and resulting in minimal lateral movement, as observed in the field.
- Secondly, several ridges were visible with intact material, and some had sharp tips pointing upwards, referred to as horsts, with tip angles mostly varying between 70-90 degrees. The field observations noted that the tip angle of the horst closely resembled the active failure angle observed in eastern Canadian clays, which is approximately 60 degrees. Other blocks within the debris had flat, horizontal tops called grabens, which were not entirely separated and could be connected by vegetation, as observed in the field.
- Finally, the soil mass moved horizontally in an active failure mode, similar to the field.

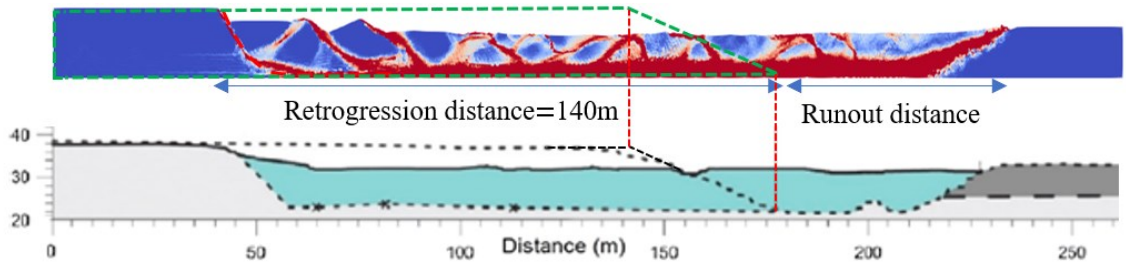

Figure 0-8. Comparison of the post-failure geometry of the simulated model and field observation from Locat et al. 2015

Comparison of the simulation results with other numerical simulations. Tran and Solwoski (2019) and Shan et al. (2021) modeled the same landslide, implementing different strain-softening equations in the Generelised Interporation MPM framework (GIMPM) and particle finite element method with the RITSS technique, respectively. Both models considered the strain rate effect on the shear strength and the depthwise variation of the peak shear strength, while the constitutive model used in this study was comparatively more simplified. However, the model presented in this study demonstrated slightly better accuracy in capturing the post-failure behavior, as shown in Figure 0-9. This could be attributed to the fact that the strain-softening equation used in this study was derived from analyzing the large-deformation stress-strain behavior of several eastern-Canadian-sensitive clay sites [151] with the large deformation parameters obtained based on laboratory direct shear test data. In contrast, other researchers employed the back analysis trial and error method to obtain these parameters. Furthermore, Shan et al.'s (2021) simulation did not comply with several field observations, such as the absence of ridges, the complete separation of the soil mass into blocks, and a retrogression distance less than that observed in the field.

CONCLUSION

In this study, a strain-softening constitutive model developed based on available data from eastern Canadian Sensitive clays was presented. The model's efficacy was demonstrated by successfully simulating a direct shear test and a real-scale sensitive clay landslide, which was compared with field observations. The model effectively captured the essential characteristics of retrogressive spread failure, consistent with previous theoretical descriptions of this type of failure. The post-failure geometry generated by the

model was more realistic than numerical simulations using other methods and constitutive models. These results highlight the model's reliability and usefulness for predicting the behavior of sensitive clays under undrained softening, as well as providing valuable insights into the mechanisms of retrogressive spread failure. Further research could explore the model's potential for incorporating complex features like strain rate effect, creep behavior, spatial variability, etc.

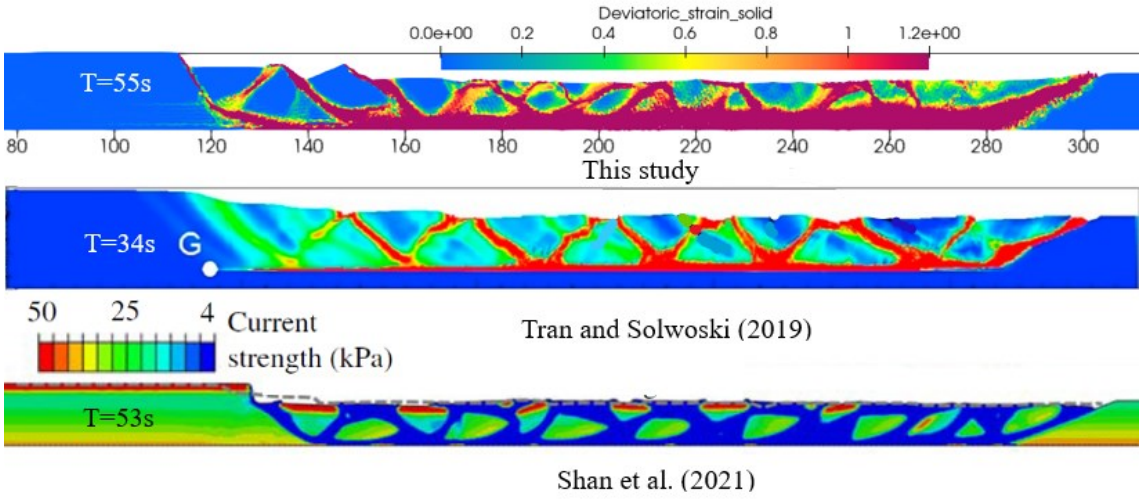

Figure 0-9. Comparison of the post-failure geometry of the simulated model and other numerical simulations of the same landslide

REFERENCES

Anura3D MPM Research Community. 2022. "<www.anura3d.com>." Anura3D Version 2022.1.0.9751 Source Code.

Bjerrum, L. 1955. "Stability of Natural Slopes in Quick Clay." Géotechnique, 5 (1): 101–119. https://doi.org/10.1680/geot.1955.5.1.101.

Carson, M. A. 1977. "On the retrogression of landslides in sensitive muddy sediments." Canadian Geotechnical Journal, 14: 582–602. https://doi.org/10.1139/t77-059.

Ceccato, F., A. Yerro, and M. Martinelli. 2018. "Modelling soil-water interaction with the material point method. Evaluation of single-point and double-point formulations." Numerical methods in geotechnical engineering IX, 351–358. CRC Press.

Locat, A., S. Leroueil, A. Fortin, D. Demers, and H. P. Jostad. 2015. "The 1994 landslide at Sainte-Monique, Quebec: Geotechnical investigation and application of progressive failure analysis." Canadian Geotechnical Journal, 52 (4): 490–504. Canadian Science Publishing. https://doi.org/10.1139/cgj-2013-0344.

Mitchell, R. J., and A. R. Markell. 1974. "Flowsliding in Sensitive Soils." Canadian Geotechnical Journal, 11: 11–31.

Odenstad, S. 1951. "The landslide in Skoptrop on the Lidan river." Royal Swedish Geotechnical Institute Proceedings No. 4.

Oliver, J., and A. E. Huespe. 2004. "Continuum approach to material failure in strong discontinuity settings." Comput Methods Appl Mech Eng, 193 (30–32): 3195–3220. https://doi.org/10.1016/j.cma.2003.07.013.

Rosenqvist, I. T. 1953. "Considerations on the sensitivity of norwegian quick-clays." Géotechnique, 3 (5): 195–200.

Rots, J., P. Natua, G. Kuster, and J. Blaauwendraad. 1985. "Smeared crack approach and fracture localization in concrete." HERON 30, 1: 3–48.

Shan, Z., W. Zhang, D. Wang, and L. Wang. 2021. "Numerical investigations of retrogressive failure in sensitive clays: revisiting 1994 Sainte-Monique slide, Quebec." Landslides, 18 (4): 1327–1336. Springer Science and Business Media Deutschland GmbH. https://doi.org/10.1007/s10346-020-01567-4.

Skempton, A. W., and R. D. Northey. 1952. "The sensitivity of clays." Géotechnique, 3 (1): 30–52. https://doi.org/10.1680/geot.1952.3.1.30.

Soga, K., E. Alonso, A. Yerro, K. Kumar, and S. Bandara. 2016. "Trends in large-deformation analysis of landslide mass movements with particular emphasis on the material point method." Geotechnique, 66 (3): 248–273. Thomas Telford Services Ltd. https://doi.org/10.1680/jgeot.15.LM.005.

Sulsky, D., Z. Chenb, and H. L. Schreyer. 1994. "A particle method for history-dependent materials." Comput Methods Appl Mech Eng, 118 (1–2): 179–196. https://doi.org/10.1016/0045-7825(94)90112-0.

Tran, Q. A., and W. Sołowski. 2019. "Generalized Interpolation Material Point Method modelling of large deformation problems including strain-rate effects – Application to penetration and progressive failure problems." Comput Geotech, 106: 249–265. Elsevier Ltd. https://doi.org/10.1016/j.compgeo.2018.10.020.

Urmi, Z. A., A. Saeidi, R. V. P. Chavali, and A. Yerro. 2023a. "Failure mechanism, existing constitutive models and numerical modeling of landslides in sensitive clay: a review." Geoenvironmental Disasters, 10 (1): 14. https://doi.org/10.1186/s40677-023-00242-9.

Urmi, Z. A., A. Saeidi, A. Yerro, and R. V. P. Chavali. 2023b. "Effect of strain softening on the prediction of post-failure runout in sensitive clay landslide ." NUMGE 2023: 10th European Conference on Numerical Methods in Geotechnical Engineering . London.

Urmi, Z. A., A. Saeidi, A. Yerro, and R. V. P. Chavali. 2023c. "Prediction of post-peak stress-strain behavior for sensitive clays." Eng Geol, 323: 107221. https://doi.org/10.1016/j.enggeo.2023.107221.

Wang, C., B. Hawlader, D. Perret, and K. Soga. 2020. "Effects of geometry and soil properties on type and retrogression of landslides in sensitive clays." Géotechnique, 1–15. Thomas Telford Ltd. https://doi.org/10.1680/jgeot.20.p.046.

Yerro, A., K. Soga, and J. Bray. 2019. "Runout evaluation of Oso landslide with the material point method." Canadian Geotechnical Journal, 56 (9): 1304–1317. https://doi.org/10.1139/cgj-2017-0630.

Yuan, W. H., K. Liu, W. Zhang, B. Dai, and Y. Wang. 2020. "Dynamic modeling of large deformation slope failure using smoothed particle finite element method." Landslides, 17 (7): 1591–1603. Springer. https://doi.org/10.1007/s10346-020-01375-w.

Zhang, X., S. W. Sloan, and E. Oñate. 2018. "Dynamic modelling of retrogressive landslides with emphasis on the role of clay sensitivity." Int J Numer Anal Methods Geomech, 42 (15): 1806–1822. John Wiley and Sons Ltd. https://doi.org/10.1002/nag.2815.